Investigating the structural and functional characteristics of coproporphyrin ferrochelatase

By:

Antonia Turberville

A thesis submitted in partial fulfilment of the requirements for the degree of Doctor of Philosophy

The University of Sheffield
Faculty of Science
Department of Chemistry

Submission Date

October 2019

Acknowledgements

I would firstly like to thank my supervisor Dr Jim Reid for all the time and support he has given me during my PhD. I have greatly benefited from his expertise especially in the more difficult aspects of enzyme kinetics. Without his help I would have never become the scientist I am today.

I would also like to thank the members of my lab group. First and foremost, I would like to thank Dr Nick Moody. He was definitely a source of amusement throughout my time in the lab even when it wasn't intentional, he also provided me with strong opinions on my choice of TV shows which I do object to. We did also have many discussions about our science which were both helpful and informative. I would like to thank Dr Chat Phansopa for all his advice and his solid foundation of knowledge in all things biological. He was particularly helpful for looking at science from a different perspective and his knowledge was greatly appreciated. Finally, I would like to thank Dhiya Zawawi she was a warm, friendly and kind addition to the lab.

In addition to the lab group, I would like to thank the members of the Staniland group for making the office a nice place to work. They are friendly and made my time in the office very enjoyable. I would like to specifically thank Dr Andrea Rawlings, not only is she one of the nicest people I have met, she is very knowledgeable and helpful. She was always able to solve many of my problems or suggest alternative methods. Another person I would like to thank is Dr Chris Marklew, his expertise was also greatly appreciated. He also provided and warm, friendly atmosphere to work in and sometimes that was all that was needed.

Abstract

Heme is an essential cofactor in most organisms, this includes bacteria and mammals. The coproporphyrin-dependent heme biosynthesis pathway is specific to Gram positive bacteria and was only discovered in 2015. Before this discovery Gram positive bacteria were assumed to synthesise heme using the same heme synthesis pathway as mammals. As a result, the enzymes within this pathway have not been fully characterised and provide novel targets for antibiotics.

Experiments were completed to investigate the protein-protein interactions between HemH and HemQ, two consecutive enzymes in the pathway as they are covalently linked in *P. acnes*. This used SEC and showed that truncations for the *P. acnes* HemH-Q protein (HemHL and HemQS) interacted 1:1 whereas other non-covalently linked HemH and HemQ proteins didn't have observable protein-protein interactions.

Kinetic investigation of the wildtype *B. subtilis* and *S. aureus* HemH proteins with their endogenous substrate (coproporphyrin) was completed as previous kinetic analysis of *B. subtilis* HemH used analogues of protoporphyrin IX in the kinetic assays. A combination of spectroscopic techniques were utilised and they show that the two proteins are very active and behave in a broadly similar way to each other. Stopped flow fluorescence spectroscopy proved a useful tool for in depth kinetic investigation into the enzymatic mechanism of coproporphyrin ferrochelatase. Rates constants for enzyme/porphyrin isomerisation, metal chelation and binding constants for substrate binding were estimated using this technique.

Finally, functionally important *B. subtilis* HemH active site mutants (K87A, H88A, E264A/Q) were characterised using similar techniques described for wildtype characterisation. K87A/H88A and E264A/Q are on the non-conserved and conserved active site face, respectively. This shows that whilst K87A, E264A/Q are relatively inactive they are capable of binding coproporphyrin and activity is diminished after binding. H88A has activity comparable to wildtype with weakened coproporphyrin binding and better at iron binding and chelation. This research could provide details for rational drug design of antibiotics that specifically target Gram positive bacteria.

Table of Contents

List of Figures and Tables

Enzymatic Schemes

Scheme 1- Two step substrate (CPIII) binding to enzyme (E)

Scheme 2- Iron binding and porphyrin metalation

Scheme 3- Enzymatic scheme of ferrochelatase reaction from start to rate determining step

Scheme 4- Overall enzymatic mechanism of ferrochelatase

Abbreviations

ABC   Ammonium bicarbonate

ACN   Acetonitrile

AFM   Atomic force microscopy

AhbA/B/C/D   Alternative heme biosynthesis A/B/C/D

ALA   δ-aminolevulinic acid

ALAS   δ-aminolevulinic acid synthase

APS   Ammonium persulphate

AUC   Analytical ultracentrifugation

B. megaterium   *Bacillus megaterium*

B. subtilis   *Bacillus subtilis*

bFC   *Bacillus subtilis* ferrochelatase

BLAST   Basic local alignment search tool

BN-PAGE   Blue native polyacrylamide gel electrophoresis

CD   Circular dichroism spectroscopy

CgDC   Coproporphyrinogen III decarboxylase

CgDH   Coproporphyrinogen III dehydrogenase

CgOX   Coproporphyrinogen III oxidase

CHAPS	3-[(cholamidopropyl)dimethylammonio]-1-propanesulfonate hydrate
ChDC	Coproheme decarboxylase
CoA	Coenzyme A
Copro	Coproporphyrin III
Copro'gen	Coproporphyrinogen III
Coproheme	Fe-coproporphyrin III
CpFC	Coproporphyrin ferrochelatase
CP_{III}	Coproporphyrin III
CPO	Coproporphyrinogen oxidase
CV	Column volumes
D. vulgaris	*Desulfovibrio vulgaris*
DDSH	12, 18-didecarboxysirohydrochlorin
D_{IX}	Deuteroporphyrin IX
EDTA	Ethylenediaminetetraacetic acid
FAD	Flavin adenine dinucleotide
FC	Ferrochelatase
FI	Fluorescence intensity

FMN	Flavin mononucleotide
GluT	Glutamyl-tRNA^{Glu}
GluTR	Glutamyl-tRNA reductase
GluTS	Glutamyl-tRNA synthetase
GSA	Glutamate-1-semialdehyde
GSAM	Glutamate-1-semialdehyde aminomutase
H. sapiens	*Homo sapiens*
HDX-MS	Hydrogen-deuterium exchange mass spectrometry
hFC	*Homo sapiens* ferrochelatase
HMB	1-hydroxymethylbilane
HMBS	Hydroxymethylbilane synthase
IAA	Iodoacetamide
IEX	Ion exchange chromatography
IMAC	Immobilised metal affinity chromatography
IPTG	Isopropyl β-D-1-thiogalactopyranoside
KLD	Kinase, ligase, Dpn1
L. monocytogenes	*Listeria monocytogenes*
LC	Liquid chromatography
M. barkeri	*Methosarcina barkeri*

MST	Microscale thermophoresis
M. tuberculosis	*Mycobacterium tuberculosis*
MP$_{IX}$	Mesoporphyrin IX
NAD	Nicotinamide adenine dinucleotide
NADP	Nicotinamide adenine dinucleotide phosphate
NirDL/G/H/J	Nitrate reductase DL/G/H/J
N-MeMP	N-methyl mesoporphyrin
OEP	Octylethylporphyrin
P. acnes	*Propionibacterium acnes*
PAA	Peracetic acid
PBG	Porphobilinogen
PBGD	Porphobilinogen deaminase
PBGS	Porphobilinogen synthase
PBS	Phosphate buffered saline
PC2	Precorrin 2
PCDH	Precorrin dehydrogenase
PCR	Polymerase chain reaction
PgDH1/2	Porphobilinogen dehydrogenase 1/2
PgOX	Porphobilinogen oxidase

PpFC   Protoporphyrin ferrochelatase

PPO   Protoporphyrinogen oxidase

Proto   Protoporphyrin IX

Proto'gen   Protoporphyrinogen

R. spheroides   *Rhodobacter spheroides*

RR   Resonance Raman

S. aureus   *Staphyloccocus aureus*

S. cerevisiae   *Saccharomyces cerevisae*

SAM   S-adenosyl methionine

SAXS   Small- angle X-ray scattering

SDS   Sodium dodecyl sulphate

SDS-PAGE   Sodium dodecyl sulphate polyacrylamide gel
                        electrophoresis

SEC   Size exclusion chromatography

SEC-MALS   Size exclusion chromatography – multiple angle light
                        scattering

SH   Siroheme

SiHC   Sirohydrochlorin

SPR   Surface plasmon resonance

SUMT	SAM-dependent uroporphyrinogen methyltransferase
TCEP	Tris(2-carboxyethyl) phosphine hydrochloride
TEMED	*N*, *N*, *N′*,*N′*-tetramethylethylene-diamine
T_m	Thermal melting point
Uro'gen	Uroporphyrinogen III
UROD	Uroporphyrinogen III decarboxylase
UROS	Uroporphyrinogen III synthase
θMR	Molar residue ellipticity

1. Introduction

1.1 Tetrapyrroles and heme

Tetrapyrroles are chains of four covalently linked pyrroles. They can be linear or cyclic such as hydroxymethylbilane (HMB) and uroporphyrinogen III (uro'gen), respectively. A specific class of cyclic tetrapyrroles are called porphyrins. Porphyrins are derived from the parent compound porphine (figure 1.1). Substitution of the hydrogen at positions 1-8 give rise to the different porphyrin compounds. Examples include coproporphyrin III (Copro or CP_{III}) which contains 4 methyl and 4 propionyl groups at positions 1-8 and protoporphyrin IX (Proto or PP_{IX}) containing 4 methyl, 2 vinyl and 2 propionyl groups at positions 1-8 (Falk, 1964).

Tetrapyrrole synthesis diverges at the last common precursor, uroporphyrinogen III. Uroporphyrinogen can be converted into a number of different products through a series of different enzymatic steps. These tetrapyrrole products include heme, chlorophyll and cobalamin (Dailey et al., 2017).
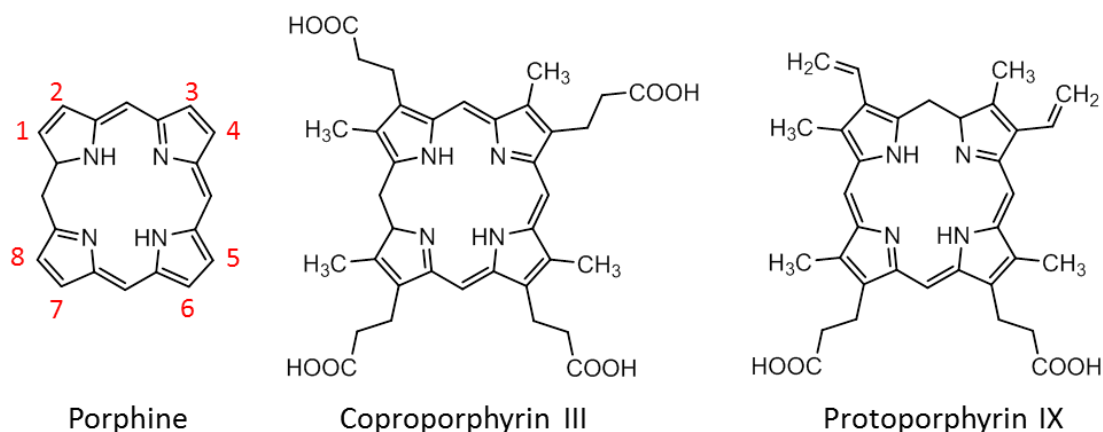
Figure 1.1 - Porphyrin structures

The parent porphyrin compound porphine contains hydrogens at potential substitution positions 1-8 (red). Coproporphyrin III and protoporphyrin IX are examples of porphyrins where positions 1-8 have been substituted with methyl, vinyl and propionyl groups.

Heme is a prosthetic group or cofactor of proteins involved in a wide range of biological processes; this includes gene regulation, cell signalling and oxygen transport. Heme is one of the most important tetrapyrroles and as a result it is found in a variety of proteins, the most commonly known examples are hemoglobin, myoglobin, cytochrome P450, peroxidases and catalases (Munro et al., 2009, Falk, 1964).

1.2 Heme biosynthesis

Heme biosynthesis occurs through three routes: the protoporphyrin-dependent (canonical or classic) route taken by Gram negative bacteria and eukaryotes, the coproporphyrin-dependent (non-canonical or intermediate) pathway utilised by Gram positive bacteria and the siroheme-dependent (alternative) pathway used by sulphate reducing bacteria and archaea (figure 1.2). The coproporphyrin-dependent pathway is the most recently discovered pathway and so investigating the enzymes in this pathway could lead to the production of novel antibiotics specifically targeted against Gram positive bacteria (Layer et al., 2010, Storbeck et al., 2010, Dailey et al., 2015).

PROTOPORPHYRIN
Gram negative bacteria, eukaryotes

ALA ⟶ URO'GEN ⟶ COPRO'GEN ⟶ HEME

COPROPORPHYRIN
Gram positive bacteria

SIROHEME
Sulphate-reducing bacteria, archae
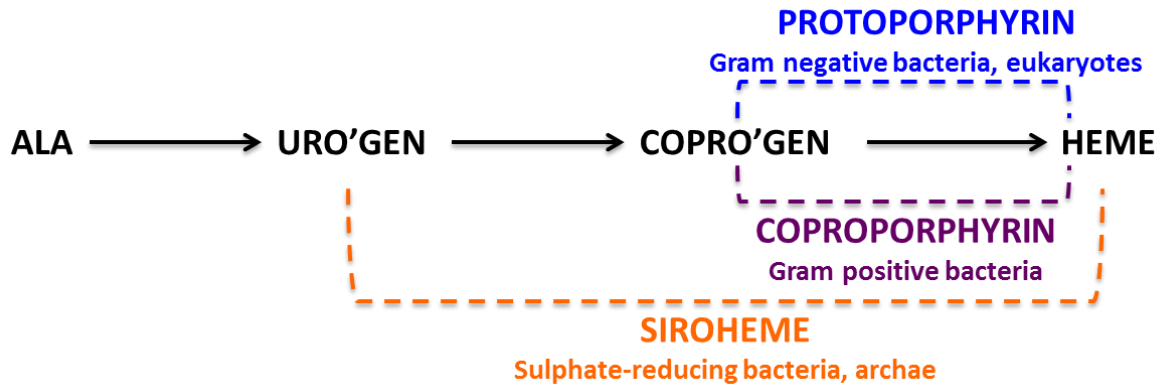
Figure 1.2 - Simple scheme of the three different heme biosynthetic pathways

The pathway from δ-aminolevulinic acid to uroporphyrinogen III is conserved in the three heme biosynthetic pathways. After the formation of uroporphyrinogen, the siroheme-dependent pathway diverts away from the conserved pathway and forms heme using different enzymes and substrates. Uroporphyrinogen is decarboxylated to form coproporphyrinogen and the protoporphyrin-dependent and coproporphyrin-dependent pathways diverge at coproporphyrinogen and synthesise heme using different enzymatic steps. **Abbreviations: ALA** (δ-aminolevulinic acid), **URO'GEN** (uroporphyrinogen III), **COPRO'GEN** (coproporphyrinogen III).

1.2.1 Conserved pathway

1.2.1.1 Formation of δ-aminolevulinic acid (ALA)
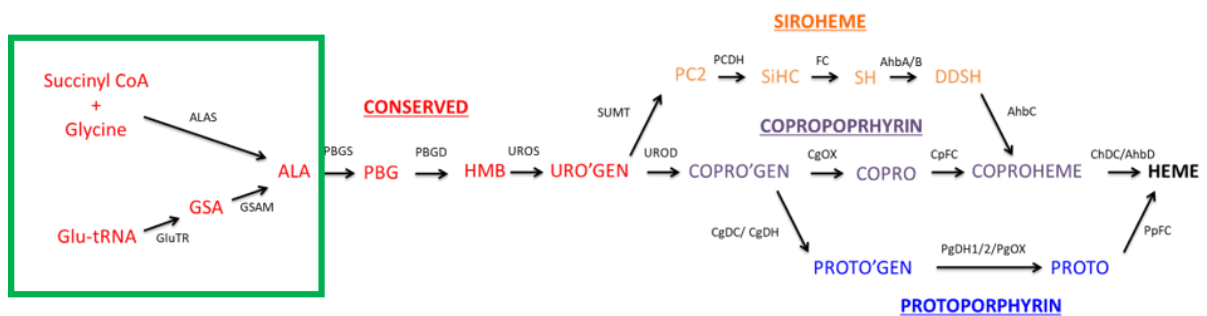
Figure 1.3 – Overall heme biosynthesis pathway

The green box highlights the current section of interest, the formation of ALA. ALA is through two pathways: the Shemin pathway and the C_5 pathway. The Shemin pathway utilises glycine and the C_5 pathway uses glutamate.

All natural tetrapyrroles are synthesised from a common precursor δ-aminolevulinic

acid (ALA) and this is formed in two different unrelated ways, the Shemin (C_4) pathway

and the C_5 pathway (figure 1.3). The route taken to form ALA is dependent on the organism (Layer et al., 2010). Mammals, fungi and α-proteobacteria produce ALA through the condensation of succinyl-CoA (coenzyme A) and glycine, catalysed by the homodimeric, pyridoxal phosphate-dependent enzyme δ-aminolevulinic acid synthase (ALAS, HemA[C4]). This is the Shemin pathway (Choi et al., 2004, Layer et al., 2010). The Shemin pathway was proposed in 1952, and the involvement of glycine and succinyl-CoA in heme biosynthesis was discovered in 1945 and 1952, respectively. These results identified δ-aminolevulinic acid as a potential precursor for heme synthesis (Shemin and Kumin, 1952, Shemin and Rittenberg, 1945)(figure 1.4).
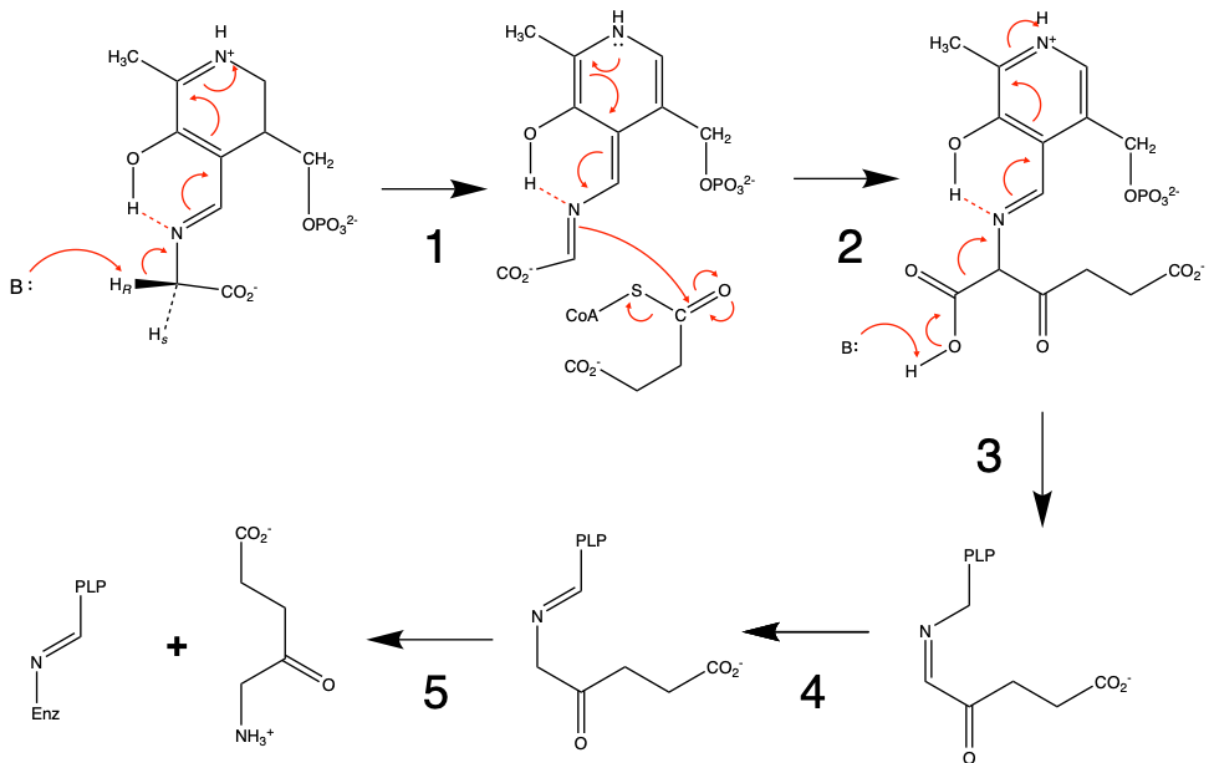
Figure 1.4- Enzyme mechanism of ALAS

The mechanism starts with the formation of a glycine-PLP imine which becomes deprotonated (1). This is followed by a Claisen-like condensation reaction with succinyl CoA (2) and decarboxylation (3). The molecule undergoes tautomerization (4) and transamination to give ALA(5).

The C_5 pathway is found in plants, archaea and most bacteria (Layer et al., 2010). It was discovered in the 1970s after it was shown that glycine was not used in heme

biosynthesis in chlorophyll-synthesising tissues (figure 1.5). Further studies indicated that glutamyl-tRNA provided the carbon and nitrogen source needed for heme biosynthesis in these tissues (Layer et al., 2010, Huang et al., 1984). The C_5 pathway begins with glutamyl-tRNA^{Glu} (GluT) which is produced via glutamyl-tRNA synthetase (GluTS) (Heinemann et al., 2008). Glutamyl-tRNA is reduced by glutamyl-tRNA reductase (GluTR, HemA^{C5}) to form the reaction intermediate glutamate-1-semialdehyde (GSA) (Kannangara and Gough, 1978, Beale et al., 1975). Glutamate-1-semialdehyde is quickly converted to δ-aminolevulinic acid by glutamate-1-semialdehyde aminomutase (GSAM, HemL) in a pyridoxal phosphate-dependent transamination reaction (Layer et al., 2010, Heinemann et al., 2008). After the formation of δ-aminolevulinic acid, the subsequent steps in heme biosynthesis are conserved across the majority of heme-synthesising organisms until the synthesis of the first cyclic intermediate uroporphyrinogen III (Heinemann et al., 2008).
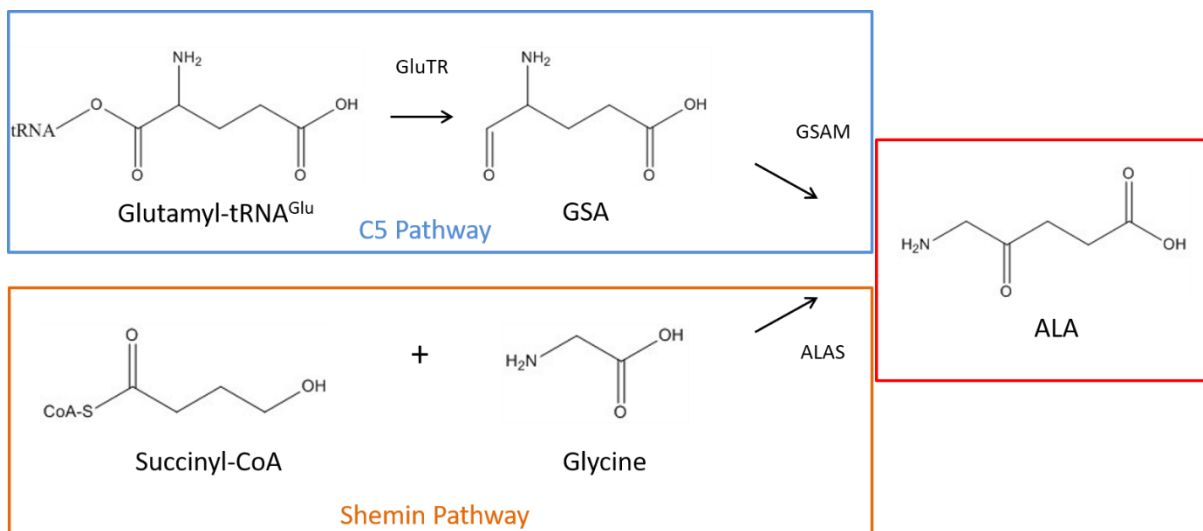
Figure 1.5 - Formation of ALA (δ-aminolevulinic acid)

Two different pathways to form the tetrapyrrole intermediate δ-aminolevulinic acid (red), the Shemin pathway (orange) and the C_5 pathway (blue) Abbreviations: **ALAS** (δ-aminolevulinic acid synthase), **ALA** (δ-aminolevulinic acid), **GSAM** (glutamate-1-semialdehyde aminomutase), **GSA** (glutamate-1-semialdehyde), **GluTR** (glutamyl-tRNA reductase).

1.2.1.2   Formation of uroporphyrinogen III (Uro'gen)
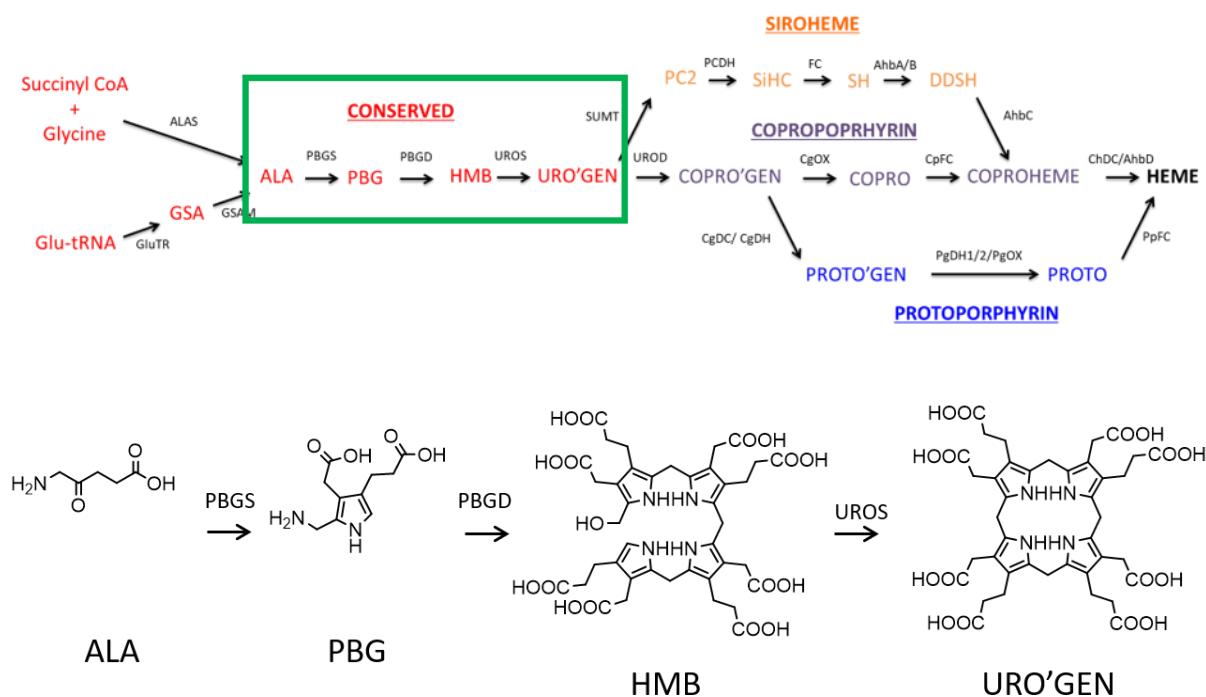
Figure 1.6– Overall heme biosynthesis pathway

The green box highlights the current section of interest, the conserved pathway, This pathway is conserved for all tetrapyrroles synthesis pathways and the main branch starts after the formation of ALA and ends in the formation of URO'GEN. In the conserved pathway δ-aminolevulinic acid is converted to uroporphyrinogen through a series of conserved enzymatic steps. Two molecules of δ-aminolevulinic acid are asymmetrically condensed to produce porphobilinogen and four molecules of porphobilinogen are covalently linked to form hydroxymethylbilane. Hydroxymethylbilane undergoes isomerisation and circularisation to produce uroporphyrinogen. Abbreviations: **ALA** (δ-aminolevulinic acid), **PBGS** (porphobilinogen synthase), **PBG** (porphobilinogen) **PBGD** (porphobilinogen deaminase), **HMB** (hydroxymethylbilane), **UROS** (uroporphyrinogen III synthase), **URO'GEN** (uroporphyrinogen III).

After the formation of ALA the main branch of the conserved pathway begins, this is common to all tetrapyrrole biosynthesis pathways and ends after the formation of uroporphyrinogen III (figure 1.6). To start, two δ-aminolevulinic acid molecules are asymmetrically condensed to produce porphobilinogen, in a reaction catalysed by porphobilinogen synthase (HemB, PBGS figure 1.7) (Bevan et al., 1980). The activity of porphobilinogen synthase is controlled by an allosteric mechanism. Different

37

multimeric states of porphobilinogen synthase indicate whether the enzyme is active or inactive. In an octameric state porphobilinogen synthase is active, the octamer dissociates to form dimers, the N-terminal arm domains of the dimers re-orientate so that the inactive hexamer can assemble. There are allosteric sites on the hexamer and octamer that stabilise each of the conformations (Jaffe and Lawrence, 2012). In human porphobilinogen synthase, zinc is required for catalysis and the magnesium binds allosterically. Of the porphobilinogen synthase sequences available 50% are predicted to require zinc for catalysis and 90% bind magnesium allosterically (Bollivar et al., 2004, Layer et al., 2010, Bevan et al., 1980).
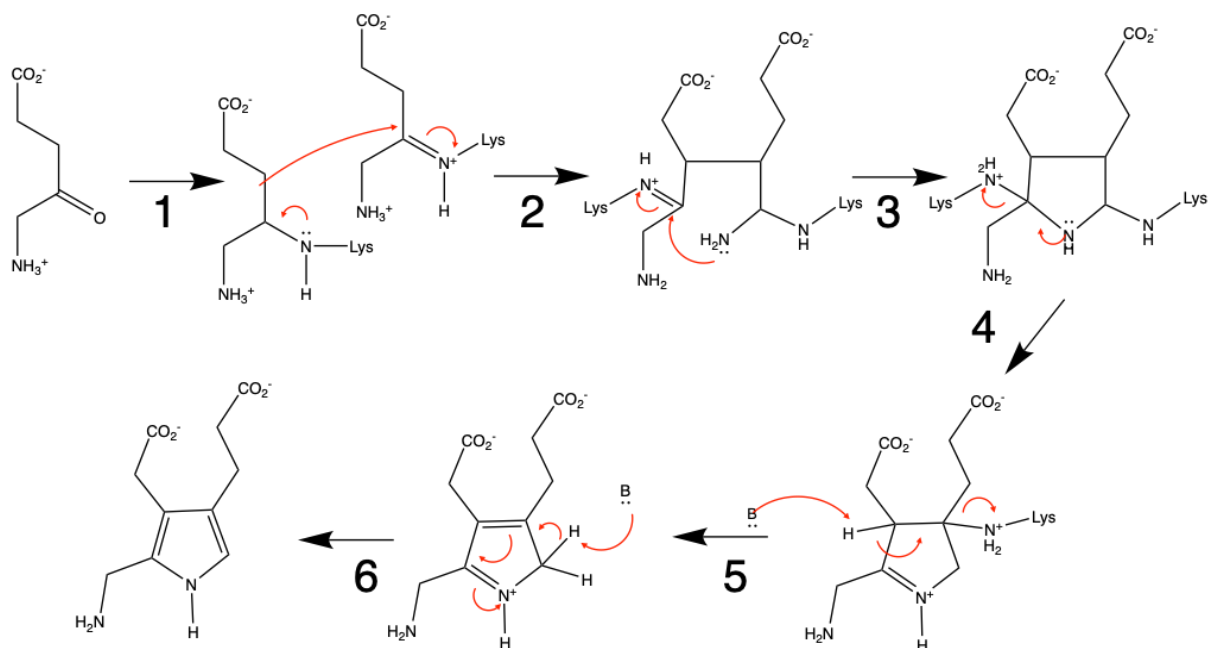
Figure 1.7- PBGS enzyme mechanism

The enzymatic mechanism for PBGS is shown. Firstly, two ALA molecules are bound to the PBGS by two imine linkages through lysine residues (1). There is nucleophilic addition of amine group from one ALA molecule to the iminium ion of the other (2). The molecule is cyclised (3) and detaches from a PBGS lysine residue (4). The second lysine residue is eliminated (5) and tautomerization of the porphobilinogen molecule occurs (6)

The next conserved step in heme biosynthesis includes the covalent linkage of four molecules of porphobilinogen through the action of porphobilinogen deaminase

(PBGD, HemC), also known as hydroxymethylbilane synthase (HMBS). Polymerisation of porphobilinogen forms the linear molecule 1-hydroxymethylbilane (HMB or pre-uroporphyrinogen). Porphobilinogen deaminase contains a dipyrromethane cofactor (two linked porphobilinogen molecules), which acts a platform for the incoming porphobilinogen molecules; it keeps the substrate in the active site and allows the construction of hydroxymethylbilane (Jordan and Warren, 1987, Warren and Jordan, 1988, Hart et al., 1987) (figure 1.8). Ring A of the tetrapyrrole ring is formed first followed by rings B, C and D before the product is released (Jordan and Warren, 1987).
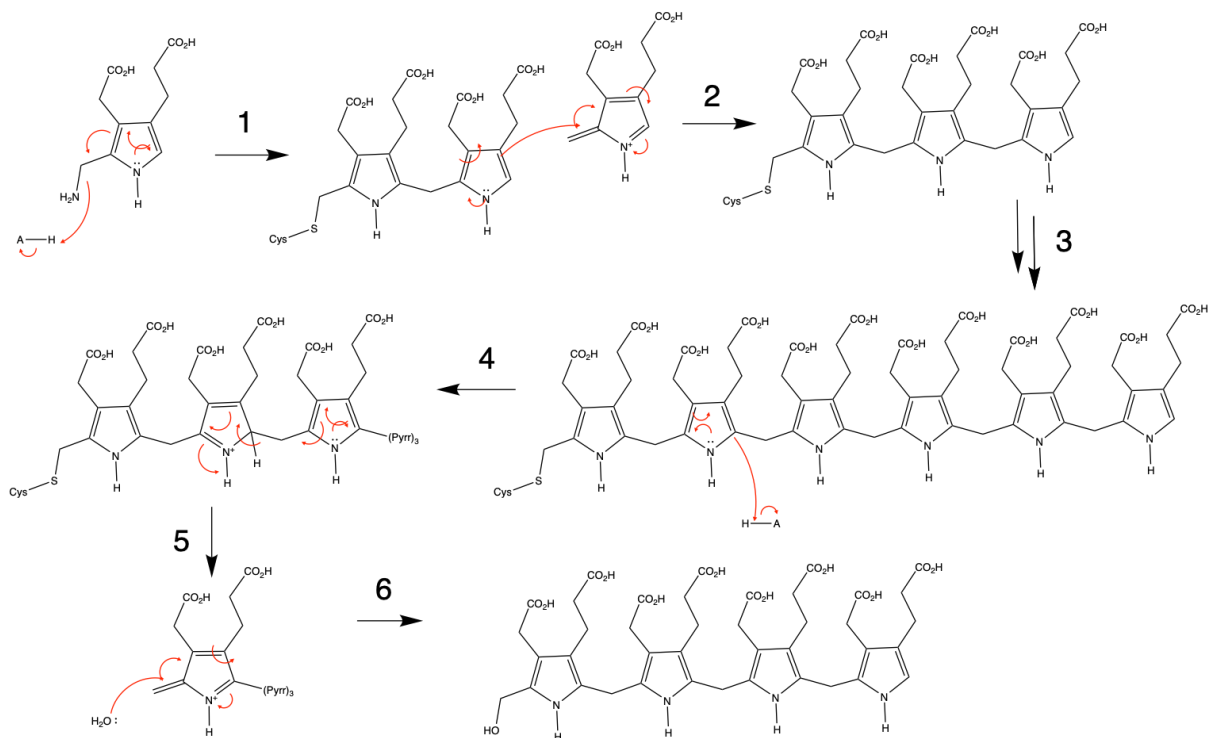
Figure 1.8- Porphobilinogen deaminase (PBGD) enzyme mechanism

The PBGD mechanism involves sequential electrophilic aromatic substitution. Porphobilinogen loses ammonia forming a cation (1) and the cation is conjugated to the dipyrromethane cofactor in PBGD (2). Another porphobilinogen cation is added to the chain to give a tetrapyrrole and this is repeated twice more yielding a hexapyrrole (3). To detach the molecule from the dipyrromethene cofactor the second pyrrole is protonated (4) and the dipyrromethene cofactor is eliminated (5). Finally, the tetrapyrrole cation reacts with water to give HMB

Following the release of hydroxymethylbilane from porphobilinogen deaminase, uroporphyrinogen III synthase (UROS, HemD) cyclises hydroxymethylbilane to uroporphyrinogen III. Uroporphyrinogen III synthase converts hydroxymethylbilane to uroporphyrinogen III in two stages; it circularises hydroxymethylbilane and catalyses ring closure by bonding the carbons either side of ring D (C16 and C20) forming a spirocyclic pyrrolenine intermediate. Then cleavage of the C15-16 bond and formation of a C15-C19 bond causes an intermolecular rearrangement in D ring allowing the D ring to flip and produce the type III porphyrinogen, uroporphyrinogen III (figure 1.9) (Crockett et al., 1991, Mathews et al., 2001). This conserved pathway is shown in figure 1.5. Without the intervention of uroporphyrinogen III synthase, 1-hydroxymethylbilane would spontaneously cyclise and form a non-physiological compound uroporphyrinogen I which can oxidise to uroporphyrin I, a toxic molecule (Aizencang et al., 2000) (figure 1.10).
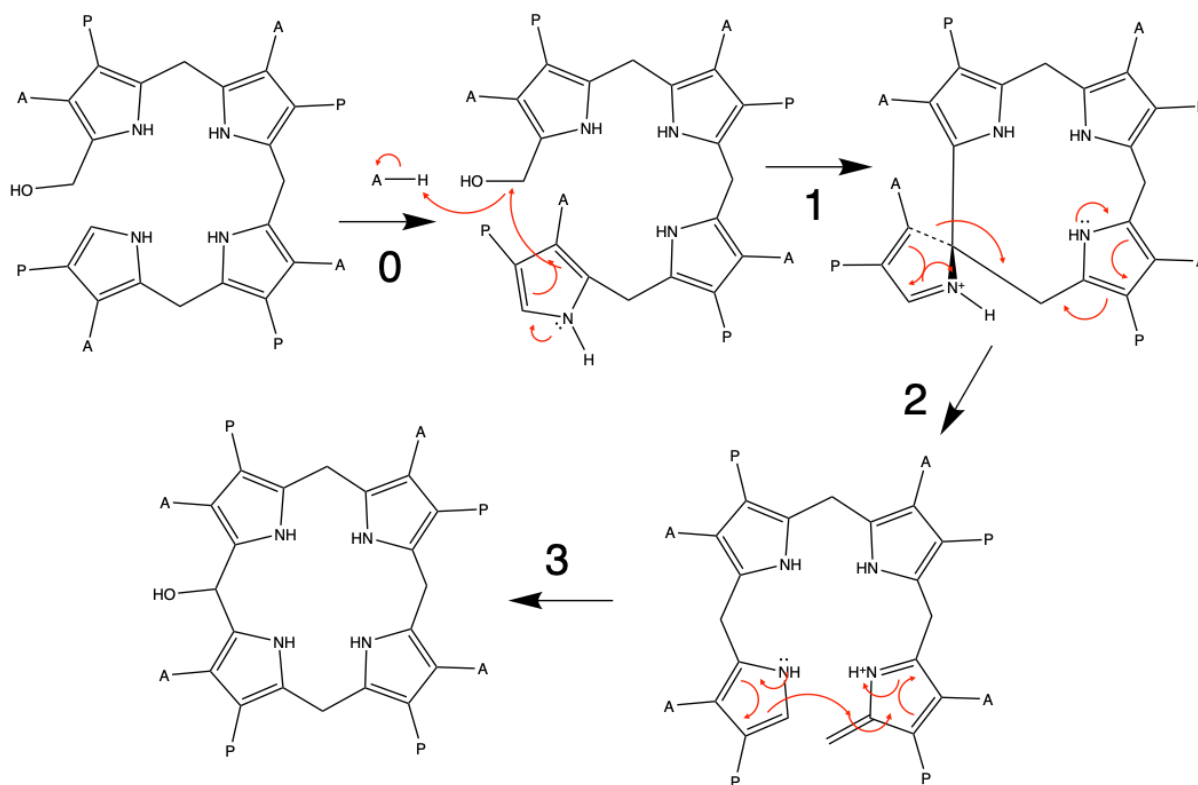
Figure 1.9 – UROS enzymatic mechanism

The enzymatic mechanism for UROS is shown. HMB must rearrange (0) before it is protonated forming a cation (1), this generates a spirocyclic intermediate. Ring is reopened to form an acyclic cation (2), the ring is then closed to using the opposite side of the pyrrole ring giving uroporphyrinogen III (3)

Uroporphyrinogen III is the first cyclic heme precursor and is common to all tetrapyrroles. Uroporphyrinogen III is the last universal precursor for all tetrapyrroles. After this point there are specialised enzymatic pathways that lead to formation of specific molecules such as heme, chlorophyll, coenzyme F430, siroheme and cobalamin (Tanaka and Tanaka, 2007).
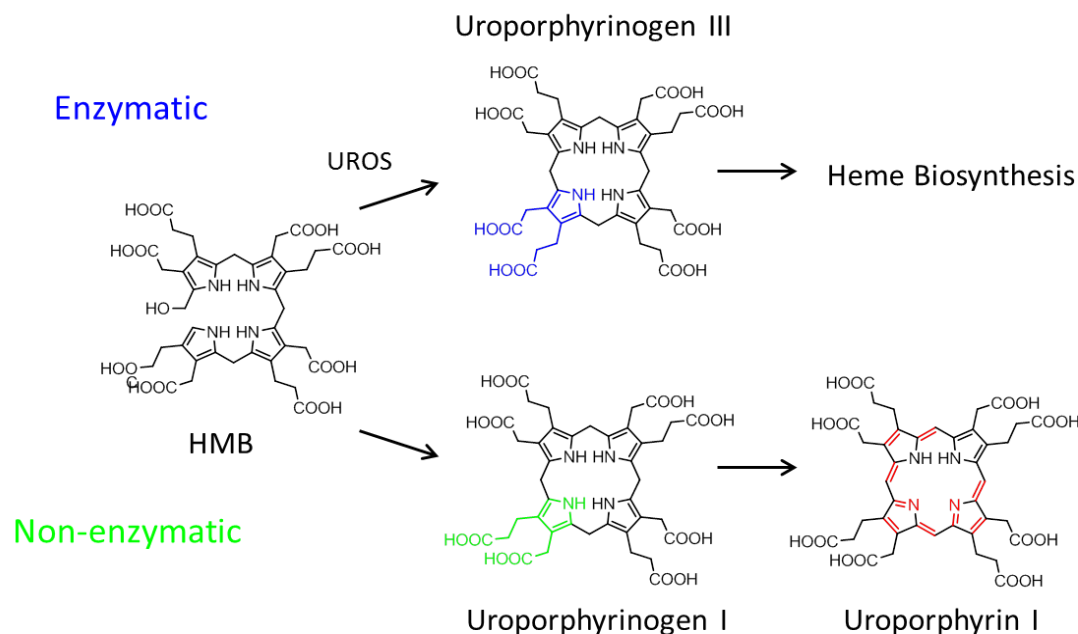
Figure 1.10 - Enzymatic and non-enzymatic pathways involving uroporphyrinogen III

The enzymatic pathway shows circularisation and isomerisation of HMB and to uroporphyrinogen III using the UROS enzyme. In the non-enzymatic pathway HMB is still circularised but isomerisation of ring D doesn't occur, this forms uroporphyrinogen I and uroporphyrinogen I is oxidised to produce uroporphyrin I, a toxic molecule. **Abbreviations: HMB** (1-hydroxymethylbilane), **UROS** (uroporphyrinogen III synthase).

1.2.2 Siroheme-dependent pathway the route to heme via siroheme

The siroheme-dependent biosynthesis pathway is the first of the three pathways to separate from the others, it was observed in heme-synthesising archaea and sulfate-reducing bacteria such as *Desulfovibrio vulgaris* (*D. vulgaris*) and *Methanosarcina barkeri* (*M. barkeri*). This pathway follows the conserved heme biosynthesis pathway until the formation of uroporphyrinogen III. At uroporphyrinogen III the siroheme-dependent pathway deviates from the main pathway (figure 1.11).

The siroheme-dependent pathway (figure 1.12) was studied using labelled methionine experiments, this revealed potential pathway intermediates (Ishida et al., 1998,

Bollivar et al., 1995). These experiments showed that methyl groups donated by S-adenosyl methionine (SAM) can be transferred onto uroporphyrinogen III at positions 2 and 7 to produce precorrin-2 (PC2). Other potential pathway intermediates that containing the methyl groups donated by SAM were sirohydrochlorin (SiHC), 12, 18-didecarboxysirohydrochlorin (DDSH), coproporphyrin III and protoporphyrin IX. Using these intermediates, the sequence of enzymatic reactions in the siroheme-dependent heme biosynthesis pathway was predicted (Ishida et al., 1998).
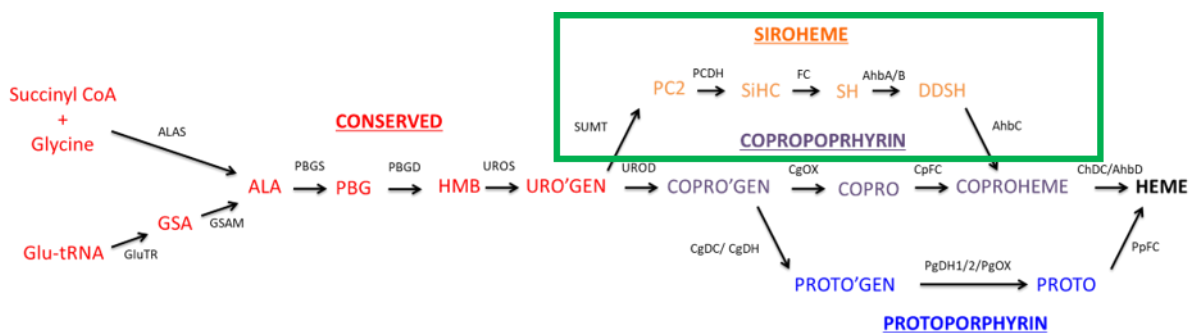
Figure 1.11 – Overall heme biosynthesis

The green box highlights the current section of interest, the siroheme dependent pathway. Uro'gen is the last common precursor for tetrapyrrole biosynthesis and ends in the formation of heme. The siroheme dependent pathway shares a pathway intermediate with the coproporphyrin-dependent pathway, coproheme

The complete siroheme-dependent biosynthetic route was established when screening for heme biosynthetic enzymes in archaea and sulfate-reducing bacteria. Archaea and sulfate-reducing bacteria contained the heme biosynthetic enzymes required to produce uroporphyrinogen but no identifiable enzymes in the protoporphyrin-dependent pathway. These organisms cannot synthesise heme *d* but do contain genes similar to those encoding enzymes found in the heme *d* biosynthetic pathway. The function of these putative heme biosynthetic enzymes were studied

using potential intermediary molecules. From these experiments the siroheme-dependent pathway was determined (Panek and O'Brian, 2002, Raux et al., 2003).
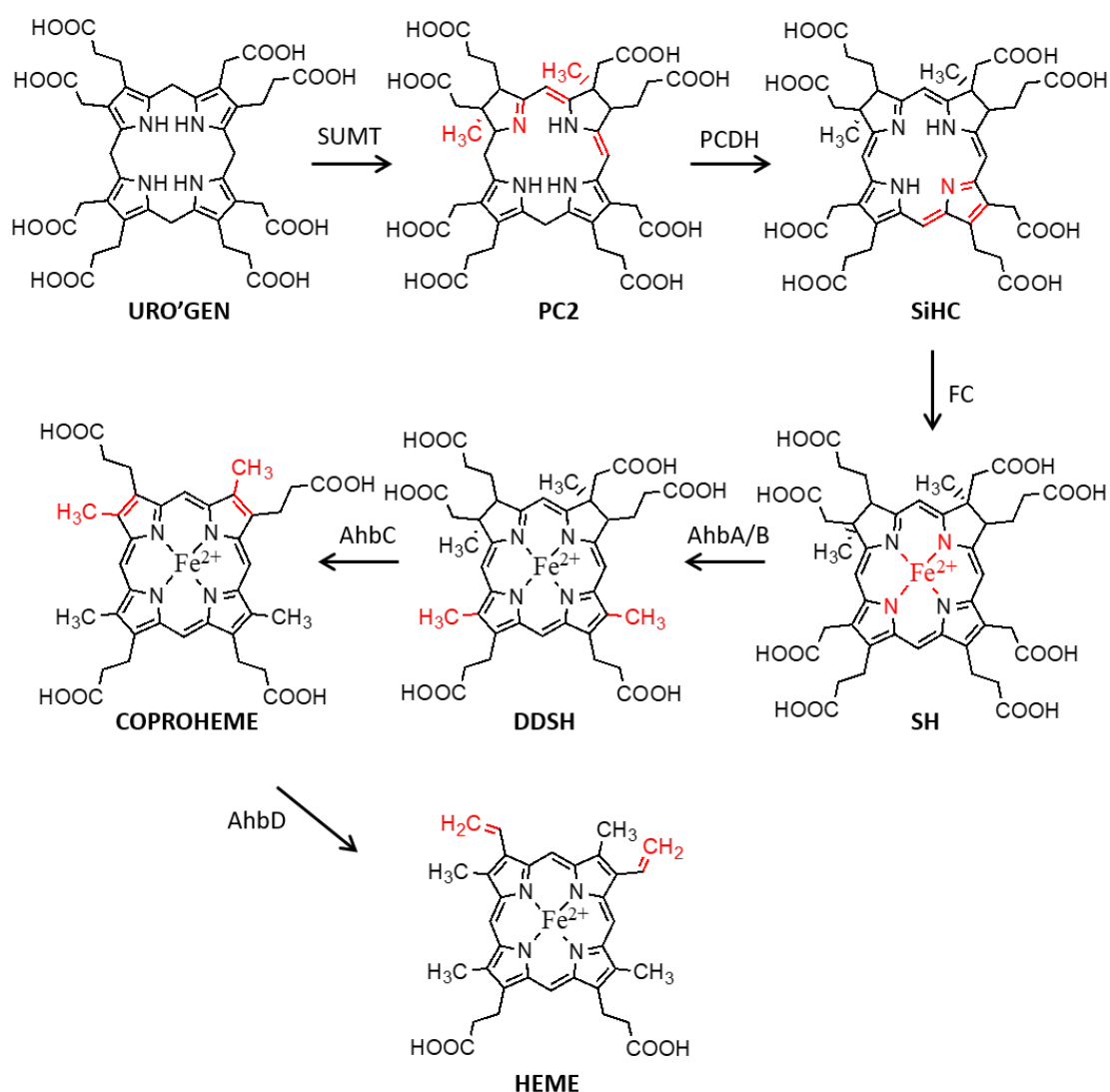
Figure 1.12– Siroheme-dependent heme biosynthesis pathway

Uroporphyrinogen III is converted to precorrin-2 through the methylation of rings A and B on uroporphyrinogen, this is catalysed by a SAM-dependent methyltransferase. Precorrin-2 is oxidised to form sirohydrochlorin and iron metalation of sirohydrochlorin forms siroheme. Siroheme is decarboxylated by AhbA/B to form 12, 18-didecarboxysiroheme after, deacetylation of 12,18-didecarboxysiroheme forms coproheme. Finally, oxidative decarboxylation of coproheme by AhbD forms heme. Abbreviations: **URO'GEN** (uroporphyrinogen III), **SUMT** (SAM (S-adenosyl methionine)-dependent uroporphyrinogen methyltransferase), **PC2** (precorrin-2), **PCDH** (precorrin-2 dehydrogenase), **SiHC** (sirohydrochlorin), **FC** (ferrochelatase), **SH** (siroheme), **AhbA/B** (alternative heme biosynthesis A and B), **DDSH** (12, 18-didecarboxysiroheme), **AhbC** (alternative heme biosynthesis C) and **AhbD** (alternative heme biosynthesis D).

1.2.2.1   Formation of heme via siroheme

Siroheme is an iron-containing isobacteriochlorin that is incorporated into sulphite and nitrite reductases as a prosthetic group (Bali et al., 2014). Three enzymatic steps are required to convert uroporphyrinogen into siroheme (SH). The enzymes required are dependent on the organism. In some cases, only one enzyme is required to catalyse all three enzymatic steps, however in others three separate enzymes are required, one for each step. Conversion of uroporphyrinogen into siroheme is shown in figure 1.12 (Bali et al., 2014, Raux et al., 1999, Raux et al., 2003).

The formation of heme through the siroheme-dependent heme biosynthetic pathway begins with the methylation of uroporphyrinogen rings A and B. The addition of the methyl groups onto uroporphyrinogen III is catalysed by a SAM-dependent uroporphyrinogen methyltransferase (SUMT), this produces precorrin-2 (Bali et al., 2014, Kuhner et al., 2014). Precorrin-2 is a precursor for siroheme, cobalamin, heme d_1 and cofactor F_{430}. There are two routes for cobalamin synthesis from precorrin-2, in an aerobic environment precorrin-2 can be converted to precorrin-3 by Cob1 and through several more enzymatic steps cobalamin is produced (Bali et al., 2014, Raux et al., 2003). In an anaerobic environment precorrin-2 is oxidised to sirohydrochlorin (SiHC) using a precorrin-2 dehydrogenase (PCDH), the next step towards the formation of SH. In cobalamin synthesis, SiHC can be chelated with cobalt using the CbiK and CbiX enzymes, diverting the pathways towards cobalamin production rather than siroheme formation (Warren et al., 2002). To direct the pathway towards siroheme and ultimately heme synthesis, iron is inserted into sirohydrochlorin by a ferrochelatase (FC) forming siroheme.

There are three enzyme catalysed reactions in this part of the siroheme pathway, a SAM-dependent uroporphyrinogen methyltransferase, precorrin-2 dehydrogenase and ferrochelatase. In *Bacillus megaterium* (*B. megaterium*) three separate enzymes are required: SirA, the SAM-dependent uroporphyrinogen methyltransferase, SirC, the precorrin-2 dehydrogenase and SirB the ferrochelatase whereas *Saccharomyces cerevisiae* (*S. cerevisiae*) only requires two enzymes Met1p and Met8p; Met8p contains both dehydrogenase and chelatase activity (Raux et al., 2003, Raux et al., 1999). In *E. coli,* one enzyme, CysG, catalyses all three steps, it contains two subunits CysG^A and CysG^B, CysG^A has methyltransferase activity and CysG^B has dehydrogenase and ferrochelatase activity (Warren et al., 1994).

1.2.2.2   *Formation of heme from siroheme*

After the formation of siroheme, there are three more enzymatic steps to form heme. The first is the decarboxylation of siroheme creating the intermediate 12,18-didecarboxysiroheme (DDSH), the acetate side chains on rings C and D of siroheme are converted to methyl groups, the enzymes AhbA and AhbB (<u>a</u>lternative <u>h</u>eme <u>b</u>iosynthesis) catalyse these reactions. Acetyl groups on rings A and B of 12,18-didecarboxysiroheme are removed by AhbC, forming Fe-coproporphyrin III (coproheme) (Bali et al., 2014, Kuhner et al., 2014). Coproheme is also an intermediate of the coproporphyrin-dependent heme biosynthesis pathway; this pathway is discussed later (section 1.4). The final step in the alternative heme biosynthesis pathway is the oxidative decarboxylation of the propionate side chains on rings A and B. AhbD catalyses the conversion of coproheme to protoheme (heme)

(Bali et al., 2014, Kuhner et al., 2014). In denitrifying bacteria the homologous enzymes are NirDL, NirG, NirH and NirJ these nitrite reductase enzymes are involved in the biosynthesis of heme *d* (Kuhner et al., 2014). NirD and NirL are often fused together and in combination with NirG and NirH they convert siroheme to 12,18-didecarboxysiroheme (as with AhbA and AhbB). If NirD or NirH is only present mono decarboxylation occurs and when NirDL or NirG and NirH are present there is a mixture of mono decarboxylation or fully decarboxylated product (Bali et al., 2011). NirJ is responsible for removing the propionate side chains on rings A and B of 12,18-didecarboxysiroheme producing dihydro-heme d_1 (Dailey et al., 2017, Bali et al., 2011)

1.2.3 The protoporphyrin-dependent pathway of heme biosynthesis found in Gram negative bacteria and eukaryotes

The protoporphyrin-dependent pathway of heme biosynthesis from uroporphyrinogen to heme (protoheme) includes four enzymatic steps (figure 1.13). These involve side chain modification, oxidation and the insertion of iron. The first step is the sequential decarboxylation (starting from ring D) of the acetyl groups on each of the four rings to form coproporphyrinogen III (copro'gen)(Jackson et al., 1976). This decarboxylation is catalysed by uroporphyrinogen III decarboxylase (UROD, HemE).
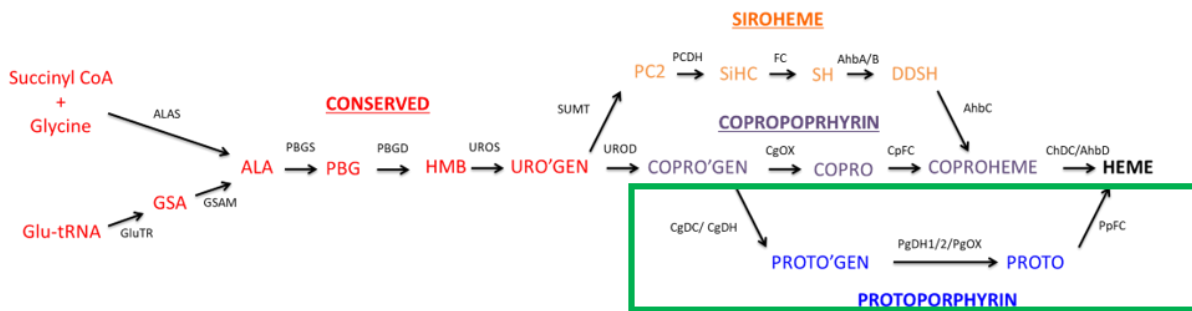
Figure 1.13 – Overall heme biosynthesis

The green box highlights the current section of interest, the protoporphyrin-dependent pathway. Uro'gen is the last common precursor for tetrapyrrole biosynthesis and this pathway ends in the formation of heme.

Human uroporphyrinogen III decarboxylase was crystallised in 1997 and a mechanism of action was proposed (Phillips et al., 1997, Whitby et al., 1998). UROD side chains D82 and Y159 are assumed to be protonated; uroporphyrinogen binds so that ring D is in hydrogen bonding distance to D82. Y159 protonates the pyrrole group causing an electronic rearrangement. The electronic rearrangement causes a release of carbon dioxide and the formation of a methylene intermediate. The methylene intermediate is protonated by D82 and Y159 removes a proton from the pyrrole ring to restore the ring to its original configuration (Martins et al., 2001).

Coproporphyrinogen III oxidase (CPO) can decarboxylate coproporphyrinogen to protoporphyrinogen IX. There are two types of CPO: oxygen-dependent (HemF also known as CgDC (coproporphyrinogen decarboxylase)) and oxygen-independent (HemN also known as CgDH (coproporphyrinogen dehydrogenase)) (Layer et al., 2010, Breckau et al., 2003). They both decarboxylate the propionate group on rings A and B to vinyl groups using a terminal electron acceptor. However they are structurally

unrelated and do not use the same mechanism (see figure 1.14 for CgDH mechanism)
(Seehra et al., 1983).
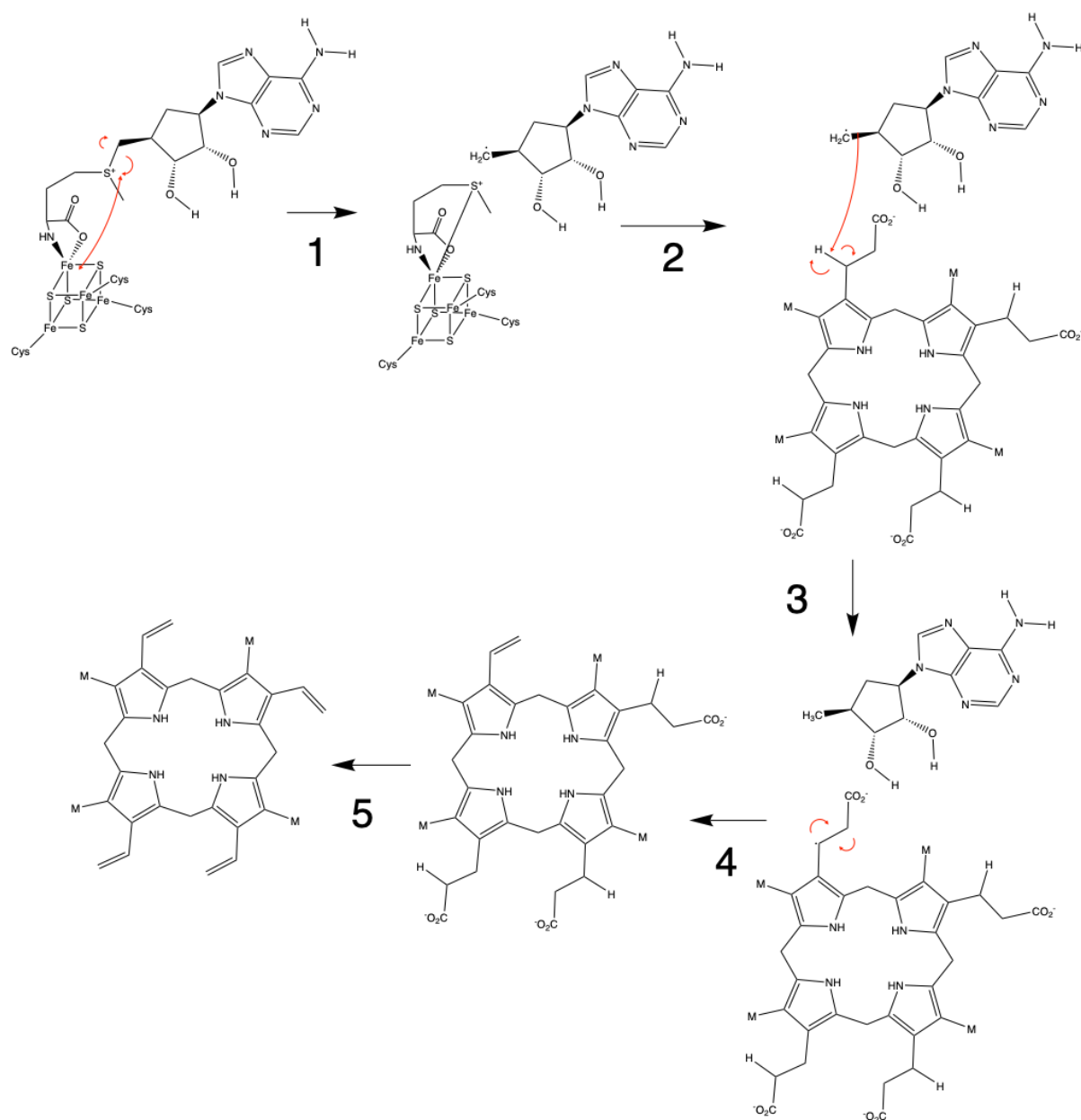
Figure 1.14 – Radical SAM mechanism of CgDH

An electron is transferred from the 4Fe-4S cluster to the sulphonium of SAM and this causes cleavage of SAM to methionine and a 5'-deoxyadenosyl radical (1,2). The radical abstracts hydrogen from the β-C in the propionate group creating a radical (3). Carbon dioxide is eliminated and electron transfer to the electron acceptor results in the formation of a vinyl group (4), this is repeated three more times to give protoporphyrinogen (5).

Coproporphyrinogen decarboxylase uses oxygen as a terminal electron acceptor and is mainly found in eukaryotes but is present in some species of bacteria (Layer et al., 2002, Troup et al., 1994). It sequentially decarboxylates ring A of coproporphyrinogen to form harderoporphyrinogen and then decarboxylates ring B to form protoporphyrinogen (Breckau et al., 2003). Coproporphyrinogen dehydrogenase is mainly found in microbes and requires an alternative terminal electron acceptor. It is a radical SAM (S-adenosyl methionine) enzyme that contains a 4Fe-4S cluster; this is coordinated by a three cysteine motif (CxxxCxxC) and a nearby SAM molecule. The mechanism of action for this enzyme involves the transfer of an electron from the iron cluster to SAM resulting in the cleavage of SAM to methionine and a 5'-deoxyadenosyl radical. This radical reacts with the propionate side chains of rings A and B on coproporphyrinogen converting them to vinyl groups producing protoporphyrinogen (Layer et al. 2003). Conversion of coproporphyrinogen to protoporphyrinogen requires NAD+ or NADP+, magnesium and SAM (S-adenosyl methionine) (Tait, 1972, Troup et al., 1994, Layer et al., 2002). In some cases both CPOs can be found in one organism, for example in *Rhodobacter spheroides (R. spheroides),* an organism which is very versatile, it can synthesise several different tetrapyrrole molecules (heme, chlorophyll and vitamin B12) and can survive in aerobic and anaerobic conditions (Seehra et al., 1983, Aizawa, 2014).
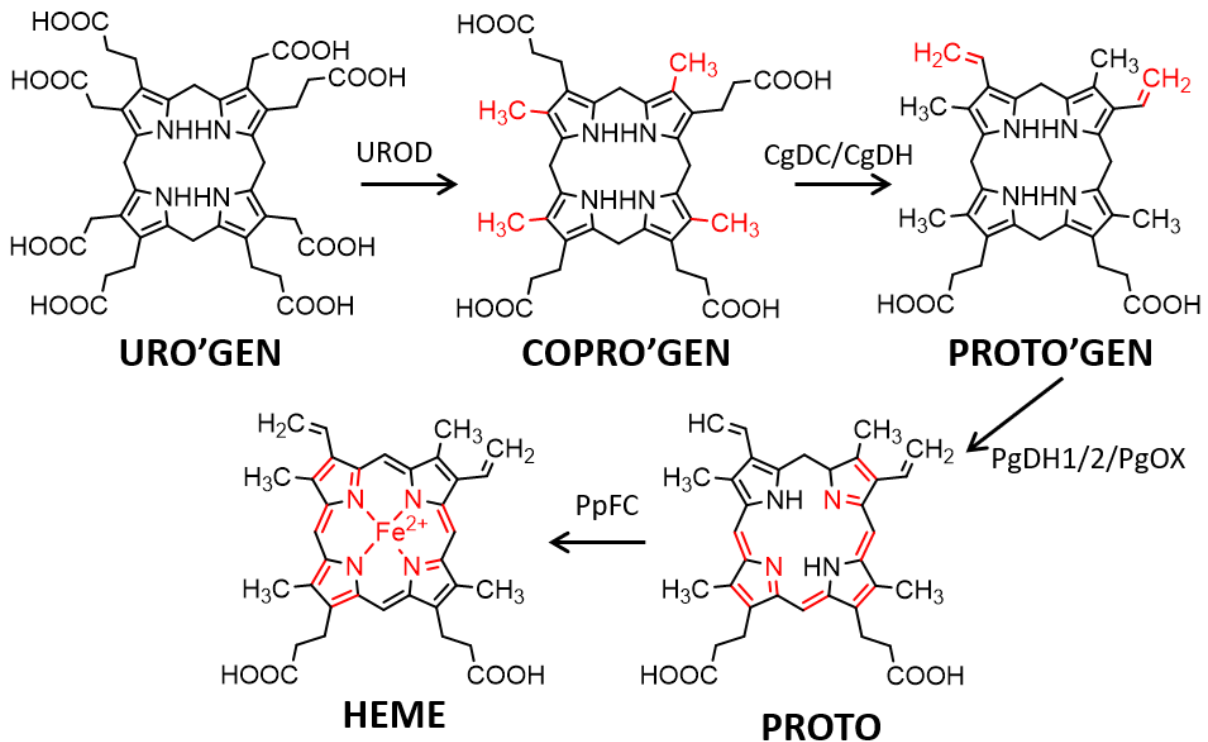
Figure 1.15 - Formation of protoheme through the canonical pathway

Protoheme is synthesised from uroporphyrinogen in a four-step reaction, uroporphyrinogen is decarboxylated to produce coproporphyrinogen which is subsequently decarboxylated again to produce protoporphyrinogen. Protoporphyrinogen is oxidised to protoporphyrin IX and ferrous iron is inserted into protoporphyrin IX, producing the metalated porphyrin, protoheme. Abbreviations: **URO'GEN** (uroporphyrinogen III), **UROD** (uroporphyrinogen decarboxylase) **CgDC** (coproporphyrinogen decarboxylase), **CgDH** (coproporphyrinogen dehydrogenase), **COPRO'GEN** (coproporphyrinogen III), **PgDH1/2** (protoporphyrinogen dehydrogenase 1 and 2), **PgOX** (protoporphyrinogen oxidase), **PpFC** (protoporphyrin ferrochelatase), **PROTO'GEN** (protoporphyrinogen IX), **PROTO** (protoporphyrin IX).

Protoporphyrinogen IX oxidase, catalyses the six-electron oxidation needed to convert protoporphyrinogen to protoporphyrin IX. There are oxygen-dependent (also known as HemY or PgOX (protoporphyrinogen oxidase)) and oxygen-independent (also known as HemG or PgDH1 (protoporphyrinogen dehydrogenase)) variants of protoporphyrinogen IX oxidase.

The oxygen-dependent protoporphyrinogen IX oxidase (HemY) is present in eukaryotes and bacteria. Initially, these were thought to be found as both soluble and membrane or membrane bound proteins, but this was before the discovery of the coproporphyrin-dependent pathway. The soluble protoporphyrinogen oxidases present in Actinobacteria and Firmicutes are in fact coproporphyrinogen oxidases (CgOX) and are capable of oxidising coproporphyrinogen to coproporphyrin and protoporphyrinogen to protoporphyrin. In humans protoporphyrinogen oxidase is located in the inner mitochondrial membrane and membrane bound protoporphyrinogen IX oxidases are found in bacterial species such as *Myxococcus* and *Aquifex* (Boynton et al., 2011, Dailey et al., 2017, Dailey et al., 2015, Lobo et al., 2015, Dailey and Dailey, 1996). The oxygen-dependent enzyme uses molecular oxygen as the terminal electron acceptor and frequently contains, as a cofactor, flavin adenine dinucleotide (FAD) or flavin mononucleotide (FMN). Flavin molecules are frequently involved in redox reactions such the conversion of protoporphyrinogen to protoporphyrin (Fagan et al., 2010).

The oxygen-independent protoporphyrinogen IX oxidase or protoporphyrinogen dehydrogenase 1 (PgDH1) requires alternative electron acceptors to oxygen, such as fumarate, nitrate and menaquinone (Boynton et al., 2009, Jacobs and Jacobs, 1976). Protoporphyrinogen dehydrogenase 1 uses menaquinone and provides a route for heme biosynthesis in anaerobic Gram negative bacteria (Boynton et al., 2009). Sequence analysis revealed that protoporphyrinogen dehydrogenase 1 is part of protein family found in γ-proteobacteria and it contains the cofactor flavin mononucleotide.

Another protoporphyrinogen IX oxidase is HemJ (also known as PgDH2 (protoporphyrinogen dehydrogenase 2); HemJ was discovered as it clustered with uroporphyrinogen decarboxylase and ferrochelatase, two enzymes involved in heme biosynthesis. Protoporphyrinogen dehydrogenase 2 is not homologous to either protoporphyrinogen dehydrogenase 1 or protoporphyrinogen oxidase and is suggested to contain no cofactors implying that it may use molecular oxygen as a terminal electron acceptor. Protoporphyrinogen dehydrogenase 2 is found in the majority of eubacteria, where there is no confirmed protoporphyrinogen oxidase, as well as cyanobacteria and all proteobacterial groups except δ-proteobacteria (Boynton et al., 2011).

The final step in the canonical pathway is the insertion of ferrous iron into protoporphyrin IX. This is catalysed by the enzyme protoporphyrin ferrochelatase (PpFC). When protoporphyrin ferrochelatase binds protoporphyrin IX, the ring becomes distorted allowing insertion of iron. Ferrochelatases are one of the most studied enzymes in the heme biosynthetic pathway and they are discussed in detail in section 1.3 (figure 1.15) (Dailey and Dailey, 2003).

1.2.4 Coproporphyrin-dependent heme biosynthetic pathway

When compared to the siroheme-dependent pathway, the protoporphyrin-dependent and coproporphyrin-dependent pathways share one more common precursor, coproporphyrinogen III. This is formed by the sequential decarboxylation of the acetyl groups on each of the four pyrrole rings. The decarboxylation of the side chains is

catalysed by the enzyme uroporphyrinogen III decarboxylase (Martins et al., 2001).

After the formation of coproporphyrinogen these heme biosynthetic pathways diverge.
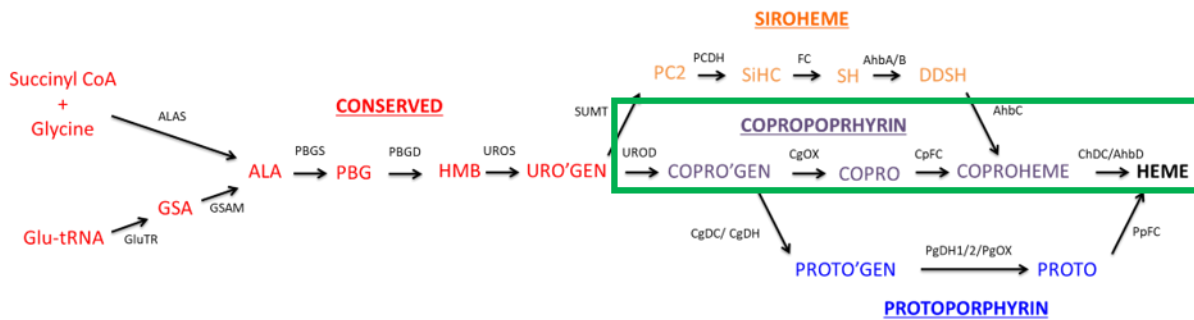
Figure 1.16- Overall heme biosynthesis

The green box highlights the current section of interest, the coproporphyrin-dependent pathway. Uro'gen is the last common precursor for tetrapyrrole biosynthesis and this pathway ends in the formation of heme.

The coproporphyrin-dependent pathway is utilised by Gram positive bacteria, more specifically Firmicutes and Actinobacteria. This pathway was first discovered when searching for enzymes capable of converting coproporphyrinogen to protoporphyrinogen in Firmicutes and Actinobacteria. HemN or HemF, the previously discovered coproporphyrinogen III oxidases, are not encoded in these genomes (Dailey et al., 2015). There are three enzymatic steps in this pathway that conclude with the formation of heme (figure 1.17).
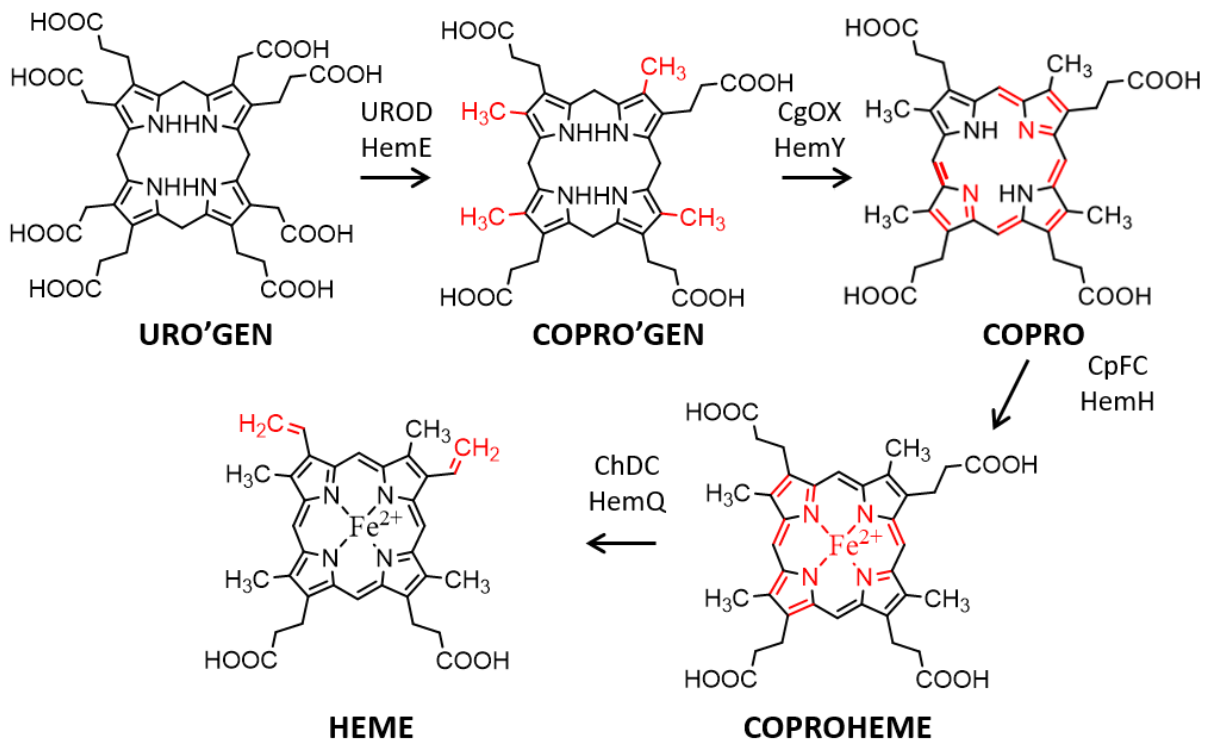
Figure 1.17 – Coproporphyrin-dependent heme biosynthesis pathway

Uroporphyrinogen is decarboxylated by UROD to produce coproporphyrinogen. Coproporphyrinogen is oxidised by CgoX to form coproporphyrin III and ferrous iron is inserted into the porphyrin ring by ferrochelatase (CpFC). ChdC decarboxylates coproheme (Fe-coproporphyrin III) to produce protoheme. **Abbreviations: URO'GEN** (uroporphyrinogen III), **UROD** (uroporphyrinogen decarboxylase), **COPRO'GEN** (coproporphyrinogen III), **COPRO** (coproporphyrin III) **CgOX** (coproporphyrinogen oxidase) **ChDC** (coproheme decarboxylase), **CpFC** (coproporphyrin ferrochelatase).

1.2.4.1   Discovery of HemY (CgOX)

HemY was originally assigned as a protoporphyrinogen oxidase. Genetic mapping of

B. subtilis revealed two operons important in heme biosynthesis, the *hemEHY* operon

and the *hemAXCDBL* operon. The *hemEHY* operon was required for heme

biosynthesis between uroporphyrinogen and heme and the *hemAXCDBL* operon was

implicated in heme biosynthesis from glutamate to uroporphyrinogen. Studies on the

hemEHY operon showed that *hemE* (uroporphyrinogen decarboxylase) had sequence

similarity to other uroporphyrinogen decarboxylases and hemH (ferrochelatase) had

activity similar to ferrochelatase when expressed in *E. coli*. The HemY protein (coproporphyrinogen oxidase) was assumed to be a coproporphyrinogen oxidase or a protoporphyrinogen oxidase (Hansson and Hederstedt, 1992, Hansson et al., 1991).

B. subtilis HemY (coproporphyrinogen oxidase) has protoporphyrinogen oxidase activity (Dailey et al., 1994) and can oxidise protoporphyrinogen to protoporphyrin IX and mesoporphyrinogen IX to mesoporphyrin IX. However, when testing *B. subtilis* HemY for coproporphyrinogen oxidase activity the substrate coproporphyrinogen III was converted to coproporphyrin III instead of protoporphyrinogen. These results led to the conclusion that *B. subtilis* HemY lacked standard coproporphyrinogen oxidase activity but possessed normal protoporhyrinogen activity. Other protoporphyrinogen oxidases, however, are not able to use coproporphyrinogen as a substrate. Despite this irregularity *B. subtilis* HemY was assigned as a protoporphyrinogen oxidase at this point in time (Dailey et al., 1994).

Homologues of HemY were found in the Gram positive bacteria *Staphylococcus aureus* (*S. aureus*) and *Mycobacterium tuberculosis* (*M. tuberculosis*). These enzymes were capable of oxidising coproporphyrinogen to coproporphyrin III as described for the *B. subtilis* HemY. Only HemY enzymes present in Gram positive bacteria could oxidise coproporphyrinogen to coproporphyrin III. The conversion of coproporphyrinogen to coproporphyrin was also faster than the oxidation of protoporphyrinogen to protoporphyrin IX. In addition, the K_m values for coproporphyrin III were much lower than those for protoporphyrin IX (Dailey and Gerdes, 2015, Dailey et al., 2015, Lobo et al., 2015). These results, in conjunction with those described for

ferrochelatase below leads to the view that these enzymes are primarily coproporphyrinogen oxidases.

1.2.4.2   Ferrochelatase (CpFC) Inserts Iron into Coproporphyrin III

In the coproporphyrin-dependent pathway, insertion of ferrous iron into the porphyrin by ferrochelatase is the penultimate step in the heme biosynthesis, rather than the final step. Coproporphyrin ferrochelatases (CpFCs) have been identified in both Firmicutes and Actinobacteria; these are structurally similar to other identified ferrochelatases. The structure of ferrochelatase is discussed in section 1.3. The coproporphyrin ferrochelatases found in *S. aureus*, *B. subtilis*, and *M. tuberculosis* are able to insert ferrous iron into coproporphyrin III much faster than into protoporphyrin IX and K_m for coproporphyrin III is lower than the K_m for protoporphyrin IX. All tested protoporphyrin ferrochelatases present in Gram negative bacteria and eukaryotes failed to insert iron into coproporphyrin at a recordable rate (Dailey et al., 2015, Lobo et al., 2015).

1.2.4.3   Coproheme   decarboxylase   (ChdC)   decarboxylates coproheme to produce heme

1.2.4.3.1   Discovery of coproheme decarboxylase (HemQ)

Genomes of Gram positive bacteria lack the genes that code for the coproporphyrinogen oxidases that convert coproporphyrinogen to protoporphyrinogen: coproporphyrinogen decarboxylase (HemF) or coproporphyrinogen dehydrogenase (HemN) which are essential in heme biosynthesis. Complementation studies using *E.*

coli and *Acinetobacter ADP1* heme auxotrophs were used to screen for the missing coproporphyrinogen oxidase in Gram positive bacteria. This process was used to identify protoporphyrinogen dehydrogenase 2 (HemJ) and protoporphyrinogen oxidase (HemY) but was unable to identify the missing coproporphyrinogen oxidase (Boynton et al., 2009, Boynton et al., 2011, Dailey and Gerdes, 2015).

Further complementation studies were carried out in *ΔhemG* or *ΔhemH E. coli*, these are *E. coli* strains lack a *hemG* or *hemH* gene and show a reduced growth phenotype. When a plasmid containing Gram positive *hemY* (coproporphyrinogen oxidase) or *hemH* (coproporphyrin ferrochelatase) was introduced into *ΔhemG* or *ΔhemH E. coli*, these plasmids cannot complement the *E .coli* strains even when they were added together (Dailey et al., 2010), implying a component is missing.

There are two major operons in heme-synthesising Actinobacteria that contain the heme biosynthetic genes. In one of these operons a gene encoding a hypothetical protein similar to chlorite dismutase was commonly found clustered with *hemY* and *hemH*. A BLAST search of this protein revealed it is frequently found in Gram positive bacteria and not in Gram negative bacteria, non-heme synthesising organisms or eukaryotes. The group of chlorite dismutase-like proteins named COG3253 were split into three groups: those with chlorite dismutases, those with no known function but are no chlorite dismutase activity or those with no known function and only present in Actinobacteria. An Actinobacteria, *Propionibacterium acnes* (*P. acnes*) contains a coproporphyrin ferrochelatase fused to a chlorite dismutase-like protein suggesting

that this protein may be involved in heme biosynthesis (Dailey et al., 2010, Dailey and Gerdes, 2015).

Complementation studies revealed that this protein, later named HemQ or ChDC (coproheme decarboxylase), was the missing component. Both Actinobacteria and Firmicute coproheme decarboxylase along with coproporphyrinogen oxidase and coproporphyrin ferrochelatase were able to return *ΔhemG* and *ΔhemH E. coli* growth to wildtype levels. Complementation did not occur when two out of the three enzymes were added to the mutated *E. coli* strains. Also, combinations of these three enzymes from different species of Gram positive bacteria (Firmicutes and Actinobacteria) were also able to complement the *E. coli* mutants (Dailey et al., 2010, Dailey and Gerdes, 2015).
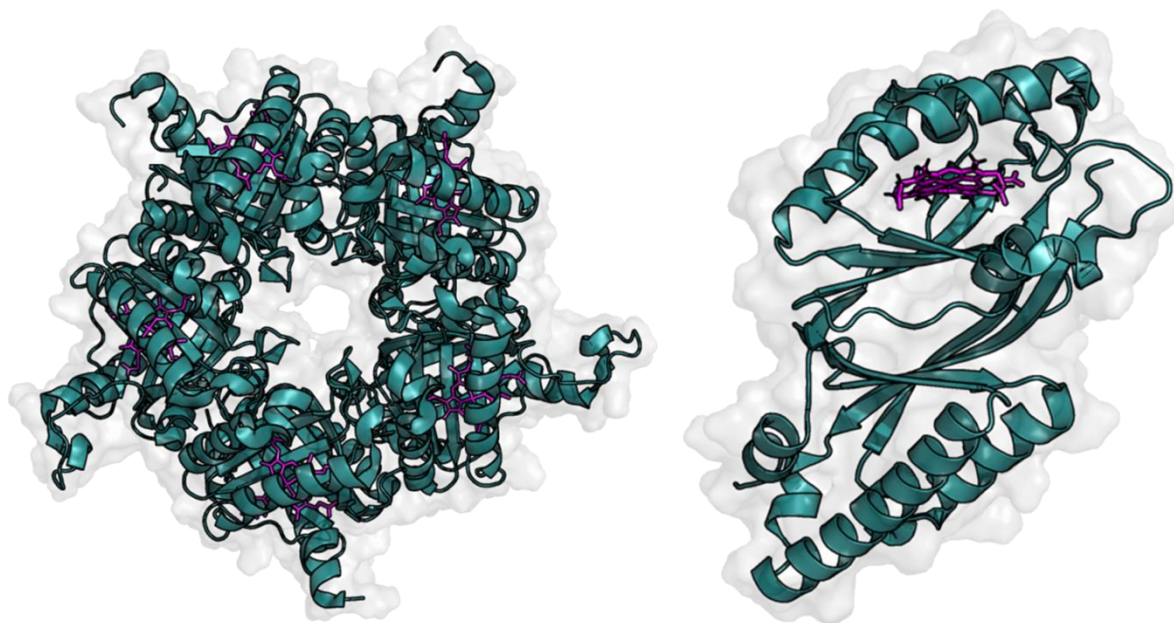
Figure 1.18 - Crystal structure of *Listeria monocytogenes* coproheme decarboxylase

The first crystal structure of a coproheme decarboxylase (PDB: 5LOQ) with coproheme (magenta) bound in the active site. The protein crystallised as a pentamer, the secondary structure is shown in teal and the protein surface in grey (adapted from (Hofbauer et al., 2016c)). **Abbreviations: ChDC** (coproheme decarboxylase).

1.2.4.3.2 *Investigating the function and stability of HemQ*

UV-Visible spectroscopy and resonance Raman (RR) spectroscopy were used to investigate the mechanism of action of coproheme decarboxylase. The UV-Vis spectrum of coproheme decarboxylase in a complex with coproheme shows an asymmetric Soret band with a maximum at 394 nm. The asymmetry of this band is thought to the partial conversion of coproheme to the intermediate harderoheme (III or IV) even in the absence of an oxidant (Celis et al., 2015).

RR spectroscopy showed propionyl bending modes in all four spectra (coproheme, harderoheme IV, harderoheme III and heme *b*) and vinyl bending modes in harderoheme and heme *b*. The addition of 10 molar equivalent of hydrogen peroxide

completely converts coproheme to heme. The reduction in propionyl bending bands and appearance of vinyl bending bands in RR spectroscopy are characteristic of an oxidative decarboxylation mechanism. Peracetic acid (PAA) was able to substitute for hydrogen peroxide, 2 molar equivalents resulted in 70% substrate turnover and 8 molar equivalents resulted in complete substrate turnover with the formation of about 85% heme (Celis et al., 2015). The catalytic efficiency for this oxidative decarboxylation is thought to be slow though biologically relevant (Hofbauer et al., 2016c). The biological source of this hydrogen peroxide is thought to come from the conversion of coproporphyrinogen to coproporphyrin in a six electron oxidation producing three molecules of hydrogen peroxide (Dailey et al., 2017).

Stopped flow spectroscopy was used to identify spectral intermediates in substrate and product binding. The high absorption coefficient for coproheme and fast binding made determining K_d difficult in stoichiometric excess so pseudo first order concentrations of coproheme were used. The binding of coproheme or hemin to apo-coproheme decarboxylase is much faster than heme binding. There are spectral changes that occur upon binding of the substrate or product which indicates the formation of spectral intermediates in both reactions (Hofbauer et al., 2016a).
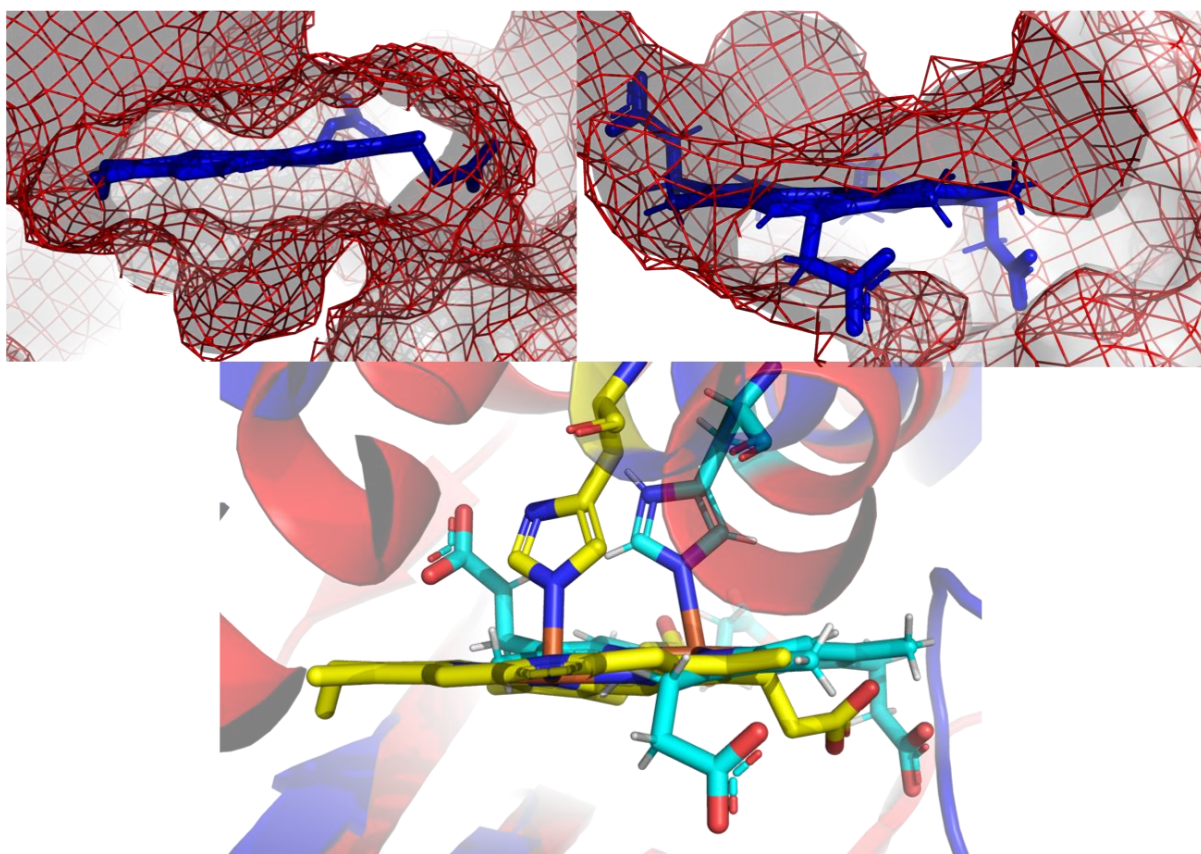
Figure 1.19 Cavity architecture of HemQ and chlorite dismutase

Chlorite dismutases (top left, PDB ID: 2VXH) and coproheme decarboxylases (top right, PDB ID:5LOQ) have similar heme cavity architecture (Hofbauer et al. 2016c, de Geus et al.,2009). The porphyrin molecules heme (top left) and coproheme (top right) are coloured blue and the surface of the proteins are shown in a red mesh and light grey surface. The bottom figure shows the coordination of heme (yellow) and coproheme (cyan) in the chlorite dismutase (blue) and coproheme decarboxylase (red) when overlaid (PDB IDs 5LOQ AND 2VXH, respectively).

Coproheme decarboxylase proteins have similar heme cavity architecture to chlorite dismutase (figure 1.19). However, coproheme decarboxylases lack a crucial arginine in the active site, which is important for chlorite degradation; HemQs do not have chlorite degrading activity. The catalytic arginine is generally replaced by serine, alanine, glutamine or leucine (Hofbauer et al., 2016b).

1.2.4.3.3   Structure of Coproheme Decarboxylase

The first coproheme decarboxylase protein was crystallised with substrate in 2016 (Hofbauer et al., 2016c) (figure 1.18). The *L. monocytogenes* coproheme decarboxylase structure was solved with coproheme bound, this crystal structure was able to confirm the coproheme binding site as well as identify the residues involved in binding of the metalated porphyrin. The substrate is anchored into the active site by a weakly bound proximal histidine (H174 in *L. monocytogenes*).   When hydrogen peroxide is at equimolar concentrations compared to coproheme-coproheme decarboxylase there is crosslinking between the protein and the heme group. (Hofbauer et al., 2016c).

Molecular dynamics simulations predict that the residue Q187 interacts with the propionate at position 2 (p2) and Y147 and S225 interacts with propionate 4 (p4) of the coproheme. These interactions were confirmed in the crystal structure also Met149 was another confirmed H-bond partner for p4 and G178 and V185 were additional interacting partners for p2 (Hofbauer et al., 2016a, Hofbauer et al., 2016c).

1.2.4.4   Confirmation of the coproporphyrin-dependent heme biosynthesis pathway

The function of each enzyme in the non-canonical heme biosynthesis pathway has been confirmed by enzyme assays (table 1.1). Enzyme assays had already been used to define a function from the coproporphyrinogen oxidase in Gram positive bacteria. This enzyme was capable of converting coproporphyrinogen III to coproporphyrin III, the first stage in the coproporphyrin-dependent pathway (Dailey et al., 1994). The

combination of enzymes coproporphyrinogen oxidase and ferrochelatase produced coproheme (Fe-coproporphyrin) when assayed with coproporphyrinogen and iron. This showed that coproporphyrinogen was converted to coproporphyrin using coproporphyrinogen oxidase and ferrous iron was inserted into coproporphyrin using ferrochelatase producing coproheme. These results indicated that the ferrochelatase was the second enzyme in the pathway.

The third enzyme in the pathway is coproheme decarboxylase. This was confirmed when an assay was performed with all three enzymes, coproporphyrinogen and ferrous iron. The end product was heme, this indicated that coproheme decarboxylase was responsible for converting coproheme to heme (Dailey et al., 2015, Dailey et al., 2010). Another coproheme decarboxylase (AhbD) is present in the siroheme-dependent heme biosynthetic pathway and is frequently found encoded in the genomes of Gram positive bacteria. 30% of Gram positive bacteria contain both coproheme decarboxylase and AhbD, HemQ is thought to be an oxygen-dependent coproheme decarboxylase whilst AhbD could be an oxygen-independent coproheme decarboxylase (Dailey and Gerdes, 2015, Dailey et al., 2015).

Table 1.1 Results of enzyme assays

SUBSTRATE(S)	ENZYMES	PRODUCT
COPROPORPHYRINOGEN + IRON	CpOX and CpFC	Fe-Coproporphyrin
COPROPORPHYRINOGEN + IRON	CpOX, CpFC and ChDC	Heme
COPROPORPHYRIN + IRON	CpFC and ChDC	Heme
FE-COPROPORPHYRIN	ChDC	Heme

The currently accepted coproporphyrin-dependent pathway branches off from the protoporphyrin-dependent pathway at coproporphyrinogen. Coproporphyrinogen is oxidised by coproporphyrinogen oxidase to form coproporphyrin III, then ferrous iron is inserted into coproporphyrin III forming coproheme (Fe-coproporphyrin) through the action of coproporphyrin ferrochelatase. Two of the propionyl groups on coproheme are oxidatively decarboxylated by coproheme decarboxylase forming vinyl groups on rings A and B creating heme (Dailey et al., 2015, Dailey et al., 2010).

These three enzymes are notably different to the three terminal heme biosynthesis enzymes in eukaryotes (i.e. the protoporphyrin-dependent pathway) and are potential therapeutic targets. The Gram positive enzymes have different substrate specificities to the eukaryotic enzymes, and this can be used as a basis for the development of antibiotics that specifically target Gram positive bacteria. Ferrochelatase is the most

studied enzyme of the three terminal enzymes and so studying and comparing ferrochelatases in the protoporphyrin and coproporphyrin-dependent heme biosynthetic pathways could lead to development of novel antibiotics (Sheldon and Heinrichs, 2015). An overview of the complete heme biosynthesis pathway is shown in figure 1.20.

Figure 1.20 - The three heme biosynthetic routes: protoporphyrin, coproporphyrin and siroheme dependent pathways

The red shows the conserved pathway that is taken by all known organisms. ALA, the first common intermediate is formed through two different routes. The siroheme-dependent pathway (orange) is present in archaea and sulfate-reducing bacteria. The protoporphyrin-dependent pathway (blue) is mainly present in eukaryotes and the majority of Gram negative bacteria whereas the coproporphyrin-dependent (purple) is mainly observed in Gram positive bacteria. **Abbreviations: ALA** (δ-aminolevulinic acid), **GSA** (glutamate-1-semialdehyde), **PBG** (porphobilinogen), **HMB** (hydroxymethylbilane), **URO'GEN** (uroporphyrinogen III), **COPRO'GEN** (coproporphyrinogen III), **COPRO** (coproporphyrin III), **PROTO'GEN** (protoporphyrinogen IX), **PROTO** (protoporphyrin IX), **SUMT** (SAM (S-adenosyl methionine)-dependent uroporphyrinogen methyltransferase), **PC2** (precorrin-2), **PCDH** (precorrin-2 dehydrogenase), **SiHC** (sirohydrochlorin), **FC** (ferrochelatase), **SH** (siroheme), **Ahb**(alternative heme biosynthesis), **DDSH** (12,18-didecarboxysiroheme), **ALAS** (δ-aminolevulinic acid synthase), **GluTR** (Glutamyl-tRNA reductase), **GSAM** (glutamate-1-semialdehyde aminomutase), **PBGS** (porphobilinogen synthase), **PBGD** (porphobilinogen deaminase), **UROS** (uroporphyrinogen synthase), **UROD** (uroporphyrinogen deaminase), **CgOX** (coproporphyrinogen oxidase), **CpFC** (coproporphyrin ferrochelatase), **ChDC** (coproheme decarboxylase), **CgDC** (coproporphyrinogen decarboxylase), **CgDH** (coproporphyrinogen dehydrogenase), **PgDH1/2** (protoporphyrinogen dehydrogenase 1 and 2), **PgOX** (protoporphyrinogen oxidase), **PpFC** (protoporphyrin ferrochelatase) .

1.3   Ferrochelatase (FC)

1.3.1 Chelatases

Chelatases catalyse the insertion of a metal ion into a tetrapyrrole ring; each tetrapyrrole biosynthetic pathway involves a chelatase that ensures the correct metal is inserted. Examples include ferrochelatase, which can catalyse the insertion of ferrous iron into protoporphyrin IX to form heme and magnesium chelatase that catalyses the insertion of magnesium into protoporphyrin IX in chlorophyll synthesis (Schubert et al., 2002). There are three categories of chelatase, class I are the ATP-dependent heterotrimeric chelatases such as magnesium chelatase. Class II contains the ATP-independent chelatases such as ferrochelatase, they are found as monomers or homodimers.   Class III chelatases are ATP-independent multifunctional homodimeric chelatases, primarily involved in siroheme biosynthesis (e.g. siroheme synthase (CysG) (Brindley et al., 2003, Al-Karadaghi et al., 2006).

1.3.2 Ferrochelatase Structure

Ferrochelatases (FCs) have very low amino acid sequence conservation, with ~12% sequence identity across eukaryotes, Gram positive and Gram negative bacteria. Conserved residues are either involved in function or maintaining the overall protein fold. Despite this low sequence identity, the monomeric structures of these enzymes are relatively well conserved (figure 1.21). The ferrochelatases from *B. subtilis* and *H. sapiens* amongst other species have been crystallised and structural models inferred from X-ray diffraction data. The human FC (hFC) was resolved to 2 Å; it is homodimeric and is associated with the mitochondrial membrane, it synthesises heme using the protoporphyrin-dependent heme biosynthetic pathway (Wu et al., 2001). In contrast,

the *B. subtilis* FC (bFC) resolved at 1.9 Å is monomeric and soluble (Al-Karadaghi et al., 1997). *B. subtilis* is a Gram positive bacterium that synthesises heme through the coproporphyrin-dependent pathway. Comparing the structure of these enzymes may reveal differences that could explain the observed substrate specificity.

The active site of FC is found between domains I and II. In *H. sapiens* ferrochelatase there is a 13-residue insert in domain I that is important in the shaping the active site; it is not present in *B. subtilis* ferrochelatase (Al-Karadaghi et al., 1997, Wu et al., 2001). There are two faces of the active site above and below the plane of the porphyrin respectively (figure 1.25). One face of the active site is the most conserved region and contains the amino acids H263 and E343; these are placed directly opposite the centre of the porphyrin and are essential in the catalytic mechanism of ferrochelatase (Dailey et al., 2007, Medlock et al., 2007a, Sellers et al., 2001, Hansson et al., 2007, Hunter et al., 2016). The second face of the active site is much less conserved and contains the residues M76, Y165 and R164 in human ferrochelatase. Two separate proposals describe binding of ferrous iron in the active site with amino acid residues in either the conserved face or non-conserved face binding iron before insertion into porphyrin. The other face not involved in iron binding is then thought to be involved in proton abstraction. There is evidence to support both hypotheses and the actual mechanism still remains controversial (Medlock et al., 2007a, Hansson et al., 2007).

Before the discovery of the copro1-dependent pathway *B. subtilis*, a Firmicute, was thought to utilise the protoporphyrin-dependent heme biosynthetic pathway, a large quantity of published kinetic analysis of *B. subtilis* ferrochelatase has used

protoporphyrin IX or an analogue of protoporphyrin (e.g. deuteroporphyrin or mesoporphyrin) as a substrate rather than the correct substrate coproporphyrin III. The *B. subtilis* ferrochelatase has been structurally resolved with bound N-methylmesoporphyrin (N-MeMP), a potent inhibitor of ferrochelatase. However, the binding of N-MeMP may not be an accurate representation of physiological substrate binding in *B. subtilis* ferrochelatase. The superposition of a monomer of *H. sapiens* ferrochelatase onto *B. subtilis* ferrochelatase is shown in figure 1.21. The structure is relatively well conserved apart from the α-helix covering the active site (N-terminal extension) and the C-terminal extension involved in binding the iron-sulphur cluster in *H. sapiens* ferrochelatase.
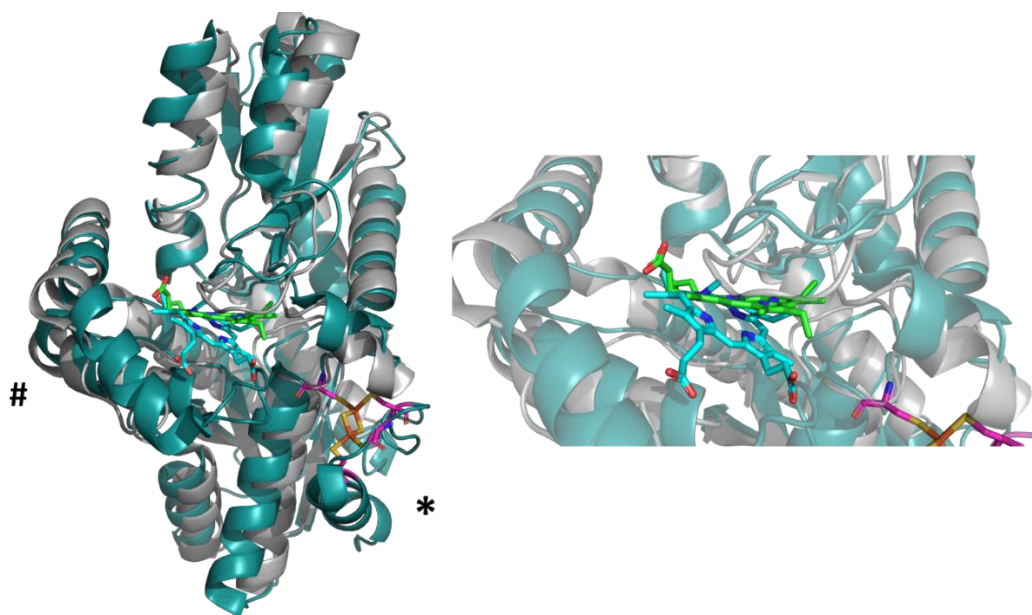
Figure 1.21 – The structural relationship between *H. sapiens* and *B. subtilis* ferrochelatase

A monomer of *H. sapiens* ferrochelatase (PDB ID: 2HRE) has been structurally aligned against *B. subtilis* ferrochelatase (PDB ID: 1C1H). *H. sapiens* ferrochelatase is shown in teal and *B. subtilis* ferrochelatase is shown in yellow. A zoomed image of the porphyrin binding in the ferrochelatase shows the difference in binding, N-methylmesoporphyrin is shown in cyan and protoporphyrin IX shown in green (Lecerof et al., 2000, Medlock et al., 2007a). The hash indicates the α helix in human ferrochelatase that sits over the active site (truncated N-terminal extension) and the asterisk highlights the helix turn helix structure involved in binding the iron-sulphur cluster (C-terminal extension). The iron-sulphur cluster is highlighted in orange and the cysteine (C196, C403, C406,C411) residues involved in its coordination are in magenta.

1.3.2.1   Domain structure

B. subtilis ferrochelatase has two domains (domain I and II), the active site is a 25 Å cleft is formed from the domains. The domains are similar and are suggested to result from a gene duplication event (Al-Karadaghi et al., 1997) (figure 1.23). They each resemble a α-β-α fold (four-stranded parallel β-sheet flanked by α-helices). The C-terminal helices of each domain interact with the β-sheet in the other domain contributing to the formation of the active site cleft (Al-Karadaghi et al., 1997).

The ferrochelatase domains contain a set of conserved glycines and prolines scattered throughout the protein, those in domain I corresponding to those in domain II. These conserved glycines and prolines are most likely involved in retaining the structure of ferrochelatase as they are commonly found in turns or the loop regions of the proteins and are involved in protein folding and compaction. Glycines and *-prolyl* bonds have relatively fast loop formation dynamics whereas dynamics around *trans-prolyl* bonds are slow (Krieger et al., 2005)(figure 1.22). Two of the conserved prolines, P91 and P233 (one in each domain) are in the *cis*-conformation and the isomerisation from *trans* to a *cis* conformation can hinder or slow correct protein folding (Al-Karadaghi et al., 1997). Mutation of any of these conserved residues could result in incorrect protein folding.
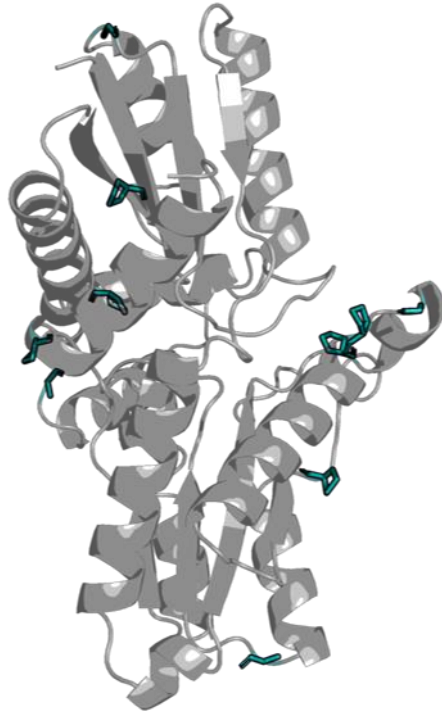
Figure 1.22- Conserved prolines and glycines in *B. subtilis* HemH

The conserved glycine and proline pairs (P16 and P186, P55 and P195, P91 and Pro 233, G52 and G193, G104 and G247) are shown on the ferrochelatase (PDB ID: 1AK1) in teal and the secondary structure is highlighted in grey. P91 and P233 are in the *cis* conformation.

Other conserved residues are found in the functional loop between β-strand 2 in domain II and α-helix 4 in domain II (residues Q221, S222, W230 and L231) or lining or in close proximity to the active site cleft. These conserved residues are thought to be functionally important. There are three major differences between the domains of *B. subtilis* ferrochelatase. Firstly, the functional loop in domain II is not present in domain I. The secondary structure elements α3 and β2 are noticeably longer in domain I. Finally, α-helices 1-3 in the domain I contain 65 amino acids whereas the corresponding region of in domain III only contains 35 residues (Al-Karadaghi et al., 1997).

```
              1          10            20            30            40
Domain I   M S R K K M G L L V M A Y G T P Y K E E D I E R Y Y T H I R R G R K P E P E M L
Domain II  - - - - E N A M L I V S - - - - - - - - - - - - - - - - - - - - - - - - - - - A

            41          50            60            70            80
Domain I   Q D L K D R Y E A I G G I S P L A Q I T E Q Q A H N L E Q H L N E I Q D E I T F
Domain II  H S L P E K I K E F G - - D P Y P D Q L H E S A K L I A E G A G V S E Y A V G W

            81          90           100           110           120
Domain I   K A Y I G - - L K H I E P F I E D A V A E M H K D G I T E A V S I V L A P H F S
Domain II  Q S E G N T P D P W L G P D V Q D L T R D L F E Q K G Y Q A F V Y V - P V G F V

           121         130           140           150           160
Domain I   - - - T F S V Q S Y N K R A K E E A E K L G G L T I T S V E S W Y D E P K F V T
Domain II  A D H L E V L Y D N D Y E C K V V T D D I G A - S Y Y R P E M P N A K P E F I D

           161         170       178
Domain I   Y W V D R V K E T Y A S M P E D E R
Domain II  A L A T V V L K K L G R - - - - - -
```

Figure 1.23 - *B. subtilis* ferrochelatase domain alignment

Sequence alignment and secondary structure alignment performed using PRALINE alignment tool of the two domains in *B. subtilis* ferrochelatase (Pirovano and Heringa, 2010). The secondary structural elements are highlighted in blue (β-strands) and red (α-helices) and are taken from the crystal structure (Al-Karadaghi et al., 1997).

The monomeric form of *H. sapiens* ferrochelatase is similar in structure to *B. subtilis* ferrochelatase, however it also contains N-terminal and C-terminal extensions. The N-terminal extension contributes to the formation of the active site changing its architecture. The C-terminal extension contains a helix-turn-helix motif that is important in binding an iron-sulphur cluster. Four cysteine residues (Cys196, Cys403, Cys406 and Cys411, *H. sapiens* ferrochelatase) coordinate the cluster, three are present in the C-terminal domain and one is in the N-terminal domain. The C-terminal extension stabilises the homodimer, of the 30 hydrogen bonds formed across the dimer interface, 18 form from residues in the C-terminal extension (Wu et al., 2001).

1.3.3 Components important in deducing the mechanism of action

The mechanism of action for ferrochelatase involves distortion of the porphyrin ring and exposure of the nitrogen lone pair orbitals of the pyrrole nitrogens to the incoming iron. A proposed mechanism includes the formation of the first coordinate bond

between the porphyrin and iron, followed by chelation and ring closure forming a sitting-a-top complex. Finally, deprotonation of the pyrrole nitrogens in the porphyrin completes metal insertion; the enzyme then releases the product (Sigfridsson and Ryde, 2003, Lecerof et al., 2003).

1.3.3.1   Porphyrin distortion

The ferrochelatase enzyme mechanism requires porphyrin distortion. Porphyrin distortion was proposed as part of the mechanism of action for ferrochelatase relatively early and several distinct approaches provide evidence to support it. The methods used include resonance Raman (RR) spectroscopy, theoretical calculations and inhibition studies. Resonance Raman spectroscopy can effectively probe the structural changes that occur in the mechanism of heme proteins, it was used to measure changes in the free-base porphyrin, mesoporphyrin IX (MP_{IX}), in the presence of yeast ferrochelatase and the metal, Hg^{2+} (Blackwood et al., 1997). Theoretical calculations defined optimal geometrics for several porphyrins and determined whether porphyrin distortion was energetically feasible (Sigfridsson and Ryde, 2003). Inhibition studies of ferrochelatase show that distorted porphyrins bind exceptionally tightly suggesting that they can be considered as transition-state inhibitors.

RR spectroscopy is capable of investigating potential porphyrin distortion as a free base or in the presence of ferrochelatase and metal. When Hg^{2+} was added to the ferrochelatase-MP_{IX} complex, bands in the spectra associated with out-of-plane modes appeared. The appearance of these bands correlated to a reduction in symmetry in the porphyrin due to static out-of-plane distortion.(Blackwood et al., 1997,

Perng and Bocian, 1992). These out-of-plane modes were similar to those seen in the spectra of ferrocytochrome c (a heme protein) and Ni-OEP. Further investigation using RR spectroscopy showed out-of-plane modes characteristic of porphyrin saddling and mutation of specific amino acids (E280Q and H209N) in murine ferrochelatase result in increased porphyrin distortion and reduced binding to hemin, a planar molecule (Franco et al., 2011, Franco et al., 2000, Shi and Ferreira, 2004).

Theoretical calculations of N-MeMP also support porphyrin distortion in the ferrochelatase active site. Tilting a neutral porphine by approximately 30° out of the porphyrin plane required less energy if metal free. A fully deprotonated metal-free porphyrin molecule containing a negative charge can easily be deformed requiring only less energy. It was suggested that a distorted porphyrin may be an intermediate in the insertion of ferrous ion into a porphyrin ring (Sigfridsson and Ryde, 2003).

Inhibition studies indicated that a variety of porphyrins act as inhibitors of human ferrochelatase; IX isomers had K_i values of 13-70 µM, similar to the K_m values for porphyrin substrates and N-alkylporphyrins had K_i values of <10 nM. N-alkylporphyrins are distorted approximately 30° compared to the planar IX isomers, the tight binding to ferrochelatase further supported the idea that a distorted porphyrin could be an intermediate in the metalation of protoporphyrin IX (Dailey et al., 2000).

Various porphyrins and metalloporphyrins were assessed as inhibitors or substrates of murine ferrochelatase and K_i or K_m values and K_d values were determined. The

metalloporphyrins assayed include Fe-protoporphyrin, Co-protoporphyrin, Zn-protoporphyrin and Sn-protoporphyrin, the K_i values ranged from 2-13 µM. The zinc, cobalt and iron metalloporphyrins are the much more effective inhibitors than tin porphyrin. Alternative porphyrins tested were protoporphyrin, mesoporphyrin, hematoporphyrin and deuteroporphyrin. The K_m values vary from 9-247 µM, deuteroporphyrin and mesoporphyrin have much higher K_m values than protoporphyrin and hematoporphyrin. N-methylprotoporphyrin has a much lower K_d than the ones tested and a K_i in the nanomolar range (10 nM) (Dailey et al., 1989).

These inhibition studies show that metallo-protoporphyrins are capable of inhibiting ferrochelatase with K_i values in the low micromolar range, these are planar molecules that cannot be easily distorted. Other related analogues of protoporphyrin such as mesoporphyrin, hematoporphyrin and deuteroporphyrin have varied K_m values indicating that they can still act as substrates. These molecules can be easily distorted by ferrochelatase and this may be why they are not inhibitory. Mesoporphyrin and deuteroporphyrin are frequently used as the porphyrin substrate in enzymatic assays and protein crystallisation as they are more soluble that protoporphyrin IX (Davidson et al., 2009, Dailey and Fleming, 1986, Medlock et al., 2009). A distorted porphyrin, N-methylprotoporphyrin, has a K_i value in the nanomolar range, significantly lower than the metallo-protoporphyrins. This suggests that a distorted porphyrin replicates the transition state however, the degree of distortion in the porphyrin molecule does not appear to be significant. These results are consistent with porphyrin distortion as part of the ferrochelatase enzymatic mechanism (Dailey et al., 1989). The crystal structure of the *H. sapiens* ferrochelatase and its substrate protoporphyrin IX reveal that the porphyrin is only moderately distorted, the actual degree of distortion shown

by the structure is approximately 12° rather than 30° seen with N-MeMP. However, the crystal structure shows the most stable enzyme-substrate complex and may not reflect a rarer conformation before catalysis (Medlock et al., 2007a, Al-Karadaghi et al., 1997).

1.3.3.2 Substrate selectivity

1.3.3.2.1 Metals

It was suggested that the degree of porphyrin distortion indicates which metal is selected and inserted into the porphyrin ring. This prediction is based mainly on steady state kinetics and structural analysis (Al-Karadaghi et al., 2006). Further work including more structural analysis and transient kinetics has been completed and these results weaken the credibility of this proposed mechanism (Medlock et al., 2009). This work shows that ferrochelatase inhibition occurs after metal insertion and product release is prevented

One plausible mechanism for the inhibition of ferrochelatase by Hg^{2+}, Pb^{2+}, Cd^{2+} and Mn^{2+} was that they bind but cannot be inserted into a porphyrin ring. This theory was tested using structural data. Crystal structures of *H. sapiens* ferrochelatase were produced using protoporphyrin or deuteroporphyrin in the presence of the metal inhibitors Hg^{2+}, Cd^{2+} or Mn^{2+} which revealed that the bound porphyrin was metalated. This indicated that metal selectivity is not determined by the degree of distortion (Medlock et al., 2009). These crystal structures proved that these inhibitory metals are inserted into the porphyrin and then the activity of ferrochelatase is inhibited by tight binding of the product (Medlock et al., 2009).

In activity assays of ferrochelatase different metals are frequently used. Zn^{2+} is used most often as it cannot be oxidised unlike the endogenous substrate Fe^{2+}. Other investigators have used Co^{2+}, Cu^{2+} and Ni^{2+} and found that there was different preference of metals dependent on the species of ferrochelatase. Eukaryotic ferrochelatase such as *H. sapiens* and *S. cerevisiae* ferrochelatase will utilise Co^{2+} and not Cu^{2+} whereas a prokaryotic ferrochelatases such as *B. subtilis* ferrochelatase use Cu^{2+} over Co^{2+}. Y13 in *B. subtilis* ferrochelatase is important in coordinating the iron in active site and directly binds to a nitrogen group on the Cu-mesoporphyrin. Sequence alignments reveal that this residue is not conserved across species and is a methionine in the *H. sapiens* and *S. cerevisiae* enzyme. Mutation of Y13 to a methionine results in metal specificity similar to the eukaryotic enzyme with a preference for Co^{2+} over Cu^{2+} (Hansson et al., 2011).

1.3.3.2.2   *Porphyrin selectivity*

The porphyrin selectivity of ferrochelatase was explained in the earliest studies on this enzyme. Ferrochelatase was harvested from mitochondria isolated from sheep liver. Assays were run using different porphyrins, with cobalt as the metal substrate. Firstly, the propionate groups present at positions 6 and 7 of the porphine ring were switched with the methyl groups at position 5 and 8, respectively. Switching the propionate at position 6 to position 5 resulted in decreased activity and substitution of both propionates resulted in complete loss of activity (figure 1.24)(Honeybourne et al., 1979).
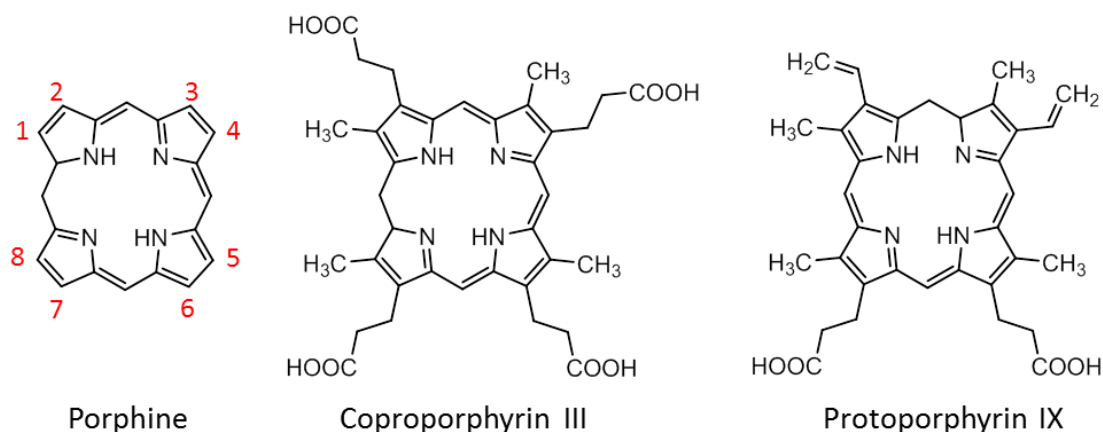
Figure 1.24 - Porphyrin structures

The parent porphyrin compound porphine contains hydrogens at potential substitution positions 1-8 (red). Coproporphyrin III and protoporphyrin IX are examples of porphyrins where positions 1-8 have been substituted with methyl, vinyl and propionyl groups.

Further studies were completed on IX porphyrin isomers. Deuteroporphyrin IX had the most activity followed by mesoporphyrin IX and then protoporphyrin IX. The different substitutions in each of the isomers are shown in table 1.2. There are hydrophobic substitutions at positions 1, 2, 3 and 4 in mesoporphyrin and protoporphyrin which unfavourably alter the V_{max} but favourably change the K_m, so these moieties maybe important in binding to a hydrophobic region in the enzyme active site. Furthermore, swapping the position 2 vinyl group in protoporphyrin IX to position 1 changes the molecule to protoporphyrin XIII and this does not alter the activity effectively. The porphyrin molecule that had the highest activity (porphyrin 1) has propionates at position 6 and 7, methyl groups at positions 5 and 8 and the other four sites were left unsubstituted (Honeybourne et al., 1979).

Table 1.2- Substitutions of each porphyrin at each position

PORPHYRIN	POSITION							
	1	2	3	4	5	6	7	8
PORPHYRIN I	H	H	H	H	Me	P	P	Me
DEUTEROPORPHYRIN IX	Me	H	Me	H	Me	P	P	Me
MESOPORPHYRIN IX	Me	Et	Me	Et	Me	P	P	Me
PROTOPORPHYRIN IX	Me	V	Me	V	Me	P	P	Me
PROTOPORPHYRIN XIII	V	Me	Me	V	Me	P	P	Me

H= Hydrogen, Me= Methyl, P= Propionate, Et= Ethyl, V= Vinyl

1.3.4 Development of a catalytic model

There have been many proposed mechanisms of for ferrochelatase. The literature reveals a controversy regarding the mechanism of iron insertion into the porphyrin and its route into the active site. One hypothesis is that the iron enters the porphyrin using the residues on the conserved face of the active site (H183 and E284 *B. subtilis* HemH) (Hunter et al., 2008, Hunter and Ferreira, 2010, Karlberg et al., 2002). The other hypothesis suggests the iron enters using the residues on the non-conserved face of the active site (K87 and H88 *B. subtilis* HemH) (Asuru and Busenlehner, 2011, Dailey et al., 2007, Sellers et al., 2001)(figure 1.25).
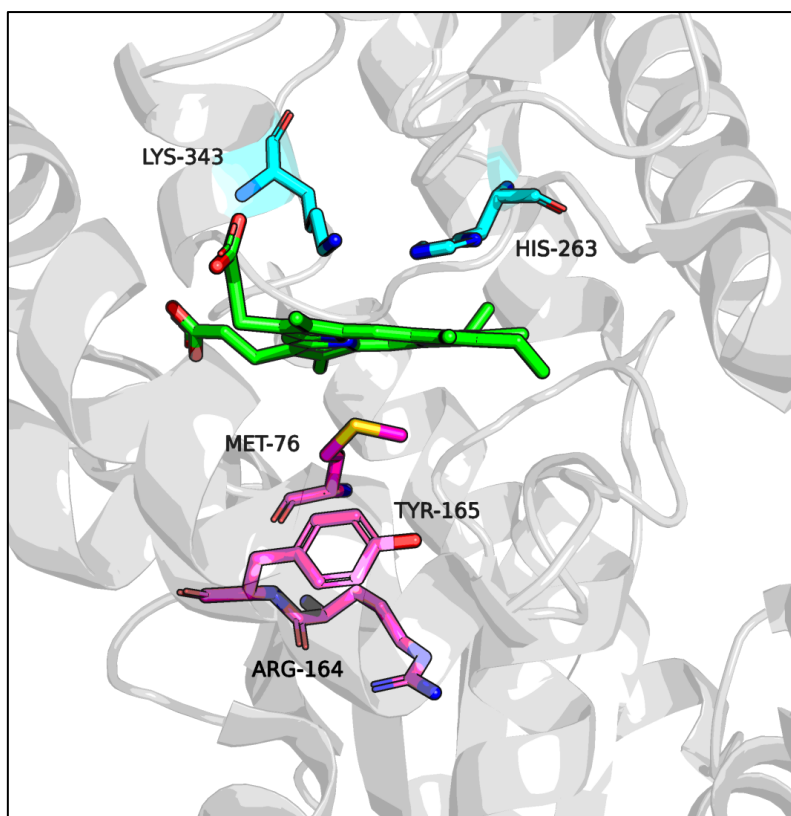
Figure 1.25 - The faces of *H. sapiens* ferrochelatase active site

The two different faces of the active site are above and below the plane of the porphyrin. Residues in the conserved face of the active site (E343 and H263) are shown in cyan however, in this structure there is an E343K mutation. The residues in the non-conserved face of the active site (M76, R164 and Y165) are shown in pink. Protoporphyrin IX is coloured green. The protein structure used in this image has PDB ID: 2QD1 (Medlock et al., 2007b).

1.3.4.1   Peripheral components of the active site

1.3.4.1.1   Hydrogen-bonding network of H. sapiens ferrochelatase

The hydrogen-bonding network present in the active site changes upon porphyrin binding, contributing to the closure of the active site mouth. There are several residues that have been implicated in the hydrogen bonding network, including H263, H341 and F337 (*H. sapiens* HemH numbering). To investigate the hydrogen-bonding network H263, H341 and F337 were mutated. The resulting mutants were structurally resolved using X-ray crystallography. H263C, H341C and F337A were structurally resolved with

no porphyrin bound and the active site architecture of each mutant was compared to R115L *H. sapiens* HemH. Analysis of the active site of each mutant showed residues that were differentially orientated. The H263C and H341C mutant proteins had different side chain orientation when compared to the R115L mutant. The residues N75, M76, R164, H263, F337, H341, and E343 all showed different orientation. In the F337A mutant the side chain orientation remained similar to R115L HemH. This suggested that both H263 and H341 are important in the hydrogen-binding network. Figure 1.26 shows the difference in side chain orientation between R115L and H263C *H. sapiens* HemH (Dailey et al., 2007).
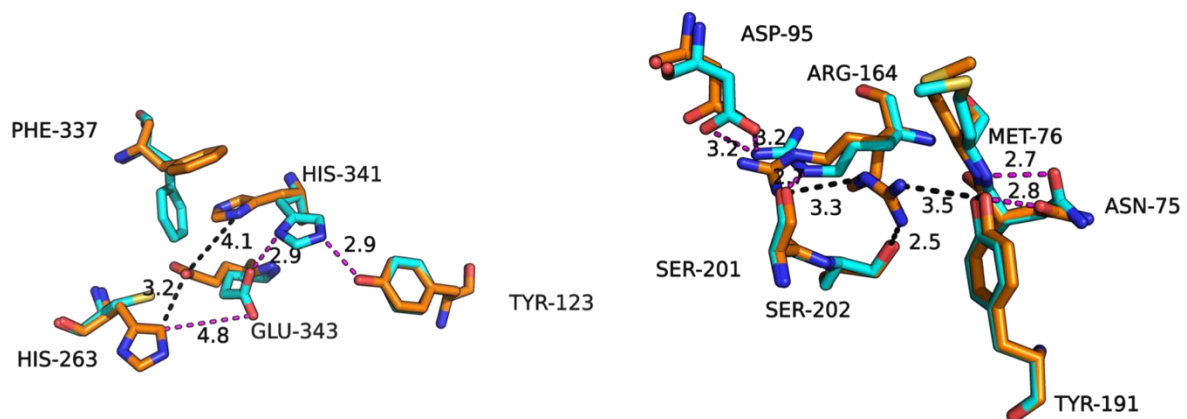
Figure 1.26 - Overlay of *H. sapiens* R115L and *H. sapiens* H263C ferrochelatase

The *H. sapiens* ferrochelatase variants are overlaid, the R115L variant (orange, PDB: 2HRC) and H263C variant (cyan, PDB ID: 2PO5). The R115L has similar structure and activity to wildtype whereas H263C has no measurable activity. The differences in these two structures are the residues highlighted. These residues are thought to be involved in the hydrogen-bonding network as mutation of H263C disrupts the hydrogen-bonding network (Dailey et al., 2007). Hydrogen bonding at rest is shown by black dashed lines and hydrogen bonding in an activated state is shown in magenta dashed line. The right image includes residues on the conserved side of the active site and the left image includes residues from the non-conserved side of the active site.

1.3.4.1.2   Solvent filled channels and the π-helix, two routes for iron entry into the active site

Another peripheral element of the active site is the presence of solvent filled channels. In *H. sapiens* ferrochelatase there are solvent filled channels, these channels form from the outside of the protein and end at the active site. Two of the channels are named after the terminal residues they interact with H240 and Q139. The Q139 channel is the shorter of the two channels and is present in *H. sapiens, B. subtilis* and *S. cerevisiae* ferrochelatase and H240 is only found in *H. sapiens and S. cerevisiae*. Both of these channels are capable of transporting water molecules and desolvated metal ions such as iron. The two channels converge at residue Phe337 (Medlock et al., 2012).

The Phe337 residue was first studied when investigating the hydrogen-bonding network in the active site of *H. sapiens* HemH (section 1.3.4.1.1). These experiments showed that Phe337 was not involved in the hydrogen-bonding network. It is now posited to function as a gate for the solvent filled channels. In the 8 mutant the channels are permanently open, this is shown through comparisons of the solvent filled channels in the R115L mutant (like wildtype) the F337A mutant ferrochelatase (Medlock et al., 2012). In the F337A mutant and the activity of the enzyme is diminished. It is also diminished in F337R mutant, but this could be because arginine prevents the expulsion of water from the active site or the entry of iron (Medlock et al., 2012, Dailey et al., 2007). In wildtype human ferrochelatase the Q139 channel is only open to the active site when porphyrin is bound and so could allow the transfer of iron into the active site.

The Phe337 residue is found in close proximity to another element of the ferrochelatase active site, the π-helix. π-helices are relatively rare compared to other helices and were originally thought to be fairly unstable due to their dihedral angles, large radius and the large entropic penalty required for them to form (Fodje and Al-Karadaghi, 2002). They are wider and flatter than α helices and the π-helix present in the active site of ferrochelatase (D340-C360 in *H. sapiens*) is dynamic and contains acidic residues (e.g. E343 and D340) along one edge, forming an acidic path into the active site (Medlock et al., 2007b).

A mutant of *H. sapiens* HemH (F110A) was crystallised and structurally resolved with heme bound. This structure imitated the product bound state of ferrochelatase. When compared to the porphyrin bound state of *H. sapiens* ferrochelatase, the π-helix is unwound between residues 340-349, it is also rotated and extended (figure 1.27). The propionate at position 6 on protoporphyrin IX is bent backward towards the centre of the porphyrin, the H263 is positioned 5 Å away from the centre of the porphyrin rather than its normal 3 Å and the active site is open. In structures containing bound Pb-protoporphyrin IX the active site architecture is similar to the heme bound ferrochelatase mutant (Medlock et al., 2007b).
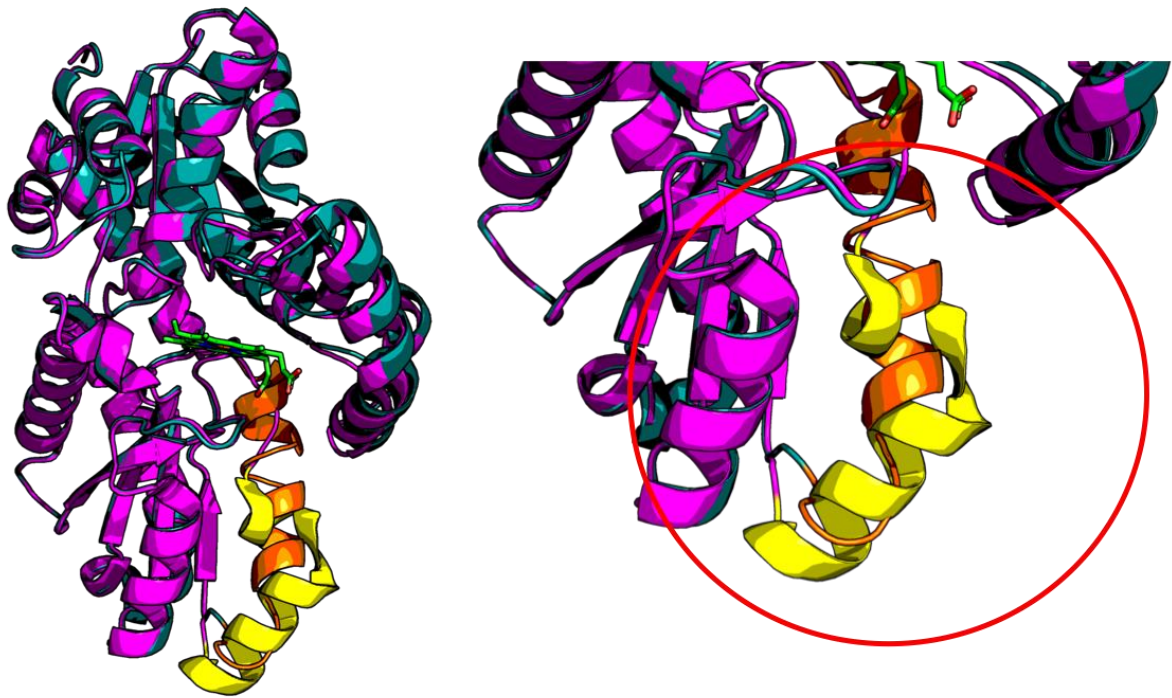
Figure 1.27- Dynamics of the π helix

An overlay of the two ferrochelatase variants R115L (teal PDB ID: 2HRC) and F110A (magenta PDB ID: 2QD2) shows the dynamics of the π helix. In R115L the π helix (orange) is fully formed and in the F110A the π helix (yellow) is unwound. F110A represents the product release conformation as the structure was crystallised with bound heme (green) and R115L variant represents the open conformation with no substrate bound. Zoomed versions of the π helices are also shown (Medlock et al., 2007a, Medlock et al., 2007b).

The nature of the π-helix in this F110A mutant suggests that ferrochelatase undergoes structural reorganisation during its catalytic cycle. The unwinding and winding of the π-helix has been hypothesised to both allow iron to enter the active site and allow product release (Medlock et al., 2007b, Fodje and Al-Karadaghi, 2002).

1.3.4.1.3   Secondary metal binding site

The final component of the active site to consider is the secondary metal binding site. The secondary metal binding site was discovered in *S. cerevisiae* ferrochelatase. Significant inhibition was observed in the activity of yeast ferrochelatase in the

presence of different divalent metal ions (Ni^{2+}, Co^{2+}, Zn^{2+}, Cu^{2+}). Inhibition was also observed in human ferrochelatase when it was assayed with Zn^{2+}; no inhibition was observed with iron (Hunter et al., 2008, Davidson et al., 2009). The magnitude of inhibition was dependent on the metal ion, the most inhibitory metal ion was Ni^{2+} followed by Co^{2+}, Zn^{2+} and then Cu^{2+}, in *S. cerevisiae* ferrochelatase. The divalent metal ions were thought to bind to the secondary metal binding site and inhibit ferrochelatase when iron is not present thus preventing the formation of other metalloporphyrins that aren't heme (Hunter et al., 2008). However, other studies show that the secondary metal binding site may serve to enhance the affinity for metal binding, it could be involved in substrate processing (Hunter and Ferreira, 2010) and is significant when ferrochelatase is bound to product (Davidson et al., 2009).

Several potential metal binding sites have been observed in crystal structures of ferrochelatase (PDB ID: 1L8X, 2HK6, 1LD3 and 1N0I) these were used to confirm the important residues in the secondary binding site (Hunter et al., 2008, Karlberg et al., 2002, Hansson et al., 2007, Lecerof et al., 2003).The most important residues in the secondary binding site were observed in murine ferrochelatase, these were H287 and F283. Both of these residues are completely conserved in ferrochelatase. Despite complete conservation of the F283 residue it is not required for high levels of *in vitro* activity. It is present at the end of the π helix and is thought to help metal binding to H287. The mutants F283L and H278L caused partial and complete elimination of the observed inhibition, respectively (Hunter and Ferreira, 2010). Crystal structures from Cd^{2+} soaked murine ferrochelatase showed metal binding at both histidines (H207 and H287) thought to be involved in binding at the two different metal binding sites (Hunter and Ferreira, 2010).

This secondary metal binding site is present in the coproporphyrin ferrochelatases from *B. subtilis* and *S. aureus*. *B. subtilis* ferrochelatase can only be structurally resolved in the presence of Mg^{2+}, this is thought to stabilise the π-helix and hold the ferrochelatase in the open conformation (Hunter et al., 2011, Medlock et al., 2012, Hansson and Al Karadaghi, 1995). The Mg^{2+} interacts with the residues E272, E268, R46 and E223; this is a secondary binding site proximal to the surface of the protein and approximately 7 Å away from the invariant H183 residue. Mutation of E272 (E272S) resulted in elimination of any stimulatory effect caused by Mg^{2+} bound in the secondary metal binding site (Lecerof et al., 2003, Hansson et al., 2006). In *S. aureus* HemH, the presence of Mg^{2+} caused the inhibition exerted by iron to occur at lower concentrations compared to the iron inhibition occurring in the absence of Mg^{2+}. Mutation of E271 in *S. aureus* (E272 in *B. subtilis*) to serine caused the elimination of the inhibition caused by iron (Hobbs et al., 2017).

1.3.4.2   *The role of the His-Glu pair as the final metal binding site before porphyrin metalation*

Amongst the ferrochelatases there is a His-Glu pair that is completely conserved despite their low sequence similarity (<20%). Mutation of the residues H263 and E343 in *H. sapiens* ferrochelatase generally result in inactive ferrochelatase, however, there are some cases where minimal activity is retained. For example the conservative mutant E343D retains some activity (Hoggins et al., 2007). All mutations at H263 results in an inactive enzyme. The addition of imidazole, a structurally similar

compound to histidine, cannot substitute the H263 residue and rescue activity (Sellers et al., 2001, Dailey et al., 2007, Medlock et al., 2007b).

This His-Glu pair together has been postulated to act as a binding site for the iron in the active site prior to porphyrin insertion. This insertion would occur from the conserved side of the active site (figure 1.28) and a range of experiments support this hypothesis (Karlberg et al., 2002, Ferreira et al., 2002, Hansson et al., 2007). Binding assays with Zn^{2+} and the *B. subtilis* ferrochelatase mutant proteins, H183A and E264V showed an increase in K_d, compared to the wildtype ferrochelatase, paired with a large reduction in catalytic activity. When residues in the non-conserved face of the active site were mutated (K87A and H88A) the effects were less substantial. The H88A mutant had a K_d for Zn^{2+} similar to wildtype (2.8 ± 0.4 µM vs. 3.7 ± 0.4 µM) but low activity (5%) and the K87A mutant had a higher K_d value (13 ± 5 µM vs 3.7 ± 0.4 µM) but retained 92% activity compared to the wildtype (Hansson et al., 2007).

The role of the His-Glu pair was investigated further using pH-dependent kinetics. The conserved face of the ferrochelatase active site contains residues that have ionisable groups (E343, H341, H263 *H. sapiens* numbering) whereas the non-conserved active site face mainly consists of residues unaffected by changes in pH. The research group reasoned that if the His-Glu pair was important in porphyrin metalation then the histidine and the glutamate would need to be deprotonated. When the pH is lower than the pK_a of the two residues the activity of the ferrochelatase should be greatly diminished. Kinetic assays at different pH revealed that porphyrin metalation in the ferrochelatase reaction is dependent on pH suggesting that the His-Glu pair may be

important in metal binding and porphyrin metalation although several other residues are affected complicating the assignment (Hunter and Ferreira, 2010, Hunter et al., 2016).

To further support the role of the His-Glu pair as the final binding site prior to insertion, a crystal structure of *B. subtilis* ferrochelatase with iron bound and *S. cerevisiae* ferrochelatase with cobalt bound in the active site were structurally resolved using X-ray crystallography (PDB ID: 2HK6 and 1L8X, respectively). They showed iron coordinated by the H183 and E264 in the *B. subtilis* structure and cobalt was bound to H235, the invariant histidine in *S. cerevisiae* (Hansson et al., 2007, Karlberg et al., 2002).
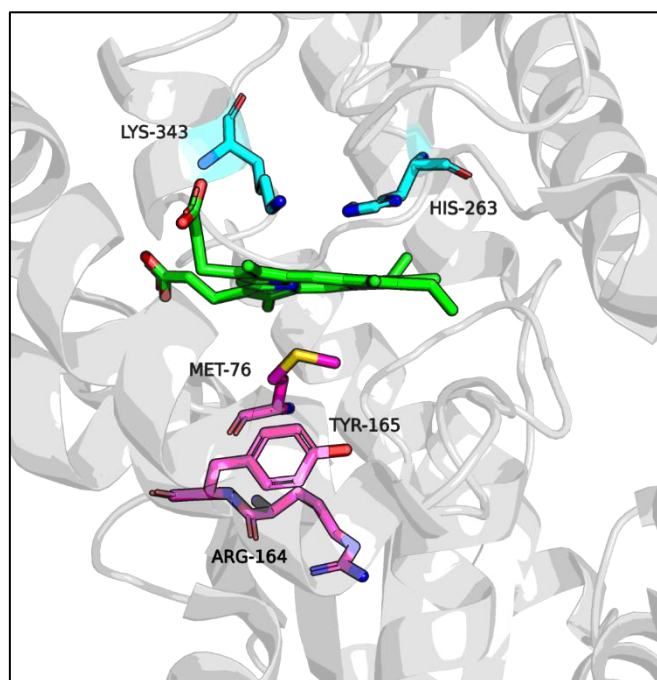
Figure 1.28 - The faces of *H. sapiens* ferrochelatase active site

The two different faces of the active site are above and below the plane of the porphyrin. Residues in the conserved face of the active site (E343 and H263) are shown in cyan however, in this structure there is an E343K mutation. The residues in the non-conserved face of the active site (M76, R164 and Y165) are shown in pink. Protoporphyrin IX is coloured green. The protein structure used in this image has PDB ID: 2QD1 (Medlock et al., 2007b).

1.3.4.3 An alternative porphyrin metalation model that utilises residues on the non-conserved side of the active site as the final metal binding site

The other proposed function for the His-Glu pair is proton abstraction. In this model, H263 (*H. sapiens*) abstracts protons from the pyrroles on the porphyrin and they exit the active site using E343 and other residues in the π helix. It has been argued that if the His-Glu pair was the terminal metal binding site this would lead to the histidine becoming an axial ligand to the heme. Histidine is frequently found as an axial ligand for heme in proteins containing heme as a cofactor and so the interaction between these would be strong and product release would not occur easily (Dailey et al., 2007, Medlock et al., 2009, Sellers et al., 2001). Kinetic assays have shown that the rate determining step in the ferrochelatase enzyme mechanism is likely to be product release (Hoggins et al., 2007).

Site-directed mutagenesis of *H. sapiens* ferrochelatase active site residues showed the significance of residues potentially involved in iron binding and porphyrin metalation. Initially H263 was mutated to H263A/C/N all of which were inactive. Due to the inactivity of these mutants the definitive role of H263 could not be elucidated. However, if H263 were an iron ligand then some activity retention in H263C would be expected. What can be concluded from the lack of activity is that this invariant histidine is clearly essential in catalysis (Sellers et al., 2001, Dailey et al., 2007). Mutation of E343 mainly resulted in an inactive ferrochelatase, E343K/H/Q mutants were completely inactive but E343D had a K_m for iron comparable to wildtype and a significantly lower V_{max} value. As these residues were hypothesised to act as proton

abstractors, mutation to a basic or an amine based residue would prevent proton abstraction and lead to the accumulation of substrate in the ferrochelatase active site. Most of these mutants were isolated with porphyrin bound in their active sites and no turnover was observed (Sellers et al., 2001).

As the His-Glu pair is proposed to be involved in proton abstraction then the insertion of the iron into the porphyrin ring is thought to occur from the opposite side of the active site, the non-conserved face (figure 1.28). The residues thought to be the metal binding site immediately prior to insertion are R164 and Y165 (*H. sapiens* HemH) equivalent to K87 and H88 in *B. subtilis* HemH (Asuru and Busenlehner, 2011, Medlock et al., 2009, Dailey et al., 2007, Sellers et al., 2001).

Site-directed mutagenesis revealed several residues that may have been involved in iron binding and/or porphyrin metalation due to the increase in their K_m^{Fe}. The mutants R164L and Y165F resulted in a 2-fold increase in K_m^{Fe} and the double mutant R164L/Y165F caused a 6 fold increase in K_m^{Fe} compared to wildtype ferrochelatase thus supporting their role as the terminal metal binding site prior to porphyrin metalation. Mutation of other residues in ferrochelatase such as D383, H231 and Y191 also resulted in higher K_m^{Fe} values. D383 and H231 are thought to be an initial binding site for iron (Wu et al., 2001, Sellers et al., 2001) and conserved residues between the active site (W227, Y191, R164 and Y165) were thought to provide a pathway for iron to enter the active site (Sellers et al., 2001), This proposal however, predated the discovery of the solvent filled channels, another potential route for iron to enter the active site (Medlock et al., 2012).

Other techniques such as amide Hydrogen/Deuterium exchange mass spectrometry (HDX-MS) were utilised to probe the residues involved in forming the final metal binding site prior to insertion. HDX-MS studied the change in backbone dynamics in Apo *H. sapiens* ferrochelatase and Fe^{2+} bound *H. sapiens* ferrochelatase. There were notable differences in the peptides 89-91, 164-173 (containing R164 and Y165), 197-203, 222-233 and 338-345 (contains the π helix) upon binding of iron. The dynamics in the region containing R164 and Y165 reduces when iron is bound, potentially indicating a role in iron binding. The peptide containing the H263, 260-269, does not alter in solvent accessibility or backbone dynamics in the presence of iron suggesting these residues do not have a role in iron binding. However, the peptide containing E343, 330-345, does show a decrease in dynamics when iron is present. Whilst this result supports E343 as a potential site for iron binding, the proton abstraction hypothesis claims that the protons would exit the active using this residue and other residues in the π helix and this could affect the dynamics of the π helix (Asuru and Busenlehner, 2011).

1.3.4.4   Summary of catalytic model

The face in which iron is inserted into the porphyrin still remains controversial, however what is clear is that the ferrochelatase undergoes significant structural reorganisation on substrate binding. Porphyrin binding leads to the reorganisation of several active site residues which ultimately causes closure of the active site mouth (Dailey et al., 2007, Medlock et al., 2007a). One group had suggested that this closure is dependent on the protonation state of the invariant glutamate (E343) (Hunter et al., 2016).

Despite the controversy surrounding the role of the conserved His-Glu pair in catalytic mechanism, it is obvious that they are essential for the ferrochelatase function. Mutagenesis of these residues results in inactive enzymes which are still able to bind porphyrin substrate but unable to turnover (Sellers et al., 2001). They are also likely to take part in the hydrogen bonding network within the active site (Medlock et al., 2009, Dailey et al., 2007).

Crystallographic studies reveal that the π helix can unwind, extend and turn and this occurs once product has formed. The unwinding of the helix is a potential mechanism for product release but presumably rewinding of the helix could provide a different function such as allowing either substrate entry into the active site (Medlock et al., 2007b, Fodje and Al-Karadaghi, 2002). The roles of the other peripheral features of the ferrochelatase active site, the solvent filled channels and the secondary metal binding site, are yet to be fully understood (Medlock et al., 2012, Hobbs et al., 2017, Hunter et al., 2008, Hansson et al., 2006).

An extensive amount of work has been completed to reveal the residues important in the enzymatic mechanism of ferrochelatase and further investigation using techniques such as stopped flow fluorescence/ absorbance spectroscopy can be used to build a detailed enzymatic mechanism (Dailey et al., 2007, Medlock et al., 2007a, Sellers et al., 2001, Hansson et al., 2007, Hunter and Ferreira, 2010, Hunter et al., 2016, Asuru and Busenlehner, 2011, Hoggins et al., 2007).

1.3.5 Kinetic characterisation of ferrochelatase

1.3.5.1 Steady state kinetics

Steady state kinetics have been utilised to define the activity of several different ferrochelatases (Sellers et al., 2001, Hoggins et al., 2007, Hobbs et al., 2017, Lobo et al., 2015, Hansson et al., 2007, Hunter et al., 2008). Most steady state kinetics were performed on a mutant of the *H. sapiens* ferrochelatase, R115L, as this ferrochelatase variant has comparable activity to the wildtype and was more stable. The steady state kinetic parameters for this ferrochelatase were deduced using UV-Vis spectroscopy: the K_m for iron (K_m^{Fe}) and deuteroporphyrin IX (K_m^{DIX}) were approximately 7.7 µM and 5.5 µM, respectively and the V_{max} was 1.21 µM min^{-1} (Hoggins et al., 2007). Several site-directed mutants of *H. sapiens* ferrochelatase have been produced targeting amino acid residues in the active site (H263, E343, R164, Y165, H341, F337, D340). These mutants were kinetically characterised using steady-state kinetics allowing comparison to the R115L mutant/ wildtype ferrochelatase (Sellers et al., 2001, Dailey et al., 2007). Combining the kinetic data of the mutants can give an indication of which residues are important in different aspects of the catalytic mechanism for an example some residues are important in iron binding, porphyrin binding or substrate turnover.

Sellers et al. completed extensive work on the kinetically characterising *H. sapiens* ferrochelatase and its mutants. Mutation of the residues D340, E343 and E347 resulted in negligible activity when mutated to alanine but when mutated conservatively these resulted in a decrease in V_{max}. There was no change in the K_m for either substrate suggesting that they are not important in substrate binding. Mutation of the aromatic residues Y165, W227 and T191 caused an increase in K_m^{Fe}

and Y123 mutation affected the V_{max} of ferrochelatase suggesting that the majority of the aromatic residues listed are important in binding iron or entry of iron into the active site. The mutation R164L causes a 2-fold increase in K_m^{Fe} and the double mutant R164L/Y165F (section 1.3.4.3) increases the K_m^{Fe} 6-fold and decreases k_{cat} 10-fold, this could be have a role in iron binding and these residues are hypothesised to bind iron prior to porphyrin metalation, as previously discussed (Sellers et al., 2001).

1.3.5.2   Transient kinetics

When kinetically characterising proteins, steady state kinetics are not sufficient to completely characterise the enzymatic mechanism. Steady state kinetics look at the overall reaction mechanism, encompassing all steps in the reaction. When looking at the effect of amino acid residue mutation on the activity of the enzyme, steady state kinetics is able to give an insight to the importance of the residue in the enzyme mechanism but not much more. Transient kinetics is capable of teasing out the rates of each step in the mechanism using different experiments and comparison of the wildtype and the site directed mutants can give a better insight to the role of the residue in the catalytic mechanism.

Limited transient kinetic investigation has been completed on ferrochelatase; these investigations have used human ferrochelatase or yeast ferrochelatase (Hunter et al., 2016, Gillam et al., 2018, Hoggins et al., 2007). Transient kinetics performed by Hunter et al., and Gillam et al., mainly focus on the pH-dependence of the ferrochelatase reaction. Hoggins et al., looks at enzymatic mechanism of ferrochelatase and the active site residues involved.

Hoggins et al. completed both steady state and transient kinetics on ferrochelatase to understand the role of a particular mutant (E343D) in the enzymatic mechanism. The activity of the R115L mutant with wildtype activity was compared to the R115L/E343D double mutant. From the steady-state kinetics of these two proteins the kinetic parameters k_{cat}, K_m^{Fe} and K_m^{DIX}, were obtained. The K_m^{Fe} values were 7.7 μM and 8.2 μM for the R115L and R115L/E343D, respectively and the K_m^{DIX} values were 5.5 μM (R115L) and 5.8 μM (R115L/E343D) showing relative consistency between the two proteins. The k_{cat} values were 1.21 μM min^{-1} (R115L) compared to 0.16 μM min^{-1} (R115L/E343D) suggesting that the mutation doesn't affect the binding of the substrates but is important in another aspect of the enzymatic mechanism (Hoggins et al., 2007).

Transient kinetics can be obtained using stopped flow absorbance or fluorescence. The transient kinetics undertaken by Hoggins et al. suggests that the mutation E343D effects several different stages in the enzyme mechanism. The concentration of active enzyme was determined using an active site titration. The E343D mutant has a substantially lower k_{cat} value and the metal chelation rates (k_{chel}) (potentially metal chelation with an isomerisation) were much greater than k_{cat} at 0.96 s^{-1} (R115L) and 0.3 s^{-1} (R115L/E343D). The substantially greater k_{chel} compared to the k_{cat} suggests that there is another much slower step involved in the enzymatic mechanism after metal insertion; this is most likely product release (Hoggins et al., 2007).

These transient kinetic studies reveal that metal chelation is fast and is not the rate determining step. There is a slower, rate determining step after metal chelation which

is most likely product release. The E343D mutant is not important in substrate binding but is important in another part of the mechanism. Mutation of E343 to aspartate (E343D) results in a 7-fold decrease in k_{cat} and a 3-fold decrease in k_{chel}, suggesting that it is involved in the iron chelation but may be important in other enzymatic steps as well. Hoggins et al. shows how powerful transient kinetics can be in deducing the enzymatic mechanism of ferrochelatase (figure 1.29) and the importance of particular residues (Hoggins et al., 2007).
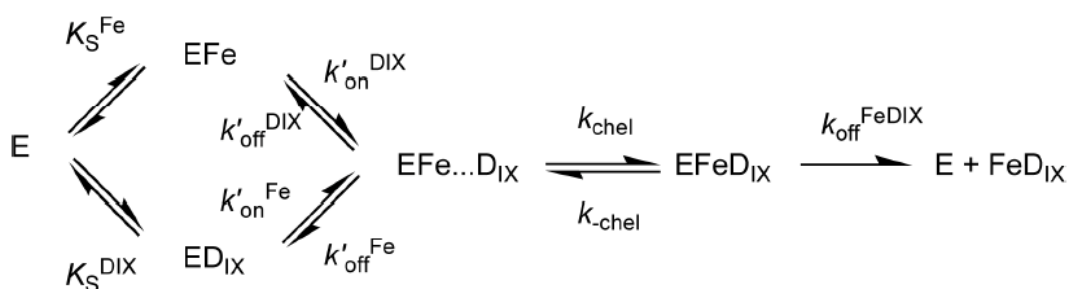
Figure 1.29 - Schematic for the mechanism of iron insertion into deuteroporphyrin IX by human ferrochelatase (FC)

This enzymatic scheme has been taken from Hoggins et al.; it shows how transient kinetics can be used to expand a simple enzymatic scheme to a more complex but more accurate scheme. **Abbreviations**: D_{IX} (deuteroporphyrin), **E** (enzyme/ ferrochelatase), **Fe** (ferrous iron, Fe^{2+}).

1.3.5.3   General considerations for kinetics studies on FC

In most kinetic studies particularly on the *H. sapiens* ferrochelatase, the endogenous substrates, protoporphyrin IX and ferrous iron have not been used. This due to the unstable nature of both substrates in solution. PP_{IX} is very hydrophobic and as a result the molecules stack and produce insoluble aggregates. Ferrous iron can be easily oxidised to produce ferric iron, which is not a substrate for ferrochelatase. Generally, the alternative substrates used are deuteroporphyrin (D_{IX}) and sometimes MP_{IX} and

zinc. The porphyrins D_{IX} and MP_{IX} are more soluble than PP_{IX} and zinc cannot be oxidised (Hunter et al., 2008, Davidson et al., 2009).

In experiments completed by Davidson et al., the kinetic properties of *H. sapiens* ferrochelatase was explored. These assays used zinc as the metal ion and D_{IX} as the porphyrin substrate. Despite the fact that these are not the physiological substrates information about the catalytic mechanism can still be obtained, however it is reasonable to assume that experiments undertaken may not relate to physiological behaviour of ferrochelatase. Deviation in the results could also occur as zinc can insert into porphyrin uncatalysed and non-physiological substrates could bind in the active site differently (Davidson et al., 2009). All the same, zinc binds to ferrochelatase in a very similar way to iron and is a more modest structural variation than site-directed mutagenesis of many amino acid side chains (Medlock et al., 2007a, Davidson et al., 2009, Hunter et al., 2008).

Zinc acts as a detergent-dependent uncompetitive substrate inhibitor as the kinetic behaviour alters in the presence of the detergent cholate. Zinc inhibition is dependent on the deuteroporphyrin concentration suggesting that zinc is the second substrate to bind. Also, a significant amount of the inhibited complex must accumulate for the inhibition to occur, implying that release of the metalloporphyrin may be rate limiting. Furthermore, as the addition of detergents like cholate alter the kinetic properties of the enzyme, this should be taken into consideration when undertaking kinetics studies on ferrochelatase (Davidson et al., 2009).

1.4 Thesis aims

Heme biosynthesis is an essential pathway in bacteria, if an enzyme in the pathway, for example ferrochelatase is knocked out it is lethal to the bacteria. Gram positive bacteria synthesise heme using the coproporphyrin-dependent pathway, which was discovered in 2015. Since the discovery of the coproporphyrin-dependent pathway, little work has been completed on the coproporphyrin ferrochelatases. The protoporphyrin ferrochelatases in the protoporphyrin-dependent pathway are well characterised especially *H. sapiens* ferrochelatase. Investigating the enzymatic mechanism of the coproporphyrin ferrochelatases kinetically and structurally could lead to the design of new antibiotics specifically targeting Gram positive bacteria.

The *P. acnes* (Gram positive bacterium) ferrochelatase is covalently linked (connected by a linker) to the subsequent enzyme in the coproporphyrin-dependent heme biosynthetic pathway, coproheme decarboxylase. This linkage is only found in this species and not in other Gram positive bacteria, which utilise the same heme biosynthesis pathway. This suggests that there may be a potential interaction between the coproporphyrin ferrochelatase and coproheme decarboxylase protein or a mechanism whereby the porphyrin molecule gets transferred directly from one protein to the other. If the two enzymes do interact then drugs can be designed which target the protein-protein interactions. In the first results chapter, I describe my investigation of the protein-protein interactions between *P. acnes* HemH and HemQ and the substrate transfer between the two proteins. Protein-protein interactions between other HemH and HemQ proteins from different bacterial species were also tested.

The *B. subtilis* ferrochelatase (coproporphyrin ferrochelatase) expresses and purifies well. However, when assayed in previous work the porphyrin substrates used were analogues of protoporphyrin IX and not of coproporphyrin III. This resulted in a ferrochelatase that appeared largely inactive and did not reflect the true activity of the *B. subtilis* ferrochelatase (Hansson et al., 2007). Since discovery of the coproporphyrin-dependent pathway there is little kinetic characterisation of Gram positive bacteria ferrochelatases (CpFC) with their physiological porphyrin substrate, coproporphyrin III. The apoprotein structure and N-methyl mesoporphyrin bound structure of *B. subtilis* ferrochelatase were resolved using X-ray crystallography (Al-Karadaghi et al., 1997). There are currently no existing structures of *B. subtilis* ferrochelatase bound to its porphyrin substrate coproporphyrin III.

The second results chapter describes the kinetic characterisation of the wildtype *B. subtilis* and *S. aureus* ferrochelatase using the physiological porphyrin substrate, coproporphyrin III. This characterisation has used both steady state kinetics and transient kinetics and a combination of UV-visible and fluorescence spectroscopy. Crystal trials have been performed on *B. subtilis* ferrochelatase in the presence of coproporphyrin to structurally resolve the ferrochelatase bound to its endogenous substrate. To date, this has been unsuccessful.

The role of active site residues in the *H. sapiens* ferrochelatase have been extensively explored by site-directed mutagenesis. This has not been completed for any ferrochelatase present in the coproporphyrin-dependent pathway in the presence of the physiological substrate. Using the same methods used to characterise the wildtype

ferrochelatases (*B. subtilis* and *S. aureus*), the active site mutants of *B. subtilis* ferrochelatase (K87A, H88A, H183A, E264A, E264Q) have also been characterised. This provides information on the role of the residues in the catalytic mechanism. The apoprotein structure of the *B. subtilis* ferrochelatase mutants H183A and K87A have already been resolved (Karlberg et al., 2008, Hansson et al., 2007). Crystal trials of K87A, H88A and E264A mutants in the presence of coproporphyrin III have been performed. The final results chapter aims to explore the role of individual amino acid side chains in the catalytic mechanism of *B. subtilis* ferrochelatase and investigate their effect on the active site structure.

2. Materials and Methods

2.1 Producing calcium competent cells

E. coli cell strains BL21, BL21-DE3, Rosetta and JM109 cells were streaked out on LB agar plates and incubated at 37 °C overnight. A single colony was selected and grown in 10 mL of LB media overnight at 37 °C; this was used to inoculate a larger volume of LB media (500 mL). After inoculation, the cells were grown at 37 °C on a shaker until a suitable optical density (OD) was reached (0.6-0.8). The optical density was measured at 600 nm on a Cary 50 UV-Vis spectrometer.

Once a suitable optical density was reached, the cells were incubated at 4 °C for 1 hour. A small volume of the growth (50 mL) was pelleted (Eppendorf 5810R centrifuge) and the supernatant was discarded. The was pellet resuspended in 10 mL 0.1 M $CaCl_2$, the suspension was incubated at 4 °C for 15 minutes before it was pelleted again. This was repeated using 5 mL 0.1 M $CaCl_2$ for resuspension. The final resuspension was in 1.5 mL 0.1 M $CaCl_2$ and 15% glycerol and the cells were snap frozen and stored at -80 °C. The centrifuge conditions were 1744 ×g, 10 minutes and 4 °C. All buffers and equipment used were pre-cooled to 4 °C beforehand and conditions remained sterile throughout.

2.2 DNA sequencing and gene cloning of *hemH* and *hemQ* genes from different Gram positive bacterial species

2.2.1 DNA sequencing of P. acnes *hemH-Q,* S. aureus *hemH and* S. aureus *hemQ and* B. subtilis *hemH*

The *P. acnes hemH-Q* plasmid construct was sequenced (Core Genomic Facility, University of Sheffield) using primers HemHQ-For 193, HemHQ-For 949, HemHQ-1262 and HemHQ-Rev 264 (table 2.1). The *S. aureus hemH* plasmid was sequenced (GATC Biotech) using the primers *S. aureus* HemH-For 179, HemH-For 671, HemH-Rev 30 and HemH-Rev 574 (table 2.1). Sequencing for *S. aureus hemQ* was attempted using *S. aureus* HemQ-For 8, HemQ-For 600, HemQ-Rev 67 and HemQ-Rev 685 and *B. subtilis hemH* sequencing was attempted using the primers N-term-For and C-term-Rev (GATC Biotech).

2.2.2 Production of P. acnes hemH-Q *truncations*

Structural alignments were performed on HemH (*P. acnes*, *S. aureus*, *B. subtilis*, *E. coli*, *H. sapiens* and *S. cerevisiae*) and HemQ (*P. acnes*, *S. aureus*, *B. subtilis*, *M. tuberculosis* and *A. meyeri).* The *P. acnes* HemH-Q fusion protein was included in both alignments. This used the alignment software PRALINE (Pirovano and Heringa, 2010). The results from the PRALINE alignment were used define crude boundaries the HemH, HemQ and the linker regions in *P. acnes* HemH-Q (not shown). The primers for the *P. acnes* HemH-Q truncations were designed from the results of DNA sequencing and the PRALINE structural alignment. The constructs designed were *P.*

acnes hemH (± linker or long/short) and hemQ (± linker or long/short); the plasmid containing the whole hemH-Q gene was used as the template DNA.

The Q5 site directed mutagenesis kit was used to amplify the DNA using the standard protocol supplied by the manufacturer. All primers were from Sigma-Aldrich and diluted in Milli-Q water to produce a primer solution of 100 µM. Further dilution resulted in a stock solution of 10 µM, the primer sequences are listed in table 2.1.

Four truncations of *P. acnes hemH-Q* were produced *hemHS* (*hemH* without the linker, *hemH* short), *hemHL* (*hemH* with the linker, *hemH* long), *hemQS* (*hemQ* without the linker, *hemQ* short) and *hemQL* (*hemQ* with the linker, *hemQ* long). The *hemHS* construct was cloned using the primers HemH-For and HemH Short-Rev whereas *hemHL* used the same forward primer (HemH-For) and a different reverse primer, HemH Long-Rev. They both used an annealing temperature of 58 °C and their extension times were 180 seconds and 300 seconds, respectively. The *hemQS* construct was amplified using the primers HemQ Short-For and HemQ-Rev (table 2.1); *hemQL* required a different forward primer, HemQ Long-For. Both the *hemQ* truncations were produced using the same conditions: an annealing temperature of 58 °C and an extension time of 165 seconds.

Table 2.1 - PCR conditions for *P. acnes* hemH-Q and *B. subtilis* hemH mutants

SPECIES	GENE CONSTRUCT	OLIGO NAME	SEQUENCE (5'-3')
B. subtilis	*K87A hemH*	K87A For	GACTGGCGCATA
		K87A Rev	ATAAACGGCTCGA
	H88A hemH	H88A For	GCGTATATCGGACT
		H88A Rev	GCTCGATAGCCTTC
	H183A hemH	H183A For	TATCCGCAGCCAG
		H183A Rev	GATTTTTTCGGCAGG
	E264A hemH	E264A For	TTGTCGCGGATC
		E264A Rev	AGCACTGCTAAGT
	E264Q hemH	E264Q For	TCGCGGATCACT
		E264Q Rev	AATCATAAAGCACTTGTA
P. acnes	*hemQ*	HemQ-Rev	GCTAGCCATACCATGAT
		HemQ Long-For	GCGGCTCGTGGTGAGGGT
		HemQ Short-For	CCCGAGGAGGTCAACGCC
	hemH	HemH-For	AAGCTTGGCTGTTTTGGCGG
		HemH Long-Rev	AATGACCGGGGTATCGCG
		HemH Short-Rev	CGCGGCCTGGGACAAGATG
	hemH-Q	HemHQ-For 193	CCGATTAACGATGCGA
		HemHQ-For 949	TTTATCGCTGATCTCGCCG
		HemHQ-For1262	CCATGTCTGATCATTCGAGT
		HemHQ-Rev 264	TCCAGTGCTGTTAGGGA
S. aureus	*hemH*	HemH-For 179	ATGACCAGGCTGATGC
		HemH-For 671	ATACAGGTACACCTTGG
		HemH-Rev 30	AGGTGTGCCATAAGCC
		HemH-Rev 574	TCTTGTGGATATGGATCATT
	hemQ	HemQ-For 8	AAGCAGCCGAAACATTAG
		HemQ-For 600	AACATTGTTCTCAGATGACG
		HemQ-Rev 67	TGGAACTAGACGTAATGATGC
		HemQ-Rev 685	CCTACAAAGAAACTACCGAA
All three species	*hemH, hemH-Q*	N-term-For	ATCATGGTATGGCTAGC
		C-term-Rev	GGCTGAAAATCTTCTCTCATC

2.2.3 Production of B. subtilis *hemH mutants by gene cloning*

The *B. subtilis hemH* gene was subjected to site directed mutagenesis causing single-or double-point mutations resulting in a single amino acid change. The site-directed mutants produced were K87A, H88A, H183A, E264A and E264Q *hemH*. The primers for these mutants were designed using the NEBaseChanger. The plasmid containing the *B. subtilis hemH* gene (pTrcHisA-*B. subtilis hemH*) was used as the DNA template. Cloning of the four of the mutants (K87A, H88A, E264A and E264Q) required the extension time of 180 seconds and the H183A mutants had an extension time of 300 seconds. The annealing temperatures for the mutations at residue E264 (E264A and E264Q) were 62 °C, for K87A, H88A and H183A they were 54 °C, 60 °C and 61 °C, respectively.

Table 2.2 – PCR conditions for *P. acnes hemH-Q* truncations and *B. subtilis* mutants

SPECIES	GENE CONSTRUCT	ANNEALING TEMPERATURE / °C	EXTENSION TIME / s
P. acnes	*hemHS*	58	180
	hemHL	58	300
	hemQS	58	165
	hemQL	58	165
B. subtilis	K87A	54	180
	H88A	60	180
	H183A	61	300
	E264Q	62	180
	E264A	62	180

2.3 Transformation of *E. coli* into a cloning strain and polymerase chain reaction (PCR) of gene

The KLD (Kinase, Ligase & DpnI) reaction was used to re-circularise the linear plasmids gained from PCR and degrade the template DNA. This reaction was performed using the manufacturer's instructions with a room temperature incubation of 30 minutes instead of 5 minutes. The circularised plasmid was introduced to DH5α *E. coli* and incubated on ice of 30 minutes. Heat shock at 42 °C for 45 seconds allowed entry of the plasmid into the *E. coli*. The *E. coli* cells were incubated on ice for a further 15 minutes and then incubated in 950 µL of SOC media (New England Biolabs Inc.) for 90 minutes at 37 °C. A volume of 50 µL was plated onto agar plates containing 100 µg mL^{-1} ampicillin and incubated overnight at 37 °C.

To obtain DNA for sequencing after mutagenesis, a single colony from the agar plate was used to inoculate a small volume of LB media and grown at 37 °C overnight. Plasmid DNA was isolated using the QIAGEN Miniprep kit. In most cases the plasmid DNA was used as a template in a second PCR, this amplified the segment of the plasmid containing the gene. The primers used for this PCR were N-term For and C-term Rev, (extension time of 60 seconds, an annealing temperature 58 °C). The DNA fragments were purified using the QIAGEN PCR clean up kit as per the manufacturer's instructions. The *S. aureus hemH* and *hemQ* plasmids were sequenced directly whereas all other constructs underwent the second PCR step and the fragment produced was sequenced. The sequencing primers used was N-term For and C-term Rev (table 2.1), the same primers used to amplify the fragment. The DNA was

sequenced by GATC Biotech and analysis of sequencing data used MEGA X and BioEdit.

2.4 Protein Expression

2.4.1 Insertion of plasmids into expression E. coli strains

All available plasmids were inserted into the *E. coli* strains BL21, BL21-DE3, Rosetta and JM109 as described in section 2.2. Expression trials were performed if the protein yield was low.

2.4.2 Expression trials

Protein expression trials for *S. aureus* HemH and HemQ, *P. acnes* HemHL, HemHS and HemQL and *B. subtilis* H183A were completed in three different *E. coli* cell lines (BL21, BL21-DE3 and Rosetta) and using two different growth mediums (LB and 2YT). *P. acnes* HemHS expression trials were more extensive, it was also trialled in JM109 *E. coli* in combination with CircleGrow media. Cell lines BL21, BL21-DE3 and Rosetta were also tested at different pre-induction temperatures in LB, 2YT media (37 °C, 30 °C and 18 °C) and ZYM-5052 auto-induction media (30 °C and 37 °C). The expression trial combinations are shown in table 2.3.

Expression trials were run in small volumes, 5 mL of media was inoculated with 50 µL of starter culture, most commonly incubated at 37 °C. In the LB and 2YT media the BL21, BL21-DE3 and Rosetta *E. coli* required induction by IPTG (isopropyl β-D-1-thiogalactopyranoside). The growths were allowed to reach an optical density of 0.6-

0.8 and 0.5 mM of IPTG was used for induction. After the addition of IPTG the temperature was reduced to 18 °C and these were incubated for 18 hours, 1 mL of the growths was centrifuged at 6000 ×g for 10 minutes, the supernatant was discarded, and the pellet resuspended. A sample was taken from the resuspended pellet and used for SDS-PAGE (sodium dodecyl sulphate polyacrylamide gel electrophoresis) analysis.

The H183A *B. subtilis* mutant protein was found in inclusion bodies, additional trials were completed to solubilise the protein during expression. Pre and post induction temperatures were lowered (18 °C) and a one hour 4 °C incubation was completed prior to IPTG induction.

Table 2.3 Protein expression conditions for *S. aureus* HemH and HemQ and the *P. acnes* truncations

SPECIES	PROTEIN	*E. coli* STRAIN	MEDIA	TEMPERATURE
S. aureus	HemH	BL21	2YT	Pre induction – 37 °C
		BL21-DE3	LB	Post induction – 18 °C
		Rosetta		
	HemQ	BL21	2YT	Pre induction – 37 °C
		BL21-DE3	LB	Post induction – 18 °C
		Rosetta		
P. acnes	HemHS	BL21	2YT	Pre induction – 18 °C,
		BL21-DE3	LB	30 °C and 37 °C
		Rosetta	ZYM-5052	Post induction – 18 °C
				30 °C and 37 °C
		JM109	CircleGrow	30 °C
	HemHL	BL21	2YT	Pre induction – 18 °C,
		BL21-DE3	LB	30 °C and 37 °C
		Rosetta		Post induction – 18 °C
	HemQL	BL21	2YT	Pre induction – 18 °C,
		BL21-DE3	LB	30 °C and 37 °C
		Rosetta		Post induction – 18 °C
B. subtilis	H183A HemH	BL21	2YT	Pre induction – 18 °C,
		BL21-DE3	LB	30 °C and 37 °C
		Rosetta	ZYM-5052	Post induction – 18 °C

2.4.3 Full scale protein expression

2.4.3.1   *Standard expression protocol and expression cell lines*

P. acnes HemH-Q, *P. acnes* HemQS, *P. acnes* HemQL and *B. subtilis* HemH were expressed in Rosetta *E. coli.* The *B. subtilis* mutants (K87A, H88A, H183A, E264A and E264Q) were expressed in BL21-DE3 *E. coli* and *P. acnes* HemHL, *P. acnes* HemHS and *S. aureus* HemQ were expressed in BL21 *E. coli*. Finally, *S. aureus* HemH

was expressed in JM109 *E. coli.* All proteins except *S. aureus* HemH were expressed in LB media. *S. aureus* HemH required CircleGrow media.

One colony of *E. coli* cells containing desired gene was grown in 20 mL of LB media at 37 °C for 18 hours. Half of the starter culture was used to inoculate 1 L of LB media and this was grown at 37 °C until the growth obtained an OD reading of 0.6-0.8. Protein expression was induced by the addition of 0.5 mM IPTG and the temperature was reduced to 18 °C, for 18 hours. Ampicillin (100 µg mL^{-1}) was added to the growth media. The cells were harvested by centrifugation at 5488 ×g, for 20 minutes at 4 °C. The resulting pellets were stored at -80 °C.

The expression of *S. aureus* HemH involves used a different expression protocol. The starter culture was produced in the same way and 10 mL was used to inoculate 1 L of CircleGrow media. The *E. coli* was grown at 30 °C for 24 hours and expression was not induced. The cells were harvested as above and ampicillin (100 µg mL^{-1}) was present throughout.

2.4.3.2   *Different* P. acnes *HemHS expression conditions*

Different growth conditions were used to express *P. acnes* HemHS. Firstly, HemHS was expressed in LB media and induced using IPTG using the same method described in section 2.3.5 however; this was attempted in three of the *E. coli* cell lines (BL21, BL21-DE3 and Rosetta). This protocol was also altered where the initial

incubation temperature before protein induction was changed from 37 °C to 30 °C and 18 °C.

2.5 Protein Purification

2.5.1 Preparation of protein sample for immobilised metal affinity chromatography (IMAC)

E. coli cell pellets stored at -80 °C, were defrosted and resuspended in binding buffer (50 mM Tris, 100 mM KCl, pH 8). At this point protease inhibitors were added, most commonly Roche cOmplete mini EDTA (ethylenediaminetetraacetic acid) free (Sigma Aldrich) but sometimes SigmaFast protease inhibitor cocktail (EDTA free) (Sigma Aldrich) or Pefabloc SC (Sigma Aldrich). Protease inhibitors were solubilised in MilliQ water before they were added to the cell pellet suspension. The resuspended cells were lysed using pulse sonication at 10 μm in ice, each pulse lasted for 30 seconds with 60 second rests in between, this was repeated six times. The lysate was centrifuged at 26902 ×g for 45 minutes at 4 °C separating the soluble and insoluble cell pellet fractions.

2.5.2 Purification using IMAC

All proteins (*P. acnes* HemH-Q, *P. acnes* HemHS, *P. acnes* HemHS, *P. acnes* HemQS, *P. acnes* HemQL, *B. subtilis* HemH, *B. subtilis* K87A HemH, *B. subtilis* H88A HemH, *B. subtilis* H183A HemH, *B. subtilis* E264A HemH, *B. subtilis* E264Q HemH, *S. aureus* HemH and *S. aureus* HemQ) used IMAC as their first purification step as all contain a N-terminal 6x histidine tag. The soluble fraction or supernatant after lysis and centrifugation was applied to a pre-equilibrated nickel/ cobalt column. *P. acnes* HemH-

Q, *P. acnes* HemQS, *P. acnes* HemQL, *B. subtilis* HemH and *S. aureus* HemQ used columns containing nickel resin in the form of a 1 mL His GraviTrap or a 1 mL or 5 mL HisTrap (GE Healthcare Life Sciences). *P. acnes* HemHL, *B. subtilis* mutants (K87A, H88A, H183A, E264Q and E264A) and *S. aureus* HemH use columns containing cobalt resin (TALON), these were in the form of 1 mL His GraviTrap TALON (GE Healthcare Life Sciences). During the optimisation of *P. acnes* HemHS purification, both cobalt and nickel resin were used.

After initial protein binding to the column the resin was washed with 20 CV (column volumes) of high salt buffer (50 mM Tris, 1 M KCl, pH 8). The resin was washed with 10 CV of low imidazole buffer (50 mM Tris, 100 mM KCl, 10-30 mM imidazole, pH 8). The protein was eluted from the column in 5 CV of elution buffer (50 mM Tris, 100 mM KCl, 300 mM imidazole, pH 8). The purification protocol of *S. aureus* HemH did not contain the high salt wash. In some experiments *S. aureus* HemH was purified using buffers that contained an addition of 1% sodium cholate and 50 mM MOPS (3-(N-morpholino) propanesulfonic acid). These conditions were also used in an attempt to solubilise H183A *B. subtilis* HemH.

Proteins that were successfully purified by IMAC (*B. subtilis* HemH mutants, *P. acnes* HemHL, *P. acnes* HemQS, *S. aureus* HemH) were desalted using a manually poured Sephadex G50 column into binding buffer to remove imidazole and stored at -80 °C. Those that required further purification (*P. acnes* HemH-Q, *P. acnes* HemQL, *B. subtilis* HemH and *S. aureus* HemQ) were also desalted in preparation for ion exchange chromatography (IEX).

2.5.3 Purification using ion exchange chromatography (IEX)

P. acnes HemH-Q, *P. acnes* HemQL, *B. subtilis* HemH and *S. aureus* HemQ required further purification after IMAC and so they were purified further using IEX. A Q Sepharose 5 mL HiTrap FF column (GE Healthcare Life Sciences) was used for IEX. The column was equilibrated in low salt buffer (50 mM Tris, pH 8) and a gradient of salt from 0 - 0.5 M was applied over 10 CV and 0.5-1 M over 5 CV. Proteins that successfully purified after IEX were stored at -80 °C.

2.5.4 Optimisations for P. acnes *HemH-Q purification*

2.5.4.1   Size exclusion chromatography (SEC)

Steps to optimise the purification protocol for *P. acnes* HemH-Q included using SEC. The SEC column used was a HiLoad Superdex 26/600 200 PG column (GE Healthcare Life Sciences). The column was pre-equilibrated in binding buffer and the protein sample containing *P. acnes* HemH-Q was applied directly to the SEC column after elution off the IMAC. The column was run for 1 CV. This purification was also repeated in two different conditions these were high salt (1 M KCl) and 1 M urea.

2.5.4.2   IMAC of P. acnes *HemH-Q in denaturing conditions*

P. acnes HemH-Q was purified in the presence of 1 M urea and 8 M urea. This was performed in the same way as the standard IMAC procedure described earlier in section 2.5.2 however, the buffers used contained either 1 M urea or 8 M urea. The 1 M urea preparation was then purified further by SEC also in the presence of 1 M urea. Due to the high viscosity of 8 M urea, SEC was not attempted under these conditions.

2.5.4.3 Treatment with EDTA to inhibit metalloproteases

To improve the yield of *P. acnes* HemH-Q 5 mM EDTA was added to cell suspension along with protease inhibitor cocktail (SigmaFast) before sonication. EDTA was added to inhibit *E. coli* metalloproteases. The cells were lysed and centrifuged as described above in section 2.5.1. The soluble fraction was treated with ammonium sulphate (80% saturation) and incubated at 4 °C for 30 minutes to pellet *P. acnes* HemH-Q. The sample was centrifuged 10,000 ×g for 15 minutes at 4 °C and the resulting pellet was resuspended in binding buffer before application to a 1 mL His GraviTrap column. Ammonium sulphate precipitation removed the EDTA before IMAC.

2.5.5 Optimisations for P. acnes HemHS purification

2.5.5.1 Solubilising P. acnes HemHS using detergents and high salt

The *P. acnes* HemHS cell pellet was resuspended in binding buffer containing either 2 % Triton-X-100, 1 % sodium cholate, 15 mM CHAPS (3-[(3-cholamidopropyl) dimethylammonio]-1-propanesulfonate hydrate) or 500 mM KCl. Cell lysis occurred by sonication and the lysate was centrifuged as in section 2.5.1. The HemHS content in the lysate, insoluble and soluble fractions were analysed by SDS PAGE (section 2.6).

2.5.5.2 Denaturing preparations of P. acnes HemHS

The cell pellet was resuspended in binding buffer, lysed by sonication and centrifuged (section 5.2.1). The insoluble fraction (pellet) was resolubilised in binding buffer containing 8 M urea and centrifuged (26902 ×g, 20 mins, 4 °C). The supernatant was applied to a pre-equilibrated 1 mL His GraviTrap, the column was washed with 20 CV

of high salt buffer containing 8 M urea and then 10 CV of a low imidazole wash also in 8 M urea. When attempting on column refolding the urea concentration was lowered in 1 M steps until the urea concentration reached 1 M then there was a final wash of 500 mM urea before the protein was eluted of the column in elution buffer containing no urea (5 CV). Each of the low imidazole washes were 5 CV.

2.6 Polyacrylamide gel electrophoresis (PAGE)

2.6.1 SDS-PAGE

The gels for SDS-PAGE were handmade, the resolving gel had an acrylamide concentration of 8-12 % and the stacking gel was 4-6 % acrylamide. The gel buffer solutions for each gel component was 1 M Tris, pH 8.8 (resolving) and 1 M Tris, pH 6.8 (stacking). A combination of APS (ammonium persulphate) and TEMED (*N*, *N*, *N'*,*N'*-tetramethylethylene-diamine) were used to polymerise the acrylamide and SDS was used to denature proteins in the sample. After the Laemmli sample buffer containing fresh reducing agent (β-mercaptoethanol) was added to the protein, the samples were loaded into the SDS-PAGE gel. The running buffer used for SDS-PAGE was 1X Tris Glycine SDS running buffer bought as a 10X stock. Each gel was run at 160-200V for 40-55 mins. SDS-PAGE was used to analyse the presence and purity of desired proteins.

2.6.2 Native PAGE

Three different types of native PAGE gels were used in the native PAGE analysis of *P. acnes* HemH-Q: tris glycine, blue native (BN) and a hybrid of the two systems. Tris

glycine gels were made in the same way as the SDS gels described in section 2.6.1 however SDS was excluded. The acrylamide concentration was varied between 6- 10 % and standard Laemmli sample buffer without SDS and reducing agent was used. BN-PAGE gels were prepared similarly using an acrylamide concentration of 8%. The sample buffer for BN-PAGE contained Coomassie G250. The hybrid of the two systems used tris glycine gels and running buffer and the BN-PAGE Coomassie sample buffer. The gels were run at 4 °C for approximately 5 hours, depending on the mobility of the protein through the gel.

2.7 Circular Dichroism (CD)

2.7.1 Denaturing P. acnes HemH-Q

P. acnes HemH-Q was exchanged in to phosphate buffered saline (PBS) and incubated with different concentrations of urea (0-4 M) or different concentrations of isopropanol (0-50 %) overnight. The secondary structure of HemH-Q after incubation was measured using circular dichroism. The spectra were measured between 220 nm and 260 nm (Jasco J-810 Spectrometer), the quartz cuvette used has a path length of 0.1 cm.

2.7.2 Determining secondary structure and thermostability of B. subtilis *HemH and its mutants*

Circular dichroism spectra of *B. subtilis* HemH and its mutants (K87A, H88A, E264A and E264Q) were taken at 200-260 nm (Jasco J-810 Spectrometer).   The

concentration of each protein was 4 μM and the spectra was measured between 200-260 nm. The thermostability was tested for the wildtype and the mutants, the ellipticity was molar residue ellipticity (θMR) was measured at 220 nm between 5-100 °C for unfolding and refolding. The rate of temperature change was 2 °C per minute. The unfolding and refolding data was fitted to the equation 1 allowing the calculation of the thermal melting temperature (T_m). In equation 1 A_B is the θMR at the base of the sigmoid, ΔA is the change in θMR between the top and base of the sigmoid, V_{50} is the temperature with causes a 50% increase in θMR, this is the T_m and slope is the steepness of the curve.

$$y = A_B + \frac{\Delta A}{1 + e^{\frac{V_{50}-x}{Slope}}} \qquad \text{Equation 1}$$

2.8 In-gel tryptic digestion and mass spectrometry (MS)

2.8.1 Destaining and dehydration of gel pieces

The protein band of interest was excised from a 10% SDS-PAGE gel. The excised band was treated with 1 mL destaining solution (50% acetonitrile (ACN) (Sigma Aldrich), 50 mM ammonium bicarbonate (ABC) (Sigma Aldrich)) and incubated on a shaker for 1 hour. The liquid was decanted off and the procedure was repeated twice more, ensuring that the gel pieces containing the protein band were thoroughly destained. The gel was dehydrated using 200 μL of ACN and incubated for 15 minutes, before the liquid was removed. Incubation steps occurred at room temperature and all following incubation steps were also at room temperature unless stated otherwise.

2.8.2 Reduction, alkylation and digestion of protein

The resulting protein sample was reduced using 200 µL 50 mM TCEP (Tris(2-carboxyethyl) phosphine hydrochloride (Sigma Aldrich) and incubated at 56 °C for 1 hour. Alkylation required 200 µL 40 mM iodoacetamide (IAA) and an incubation of 30 minutes in the dark. The supernatant was removed, and the protein sample was washed with 200 µL of 50 mM ABC twice, 15 minutes each time. A third wash used 200 µL of the destaining solution. The gel was dehydrated again as previously stated. The supernatant was removed, and the gel pieces were left for 5 minutes to ensure all ACN had evaporated. Finally, 30 µL of trypsin solution (Sigma Aldrich) was added to the sample and digestion occurred overnight at 37 °C.

2.8.3 Peptide extraction and mass spectrometry

To stop digestion after overnight incubation 15 µL of ACN was added to the digested peptides and incubated for 15 minutes. A 30-minute incubation followed in 150 µL 0.5% formic acid (Sigma Aldrich) and extracted peptides were transferred to a new tube. The following steps were repeated three times: a 15-minute incubation with 100 µL formic acid, 15 minutes incubation with 50 µL ACN and transfer of extracted peptides into tube. The peptides were dried down in a speed-vac and stored at -20 °C.

The dried peptides were resuspended in 40 µL 0.5% formic acid and the resuspended peptides were sonicated in a water bath for 5 minutes. After sonication, the peptides were centrifuged at 12,000 ×g for 5 minutes and transferred into a mass spectrometry vial. The peptide sample was run down a 50 cm C18 liquid chromatography (LC)

column; a gradient of acetonitrile (0-72%) was applied. As the peptides eluted off the column, they were analysed by mass spectrometry.

2.9 Kinetic characterisation of *B. subtilis* HemH and *S. aureus* HemH

2.9.1 Preparation and concentration determination of ferrochelatase and its substrates

2.9.1.1 Concentration determination of ferrochelatase

The concentration of *B. subtilis* HemH and its mutants (K87A, H88A, E264A and E264Q) were determined using an absorbance reading at 280 nm on a NanoDrop (ThermoFisher) with an extinction coefficient of 48820 M^{-1} cm^{-1}. *S. aureus* HemH had an extinction coefficient of 47790 M^{-1} cm^{-1}(Hobb et al., 2017, Lobo et al., 2015). The enzyme concentrations were calculated using the Beer-Lambert law.

2.9.1.2 Ferrous iron solution

Approximately 40 mg of ferrous ammonium sulphate and 9 mg of L-ascorbic acid was solubilised in 20 mL of MilliQ water to form a ferrous iron solution. A small amount of ferrozine was resuspended in 1 mL of MilliQ water. An iron sample was constructed in a 1 mL cuvette: 2 µL iron solution, 100 µL ferrozine and 900 µL Milli-Q water. The concentration of ferrous iron was determined using a Cary 50 UV-Vis spectrometer. Using the measured the absorbance at 563 nm and the extinction coefficient for the

iron ferrozine complex, 28000 M^{-1} cm^{-1} (Stookey, 1970) the concentration of iron can be determined using the Beer-Lambert law.

2.9.1.3   Coproporphyrin III (CP$_{III}$) solution

A small amount of coproporphyrin III dihydrochloride was diluted in 1 mL assay buffer (0.1 M Tris, pH 8). Once completely resuspended the solution was diluted further in assay buffer until at a suitable working concentration. This solution was transferred into black centrifuge tubes and stored at -20 °C.

To determine the concentration of CP$_{III}$, 2 µL CP$_{III}$ solution was added to 1 mL 0.1 M HCl. A Cary 50 UV-Vis spectrometer measured the absorbance between 350-450 nm. The extinction coefficient for coproporphyrin III at 401 nm is 470000 M^{-1} cm^{-1} (Falk, 1964) and the Beer-Lambert law was used to calculate the concentration of CP$_{III}$.

2.9.2 Preliminary kinetics

2.9.2.1   Scanning kinetics

Two experiments were conducted using scanning kinetics to investigate the behaviour of *B. subtilis* HemH and its mutants. The first experiment used looked at absorbance peaks change in absorbance as the reaction progressed. The wildtype HemH was assayed with its substrates ferrous iron and coproporphyrin III in assay buffer (0.1 M Tris, pH8.0). The reaction was monitored between 350-600 nm and a spectrum was taken every 30 seconds for 30 minutes. In these assays the ferrous iron concentrations

were 0.8 μM, 8 μM or 80 μM and the CP_{III} concentrations were 2 μM and 10 μM. The ferrochelatase concentration for each of these assays was 50 nM. These spectra were monitored on a Cary 1 UV-Vis spectrometer at 25 °C.

The second experiment looked at spectral shifts that occurred when CP_{III} was bound to enzyme. The spectral shifts were monitored between 350-450 nm, each scan was 6 seconds for the first 10 minutes and every 30 s a spectrum of 2 uM CPIII was recorded. Firstly, in wildtype *B. subtilis,* to ensure the spectral shifts were a result of enzyme-substrate complex (2 μM CP_{III} and 2 μM HemH), the complex was denatured in ~30% ethanol. The samples were also spiked with 10 μM $ZnCl_2$ to replicate zinc contamination. The wildtype *S. aureus* HemH and *B. subtilis* HemH and the *B. subtilis* HemH mutants' spectral properties in the presence of porphyrin were also investigated. Initially, the spectra of 2 μM CP_{III} were recorded, then 2 μM of ferrochelatase was added. The spectral shift was monitored and when complete 20 μM ferrous iron was added and the further reaction was monitored. This was also performed for each of the *B. subtilis* HemH mutants (K87A, H88A, E264Q and E264A) and *S. aureus* HemH. These spectra were monitored on a Cary 1 UV-Vis spectrometer at 25 °C.

2.9.2.2 B. subtilis *and* S. aureus *HemH activity assays*

The progression of the reaction between *B. subtilis* HemH and *S. aureus* HemH and its substrates was monitored by a Cary 1 UV-Vis spectrometer at 25 °C at 393 nm. The absorbance was monitored continuously until the endpoint of the reaction was reached. The ferrous iron concentration was either 50 μM or 100 μM, the CP_{III} concentration was 4 or 10 μM and the ferrochelatase concentration remained constant

at 0.2 µM. The molar extinction coefficient for the reaction was calculated as 70410 M^{-1} cm^{-1}. To compare the activity of the *B. subtilis* HemH mutants, endpoint assays were completed on them using 0.2 µM enzyme, 4 µM CP_{III} and 50 µM ferrous iron.

2.9.3 Steady State Kinetics

The steady-state kinetic parameters of *B. subtilis* HemH and *S. aureus* HemH were determined using the substrates ferrous iron and coproporphyrin III in a spectrophotometric assay on a Cary 1 UV-Vis spectrometer at 25 ˚C.

In wildtype *B. subtilis* HemH, *S. aureus* HemH and *B. subtilis* H88A HemH the change in absorbance was monitored at 393 nm and the enzyme concentration remained constant at approximately 10 nM (when CP_{III} is varied) or 0.1 µM (when iron is varied). Whilst one substrate was held at saturating conditions the other was varied. The concentration of iron was varied between 0-200 µM and the CP_{III} concentration was held at approximately 0.5 µM, 1 µM, 1.7 µM (*B. subtilis* HemH only) and 2 µM in the wildtype proteins. In the H88A mutant the CP_{III} concentration was held at 2 µM and the different iron concentrations were repeated in triplicate. When the concentration of CP_{III} was varied (0-4 µM), iron was held at approximately 5 µM, 10 µM or 100 µM when assaying the wildtype proteins. In the H88A mutant the iron concentration was held at 100 µM and the different CP_{III} concentrations were repeated in triplicate. Rates for each reaction were calculated from the instrument software and converted into µM s^{-1} using the extinction coefficient for the reaction. The data were further processed by dividing the rate by the enzyme concentration to obtain values independent of enzyme concentration. These values were plotted against substrate concentration using Igor

Pro 8 (Wavemetrics). Equation 2A was fitted to the data in a multivariate fit (*B. subtilis* HemH and *S. aureus* HemH) where each of the two data sets for each enzyme was considered separately. This produced estimates for the kinetic parameters k_{cat} and K_m^{Fe}, K_m^{CP} and $K^{CP.Fe}$. The *B. subtilis* H88A mutant data was fitted to the Michaelis-Menten equation (equation 2B). This equation estimates the kinetic parameters k_{cat} and K_m^{Fe}, K_m^{CP}.

$$v_i = \frac{V}{1 + \frac{K_m^{Fe}}{[Fe]} + \frac{K_m^{CP}}{[CP]} + \frac{K^{CP.Fe}}{[Fe][CP]}} \quad \text{Equation 2A} \qquad v_i = \frac{V[S]}{K_m + [S]} \quad \text{Equation 2B}$$

2.10 Static substrate binding assays

Fluorescence quenching studies looking at binding between the substrates and enzymes were completed on a Fluoromax 3 (Horiba) at 25 °C. A 560 nm band pass filter was placed in front of the emission line to remove second-order scattered light when protein is excited at 280 nm. *B. subtilis* HemH, the mutants (K87A, H88A, H183A, E264A and E264Q) and *S. aureus* HemH were held at 50 nM and were excited at 280 nm. The emission was recorded from 300-700 nm in the presence of different concentrations of CP$_{III}$ (0-100 μM). The emission peak between 330-510 nm was integrated and the peak area was plotted against substrate concentration using Igor Pro 8 (Wavemetrics). The appropriate equations were fitted to the data (equation 3A or 3B).

$$FI = F + \Delta F \frac{([S]+[E]+K_d) - \sqrt{([S]+[E]+K_d)^2 - 4[S][E\}}}{2[E]} \quad \text{Equation 3A}$$

$$FI = \frac{F}{1 + \frac{[S]}{K_d}} \quad \text{Equation 3B}$$

2.11 Stopped flow fluorescence spectroscopy

There are three different experiments used in stopped flow fluorescence that look at different parts of the ferrochelatase mechanism. The reactions are observed using an Applied Photophysics Pi-star spectrophotometer with a 2 mm light path in fluorescence mode. Coproporphyrin was excited at 393 nm detected at 90° through a 405 nm cut off filter (OG405). Ferrochelatase was excited at 280 nm detected at 90° through a blue cut off filter removing wavelengths before 300 nm and after 600 nm (table 2.4). The *B. subtilis* HemH and *S. aureus* HemH complex with CP_{III} was excited at 405 nm and the H88A mutant CP_{III} complex was excited at 396 nm, emission was detected at 90° through a 515 nm cut off filter (OG515). Each reaction was recorded on a 0.5-10 second time base and at least three reactions were run and averaged. An observed rate constant (k_{obs}) was calculated by fitting equations (equation 4A or 4B) to the reactions using the Pi-Star fitting software (Pro-data 1.43). All experiments were performed at 25 °C and in 0.2M Tris, pH 8 assay buffer.

Table 2.4- Band pass filters

FILTER	WAVELENGTH RANGE	SIGNAL USED	STOPPED FLOW EXPERIMENT
405 nm	>410 nm	CP_{III} – 393 nm CP_{III}-FC complex – 396 nm	CP binding and Fe binding and metalation
515 nm	>520 nm	CP_{III}-FC complex – 405 nm	Fe binding and metalation
Blue	300-590 nm	FC – 280 nm	CP binding

$$[P]_t = Ae^{-k_{obs}t} \quad \text{Equation 4A}$$

$$[P]_t = Ae^{-k_{obs}t} + v_it \quad \text{Equation 4B}$$

$$[P]_t = A_1e^{-k_1t} + A_2e^{-k_2t} + v_it \quad \text{Equation 4C}$$

2.11.1   CP$_{III}$ Binding

The first experiment looks at CP$_{III}$ binding, ferrochelatase and CP$_{III}$ are prepared in separate syringes. The reaction is excited at 280 nm or 393 nm, at 280 nm when the CP$_{III}$ concentration is varied (2-100 µM) and the enzyme concentration remained constant (0.1 or 0.2 µM). When the reaction is excited 393 nm the CP$_{III}$ concentration is held at 50 nM and the enzyme concentration is varied 0.5 - 5 µM. To gain an observed rate constant these runs were fitted to equations 4A, the H88A mutant traces could be fit to equation 4C in some concentrations. The k_{obs} value was plotted against substrate/enzyme concentration and the data were fit to equation 5. By fitting equation 5 to the data the K_{CP} and k_{iso} values were estimated, the k_{-iso} value was held at zero. This was completed for *S. aureus* HemH wildtype, *B. subtilis* HemH wildtype, K87A, H88A, E264Q and E264A.

$$k_{\text{obs}} = k_{-iso} + \frac{k_{\text{iso}}}{1 + \frac{K_{\text{CP}}}{[\text{CP}]}} \quad \text{Equation 5}$$

2.11.2   *Iron binding and metalation of the porphyrin*

This experiment focuses on iron binding and metalation of CP$_{III}$. This experiment was not completed on *S. aureus* HemH. The reaction is excited at 405 nm (wildtype *B. subtilis* ferrochelatase) or 396 nm (H88A *B. subtilis* HemH). Ferrochelatase and CP$_{III}$ are incubated in one syringe together at equimolar concentrations (1 µM). The ferrochelatase (1 µM) and the different concentrations of iron (0-400 µM) are also incubated in the other syringe. The final concentration of CP$_{III}$ is 0.5 µM and ferrochelatase is 1 µM. To gain an observed rate constant the averaged data was fitted to equation 4B. The estimated k_{obs} value was plotted against iron concentration. These

data were fitted to equation 6 to estimate K_{Fe} and k_{chel} values whilst k_{-chel} was held at zero.

$$k_{\mathrm{obs}} = k_{-\mathrm{chel}} + \frac{k_{\mathrm{chel}}}{1 + \frac{K_{\mathrm{Fe}}}{[\mathrm{Fe}]}} \text{ Equation 6}$$

2.11.3   Burst kinetics

The third setup looks at the collective rate constants for the enzymatic steps prior to the rate determining step. The ferrochelatase is in one syringe and both substrates are incubated in the second syringe. The porphyrin is excited at 393 nm, the ferrochelatase concentration is held at 0.2 µM and the CP_{III} concentration is 2 µM. The ferrous iron concentration is varied (1-200 µM). The k_{obs} value for *S. aureus* HemH was calculated by fitting the averaged reactions to equation 4B and these k_{obs} values was plotted against ferrous iron concentration. A line was fitted to the data using equation 7 allowing estimation of the kinetic parameter K_{Fe} and k_{burst}. In *B. subtilis* HemH wildtype and its H88A mutant the rate constants gained from the previous two stopped flow experiments were plotted onto the averaged data using equation 4C.

$$k_{\mathrm{obs}} = k_{-\mathrm{burst}} + \frac{k_{\mathrm{burst}}}{1 + \frac{K_{\mathrm{Fe}}}{[\mathrm{Fe}]}} \text{ Equation 7}$$

2.11.4   Rapid scanning kinetics

Rapid scanning kinetics (OLIS DB 620 Spectrophotometer) were performed on the *B. subtilis* HemH mutants (K87A, H88A and E264A) and wildtype and the *S. aureus* HemH protein. The interaction between 1 µM enzyme and 0.64 µM CP_{III} was observed between 350 and 450 nm for 0.5-10 s. The scanning rate was 32 scans per second. To reduce the signal to noise ratio, scans were arrayed with 5 (K87A HemH) or 10

(wildtypes, K87A and E264A mutants) giving a time resolution of 0.15 seconds and 0.3 seconds (32 scans per second), respectively. These spectra were processed and generated using Igor Pro 8 (Wavemetrics).

2.12 Crystallisation trials

Pre-crystallisation trials were performed on the *B. subtilis* HemH wildtype proteins and the K87A, H88A and E264A *B. subtilis* HemH mutants using the Hampton Research pre-crystallisation test protocol. Each of the proteins were screened in the presence of equimolar coproporphyrin III (well concentrations of approximately 100 µM for each). The screening process used the common crystallisation screens listed: Morpheus, JCSG+, PACT, pH Clear, Proplex, MPD and ammonium sulphate. The resulting crystal trays were produced using the Mosquito crystallisation robot. Crystal plates were screened for crystals using a light microscope.

3. Expression and purification of HemH and HemQ from different species to determine interaction between two consecutive enzymes in the coproporphyrin-dependent heme biosynthetic pathway

3.1 Introduction

In the coproporphyrin-dependent heme biosynthetic pathway found in Gram positive bacteria, three enzymes differ from those in the protoporphyrin-dependent pathway found in eukaryotes (section 1.2.3 and 1.2.4). These three enzymes have homologous roles but are positioned differently in each of the pathways, giving rise to different substrate requirements. For example HemF (CgDC) and HemQ (ChDC) both decarboxylate the propionyl groups on rings A and B to form vinyl groups, however HemF is the first of the three enzymes in the protoporphyrin-dependent pathway and decarboxylates coproporphyrinogen to protoporphyrinogen whereas HemQ is the final enzyme in the coproporphyrin-dependent pathway and decarboxylates coproheme to heme (Dailey and Gerdes, 2015, Dailey et al., 2015).

In the Gram-positive bacterial species *Propionibacterium acnes* (*P. acnes*) the HemH and HemQ proteins are fused into a single polypeptide. This observation led the hypotheses, firstly that the two enzymes interact and secondly that this interaction allows direct transfer of porphyrin from one active site to the other. The third, more general, hypothesis is that this interaction and substrate transfer between the HemH and HemQ proteins is a general property of the coproporphyrin-dependent pathway of heme biosynthesis.

To test the interaction between *P. acnes* HemH and HemQ four truncations of the protein were produced using gene cloning, two for HemH (with and without the linker region) and two for HemQ (with and without the linker region). Four truncations were produced so that there was a greater chance of testing the interaction using truncations that make up the whole protein. HemH without linker (HemHS) was found in inclusion bodies upon expression and HemQ with linker (HemQL), when purified, gave poor yields. As a result, HemH with linker (HemHL) and HemQ without linker (HemQS) were used to test interaction between the two enzymes and so HemHS and HemQL were not needed. Size exclusion chromatography was used to identify whether the proteins were interacting with each other and results showed that HemHL and HemQS formed a complex.

As the truncations showed that there was a complex forming between HemHL and HemQS, the purification of the full HemH-Q protein was attempted. The HemH-Q protein was required to test the substrate transfer mechanism between HemH and HemQ. Due to the fluorescent and absorbent nature of porphyrins this could be monitored using fluorescence and UV-vis spectroscopy. However, *P. acnes* HemH-Q proved difficult to purify due to its propensity to degrade. Steps were taken to reduce or prevent this cleavage or stabilise the protein however these were unable to prevent HemH-Q breaking apart.

Finally, testing the interaction between HemHs and HemQs from different species using SEC would indicate whether the interaction observed in *P. acnes* HemH-Q is specific to *P. acnes* or occurs in other species such as *S. aureus* where HemH and

HemQ are not covalently linked. In addition, interaction between HemHs and HemQs across species were also tested to investigate whether the interaction may be species specific. The results showed that there was no interaction between *S. aureus* HemH and HemQ or across the species. The *P. acnes* truncations were the only set tested that were positive for interaction.

Recently, the naming of these two genes (*hemH* and *hemQ*) and therefore their corresponding proteins have been changed to avoid confusion by distinguishing between the coproporphyrin and protoporphyrin-dependent ferrochelatases. The HemH protein is also called CpFC (coproporphyrin III ferrochelatase) and HemQ is called ChdC (coproheme decarboxylase) (Dailey et al., 2017). However, as this thesis focuses on the coproporphyrin ferrochelatases and coproheme decarboxylases, there is no ambiguity and HemH and HemQ will be used throughout.

3.2   Investigating the interaction between HemH and HemQ using size exclusion chromatography

The ferrochelatase in the species *P. acnes* is covalently linked to the subsequent enzyme in the coproporphyrin-dependent pathway, coproheme decarboxylase (HemQ), due to this linkage it was suggested that there may be an interaction between HemH and HemQ. To investigate this interaction the four truncations of *P. acnes* of HemH-Q (HemHS, HemHL, HemQS and HemQL) were produced via gene cloning. The four truncations produced were HemH with and without the linker and HemQ with and without linker; HemHL, HemHS, HemQL and HemQS, respectively. The

truncations were expressed and purified and the interaction between them were tested using size exclusion chromatography.

3.2.1 Gene cloning of P. acnes *HemH-Q truncations*

The plasmid (pTrcHisA) containing the *P. acnes hemH-Q* gene was a gift from Professor H Dailey (University of Georgia) and was used to produce the HemH-Q truncations (appendix 7.2). To obtain approximate boundaries of each enzyme in the HemH-Q protein a structure based alignment was performed on the protein sequences of HemH and HemQ protein from different species using PRALINE (Pirovano and Heringa, 2010). The secondary structure from the *B. subtilis* ferrochelatase crystal structure (PDB: 1AK1) was superimposed onto this alignment (for HemH) and crude boundaries for HemH and the HemQ and linker domain were deduced (Al-Karadaghi et al. 1997)(appendix 7.1)The TrcHisA vector containing the *P. acnes* gene was sequenced and primers were designed for the truncations (table 2.1) The four truncations that needed to be cloned were *hemH*, with and without linker, forming *hemHL* and *hemHS,* respectively and *hemQ* with and without the linker forming *hemQL* and *hemQS* (figure 3.1).

The *P. acnes hemH-Q* truncated gene constructs were produced using the Q5 site-directed mutagenesis method. The *hemH* and *hemQ* constructs were cloned with an annealing temperature of 58 °C and an extension time of 165 seconds (*hemHS*), 300 s (*hemHL*) and 180 seconds (*hemQS* and *hemQL).* The vector was inserted into highly competent DH5α *E. coli* cells and the plasmids were isolated for sequencing.

HemHQ
1-683 aa
74kDa

HemHQ
1-683 aa
74kDa

HemHL
1- 459 aa
48 kDa

HemQS
461-683 aa
25 kDa

HemHS
1-330 aa
35 kDa

HemQL
331-683 aa
38 kDa
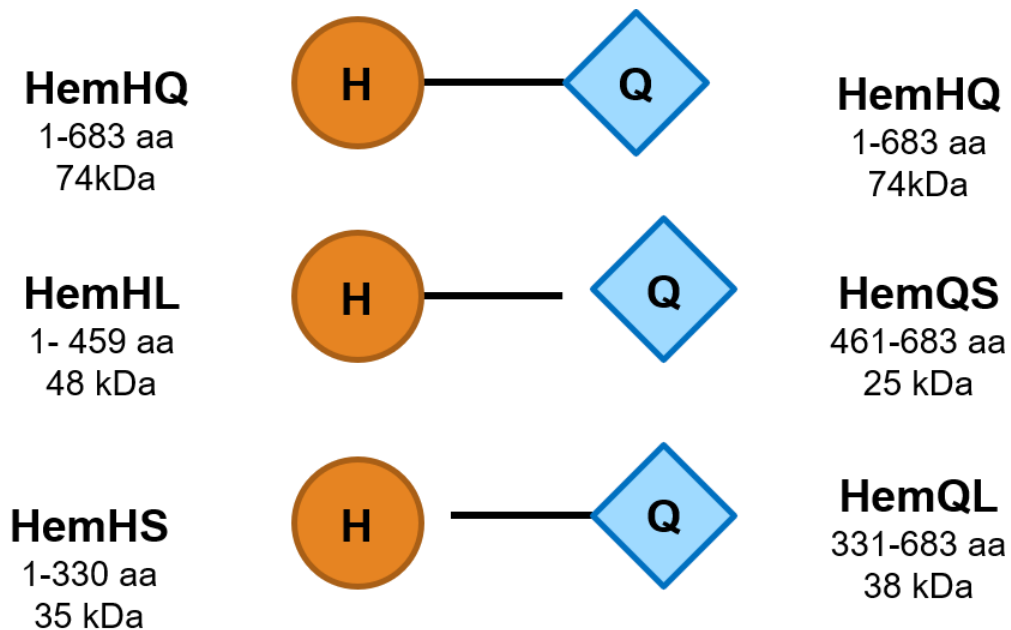
Figure 3.1 – HemH-Q Truncations

A simple diagram of each of the main parts of the protein HemH-Q and the truncations derived from this protein.

3.2.2 Optimisation of protein expression of P. acnes *HemH-Q truncations*

All truncations of the *P. acnes hemH-Q* gene were used to transform into several different strains of *E. coli* to evaluate them for protein expression. Expression trials were performed on the three of the four *P. acnes* HemH-Q truncations (HemHL, HemHS and HemQL, appendix 7.4) as optimising expression of HemQS was not required, due to excellent yields (table 3.1).

Table 3.1 – Optimal expression conditions for the *P. acnes* truncations

PROTEIN	*E. COLI* STRAIN	MEDIA
HemHS	BL21-DE3	LB
HemHL	BL21	LB
HemQS	Rosetta	LB
HemQL	Rosetta	LB

Pre and post induction temperatures were 37 °C and 18 °C, respectively.

3.2.3 Successful purification of P. acnes *HemHL, HemQS and HemQL*

Three truncations (HemHL, HemQS and HemQL) were successfully purified. These three proteins contained a N-terminal histidine tag and so they could be purified using immobilised metal affinity chromatography (IMAC). In general, the metal resin used contained nickel but resin containing cobalt has previously proven to be effective in the purification of ferrochelatase proteins (Dailey and Dailey, 2002, Hobbs et al., 2017). Initially, all the truncation purifications were attempted using nickel resin (Ni-NTA), if this failed cobalt resin (Talon, GE Healthcare) was used. If the proteins were not fully purified than an additional anion exchange chromatography step was added. Purification of HemHL and HemQS required a single purification step by IMAC, HemHL used cobalt resin (Talon, GE Healthcare) and HemQS used nickel resin (Ni-NTA), SDS PAGE analysis of the purification of these proteins are shown in figure 3.2. HemQL purification required an additional ion exchange chromatography step. Anion exchange chromatography (Q sepharose) was therefore used to further purify HemQL (appendix 7.5).
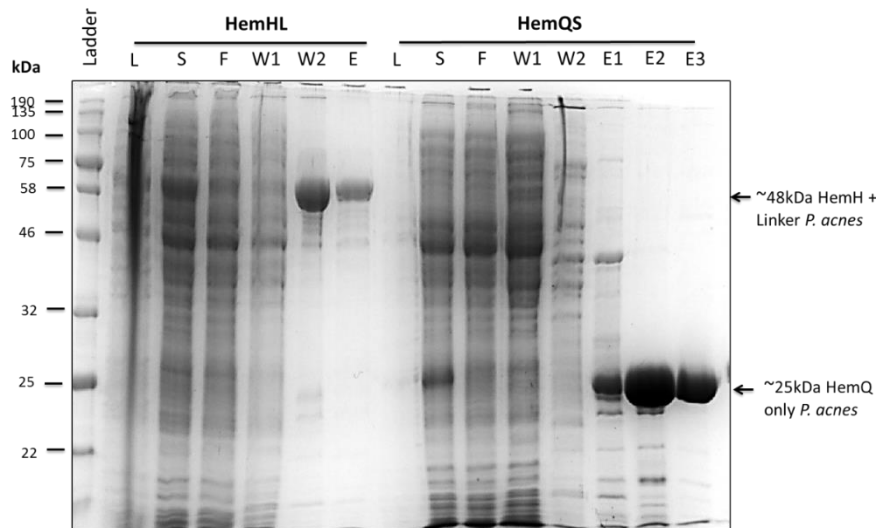
Figure 3.2- SDS PAGE of the purification of _P. acnes_ HemHL and HemQS

The SDS PAGE gel shows the progressive purification of HemHL and HemQS. L represents the lysed sample, S is the soluble fraction after centrifugation, F is the flow-through sample, the unbound protein. Washes 1 and 2 (W1, W2) are high salt (1 M KCl) and low imidazole wash (30 mM), respectively. E is the protein eluted off the column in high imidazole (300 mM) The arrows indicate the expected migration of each of the proteins.

3.2.4 Purifying P. acnes _HemHS_

As previously stated, protein expression of _P. acnes_ HemHS showed that the majority of the protein was present in the insoluble fraction. However, purification of HemHS was attempted to see if any of HemHS was still soluble. Purification using IMAC (Ni-NTA resin) and SDS PAGE analysis revealed that all of the protein was present in the insoluble fraction (figure 3.3). Other growth conditions using different _E. coli_ cell lines (BL21-DE3 and Rosetta), media (LB, 2YT, ZYM-5052) and induction temperatures (18 °C, 30 °C and 37 °C) were used in an attempt to increase the over-expression of soluble protein (appendix 7.4.2). This proved unsuccessful. As a result, several methods were used to attempt to solubilise HemHS after expression.
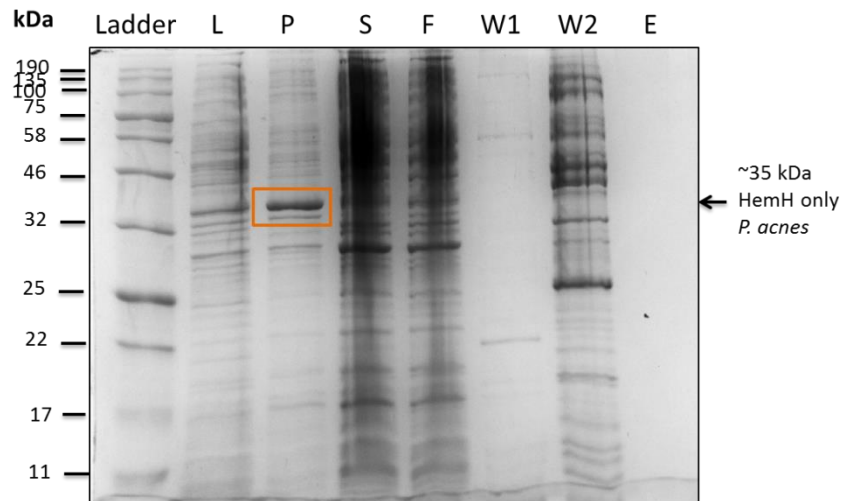
Figure 3.3 - Purification of *P. acnes* HemHS

The SDS PAGE gel of the purification of *P. acnes* HemHS by metal affinity chromatography, each of the lanes correspond to stages in the purification. L indicates the protein sample after lysis, P is the insoluble fraction after centrifugation and S is the soluble fraction. F is flow through, protein that doesn't bind to the nickel resin and W refers to washes with high salt (1) and low imidazole (2), E is the eluted protein. The protein band corresponding to HemHS is highlighted (arrow) and the presence of HemHS in the pellet (insoluble) fraction is highlighted by the orange box.

3.2.4.1 Solubilisation of the HemHS inclusion bodies with detergents and high salt concentrations.

As HemHS is present in the insoluble fraction, detergents were utilised to attempt to bring HemHS into the soluble fraction. To solubilise HemHS three different detergents were used because of their different properties. Triton-X-100 is a very effective non-ionic detergent, it is effective at solubilising protein from inclusion bodies (Kalipatnapu and Chattopadhyay, 2005), however its low critical micelle concentration (0.2-0.9 mM, ~0.01 %) makes it difficult remove by dialysis. CHAPS was used as it has a high critical micelle concentration (8-10 mM, ~0.49 %) this means the detergent can easily be removed by dialysis. Sodium cholate (critical micelle concentration: 9-15 mM, ~0.41 %) has previously been used to solubilise *H. sapiens* ferrochelatase (Wu et al., 2001) and may be able to successfully solubilise the HemHS protein.

Each of the detergents (15 mM CHAPS, 1% sodium cholate, 2% triton-X-100) were added to the standard binding buffer and used to resuspend the pellet of *E. coli* cells after expression of HemH. The cells were lysed by sonication and the insoluble and soluble fractions were separated by centrifugation. The soluble and insoluble fractions were run on an SDS PAGE gel to determine the presence of HemHS in each of the fractions. These detergents failed to solubilise HemHS and HemHS remained in the insoluble fraction. As the detergents failed to solubilise HemHS, purification of HemHS was attempted in high salt conditions.

The affinity purification of HemHS was repeated in high salt conditions (500 mM KCl). This increase in salt concentration could stabilise and solubilise HemHS, as seen with other proteins (Arakawa and Timasheff, 1982). Despite the increase in salt concentration HemHS remained insoluble and the stabilisation of HemHS was unsuccessful.

3.2.4.2 *Denaturation and refolding*

As it proved difficult to purify HemHS in native conditions, a denaturing purification strategy was attempted. In this case, the protein was completely denatured in 8 M urea and purified by IMAC chromatography. The resulting protein would then need to be refolded before biophysical or kinetic analysis. Refolding can either be attempted in solution, using stepwise dialysis to reduce the urea concentration, or with the protein immobilised and bound to the IMAC column (on column refolding).

3.2.4.2.1   Purification of HemHS in 8 M urea with on-column refolding

In this preparation the cell pellet was resuspended and lysed as normal. The soluble and insoluble fractions are separated by centrifugation and the insoluble fraction was resuspended in a buffer containing 8 M urea. The high concentration of urea will solubilise protein aggregates and subsequent centrifugation removes heavy cellular structures leaving only solubilised protein. The resulting protein sample is bound to the nickel column and the urea concentration is slowly reduced allowing the protein to slowly refold. Once the concentration of urea has dropped to zero the protein is eluted in standard elution buffer (Veldkamp et al., 2007, Tsumoto et al., 2003).

On column refolding allows quick and efficient refolding of a desired protein whilst simultaneously purifying it. There are potential problems with this method since reducing the urea concentration may lead to improper or non-native folding as well as an increased chance of precipitation occurring on the column. In addition, the immobilisation of the protein on the column may hinder correct folding. Purification of HemHS by on column refolding was not successful. Further purification of HemHS was halted in favour of using the more soluble HemHL protein.

3.2.5 Interaction between P. acnes *HemHL and HemQS using size exclusion chromatography*

Size exclusion chromatography is a quick efficient technique to determine if two proteins interact. SEC reveals strong interactions and not weak or transient

interactions so a negative result states that there are no strong interactions between the two proteins. The SEC column used was HiLoad Superdex 26/600 200 PG, calibrated before interaction studies.

The *P. acnes* HemH-Q protein contains both HemH and HemQ linked together. As *P. acnes* HemH and HemQ is naturally linked, running HemHL and HemQS down a SEC column is the most likely combination to interact. The truncations of *P. acnes* HemHL and HemQS make up the full protein; these were purified separately and run alone first for comparison. The A_{280} trace produced by *P. acnes* HemHL (48 kDa) shows a single peak at ~95 kDa this indicates the formation of a dimeric structure; ferrochelatases have been found as dimers (*H. sapiens*) and monomers (*B. subtilis*) so this is not unusual (Al-Karadaghi et al., 1997, Wu et al., 2001). The SEC chromatogram of HemQS (25 kDa) shows an elution peak at approximately ~79 kDa indicating the formation of a trimer. HemHL and HemQS were then mixed together and this was injected onto the SEC column. The SEC trace indicates the presence of one peak ~86 kDa, this is close to the full HemH-Q protein (74 kDa) and the trimeric HemQS (~75 kDa). An SDS PAGE gel was used to confirm the presence of both HemHL and HemQS in the SEC peak (figure 3.4).

These results show that there is non-covalent interaction between the two *P. acnes* truncations HemHL and HemQS. This interaction is strong enough to prevent the dimer/trimer interactions observed when HemHL and HemQS are run down the SEC column alone and the interaction between HemHL and HemQS appears to be 1:1.
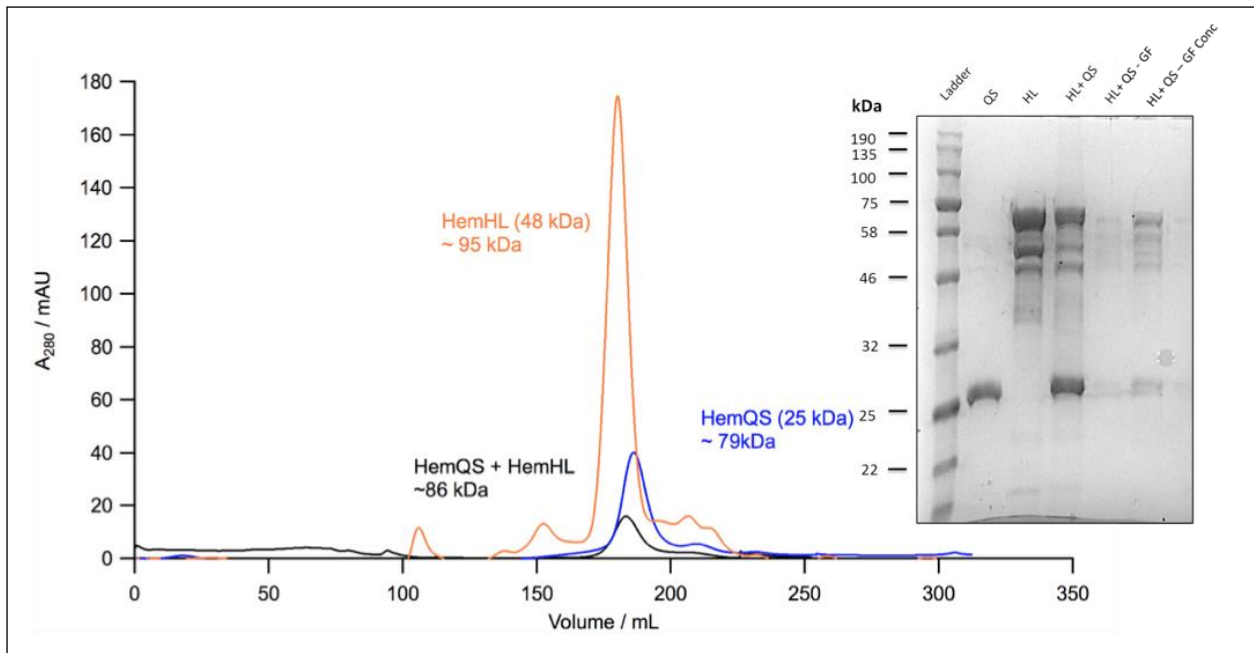
Figure 3.4 – Analytical SEC filtration trace of _P. acnes_ HemHL and HemQS

The A_{280} traces produced by an ÄKTA pure during analytical SEC are shown. The orange trace indicates the peak produced by HemHL (48 kDa) only, the blue trace indicates the peak produced by HemQS (25 kDa) only. The black trace indicates the peak produced when HemHL and HemQS is run together. The SDS PAGE gel (inset) shows the proteins samples during the analytical SEC of the two proteins. QS is HemQS only, HL is HemHL only, HL+QS is both proteins mixed together, HL +QS –GF is the sample taken from the main peak after SEC and HL+QS- GF conc it the SEC protein sample after it has been concentrated.

3.3 Investigating substrate transfer between HemH and HemQ in the _P. acnes_ fusion protein

The _P. acnes_ fusion protein provides a unique opportunity to look at the substrate transfer mechanism of ferrochelatase to coproheme decarboxylase. As the enzymes are covalently linked substrate transfer assays can be developed to determine whether the coproporphyrin binds to ferrochelatase, is converted to coproheme and funnelled directly into the active site of coproheme decarboxylase or coproheme is released by ferrochelatase and then taken up by coproheme decarboxylase. To answer this question _P. acnes_ HemH-Q must first be expressed and successfully purified.

However, purification of HemH-Q proved difficult and this was most likely due to spontaneous cleavage.

3.3.1 P. acnes ferrochelatase fusion protein expression

The plasmid containing the *P. acnes hemH-Q* (gift from Professor H Dailey) was inserted into Rosetta *E. coli* and grown in LB media. The HemH-Q protein was expressed using a standard IPTG protocol. The *E. coli* was incubated at 37 °C pre-induction and 18 °C post induction. Due to the high yields of protein produced the protein expression was not further optimised.

3.3.2 Purification of the P. acnes HemH-Q fusion protein

The *P. acnes* HemH-Q protein contains a histidine tag, so it can be purified using metal affinity chromatography. The same protocol for the IMAC purification of the truncations (HemQS, HemHL and HemQL) was used to purify the HemH-Q. This resulted in an impure sample. In order to obtain higher purity, optimisation of the IMAC purification step was attempted, an imidazole gradient was used but this did not result in purer protein. The main problem was a persistent contaminant, a protein weighing approximately 27 kDa. In addition to optimising the IMAC purification step, additional purification steps such as ion exchange chromatography (IEX) and size exclusion chromatography (SEC) were added in an attempt to completely purify HemH-Q.

The IEX of HemH-Q resulted in one main single peak at A_{280} at one salt concentration but SDS analysis revealed the protein sample contained more than one protein indicating incomplete purification (figure 3.5). The second purification step was

exchanged for SEC as this separates proteins based on their molecular weight rather than the surface charge of the protein. SEC of HemH-Q also produced a single peak at a single exclusion volume and while the sample showed fewer contaminating protein bands, one other protein was observed in the SDS PAGE gel (figure 3.5). The persistent contaminant at approximately 27 kDa is present in the purified protein samples after IEX and SEC. This suggests that the contaminant has similar charge properties to HemH-Q which has a theoretical isoelectric point (pI) of 4.95 (Wilkins et al., 1999). SEC was used as the 27 kDa protein and HemH-Q differed greatly in molecular weight (27 kDa and 74 kDa). SEC should have been easily able to separate these two proteins using the HiLoad Superdex 26/600 200 PG column.
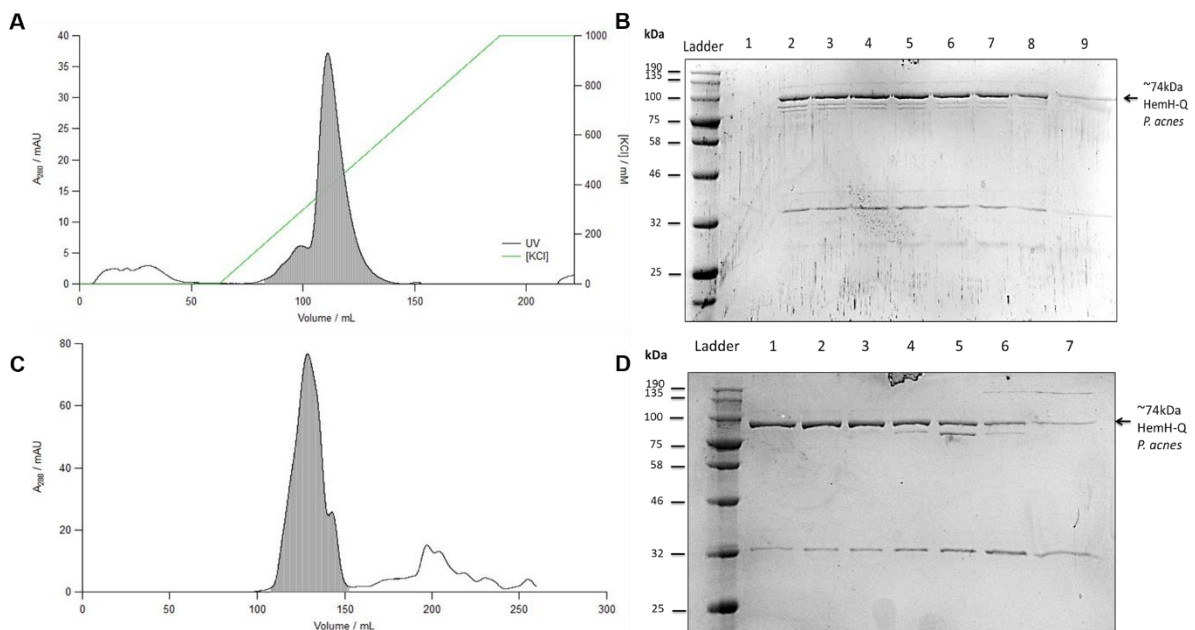
Figure 3.5 - Purification of *P. acnes* HemH-Q by IEX and SEC

Two A_{280} traces for IEX (**A**) and SEC (**C**) purification of the HemH-Q protein produced by the ÄKTA purifier. The filled in peak indicates the peak corresponding to the HemH-Q protein. The chromatograms show the absorbance at 280 nm in black and the salt gradient applied in IEX is shown in green. The SDS PAGE gels resulting from these purifications are shown adjacent to the graphs (**B** and **D**). The numbers on the lanes represent fractions within the shaded absorbance peak.

3.3.2.1 Reducing proteolysis

From these purifications it was deduced that the one remaining band may be a proteolytic fragment. To reduce proteolysis the serine protease inhibitor Pefabloc was replaced by SigmaFast protease inhibitor cocktail (No EDTA) this inhibited aspartate, cysteine and serine proteases as well as aminopeptidases and thermolysin-like proteins. The use of SigmaFast didn't prevent the formation of the 27 kDa protein. SigmaFast doesn't contain EDTA which inhibits metalloproteases, so the purification protocol was altered to include 5 mM EDTA.

EDTA can inhibit metalloproteases but as it chelates metal ions it is not compatible with IMAC. The EDTA was added before lysis of the cell pellet and an 80% saturation cut of ammonium sulphate and subsequent centrifugation was used to remove the EDTA. After the removal of EDTA the purification by IMAC proceeded. Attempts to reduce proteolysis failed to prevent the appearance of the 27 kDa protein band.

3.3.3 Confirming interaction between HemH-Q and contaminating protein

The SEC column used to purify *P. acnes* HemH-Q should be capable of separating a protein of ~27 kDa and *P. acnes* HemH-Q (74 kDa). As this separation is not observed, it is possible that the contaminating protein interacts with the HemH-Q protein this may also indicate why separation was not observed when using ion exchange chromatography as well.

3.3.3.1   Verifying the mass of HemH-Q by analytical SEC

To test the hypothesis that the HemH-Q protein and the 27 kDa contaminating protein formed a complex, analytical SEC was used to determine the mass of the HemH-Q complex. A HiLoad Superdex 26/600 200 PG column was calibrated using the protein standards: blue dextran (1000 kDa), β-amylase (200 kDa), alcohol dehydrogenase (150 kDa), bovine serum albumin (66 kDa), carbonic anhydrase (29 kDa) and cytochrome C (12.4 kDa). HemH-Q eluted at 131 mL, the calculated mass for HemH-Q was 411 kDa, much higher than the predicted 74 kDa from the primary sequence (figure 3.6). This provides evidence for a multimeric structure however as the protein sample is not pure and contains the 27 kDa protein the number of HemH-Q molecules involved in this structure cannot be determined. To further support the formation of a multimeric structure native PAGE was utilised, the protein was so large it was barely able to penetrate the resolving gel despite several optimisations. Gel filtration and native PAGE of HemH-Q to determine the molecular weight shows the formation of a high order complex.
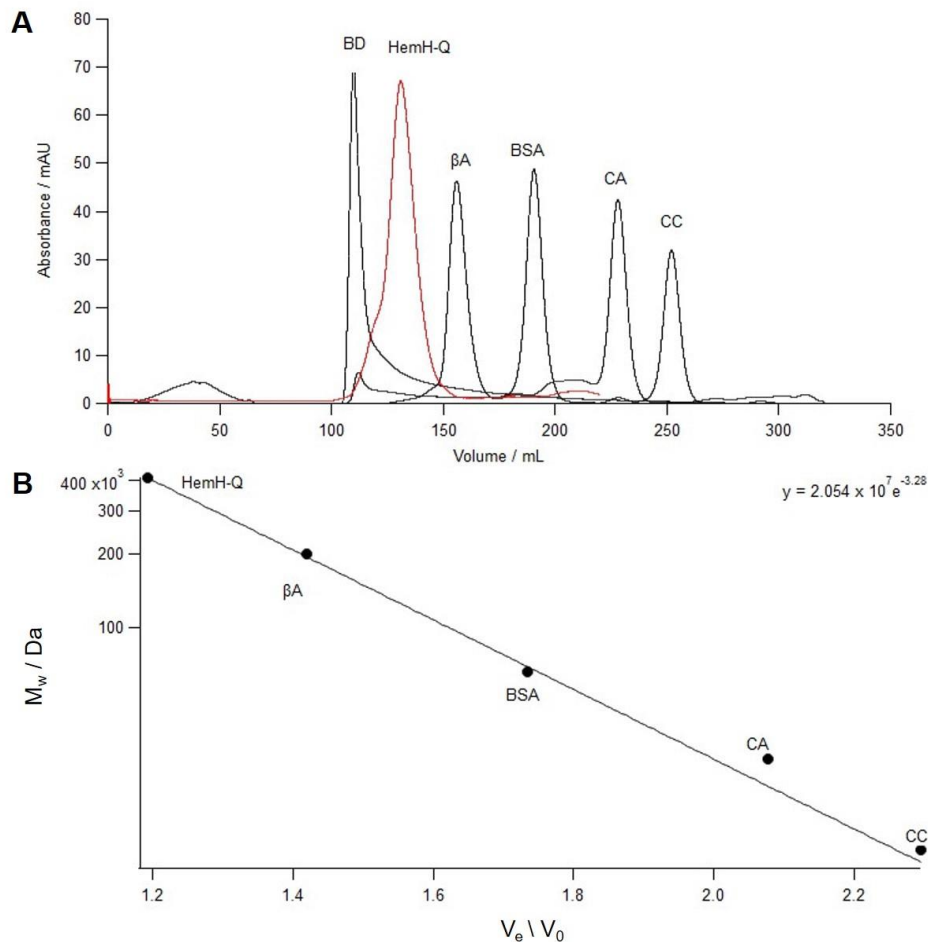
Figure 3.6 – Analytical gel filtration of HemH-Q

A shows the A_{280} traces of each of the standards and the HemH-Q protein. **B** shows the calibration curve for molecular weight determination of the HemH-Q protein, the HemH-Q run is shown in red. The standards are: CC (cytochrome C), CA (carbonic anhydrase), BSA (bovine serum albumin), βA (β-amylase) and BD (blue dextran).

3.3.4 Determining the interaction between HemH-Q and the 27 kDa protein

To tackle the interaction occurring between the two proteins an approach was to prevent the binding of the 27 kDa protein to HemH-Q. This utilised IMAC, SEC and circular dichroism (CD). A range of different solution conditions were used to separate the two proteins, including high concentrations of salt, different concentrations of organic solvent (0-50% isopropanol), different concentrations of chemical denaturants

(0-4 M urea), detergents (cholate, Triton X-100, SDS), and varying the pH (±1 unit). None of these proved successful. Perhaps identifying the contaminating protein would lead to its removal.

3.3.5 Identification of the 27 kDa protein by mass spectrometry (MS)

The 27 kDa protein was isolated from a SDS-PAGE gel containing the partially purified HemH-Q protein. It was reduced, alkylated, digested with trypsin and loaded onto a C18 reverse phase chromatography column. A gradient of acetonitrile was applied to the column and peptides eluted dependent on their hydrophobicity. Analysis by mass spectrometry determined that the protein mainly consisted of a C-terminal fragment of HemH-Q (this work was completed by Dr Adelina Acosta-Martin). This fragment contained 246 amino acids starting from D437 and continued until it reached the end of the protein (figure 3.7).

```
        10         20         30         40         50         60
MTANPYAAPT DPLAPYSAVL VVSFGGPRSP EEVMPFLRRV SHGRIPEERL ADVARHYDRF

        70         80         90        100        110        120
GGVSPINDAT DVFVNAIGNE LRRHGVRVPV LLGNRNGTPF LEEALTDMHA HGVRRVLAVV

       130        140        150        160        170        180
TSAYASYSGC RQYREEIATA LAHAGITDMQ VDKVPPFNEA PGFIRANAEA LMQAFMRIPP

       190        200        210        220        230        240
TPLEATRVVF VTHSIPDSMQ DASGAGQPGT DYISQHKAVC ERVAGQVRQV FGNMPQWDLA

       250        260        270        280        290        300
YCSRSGRPSD PWLEPDIIDH LRSLPEQGVQ SVVVAPIGFV ADHMEVVNDL DYEAAEAAKE

       310        320        330        340        350        360
SGLAFTRAAT AGTHSAFIAD LAGLILSQAA AARGEGGNLT SWPAPCVAGC CRRYPDAQDI

       370        380        390        400        410        420
PAVSGGDVES VAAGADVVDA EPGGVDFVPS GSASAVDRPG PEAVELETPP SPYNPLTKET

       430        440        450        460        470        480
PMSDHSSADS VIEGPRDDEV PAGSYTAPTD PRDTPVIPEE VNASSKWAMY SVFRVATALP

       490        500        510        520        530        540
AEDDERRRLV EGSDEWAGQS GVDTRGWYDL SGLRANADLL VWWVSDDPAV LQDAYHRFRA

       550        560        570        580        590        600
SGLGRHLEPV WSNVGVHRPA EFNKSHLPSC FAGIAPRRWA AFYPFIRSKE WYLLPAADRS

       610        620        630        640        650        660
RMLREHGIVG AASSDVKAST LAAFALGDYE WILALEGDDL ARIVDVMKDL RYVEARRYVD

       670        680
VDTPFFTGER VSPVVWADRQ MRA
```

Figure 3.7- In-gel tryptic digest and mass spectrometry

The amino acid sequence of HemH-Q is shown; the red box indicates the part of the protein that is mainly found in the 27 kDa protein on the SDS gel. This sequence is consistent with a 27 kDa protein

3.3.5.1 *Cleavage of HemH-Q may be due to labile bonds in the protein*

As mass spectrometry revealed that the contaminating protein is a fragment of the HemH-Q protein, potential mechanisms of protein hydrolysis needed to be reconsidered. Proteolysis by proteases present in the *E. coli* expression strain has been discussed above (section 3.3.2.1) and it is notable that use of protease inhibitors and *E. coli* strains with a reduced number of proteases was ineffective at removing the contaminating C-terminal fragment. One additional cleavage mechanism arises as aspartyl-prolyl bonds are heat labile and can be spontaneously broken during sample

preparation for SDS-PAGE gel electrophoresis (Kurien and Scofield, 2012). There are several of these bonds present in the HemH-Q amino acid sequence.

Heat trials were performed to test for aspartyl-prolyl bond cleavage during SDS PAGE. SDS PAGE heat trials were completed to see if there was an increase in band intensity of contaminating protein in a SDS PAGE upon heating. The protein samples were heated to either 75 °C or 95 °C for 5, 20 or 60 minutes and run on a SDS PAGE gel. Analysis by SDS PAGE showed an increase in proteolytic fragments upon heating but no increase in band intensity of the 30 kDa proteolytic fragment. This shows that the whole HemH/Q protein is sensitive to heat and so is the proteolytic fragment and it is unlikely to be an SDS PAGE artefact.

3.4 Testing the interaction between non-covalently linked HemH and HemQ from different bacterial species and across species

As *P. acnes* HemH and HemQ are shown to interact using size exclusion chromatography other HemH proteins (*B. subtilis, S. aureus* and *P. acnes)* HemQ proteins (*S. aureus* and *P. acnes*) were tested for interaction. *S. aureus* has a HemH and HemQ that are not covalently linked. Investigating the interaction between these proteins would show whether the interaction was specific to *P. acnes* or present in other Gram positive bacteria. Different combinations of HemH proteins and HemQ proteins from different species were also investigated to indicate whether the HemH and HemQ proteins must originate from the same species for interaction to occur.

Firstly, protein expression and purification of all the HemH and HemQ proteins were required.

3.4.1 Expression of S. aureus *HemH and HemQ and* B. subtilis *HemH*

Plasmids containing the genes for *S. aureus* HemH and *S. aureus* HemQ were a gift from Dr. M Shepherd (University of Kent), the *S. aureus* HemH was cloned into a TrcHisA plasmid and *S. aureus* HemQ was inserted into a pET14b plasmid. The plasmid containing *B. subtilis* HemH was a gift from Dr H Dailey (University of Georgia). The plasmid constructs were isolated and used to transform different *E. coli* strains (BL21, BL21-DE3, Rosetta and JM109).

An expression protocol for *S. aureus* HemH was previously published (Hobbs, et al. 2017), using CircleGrow media and JM109 *E. coli* cells. This expression protocol was originally developed for production of *H. sapiens* ferrochelatase as the high concentrations of human ferrochelatase produced in conventional IPTG induced systems are toxic and yields are low. In contrast, bacterial ferrochelatases such as those from *B. subtilis* and *P. acnes* express well when a standard IPTG induction protocol is used. Expression trials on *S. aureus* HemH was completed to see if standard IPTG induction was a feasible route that could increase the protein yield. Optimal expression conditions for the *S. aureus* HemQ protein was also investigated. The conditions investigated (*i.e.* cell type, media, growth temperature) were the same as those previously described (section 3.2.2) when producing the *P. acnes* HemH-Q truncated proteins (see table 2.2).

It appeared that the optimal conditions for *S. aureus* HemH expression were the use of JM109 *E. coli* and CircleGrow media as previously published (Hobbs et al., 2017). Both *S. aureus* HemQ and *B. subtilis* HemH require LB media and BL21 and Rosetta *E. coli*, respectively (table 3.2).

Table 3.2 – Expression conditions for the *S. aureus* HemH and HemQ and *B. subtilis* HemH

SPECIES	PROTEIN	*E. COLI* STRAIN	MEDIA	TEMPERATURE
S. aureus	HemH	JM109	CircleGrow	Incubation 30 °C No IPTG induction
	HemQ	BL21	LB	Pre induction - 37 °C Post induction - 18 °C
B. subtilis	HemH	Rosetta	LB	Pre induction - 37 °C Post induction - 18 °C

3.4.2 Purification of S. aureus *HemH and HemQ and* B. subtilis *HemH*

All three proteins contain a N-terminal His tag and the first purification step is IMAC, *S. aureus* HemH was purified on a cobalt resin column (Talon) and *B. subtilis* HemH and *S. aureus* HemQ were purified on a nickel resin column (Ni-NTA). *S. aureus* HemH purification requires just the single purification step (Hobbs et al., 2017) whereas *B. subtilis* HemH and *S. aureus* HemQ need an extra IEX step for polishing. The IEX step uses the anion exchange media, Q Sepharose, this extra step successfully purifies both proteins in high yields (table 3.3). All three of these proteins have published purification protocols, these were used for the *S. aureus* proteins but not for *B. subtilis*

HemH. This *B. subtilis* HemH contained a histidine tag which was utilised in its purification; the published protocol used a construct of *B. subtilis* HemH which did not contain a histidine tag (Hobbs et al., 2016, Hobbs et al., 2017, Hansson and Al Karadaghi, 1995)

Table 3.3- Purification conditions of *S. aureus* HemH and HemQ and *B. subtilis* HemH

SPECIES	PROTEIN	PURIFICATION STEPS	PURE?
S. aureus	HemH	IMAC (Talon)	Yes
	HemQ	IMAC (Ni-NTA) IEX (Q Sepharose)	Yes
B. subtilis	HemH	IMAC (Ni-NTA) IEX (Q Sepharose)	Yes

3.4.3 Interaction between HemH and HemQ from different Gram-positive bacterial species using size exclusion chromatography

After the successful interaction of the HemHL and HemQS protein from *P. acnes*, HemH and HemQ proteins from different species were tested. There were three HemH proteins (*P. acnes, S. aureus, and B. subtilis*) and two HemQ proteins (*P. acnes, S. aureus*) available making up four possible cross species tests, these were run in the same way as the *P. acnes* proteins (section 3.2.5).

3.4.3.1 *The* P. acnes *HemQS protein and* S. aureus *HemH or* B. subtilis *HemH do not interact*

The pure *P. acnes* HemQS (25 kDa) protein elutes off the SEC column as a molecular weight of ~79 kDa indicating the presence of a trimer. In these experiments, *S. aureus* HemH (35 kDa) did not express well and as a result it was difficult to obtain at a high concentration of pure protein without a larger scale up. *S. aureus* HemH elutes off of the SEC column at volume representative of a protein with molecular weight ~33 kDa near to the 35 kDa weight of *S. aureus* HemH (figure 3.9B).

When the *P. acnes* HemQS and *S. aureus* HemH are run together the elution profile shows one peak ~79 kDa corresponding to the *P. acnes* HemQS trimer and a cluster of peaks at ~35 kDa indicating the presence of *S. aureus* HemH. Other peaks present are below the void volume or very close to the void volume indicating a high molecular protein or aggregate. These peaks suggest that there is no interaction between these two proteins; the absence of any strong peak at an elution volume indicating a protein of 60 kDa supports the lack of interaction (figure 3.8B).

The *B. subtilis* HemH (~36 kDa) protein produces one peak in the SEC chromatogram. This peak corresponds to a protein ~32 kDa in weight. *B. subtilis* HemH is mixed together with *P. acnes* HemQS and the resulting elution profile shows two distinct peaks corresponding to *B. subtilis* HemH at ~32 kDa and *P. acnes* HemQS at ~79 kDa (figure 3.8A). The lack of any other peaks other than those matching the separate HemH and HemQ proteins indicates that there is no interaction between *P. acnes* HemQS and *B. subtilis* HemH.
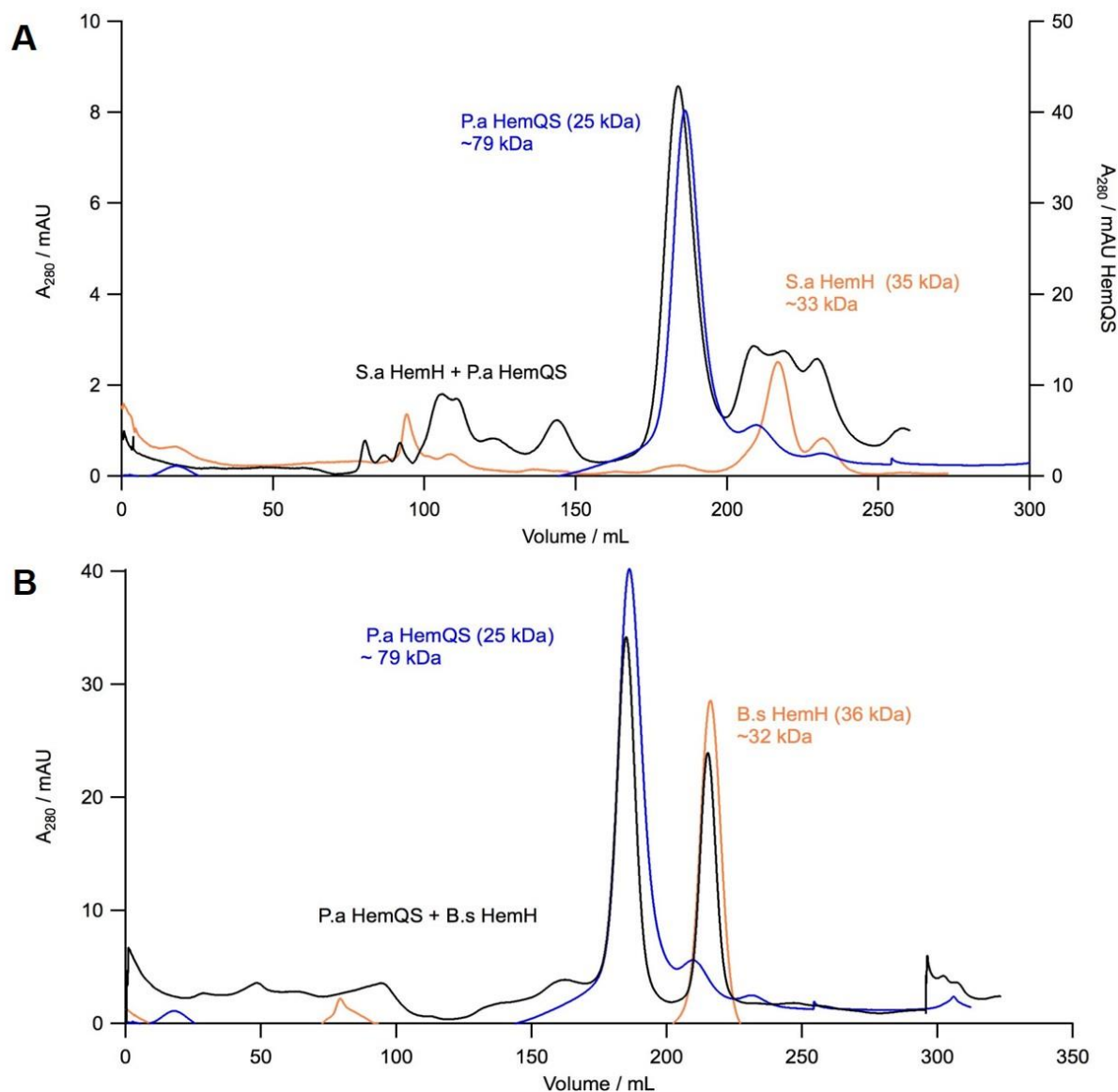
Figure 3.8 –Analytical SEC chromatogram of *P. acnes* HemQS and *S. aureus* HemH or *B. subtilis* HemH

A shows a SEC chromatogram of *P. acnes* HemQS and *S. aureus* HemH, **B** shows a SEC chromatogram of *P. acnes* HemQS and *B. subtilis* HemH. The traces represent the A_{280} traces produced by an ÄKTA pure during analytical SEC. The blue trace shows the chromatogram produced when *P. acnes* HemQS (25 kDa) is run alone. The orange trace indicates the peak produced by *S. aureus* HemH (35 kDa) only (**A**) or *B. subtilis* HemH (36 kDa) only (**B**). The black traces indicate the A_{280} trace produced when either *S. aureus* HemH and *P. acnes* HemQS (**A**) or *B. subtilis* HemH and *P. acnes* HemQS (**B**) are run together.

3.4.3.2 S. aureus *HemQ and* P. acnes *HemHL or* B. subtilis *HemH*

S. aureus HemQ forms a multimeric structure. *S. aureus* HemQ elutes off the column at a volume corresponding to the molecular weight of ~124 kDa, the monomeric weight of *S. aureus* HemQ is ~29 kDa (figure 3.9). This molecular weight suggests the HemQ forms a tetramer. *P. acnes* HemQS forms a trimer and the first crystallised structure of HemQ from *L. monocytogenes* was crystallised as a pentamer (Hofbauer et al., 2016c)(figure 1.18). HemQs from different bacterial species appear to form different multimeric states.

P. acnes HemHL forms a dimer when subjected to size exclusion chromatography, this gives the molecular weight of ~95 kDa which is not clearly resolvable on SEC from the *S. aureus* HemQ at 124 kDa. The two different proteins can be still be observed as *P. acnes* HemHL causes the appearance of a slight shoulder on the merged peak. As the peak is merged the peak spans a much larger elution volume encompassing both proteins, the appearance of this absorbance peak suggests that these two proteins do not interact (figure 3.9A).

When *B. subtilis* HemH and *S. aureus* HemQ are injected onto the column together there are two distinct peaks on the SEC chromatogram corresponding to the absorbance peaks of each of the proteins suggesting no interaction (figure 3.9B). From these investigations, there is strong evidence to suggest that the cross-species combinations of HemH and HemQ do not interact when subjected to SEC.
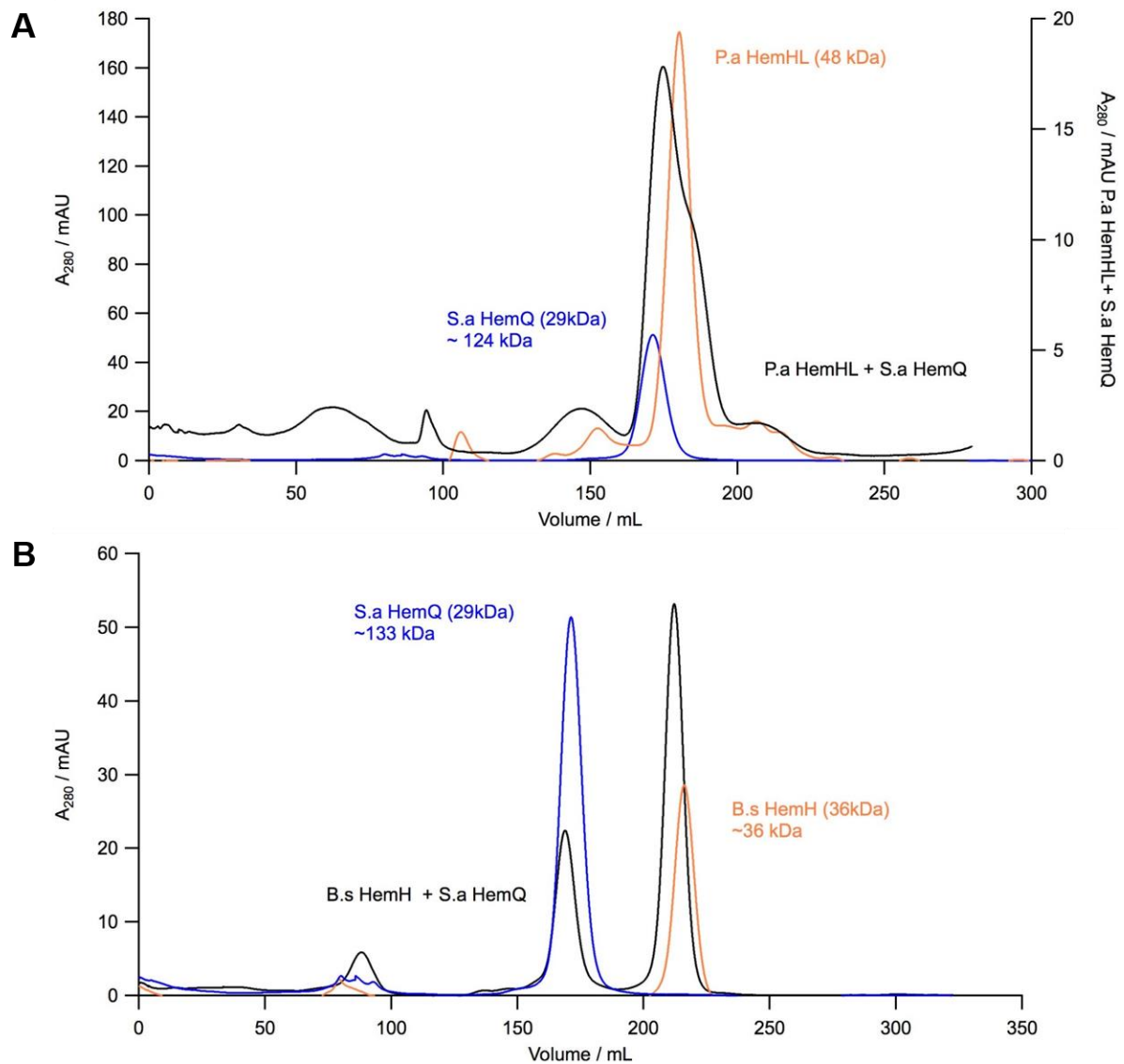
Figure 3.9- Testing the interaction between *S. aureus* HemQ and *P. acnes* HemHL or *B. subtilis* HemH

The SEC chromatograms show an absorbance (A_{280}) trace produced by an ÄKTA pure. **A** shows the SEC chromatogram corresponding to *S. aureus* HemQ and *P. acnes* HemHL. **B** shows the SEC chromatogram corresponding to *S. aureus* HemQ and *B. subtilis* HemH. The blue line indicates the elution profile for *S. aureus* HemQ (29 kDa) alone. The orange trace corresponds to *P. acnes* HemHL (**A**) alone (48 kDa) and *B. subtilis* HemH (**B**) alone (36 kDa). The black line for the chromatogram in **A** indicates a run of *S. aureus* HemQ and *P. acnes* HemHL whereas the chromatogram in **B** is a run of *S. aureus* HemQ and *B. subtilis* HemH.

3.4.4 Investigation into the interaction between S. aureus *HemH and*

S. aureus *HemQ*

Testing the interaction between HemH and HemQ from different species showed that there was no interaction when detected by SEC. The *P. acnes* HemHL and HemQS do interact and eluted off the SEC column together however, these proteins are naturally linked. *S. aureus* HemH and HemQ are not naturally linked but are derived from the same species so there may be an interaction that occurs between the two enzymes.

These proteins *S. aureus* HemH and HemQ are run alone and the peaks produced are as expected from the parallel to molecular weights 32 kDa and 124 kDa, respectively. When these two proteins are run down the column the elution profile shows two peaks around the elution volumes of HemH and HemQ indicating no interaction between the two enzymes under these conditions (figure 3.10).
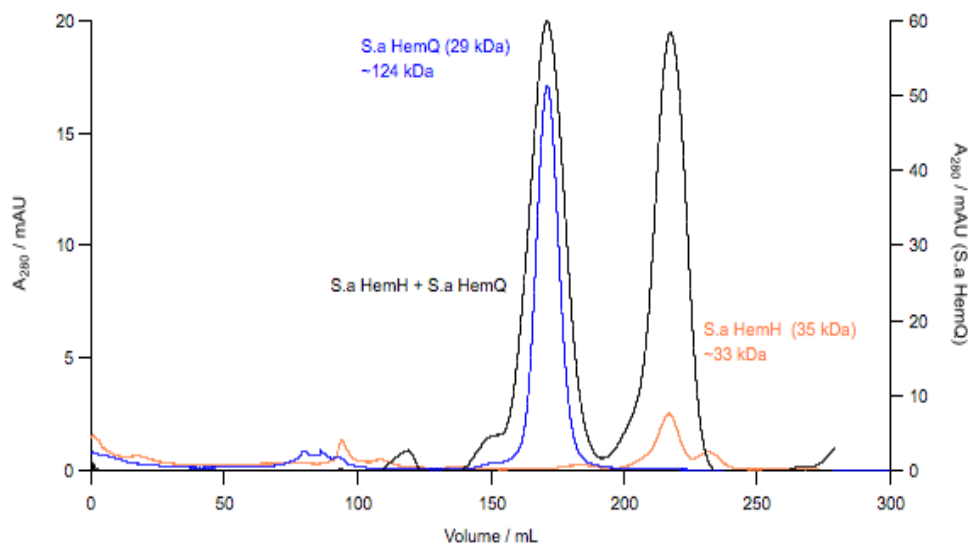
Figure 3.10- Analytical SEC of *S. aureus* HemH and HemQ

The SEC chromatogram was produced by an ÄKTA pure which measured the absorbance at A_{280}. The blue and orange trace reflects the elution profiles of *S. aureus* HemQ and HemH alone, respectively. The black line indicates the elution profile of *S. aureus* HemQ and HemH when they are run together.

3.5 Chapter Summary

Four truncations of *P. acnes* HemH-Q (HemHS, HemHL, HemQS and HemQL) were produced. The expression and purification of the truncations were optimised. HemHL, HemQS and were successfully purified whereas HemHS purification was unsuccessful. Several different methods were used to optimise the HemHS purification but the HemHS protein remained insoluble. As the truncation pair HemHL and HemQS were successfully purified these were used to analyse interactions between the two proteins, HemH and HemQ. The HemHS and HemQL truncations were no longer required as HemHL and HemQS could be used instead. Size exclusion chromatography revealed that these two proteins interact in a 1:1 ratio.

The second part of the chapter investigated the substrate transfer mechanism using the full *P. acnes* HemH-Q protein. However, the HemH-Q protein could not be

successfully purified. Due to the unstable nature of this multi-domain protein self-cleavage was an issue. Steps were taken to attempt to reduce the proteolysis of HemH-Q however these failed. Cleavage occurred in the N-terminal part of the HemQ and the C-terminal cleavage product interacted with the remaining intact HemH-Q protein. The cleavage product would only disentangle from the full protein in the detergent SDS and was visible on a SDS PAGE. The identity of the cleavage product was confirmed using tryptic digestion and mass spectrometry.

When subjected to SEC *P. acnes* HemH-Q eluted off the column at a much higher molecular weight indicating that not only was the C terminal cleavage product interacting with the intact HemH-Q protein, but the HemH-Q protein was also interacting with other intact HemH-Q proteins.

In the final part of the chapter, the interaction between different HemH and HemQ proteins was tested using SEC. In this investigation the *P. acnes* truncations HemHL and HemQS were used as well as *S. aureus* and *B. subtilis* HemH and *S. aureus* HemQ. All cross-species combinations of the HemH and HemQ proteins were tested and all showed that there was no interaction between the two proteins. In addition to these experiments, the interaction between *S. aureus* HemH and HemQ was assessed. These two proteins were from the same species but were not covalently linked. The result of this experiment showed that there were no strong non-covalent interactions between the two proteins.

The lack of strong interaction between *S. aureus* HemH and HemQ suggests that a strong complex is not formed between these proteins. These results do not rule out the formation of any transient or weak complexes. No observed interaction between HemQ and HemH in *S. aureus* opposes a substrate funnelling mechanism where the coproheme in the ferrochelatase active site is funnelled direct into the active site of HemQ. However, these interaction studies were completed in the absence of substrate. Substrate binding and product release in *B. subtilis* and *S. aureus* ferrochelatase have been associated with isomerisations that could reveal interaction surfaces for HemQ.

4. Investigating the kinetic properties of *B. subtilis* and *S. aureus* HemH

4.1. Chapter introduction

The two bacterial species *B. subtilis* and *S. aureus* synthesise heme utilising the coproporphyrin-dependent pathway and belong to the same phylum, the Firmicutes. Typically, ferrochelatases are known to be structurally conserved but have low sequence similarity (~20%), these bacterial ferrochelatases have approximately 60% sequence identity (Needleman and Wunsch, 1970) and as a result are expected to behave similarly.

In the past, investigation into *B. subtilis* HemH has been extensive. *B. subtilis* HemH was the first ferrochelatase structurally resolved (Al-Karadaghi et al., 1997) and a second structure was published with N-methyl mesoporphyrin bound (Lecerof et al., 2000). In addition to structural analysis kinetic characterisation of *B. subtilis* HemH was attempted (Hansson et al., 2007); the enzyme appeared largely inactive when compared to *H. sapiens* HemH. These kinetic studies on *B. subtilis* HemH were performed under the misconception that protoporphyrin IX was the endogenous porphyrin substrate. Recent work has revealed that the endogenous porphyrin substrate is coproporphyrin III (Dailey et al., 2015). The low activity observed with the *B. subtilis* ferrochelatase was due to the use of protoporphyrin IX and protoporphyrin analogues in the kinetic assays.

Since the discovery of the coproporphyrin-dependent heme biosynthetic pathway there has been little kinetic investigation of any coproporphyrin ferrochelatase (Hobbs et al., 2017, Dailey et al., 2015, Lobo et al., 2015) and in general, there has been little kinetic characterisation of any ferrochelatase using transient kinetics (Hoggins et al., 2007, Hunter et al., 2016, Gillam et al., 2018).

B. subtilis and *S. aureus* HemH have been successfully expressed and purified. Circular dichroism spectroscopy has shown that these proteins contain secondary structure elements, and thermo-melts have been performed to determine thermal melting temperatures. Fluorescent binding assays have been completed showing that CP_{III} can tightly bind to both ferrochelatases and steady state kinetics have allowed the determination of k_{cat}, K_m^{Fe} and K_m^{CP} values. Stopped flow fluorescence spectroscopy was used in three different experimental designs to reveal the rates constants for CP_{III} binding, Fe^{2+} binding and porphyrin metalation.

4.2. Transformation and protein expression

To produce the ferrochelatase proteins, the plasmids containing the genes for *B. subtilis* and *S. aureus* HemH was used to transform *E. coli.* The plasmid containing *B. subtilis* HemH was a gift from Professor H Dailey (University of Georgia) and the *S. aureus* HemH was a gift from Dr M Shepherd (University of Kent). *B. subtilis* HemH was incorporated into Rosetta *E. coli* and grown in LB media, protein expression was induced using IPTG. Expression of *B. subtilis* HemH through IPTG induction resulted

in a large amount of protein. The large amount of protein expressed meant that further optimisation expression was not required.

Previous publications (Hansson and Al Karadaghi, 1995) outline the method that they used to express HemH, the plasmid (pLUGT7-H) containing the *B. subtilis hemH* gene was used to transform BL21-DE3 *E. coli* and grown on tryptose blood agar plates containing ampicillin (50 mg mL^{-1}) and glucose (0.4% w/v). The *E. coli* was grown in LB media (with 100 mg mL^{-1} ampicillin) and protein expression was induced using IPTG (0.5 mM) at OD (0.4-0.5), the cells were harvested four hours after IPTG induction. The method used to express *B. subtilis* HemH was similar to the published method however the plasmid system used was different and so minor changes were made.

The protein expression of *S. aureus* HemH was trialled using similar conditions those used in the protein expression of *B. subtilis* HemH using derivatives of BL21 *E. coli* and standard IPTG induction (table 2.2). Optimisation of protein expression using a standard IPTG induction system failed to produce high yields of *S. aureus* HemH. In a recent publication, the expression of *S. aureus* HemH was described using JM109 *E. coli* and CircleGrow media (Hobbs et al., 2017). In this protocol protein expression was not induced by IPTG. This method was also used in the expression of *H. sapiens* HemH and was able to produce high yields of *S. aureus* HemH (Burden et al., 1999, Hobbs et al., 2017)

4.3. Purification of *B. subtilis* HemH and *S. aureus* HemH

The *B. subtilis* HemH protein contains an engineered histidine tag so it could be purified using metal affinity chromatography. A nickel column was used as the first purification step and an ion exchange column in the second step. The protein was eluted from the nickel column at 300 mM imidazole and desalted using a manually poured Sephadex G50 column removing the imidazole. Ion exchange chromatography completed purification and *B. subtilis* HemH eluted off the column at approximately 400 mM salt; the purification of *B. subtilis* HemH is shown in figure 4.1A.

The method used to purify *B. subtilis* HemH is different to the published protocol. The published protocol uses two rounds of ammonium sulphate precipitation (70% and 90%), overnight dialysis and ion exchange chromatography (Al-Karadaghi et al., 1997, Hansson and Al Karadaghi, 1995). This protocol avoids using immobilised metal affinity chromatography (IMAC) as this could cause metal ion contamination. Potential metal ion contamination can be an issue when assaying ferrochelatase as ferrochelatase is capable of inserting divalent metal ions such as Ni^{2+} into the porphyrin substrate (Hunter et al., 2008, Hansson and Hederstedt, 1994, Medlock et al., 2009, Davidson et al., 2009). However, the method using IMAC to purify *B. subtilis* HemH has been used to purify other ferrochelatases (Hobbs et al., 2017, Burden et al., 1999) and is quicker, purifications can be completed in hours rather than days. Control experiments show minimal metal ion contamination and chelex 100 is used to remove and metal ions from the assay buffer prior to functional studies.

S. aureus HemH was purified using a previously published protocol (Hobbs et al., 2017), although it was also successfully purified without the addition of 50 mM MOPS

and 1% sodium cholate to the buffer (figure 4.1B). *S. aureus* HemH was purified using a single cobalt (Talon) column; it was washed with low imidazole (15 mM) and eluted in high imidazole (300 mM). The protein was then buffer exchanged into binding buffer to remove imidazole. The purification of *S. aureus* HemH is shown in figure 4.1B.
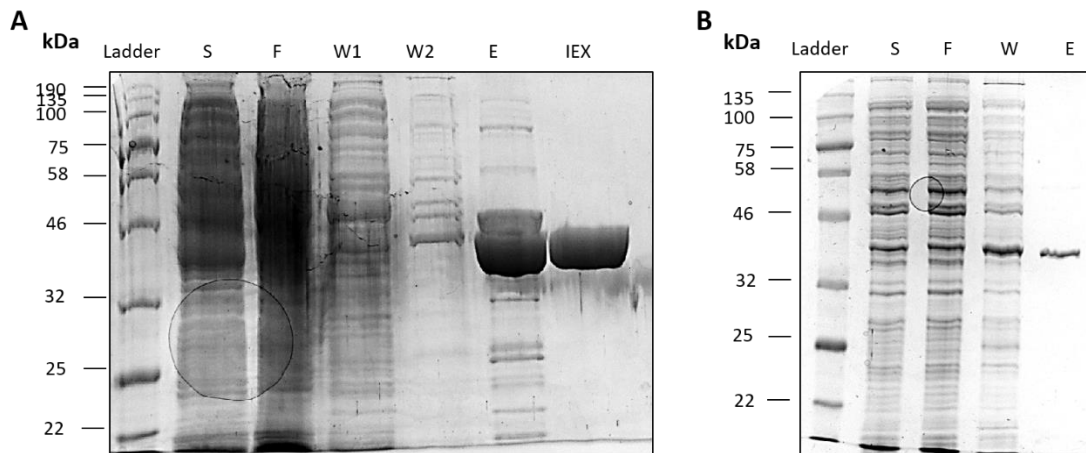
Figure 4.1 Purification of *B. subtilis* HemH and *S. aureus* HemH

A SDS PAGE gel of the purification of B. subtilis HemH (A) and S. aureus HemH (B), S represents the soluble fraction after lysis and centrifugation, F is the flow-through (unbound protein), W1 corresponds to a high salt washes whereas W and W2 correspond low imidazole washes 15 mM and 30 mM imidazole, respectively. E is the protein eluted off the IMAC column and IEX is the protein sample after IEX.

4.4. Probing the secondary structure of *B. subtilis* and *S. aureus* HemH using circular dichroism

4.4.1. Circular dichroism shows spectra consistent with the presences of secondary structure

After successful purification of the HemH proteins, circular dichroism (CD) was used to confirm whether the proteins contained secondary structure. Unfolded and folded protein produce distinctive spectra when measuring the ellipticity across a mid UV range (200-260 nm).

CD of the two ferrochelatases reveal a broad trough in negative ellipticity range (figure 4.2). The broad trough spans a large part of these spectra, this indicates the presence of both α helix and β sheet structures. Both ferrochelatases contain of two four-stranded β sheets flanked by helices so the spectra are consistent with the expected protein fold (Al-Karadaghi et al., 1997, Hobbs et al., 2017). Analysis of the B. subtilis HemH spectrum using the K2d method on Dichroweb (Andrade et al., 1993) predicts that protein structure contains 37% α helix and 26% β sheet, the B. subtilis HemH crystal structure (PDB ID: 1AK1) states that the structure consists of 49% α helix and 17% β sheet. This is reasonably consistent given the limited wavelength range (Andrade et al., 1993, Al-Karadaghi et al., 1997). The inconsistency in ellipticity between the two ferrochelatases is likely due to inaccurate protein determination.
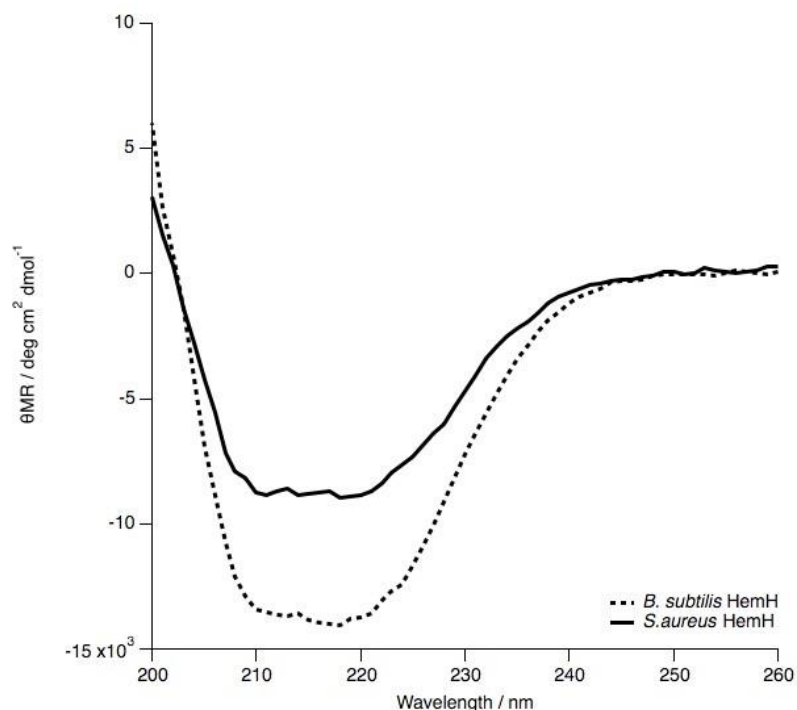
Figure 4.2- Circular dichroism spectra of *B. subtilis* and *S. aureus* HemH

The CD spectra of *B. subtilis* HemH and *S. aureus* HemH each at approximately 4 µM, these spectra were normalised to protein concentration.

4.4.2. Testing the thermostability of B. subtilis *and* S. aureus *ferrochelatase*

The thermostability of a protein can be determined by its melting temperature (T_m). The T_m of the HemH proteins can be measured using CD spectroscopy. The ellipticity at 222 nm is a strong signal for α helical structure, but 220 nm appeared a more appropriate wavelength to use. The temperature was increased from 5 °C to 100 °C and the ellipticity was monitored at 220 nm, after protein unfolding the temperature was slowly reduced to 5 °C allowing the protein to refold (figure 4.3).

The T_m of HemH unfolding and refolding was calculated using equation 1, the calculated T_m for HemH unfolding were 53 °C and 44 °C for *B. subtilis* HemH and *S. aureus* HemH, respectively. The difference in T_m for the unfolding of two proteins show that *B. subtilis* HemH is more thermally stable by approximately 10 °C (figure 4.3A and C). The T_m for refolding in *B. subtilis* and *S. aureus* HemH were calculated at 52 °C and 63 °C (figure 4.3B and D). Refolding of both proteins showed less negative ellipticities than the protein before unfolding, this could be because of degradation or precipitation of the protein.
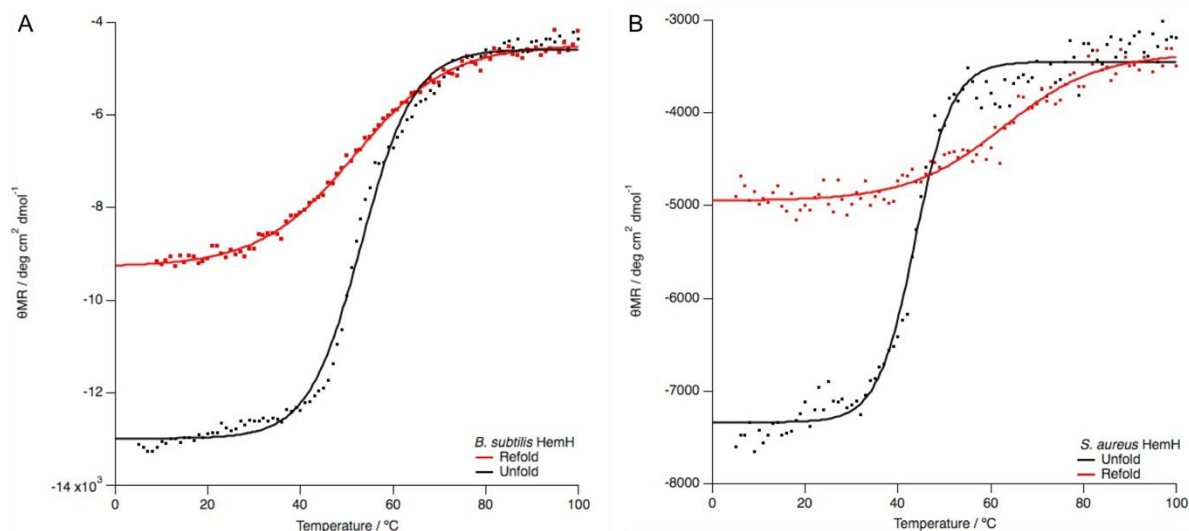
Figure 4.3- Testing the thermostability of *B. subtilis* and *S. aureus* ferrochelatase

The thermostability of the ferrochelatases were tested between 5-100 °C; the ellipticity was measured at 220 nm. During protein unfolding and refolding (**A**) the temperature was changed between 5-100 °C and the calculated melting temperature (T_m) was 53 ± 0.2 °C for unfolding (black) and 52 ± 0.3 °C (red) for *B. subtilis* HemH. (**B**) The temperature was changed between 5-100 °C and the calculated melting temperature (T_m) was 44 ± 0.3 °C for unfolding (black) and 63 ± 1 °C (red) for *S. aureus* HemH. The errors given are ± one standard deviation.

4.5. Kinetic characterisation of *B. subtilis* HemH and *S. aureus* HemH

4.5.1. Preliminary kinetics of coproporphyrin *ferrochelatase to define parameters of the experiment*

4.5.1.1. Scanning kinetics determines a suitable wavelength for steady-state kinetics

Scanning kinetic assays were performed on the two ferrochelatases to identify a suitable wavelength to monitor the reaction. These assays were performed in the presence of the endogenous substrates coproporphyrin III and ferrous iron. The changes in absorbance were monitored in the wavelength range 350-600 nm and the spectra revealed peaks at 393 nm, 500 nm, 536 nm and 556 nm (figure 4.4). The

greatest change in absorbance was observed at 393 nm and this wavelength was selected to monitor the ferrochelatase reaction.
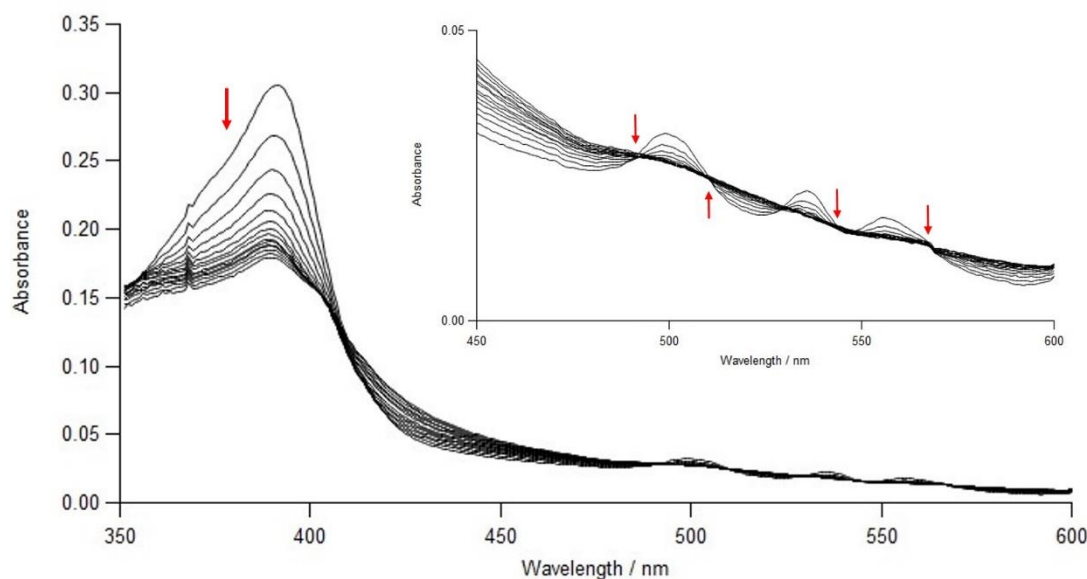
Figure 4.4 – Scanning kinetics of *B. subtilis* ferrochelatase

Change in absorbance as the ferrochelatase reaction proceeds across the wavelength range 350-600 nm. The inset shows an expanded view of the wavelength range 450-600 nm. The ferrochelatase, coproporphyrin III and ferrous iron concentrations were 50 nM, 2 µM and 8 µM, respectively.

4.5.1.2. Endpoint assay allows the determination of extinction coefficient of reaction

After 393 nm was selected from the scanning kinetic assays, the extinction coefficient for the reaction must be obtained. This cannot be directly estimated from the extinction coefficient of the substrate as the product is highly absorbing. In the absence of pure product extinction coefficients for reactions can be determined by running the reaction to its endpoint, this is based on the assumption that the equilibrium constant is sufficiently large that essentially no substrate porphyrin remains. This is required to gain the absorbance change (ΔA) for the reaction; the ΔA can be divided by the concentration of the limiting substrate to gain the extinction coefficient for the reaction.

These assays were run at different substrate concentrations (Fe^{2+} 50 µM and 100 µM) to ensure the calculated extinction coefficient remained relatively consistent throughout and there are no issues with equilibrium (figure 4.5). The calculated extinction coefficient for this reaction using *B. subtilis* HemH and *S. aureus* HemH at 393 nm is 70410 M^{-1} cm^{-1}.
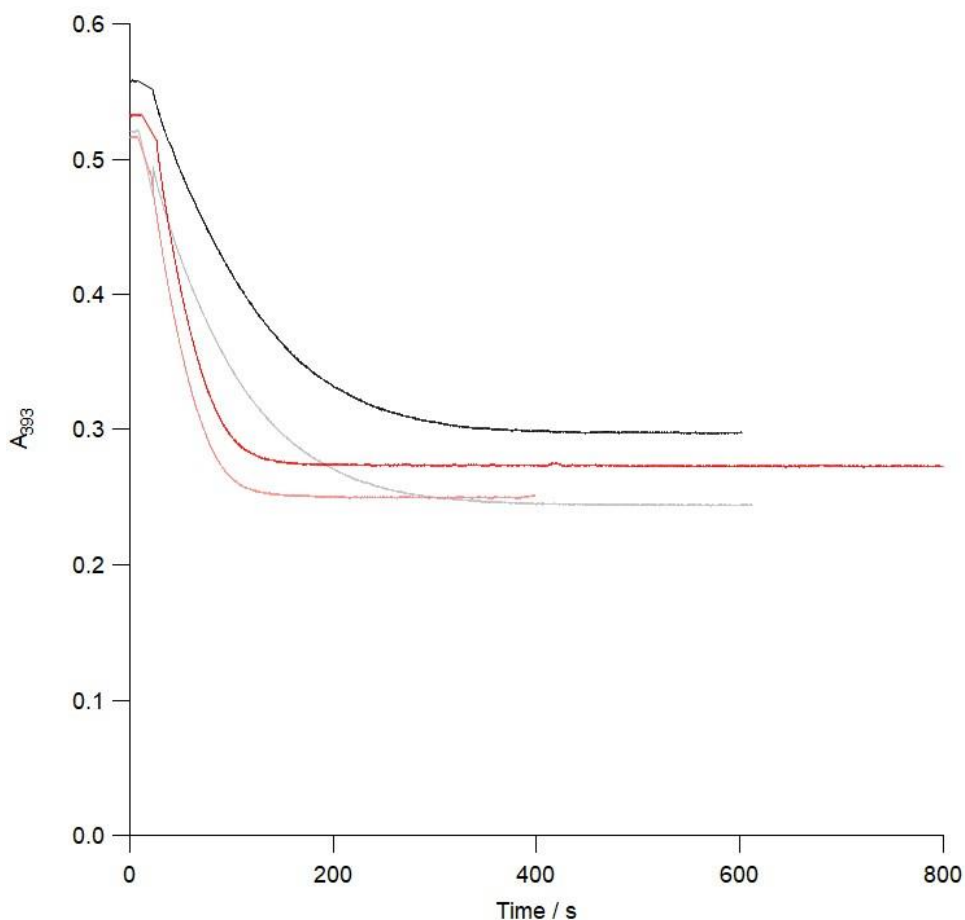
Figure 4.5- Endpoint assay of *B. subtilis* HemH and *S. aureus* HemH to determine molar extinction coefficient for the ferrochelatase reaction.

Graph shows the ferrochelatase reaction of *B. subtilis* and *S. aureus* HemH running to completion at different substrate concentrations. All assays contain 0.2 µM ferrochelatase. The black and grey traces contain *B. subtilis* HemH and the red and pink traces contain *S. aureus* HemH. The black and red traces substrate conditions are 4 µM coproporphyrin III and 100 µM ferrous iron whereas the grey and pink traces contain 4 µM coproporphyrin III and 50 µM ferrous iron.

4.5.2. Steady state kinetics of B. subtilis *HemH* and S. aureus *HemH*

Steady state kinetics were performed on *B. subtilis* HemH and *S. aureus* HemH where one substrate was held under constant conditions whilst the other was varied. The reaction was monitored at 393 nm using a UV-Vis spectrometer and initial rates were obtained using the calculated extinction coefficient (70410 M^{-1} cm^{-1}).

The steady state data was analysed using a multivariate fit and the two-substrate equation (equation 2A), each of the four data sets shown in figure 4.6 were fitted in isolation to allow accurate calculation of steady-state parameters. When the two data sets for each ferrochelatase (figure 4.6A and B for *B. subtilis* HemH and figure 4.6C and D for *S. aureus* HemH) were analysed globally there were slight inconsistencies between the datasets most likely due to different amounts of active enzyme. When varying the concentration of coproporphyrin III (0-4 µM), ferrous iron was held at approximately 5, 10 and 100 µM. The enzyme concentrations were approximately 10 nM, this low concentration was used to maintain steady-state conditions as low concentrations of CP_{III} were required to estimate the K_m^{CP} value. The estimated K_m^{CP} values were calculated as 0.14 and 0.15 µM (*B. subtilis* HemH) and 0.1 and 0.2 µM (*S. aureus* HemH), demonstrating that the K_m^{CP} values in *B. subtilis* and *S. aureus* HemH are similar (figure 4.6A and C). When investigating the second substrate, ferrous iron, the concentration of iron was varied (0-140 µM) and the concentrations of CP_{III} were 2, 1.7 (*B. subtilis* HemH only), 1 and 0.5 µM. The ferrochelatase concentration was 10-fold higher than those used in the previous assays at 0.1 µM as this gave more reliable rates. The calculated K_m^{Fe} values were 1.8 and 3.8 µM and 0.58 and 1.1 µM for *B. subtilis* HemH and *S. aureus* HemH, respectively. The slightly

lower $K_m{}^{Fe}$ in *S. aureus* HemH indicates that it is more active than the *B. subtilis* enzyme at lower iron concentrations (figure 4.6B and D, table 4.7).

The k_{cat} value for the ferrochelatase reaction in each of the species was calculated. The k_{cat} value for *B. subtilis* HemH was 0.32 and 0.35 s^{-1} and 0.36 and 0.44 s^{-1} for *S. aureus* HemH. The two enzymes have similar turnover numbers (k_{cat}) however the *S. aureus* HemH protein is slightly faster showing that it there may be parts of its enzymatic mechanism that it does more effectively than the *B. subtilis* enzyme. In contrast to the $K_m{}^{CP}$, $K_m{}^{Fe}$ and k_{cat} values, $K^{CP.Fe}$ was not calculated. The $K^{CP.Fe}$ value in this mechanism corresponds to the dissociation constant of the ternary complex, however, in general the definition of this term depends on the mechanism. In the analysis of the steady state curves the $K^{CP.Fe}$ value was constrained at either 0.1 or 0.01 µM^2 (figure 4.6A, B and D), as unconstrained curve fitting resulted in a physically unrealistic negative value. The value of this coefficient is low when compared to the product of the two substrate concentrations. Changing the value from 0.1 to 0.01 or 0.001 did not substantially change the best fit estimates of $K_m{}^{CP}$, $K_m{}^{Fe}$ and k_{cat}. In the analysis shown in figure 4.6C this value was optimised as 0.023 µM^2, however the large standard error suggests that the only reliable statement that can be made about this parameter is that it has a much lower value than the lowest product of substrate concentrations reached experimentally (table 4.7).
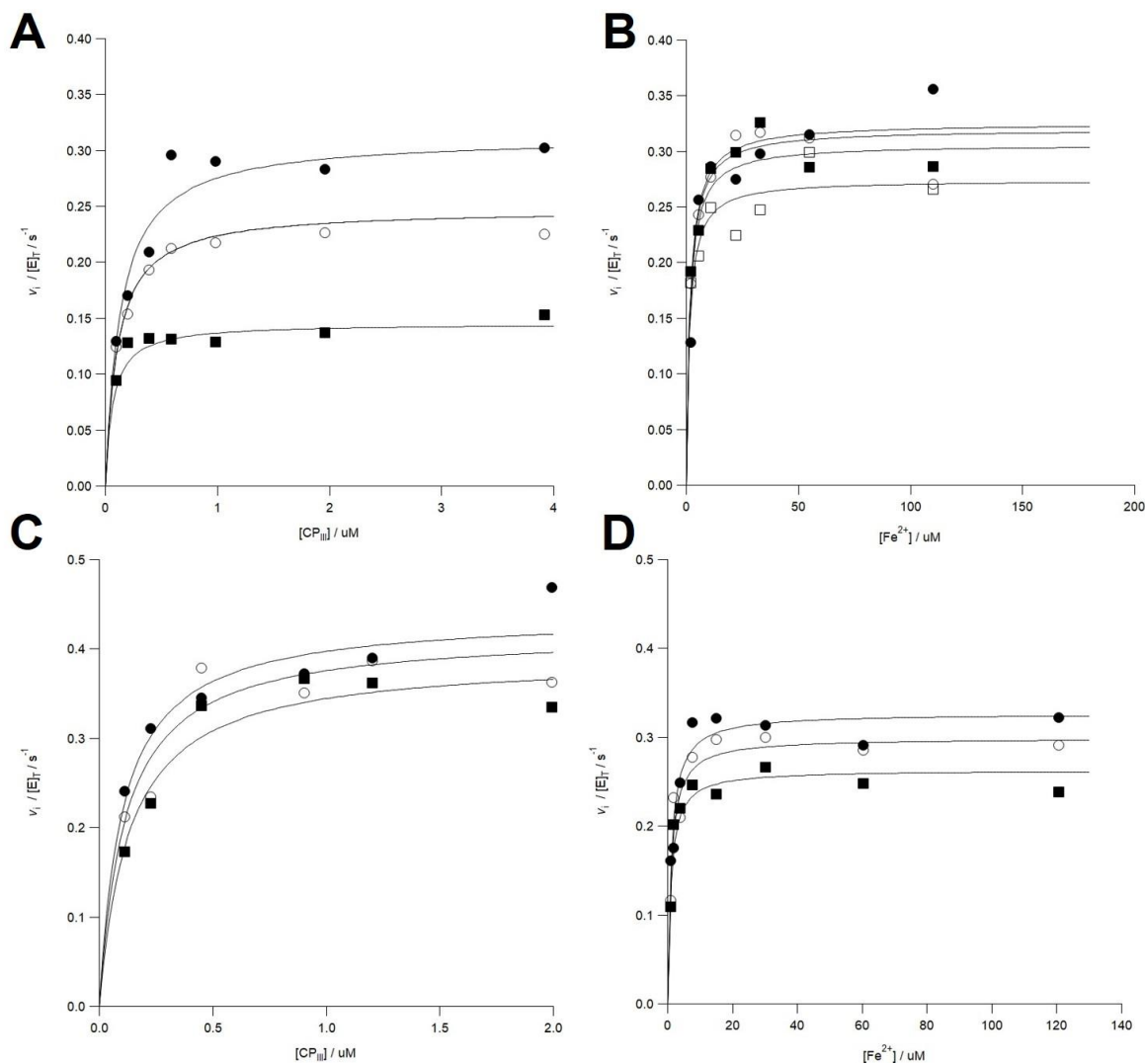
Figure 4.6- Steady-state kinetics of *B. subtilis* HemH and *S. aureus* HemH

Steady-state kinetics of *B. subtilis* HemH (**A** and **B**) and *S. aureus* HemH (**C** and **D**). Part **A** shows when CP_{III} is varied (0-4 µM) and ferrous iron (Fe^{2+}) is held at 107 µM (●), 12 µM (○) and 3 µM (■). B shows when Fe^{2+} is varied (0-100 µM) and CP_{III} is held at 2.2 µM (●), 1.7 µM (○), 1 µM (■) and 0.5 µM (□). These curves were produced using the two-substrate equation (equation 2) in a multivariate fit. The calculated kinetics parameters in **A** were k_{cat} 0.32 ± 0.01 s^{-1}, K_m^{Fe} 3.8 ± 0.4 µM, K_m^{CP} 0.14 ± 0.02 µM and was constrained $K^{CP.Fe}$ at 0.01 µM². The calculated parameters for **B** were k_{cat} 0.35 ± 0.01 s^{-1}, K_m^{Fe} 1.8 ± 0.3 µM, K_m^{CP} 0.15 ± 0.05 µM and $K^{CP.Fe}$ was held at 0.01 µM². Graph **C** shows the activity of *S. aureus* HemH when the CP_{III} is varied (0-2 µM) and Fe^{2+} is held at 114 µM (●), 11 µM (○) and 4.5 µM (■). The traces in part **D** show when iron is varied between (0-140 µM) and CP_{III} is held at 2 µM (●), 1 µM (○) and 0.6 µM (■). The calculated kinetics parameters in **C** were k_{cat} 0.44 ± 0.02 s^{-1}, K_m^{Fe} 0.58 ± 0.05 µM, K_m^{CP} 0.1 ± 0.03 µM and $K^{CP.Fe}$ 0.023 ± 0.2 µM². The calculated parameters for **D** were k_{cat} 0.36 ± 0.02 s^{-1}, K_m^{Fe} 1.1 ± 0.2 µM, K_m^{CP} 0.21 ± 0.06 µM and $K^{CP.Fe}$ was constrained at 0.1 µM². Calculated errors are ± one standard deviation. Each data point was a single reading taken from a single cuvette.

171

Table 4.7- Steady-state kinetics values of B. subtilis HemH and S. aureus HemH

Experiment	Parameters	*B. subtilis* HemH	*S. aureus* HemH
STEADY STATE KINETICS [1]	K_m^{CP} / µM	0.14 ± 0.02	0.1 ± 0.03
		0.15 ± 0.05	0.21 ± 0.06
	K_m^{Fe} / µM	3.8 ± 0.4	0.58 ± 0.05
		1.8 ± 0.3	1.1 ± 0.2
	k_{cat} / s^{-1}	0.32 ± 0.01	0.44 ± 0.02
		0.35 ± 0.01	0.36 ± 0.02
	$K^{CP.Fe}$ / $µM^2$	0.01 ± 0 (held)	0.023 ± 0.2
		0.01 ± 0 (held)	0.1 ± 0 (held)

Most previous steady state kinetics performed on *B. subtilis* and *S. aureus* HemH used protoporphyrin IX or porphyrin molecules related to protoporphyrin (deuteroporphyrin and mesoporphyrin). Also, the endogenous metal ion Fe^{2+} is frequently replaced by Zn^{2+} (Hansson and Hederstedt, 1994b, Hansson et al., 2006, Hansson et al., 2007, Olsson et al., 2002). The results of those kinetic investigations have shown that the *B. subtilis* enzyme is relatively inactive in those conditions compared to *H. sapiens* ferrochelatase. In this work, kinetic characterisation of *B. subtilis* HemH the endogenous substrates CP_{III} and Fe^{2+} have been used, providing a more natural insight to function of ferrochelatase.

CP_{III} is more soluble than stable protoporphyrin IX and deuteroporphyrin. As a result, detergents such as Tween 20 were not required to solubilise CP_{III}. Oxidation of ferrous iron was a possible issue but exchanging Fe^{2+} for Zn^{2+} presented more problems. Zinc can insert into coproporphyrin III without the help of ferrochelatase in an uncatalysed reaction. This uncatalysed reaction is fast and high enzyme concentrations are required to outcompete the uncatalysed reaction (appendix 7.6.1). As a result, high concentrations of substrates are also required to maintain steady-state conditions. This prevents inaccurate estimation of kinetic parameters especially as K_m values were low. An uncatalysed chelation was also observed when Co^{2+} was used although the reaction was slower (unpublished data).

Recent steady-state characterisation has been completed on *S. aureus* HemH (Hobbs et al., 2017, Lobo et al., 2015) and *B. subtilis* HemH (Bali et al., 2011, Lobo et al., 2015) using both of the endogenous substrates (Lobo et al., 2015, Hobbs et al., 2017). In these papers there are small changes in the production, purification and characterisation of the ferrochelatase that could alter the activity of the enzymes.

The kinetic characterisation of *B. subtilis* and *S. aureus* in both papers show that when iron is varied and CP_{III} is held at 1 µM or 10 µM there is significant substrate inhibition observed at low concentrations of iron (<12 µM). In this work, this inhibition was not observed when these enzymes were assayed where CP_{III} was held at 2 µM and iron was varied (0-200 µM), standard Michaelis-Menten kinetic behaviour was observed. In addition, the k_{cat} values were different from those measured in this work (see table 4.8) and were not consistent with each other. The K_m^{Fe} values for *S. aureus* HemH are

consistent (0.60, 0.27 and 0.58 µM). The K_m^{Fe} values for *B. subtilis* HemH inconsistent with at least 10-fold difference (1.8 and 3.8 vs 0.15 µM). In the experiments where CP_{III} was varied (this work and Hobbs et al.) the results are notably different from the each other with a 10-fold difference in K_m^{CP} values (0.1 and 0.21 vs 1.5 µM).

Table 4.8 – Results of kinetic studies from the literature

SOURCES	HEMH SPECIES	KINETIC PARAMETERS			
		k_{cat} / s^{-1}	K_m^{Fe} / µM	K_m^{CP} / µM	K_i^{Fe} / µM
LOBO ET AL.	*B. subtilis*	1.3 ± 0.2	0.15 ± 0.03	ND	2.8 ± 0.5
	S. aureus	2.8 ± 0.9	0.6 ± 0.1	ND	0.8 ± 0.2
HOBBS ET AL.	*S. aureus*	0.18 ± 0.007	0.27 ± 0.04	1.5 ± 0.2	-
THIS WORK	*B. subtilis*	0.32 ± 0.01	3.8 ± 0.4	0.14 ± 0.02	-
		0.35 ± 0.01	1.8 ± 0.3	0.15 ± 0.05	-
	S. aureus	0.44 ± 0.02	0.58 ± 0.5	0.1 ± 0.03	-
		0.36 ± 0.02	1.1 ± 0.2	0.21 ± 0.06	-

The differences in the kinetic parameters calculated in all three research groups can possibly be explained by different protein constructs used as well as slightly different protein expression, purification and assay conditions. In the Lobo et al. paper, the plasmid construct is different (gene contained in pET23b rather than pTrcHisA) and protein expression of growth media is supplemented with iron. The purification of the ferrochelatase follows a standard IMAC and buffer exchange and purified protein is

stored in the assay buffer 0.1 M Tris, pH 8 (same assay buffer as in this work). In the activity assay the CP_{III} solubilised in water with a few drops of NH_4OH, this consistent with the preparation of CP_{III} in Hobbs et al.

In Hobbs et al., the plasmid construct and protein expression and purification protocols are the same as those used in these experiments, the major difference is the purification buffers. Hobbs et al. use MOPS and sodium cholate in their buffers, sodium cholate has been shown to affect enzymatic activity in *H. sapiens* ferrochelatase (Davidson et al., 2009) and the same is true for *S. aureus* HemH. In an endpoint assay the turnover of substrate by *S. aureus* HemH in the presence of detergent was much slower when compared to the assay in the absence of detergent (data incomplete, appendix 7.6.2).The assay buffer for the kinetic assays is also different, it contains 0.1 M Tris, 0.5% sodium cholate, 0.5% Tween 20 and 1 mM β-mercaptoethanol, pH 8.1. It is reasonable to assume that these differences could lead to different enzyme activity.

4.5.3. Investigating binding between B. subtilis *and* S. aureus *ferrochelatase and their endogenous substrates*

Characterisation of *B. subtilis* and *S. aureus* HemH by steady-state kinetics looks at the whole of the reaction and not specific steps in the enzymatic mechanism. The k_{cat} value determines the rate of the rate-determining step but not which part of the mechanism is rate determining. The k_{cat} can be estimated using a standard UV-vis or fluorescence spectroscopy however faster steps in the mechanism require other techniques such as stopped flow spectroscopy. Stopped flow fluorescence

spectroscopy can be used to dissect the enzymatic mechanism of the two ferrochelatases and using different experimental designs the rate constants for each of the enzymatic step can be deduced.

The first enzymatic step assessed was substrate binding, ferrochelatase binds its two substrates in an ordered mechanism, the CP_{III} binds first and the Fe^{2+} is second. Before using stopped flow fluorescence spectroscopy to deduce the rates of CP_{III} binding, binding equilibrium assays between ferrochelatase and CP_{III} were performed. This allowed the estimation of K_d values for CP_{III} binding in *B. subtilis* and *S. aureus* which aided experimental design for the CP_{III} binding kinetics.

4.5.3.1.   Static quenching of tryptophan fluorescence in ferrochelatase in the presence of CP_{III}

In preparation for assessing the kinetics of substrate binding, static binding assays were completed. The ferrochelatases have strong intrinsic tryptophan fluorescence, when they are excited at 280 nm an emission peak is detected between 330-510 nm with a maximum at approximately 371 nm. This tryptophan fluorescence is quenched in the presence of both substrates CP_{III}. Emission spectra of ferrochelatase in the presence of CP_{III} show that the peak representing tryptophan fluorescence between 330-510 nm decreases as the concentration of CP_{III} increases. Excitation at 280 nm is also capable of exciting the porphyrin directly and energy transfer from the tryptophan residues to the porphyrin molecule occurs too. This direct excitation and energy transfer results in an increase in fluorescence intensity in the two emission peaks between 600 and 700 nm that correspond to coproporphyrin (figure 4.9A). The

tryptophan emission peak produced by excitation of *B. subtilis* and *S. aureus* HemH was integrated (330-510 nm) for each concentration of CP_{III} and the peak areas were plotted against CP_{III} concentration to produce a binding curve (figure 4.9B and C). The binding curves for both proteins show tight binding between the enzyme and coproporphyrin strongly indicating the formation of a complex between substrate and enzyme. The data was fitted to the tight binding equation (equation 3A) and the K_d for this interaction was calculated as 0.048 µM (48 nM) for *B. subtilis* HemH and 0.046 µM (46 nM) for *S. aureus* HemH.
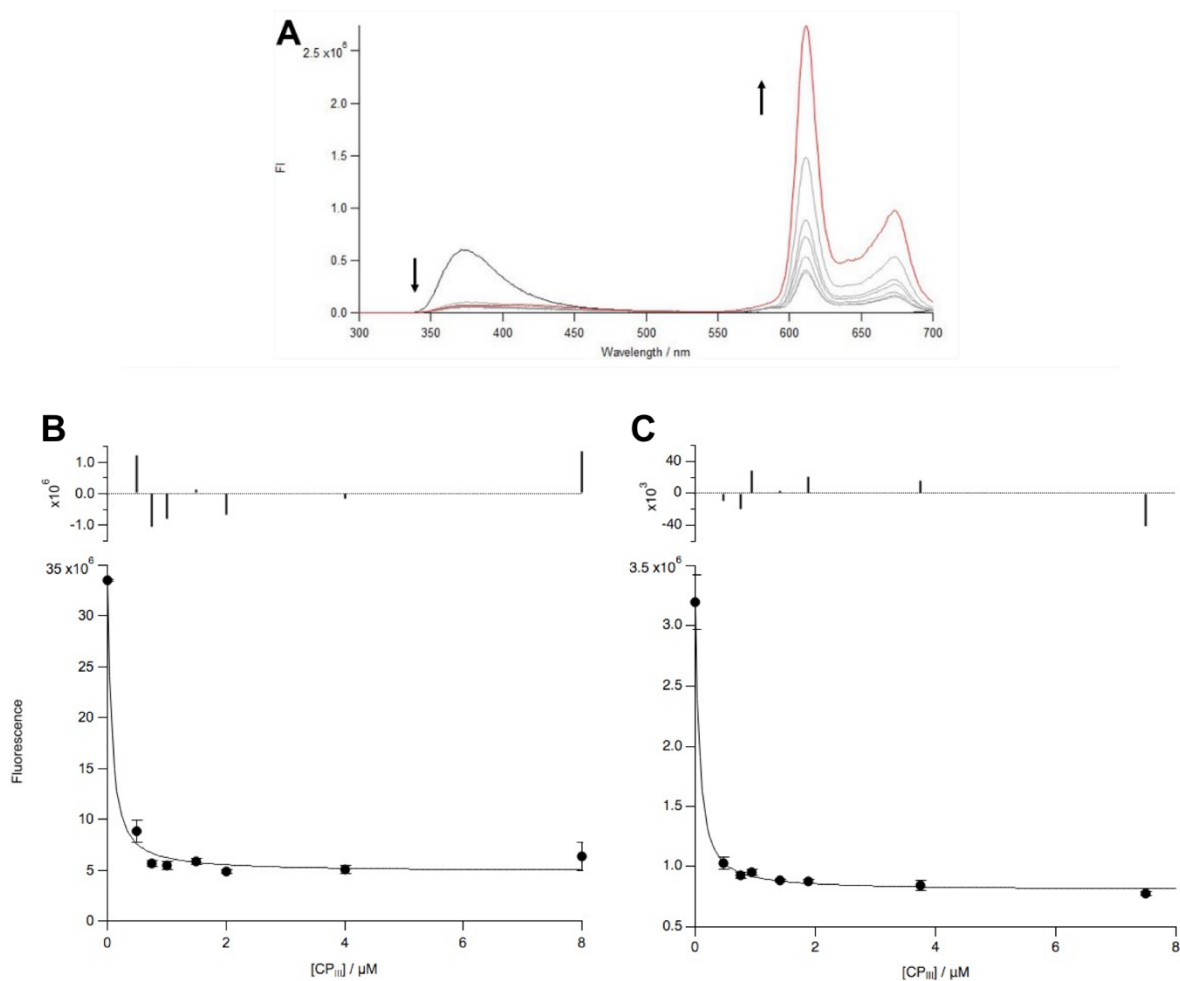
Figure 4.9 – Static quenching of ferrochelatase tryptophan fluorescence by CP$_{III}$

A shows a representative emission spectra of 50 nM *B. subtilis* ferrochelatase in the presence of increasing concentrations of CP$_{III}$ (0-8 µM) when excited at 280 nm. The peak at 371 nm represents the tryptophan fluorescence and the two peaks between 600-700 nm represent emission produced by excitation of porphyrin. Coloured black is emission of FC in the absence of CP$_{III}$ and coloured red is the emission of FC and the highest concentration of CP$_{III}$ (8 µM). The peak representing tryptophan fluorescence of FC is integrated between 330-510 nm and plotted against CP$_{III}$ concentration giving rise to the binding curves in **B** (*B. subtilis)* and **C** (*S. aureus*). Each data point is an average of three and the error bars are ± one standard deviation. The curve was fitted using equation 3A and the calculated K_d was 0.048 ± 0.02 µM and 0.046 ± 0.07 µM for *B. subtilis* and *S. aureus* HemH, respectively.

Ferrous iron binding to ferrochelatase was also tested, ferrous iron is capable of quenching the tryptophan fluorescence of ferrochelatase. It can also quench CP$_{III}$ fluorescence indicating that the quenching mechanism may be non-specific (dynamic) so K_d values for the interaction between iron and ferrochelatase cannot not be determined using this method.

4.5.3.2. Using stopped flow fluorescence spectroscopy to deduce the rates of CP_{III} binding to ferrochelatase

Stopped flow fluorescence spectroscopy was required to deduce the individual rates of steps in the enzymatic mechanism of ferrochelatase. The binding equilibrium assays revealed that there is tight binding between CP_{III} and HemH. This data provided basic guidelines for investigating CP_{III} binding by stopped flow fluorescence spectroscopy.

The experimental design for assessing CP_{III} binding involves preparing the enzyme and CP_{III} in two separate syringes, this prevented any interaction between them. The reaction was monitored at 280 nm or 393 nm depending on whether the coproporphyrin III or ferrochelatase was varied. When investigating the binding in *B. subtilis* HemH both wavelengths were used, and the 280 nm wavelength was used for *S. aureus*, this was because high concentrations of enzyme were unobtainable.

$$E + CP_{III} \xrightleftharpoons{K_{CP}} ECP_{III} \xrightleftharpoons[k_{-iso}]{k_{iso}} E'CP_{III}$$

Scheme 1- Two step substrate (CP_{III}) binding to enzyme (E)

When monitoring the emission of CP_{III} the concentration of CP_{III} was held at 50 nM whilst the *B. subtilis* ferrochelatase concentration was varied between 0.5-5.5 μM. The average trace was fit to a single exponential (equation 4A) and the k_{obs} value was

calculated. The k_{obs} value was plotted against ferrochelatase concentration and fitted to equation 5. The curve was consistent with two step binding where the first stage was initial binding (K_{CP}) and the second stage was likely a reversible isomerisation (k_{iso}) as shown by scheme 1. The rate constant for the backward reaction in step 2 (k_{-iso}) was held at zero as the data show that k_{-iso} is very small. The K_{CP} was calculated as 5.5 μM and the forward reaction in step 2 (k_{iso}) has a rate constant of 46.0 s^{-1} (figure 4.10).
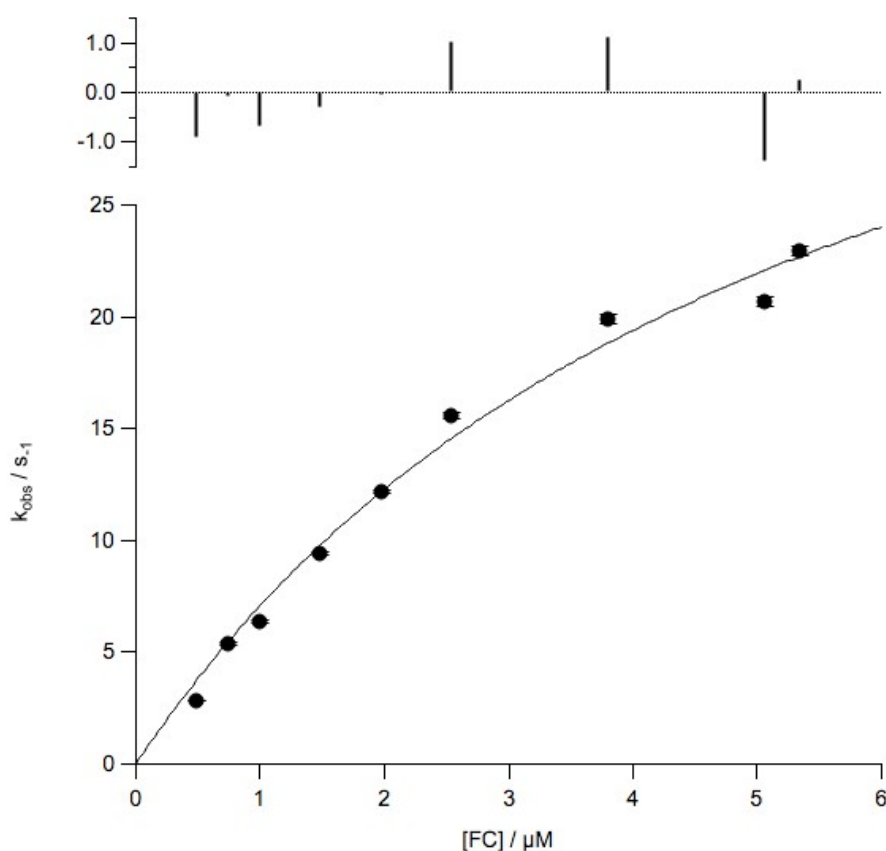
Figure 4.10 - CP$_{III}$ Binding in *B. subtilis* HemH when ferrochelatase is varied

The k_{obs} of the reaction for substrate binding when excited at 393 nm, the CP$_{III}$ concentration was held at 50 nM, the ferrochelatase concentration was varied (0.5- 5.5 μM). A curve was fitted to the data using equation 5, the calculated K_{CP} and k_{iso} values were 5.5 ± 1 μM, 46 ± 5 s^{-1}, respectively and k_{-iso} was constrained at zero. Error bars are ± one standard deviation.

When monitoring the tryptophan fluorescence of ferrochelatase, a blue cut off filter is used, this prevents excitation and emission at the same wavelength and prevents emission beyond 600 nm. The peaks corresponding from direct porphyrin emission span 590-700 nm; this means that the filter removes the majority of the emission generated from direct excitation of porphyrin. Light in the wavelength range 590-600 nm is not completely removed by the filter, however the fluorescence intensity here is very low (<5 %) compared to the fluorescence intensity at λ_{max} (table 2.4). In addition, the transmittance of the filter at this wavelength is also very low. Even in high concentrations of porphyrin there is negligible excitation of free porphyrin detected.

When observing tryptophan quenching, the ferrochelatase concentration can be held at 0.1 μM and the CP_{III} concentration is varied (1-70 μM). The traces are similar to those observed when exciting the porphyrin. The data was also fitted to a single exponential (equation 4A) and the calculated k_{obs} values were plotted against CP_{III} concentration. Again, the data was fitted to equation 5, k_{-iso} was held at zero and the curve fitting was distinctly two-step binding in both ferrochelatases (figure 4.11). The calculated K_{CP} value was 5.6 μM in *B. subtilis* HemH and 7.6 μM in *S. aureus* HemH. These two K_{CP} values are similar as their errors overlap. In addition, the two different binding kinetics approaches performed on *B. subtilis* HemH show that the K_{CP} values are consistent (5.5 vs 5.6 μM).

The forward rate for the isomerisation (k_{iso}) were calculated as 25 and 70 s^{-1} in *B. subtilis* and *S. aureus* HemH, respectively. This shows that isomerisation is almost three-fold faster in *S. aureus* HemH compared to *B. subtilis* HemH. The higher rate of

isomerisation in *S. aureus* HemH could explain the slightly higher k_{cat} value observed in the steady-state kinetics (section 4.5.3). The two different experimental designs (when CP_{III} concentration is varied and when ferrochelatase concentration is varied) in CP_{III} binding kinetics for *B. subtilis* HemH are not consistent in their k_{iso} values. When CP_{III} is held at 50 nM and HemH is varied the k_{iso} value is approximately 2-fold higher at 46 s^{-1} compared to 25 s^{-1}. Systematic errors such as inaccurate calculation of CP_{III} and HemH concentration could give rise to this observed discrepancy. A global fit was applied to both data sets to check for consistency (appendix 7.6.4); this showed that the two datasets were broadly consistent when errors in concentration were corrected for.
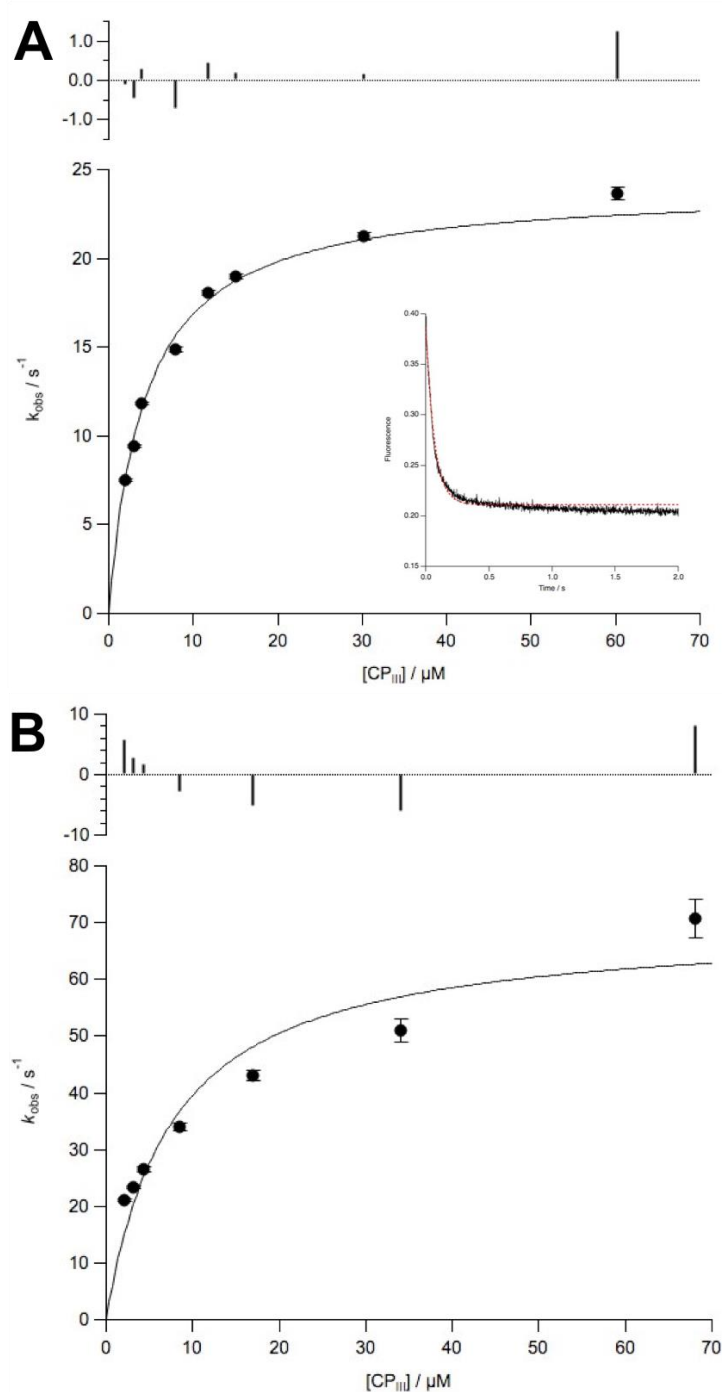
Figure 4.11 – CP$_{\text{III}}$ binding to *B. subtilis* and *S. aureus* ferrochelatase

A shows the k_{obs} of the reaction for substrate binding in *B. subtilis* HemH when excited at 280 nm, the enzyme concentration is held at 0.2 µM and the CP$_{\text{III}}$ is varied (1-60 µM). **B** shows the k_{obs} of the reaction for substrate binding in *S. aureus* HemH, the enzyme concentration is held at 0.2 µM and the CP$_{\text{III}}$ is varied (1-70 µM). Equation 5 was used to fit a curve to the data, a representative example is shown in inset on **A** (black – raw data, red- fitted line). From this fitting the K_{CP}, k_{iso} and $k_{\text{-iso}}$ values were estimated. In *B. subtilis* HemH the calculated K_{CP} and k_{iso} values were 4.8 ± 0.3 µM and 25 ± 0.4 s^{-1}, respectively and in *S. aureus* HemH the calculated K_{CP} was 7.6 ± 2 µM and the k_{iso} was 70 ± 7 s^{-1}. The error bars are ± one standard deviation

4.5.3.3.   Scanning kinetics of the ferrochelatase-CP$_{III}$ complex

In conjunction with binding kinetics of CP$_{III}$ and ferrochelatase, scanning kinetics were performed. Initially scanning kinetics were performed at 350-450 nm using the *B. subtilis* HemH. To start CP$_{III}$ (2 µM) was scanned alone and then 2 µM of ferrochelatase was added. The scanning kinetics of this enzyme-substrate complex in equimolar concentrations showed a red shift in λ$_{max}$ of the Soret band from 393-405 nm (figure 4.12). This spectral shift is not evident when steady-state conditions are used as there is only a low concentration of the bound complex compared to free porphyrin. To determine whether this spectral change was actually due to complex formation between *B. subtilis* ferrochelatase and CP$_{III}$ a few tests were completed.

A concern was that there may be zinc contamination and this would cause the shift in the peak. Zinc can be easily inserted in coproporphyrin III without the help of ferrochelatase forming Zn-coproporphyrin III however, when the reaction is spiked with 10 µM Zn^{2+} a highly absorbing narrow peak with a λ$_{max}$ at 403 nm forms, indicating that the spectral shift does not occur as a result of zinc contamination (figure 4.12A). Furthermore, after the enzyme-substrate complex had formed it was treated with ~30% ethanol which denatured the ferrochelatase and the Soret band shifted back to 394 nm, the same λ$_{max}$ as CP$_{III}$ in the presence of ~30 % ethanol (figure 4.12B), demonstrating that the spectral shift is a result of complex formation between HemH and CP$_{III.}$ The spectral shift that occurs in when CP$_{III}$ binds *B. subtilis* HemH is also observed when CP$_{III}$ binds to *S. aureus* HemH (figure 4.13B).
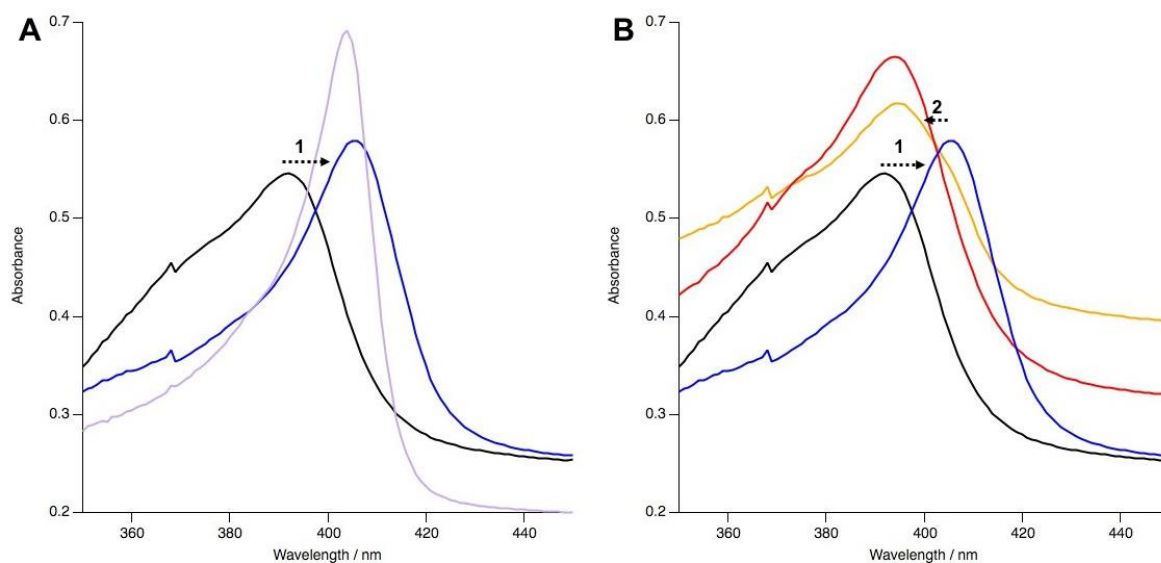
Figure 4.12- Determining whether spectral shift is a result of complex formation

A shows the spectral shift when 2 μM CP_{III} shown by the (black) complexes with 2 μM *B. subtilis* HemH to give the spectrum coloured blue. The shift is shown by the arrow labelled 1 and λ_{max} changes from 393 nm to 405 nm. The spectrum given for Zn-coproporphyrin is shown in purple for comparison. **B** shows the spectral shift is due to complex formation between the CP_{III} and ferrochelatase. The spectrum of 2 μM CP_{III} in assay buffer (λ_{max} 393 nm) and 30% ethanol + assay buffer (λ_{max} 394 nm) is shown in black and red, respectively, these are controls. Addition of 2 μM ferrochelatase to CP_{III} in assay buffer causes a red shift in the Soret band (λ_{max} 405 nm, blue). After complex formation the solution was added to an ethanol solution to form a solution containing the FC-CP_{III} complex in 30% ethanol which is shown by the orange trace (λ_{max} 394 nm). The arrow numbered 1 indicates the initial shift that occurs when enzyme-substrate complex is formed and the arrow numbered 2 shows a blue shift from 405 nm to 394 nm which occurs in the presence of 30 % ethanol when the complex breaks apart.

Rapid scanning kinetics were completed so that the spectral shift could be visualised on a millisecond time scale. The appearance of one isosbestic point indicated that there were two distinct species these an unbound porphyrin and a ferrochelatase bound porphyrin species (figure 4.13). Strangely, the rapid scanning kinetics in *B. subtilis* HemH showed the Soret band λ_{max} move from 393 nm to 411 nm, the reason for this is unknown. All metal was removed with chelex 100 so metal contamination was not the issue, perhaps the batch of enzyme was older and losing activity and so different spectral properties were observed. As pseudo-first order conditions were not used rate constants for this could not be obtained.
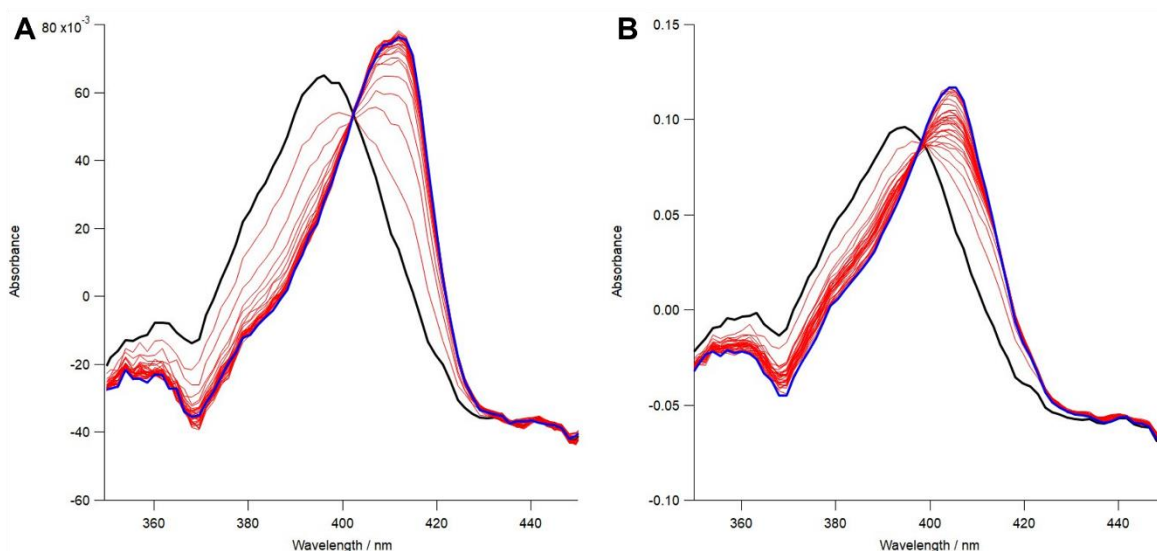
Figure 4.13- Rapid scanning kinetics of ferrochelatase and CP$_{III}$ complex formation

The spectra show rapid scanning kinetics of *B. subtilis* (**A**) and *S. aureus* (**B**) complexion with CP$_{III}$. The spectral shift is measured over 5 s (*B. subtilis*) or 10 s (*S. aureus*). The concentrations of the ferrochelatases were 1 µM and the CP$_{III}$ concentration was 0.64 µM. In **A** the λ_{max} of CP$_{III}$ shifts from 393 nm to 411 nm and in **B** the λ_{max} of CP$_{III}$ shifts from 393 nm to 405 nm. Each single trace is an average of 10 consecutive scans, this reduced noise.

4.5.4. Investigating iron binding and porphyrin metalation

The next step in the enzymatic mechanism investigated was iron binding to the complex ferrochelatase-CP$_{III}$ complex and then metalation of the porphyrin. To assess these enzymatic steps a combination of stopped flow fluorescence and UV-visible spectroscopy was utilised. The experimental design involved preassembling HemH and CP$_{III}$ in equimolar conditions and adding ferrous iron in greater than 10-fold excess, the enzymatic scheme that highlights the mechanistic steps that are being investigated is shown in scheme 2.

$$\text{E'CP}_{III} \underset{}{\overset{K_{Fe}}{\rightleftharpoons}} \text{E'CP}_{III}\ldots\text{Fe} \underset{k_{-chel}}{\overset{k_{chel}}{\rightleftharpoons}} \text{E'CP}_{III}\text{Fe}$$
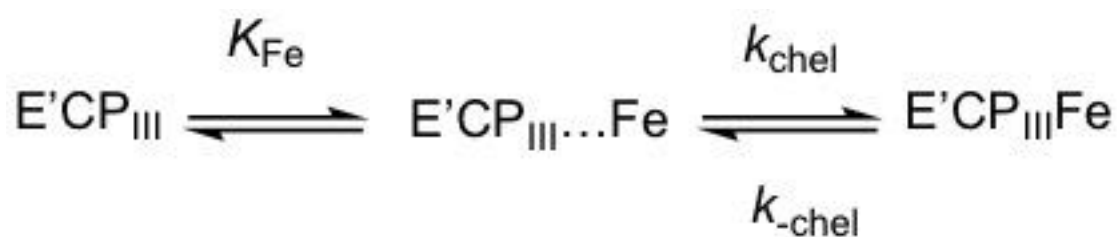
Scheme 2- Iron binding and porphyrin metalation

Scanning kinetics were performed to determine the spectra for product formation. Addition of 10-fold excess of ferrous iron to the ferrochelatase-CP$_{III}$ complex shows rapid decrease in absorbance at 405 nm (figure 4.14). This shows that 405 nm can be used to determine rate constants for iron binding and porphyrin metalation.
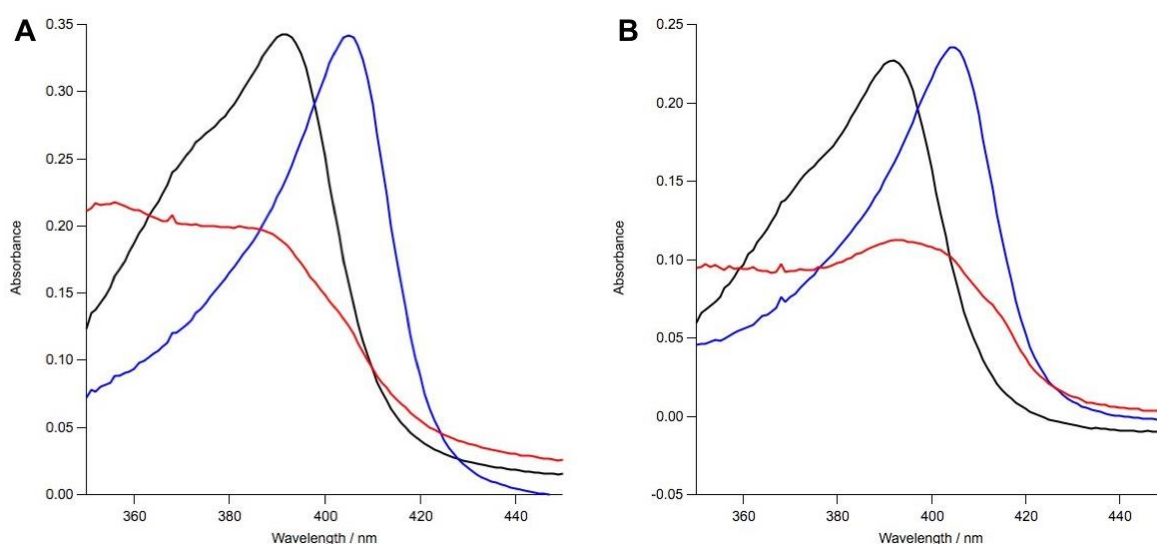
Figure 4.14 – Spectral shift upon complex formation in *B. subtilis* and *S. aureus* HemH

The spectral shift upon complex formation of HemH and CP$_{III}$ is shown with *B. subtilis* HemH (**A**) and *S. aureus* HemH (**B**). CP$_{III}$ (2 μM) alone is shown by the black spectra, the spectra of equimolar CP$_{III}$ and HemH is blue and the addition of 10-fold excess ferrous iron is red. The spectral shift in both proteins moves the λ$_{max}$ of the CP$_{III}$ Soret band from 393 nm to 405 nm.

4.5.4.1. Investigation of the rates of iron binding and porphyrin metalation using stopped flow fluorescence

After investigating complex formation between CP$_{III}$ and ferrochelatase using scanning kinetics, rates of metal binding and porphyrin metalation were assessed again using stopped flow fluorescence spectroscopy. In this experimental design, the reaction was excited at 405 nm, the λ$_{max}$ of the Soret band after complex formation between CP$_{III}$ and ferrochelatase. The ferrochelatase and CP$_{III}$ (1 μM) were incubated together in equimolar conditions. Incubation proceeded for a few minutes to ensure all CP$_{III}$ was

bound to the enzyme and was then exposed to 10-fold excess of ferrous iron. Both syringes contained 1 µM ferrochelatase so that when they were mixed the concentration of ferrochelatase remained constant (1 µM). This design prevents an artefactual change in the porphyrin binding equilibrium. This experiment was only completed for *B. subtilis* HemH in with this design (figure 4.15).

The raw traces for these experiments appeared to be single exponential with an additional linear phase, as a result they were fit to equation 4B and k_{obs} values were estimated. When the k_{obs} values were plotted against Fe^{2+} concentration, the data was fit to equation 6 and indicated the presence of two steps; iron binding (K_{Fe}) and porphyrin metalation (k_{chel}). The estimated binding (K_{Fe}) and rate constants (k_{chel}) for *B. subtilis* were 90 µM and 16 s^{-1}, respectively.
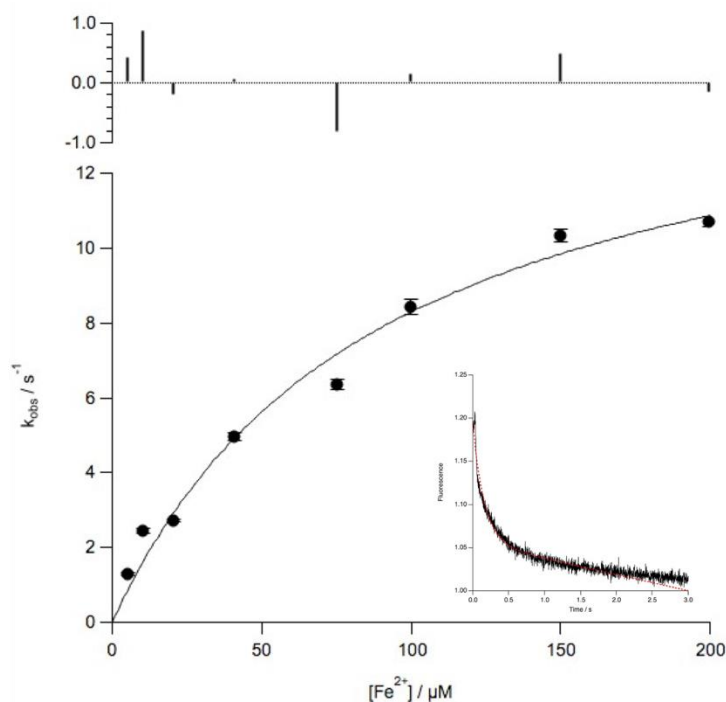
Figure 4.15- Determining the rate of iron binding and porphyrin metalation in *B. subtilis*

The rate constants for the iron binding and porphyrin metalation in *B. subtilis* HemH was determined using stopped flow fluorescence spectroscopy. The enzyme-CP$_{III}$ complex was preassembled in equimolar conditions 1 µM. The syringe containing ferrous iron (Fe^{2+}) also contained 1 µM enzyme. The final concentration of CP$_{III}$ was 0.5 µM and HemH was 1 µM. The Fe^{2+} concentration was varied between 0-200 µM and the reaction was excited at 405 nm. A representative raw data trace is show in the inset in **A** (raw data – black, fitted curve- red). The K_{Fe} value were calculated as 90 $\pm$ 20 µM for *B. subtilis* HemH and the k_{chel} value for *B. subtilis* HemH were 16 $\pm$ 1.6 s^{-1}. The k$_{-chel}$ values were held at zero and error bars are $\pm$ one standard deviation.

4.5.5. Determining the rate constants in ferrochelatase mechanism from the beginning until the rate determining step

The final experimental design used in the stopped flow spectroscopy looks at the rates of all the enzymatic steps in the ferrochelatase mechanism before the rate-determining step. The rate determining step occurs after porphyrin metalation and is most likely to be product release. The approximate rates for the rate determining step for each enzyme are the k_{cat} values gained in the steady state kinetics (sections 4.5.3) 0.32 and 0.35 s^{-1} and 0.36 and 0.44 s^{-1} for *B. subtilis* and *S. aureus* HemH, respectively.

The experimental design ensures that the ferrochelatase is separate from the substrates; the substrates are incubated together and are exposed to ferrochelatase at the same time. The reaction was excited at 393 nm and the enzyme and CP_{III} concentrations were held at 0.2 µM and 2 µM, respectively. The ferrous iron concentration was varied between 2-200 µM. The raw traces were similar in appearance to those observed in the previous experiment (section 4.5.5.1), where there was an exponential phase followed by a linear phase. Using the *B. subtilis* HemH data from the previous two experiments the rate constant (k_{iso}) for CP_{III} binding (at 2 µM) and the rate constant for chelation (k_{chel}) were at specific iron concentrations (2, 3, 4, 5, 10, 20, 80 and 200 µM) were used to fit a double exponential equation (equation 4C) to the third stopped flow experiment (figure 4.16). This approach was used as the rate constants for k_{iso} and k_{chel} were too similar. As these values were too similar it was difficult to distinguish the two separate exponential phases. To distinguish between the two exponential phases there must be at a 10-fold difference in their rate constants. At lower concentrations of ferrous iron this was obtainable but not at ferrous iron concentrations higher than 4 µM. The data analysis of this experiment show that it is consistent with the binding kinetics and iron binding and porphyrin metalation kinetics described in section 4.5.4.3 and 4.5.5.1.
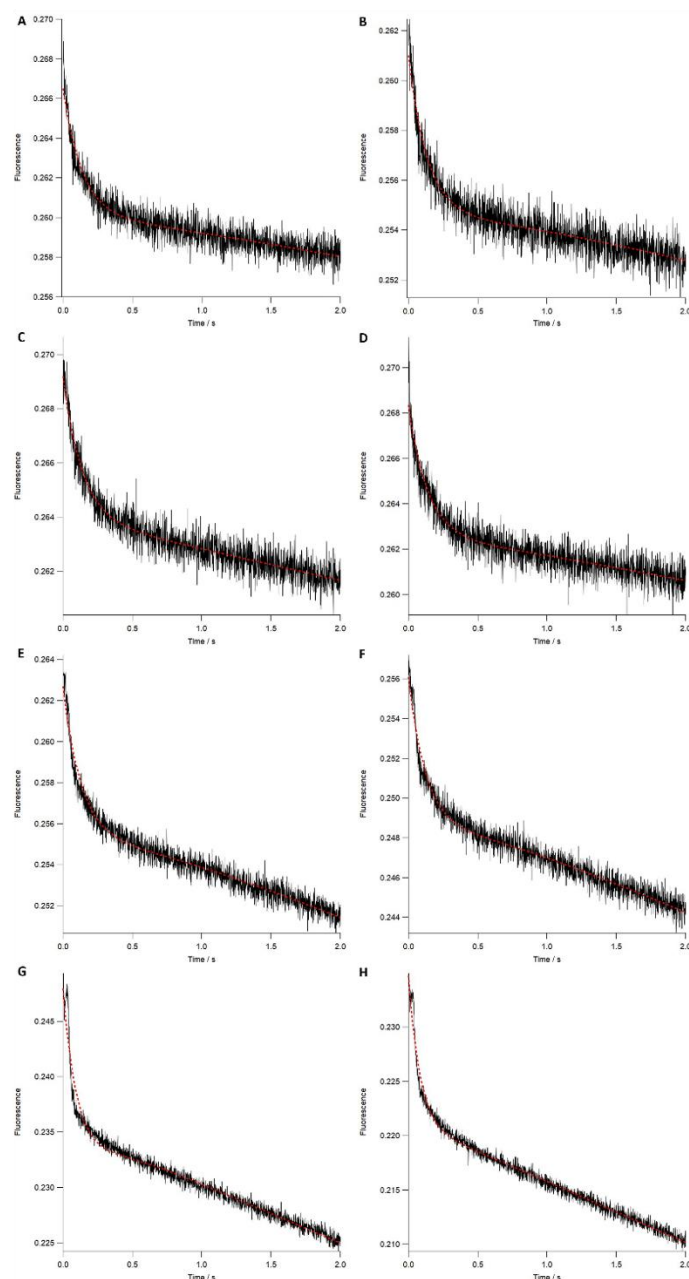
Figure 4.16- Determining the rate of enzymatic steps in the *B. subtilis* HemH mechanism prior to the rate-determining step

The rate of the enzymatic steps prior to the rate determining step in *B. subtilis* was determined using stopped flow fluorescence spectroscopy. The enzyme concentrations and CP_{III} concentration were held at 0.2 µM and 2 µM, respectively. The ferrous iron (Fe^{2+}) concentration was varied (2 µM (**A**), 3 µM (**B**), 4 µM (**C**),5 µM (**D**), 10 µM (**E**), 20 µM (**F**), 80 µM (**G**) and 200 µM (**H**)). The porphyrin was excited at 393 nm and progress curves measured the change in fluorescence (black). The progress curves were fitted to a double exponential equation (equation 4C). The rate of the first exponential phase was held at 7.35 s^{-1}(the rate constant for the CP_{III} binding at 2 µM). The rate of the second exponential phase was held at rate constants for the porphyrin metalation at different iron concentrations (0.348 s^{-1} (**A**), 0.516 s^{-1} (**B**), 0.681 s^{-1} (**C**), 0.842 s^{-1} (**D**), 1.60 s^{-1} (**E**), 2.91 s^{-1} (**F**), 7.51 s^{-1} (**G**) and 11.0 s^{-1} (**H**). The curve fitting for the double exponential equation is shown in red.

This stopped flow spectroscopy experiment was also completed in *S. aureus* HemH. However, as the iron binding and porphyrin metalation kinetics were not performed on *S. aureus* HemH the data analysis used on *B. subtilis* HemH cannot be used. The progress curves obtained in this experiment were fitted to a single exponential and a linear phase (equation 4B). Fitting to a double exponential equation resulted in a large range of values for the second exponential phase. After k_{obs} values were obtained they were plotted against iron concentration and fit to equation 7. The estimated K_{Fe} value was 1.1 μM and the estimated k_{burst} value was 30 s^{-1} (figure 4.17).
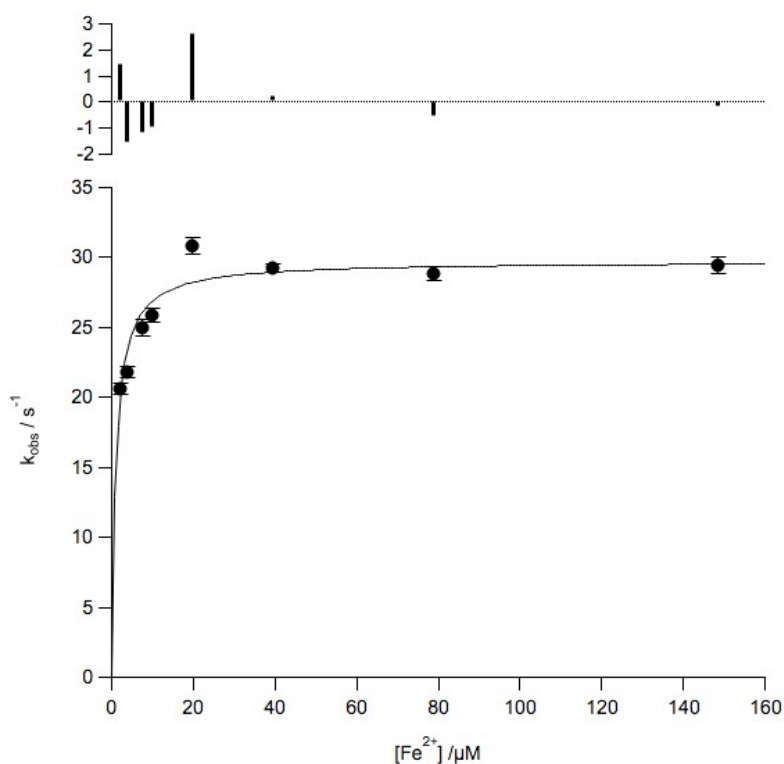
Figure 4.17- Determining the rate of enzymatic steps in the *S. aureus* HemH mechanism prior to the rate-determining step

The rate of the enzymatic steps prior to the rate determining step in *S. aureus* was determined using stopped flow fluorescence spectroscopy. The enzyme concentrations and CP$_{III}$ concentration were held at 0.2 μM and 2 μM, respectively. The ferrous iron (Fe^{2+}) concentration was varied between 0-200 μM and the reaction was excited at 393 nm. The K_{Fe} value was estimated as 1.1± 0.2 μM for *S. aureus* HemH. The k_{burst} value was 30 ± 0.8 s^{-1}, respectively. The k$_{-burst}$ values were held at zero and error bars are ± one standard deviation.

The k_{burst} value is a combined rate constant for k_{iso} and k_{chel}. As the CP$_{III}$ concentration is not at saturating conditions with respect to the K_{CP} values in the binding kinetics (but are with respect to K_m^{CP} and K_d values) the rate constant calculated is a combination of the ferrochelatase isomerisation and iron binding and porphyrin metalation rather than just iron binding and porphyrin metalation. The scheme for this reaction is shown in scheme 3.
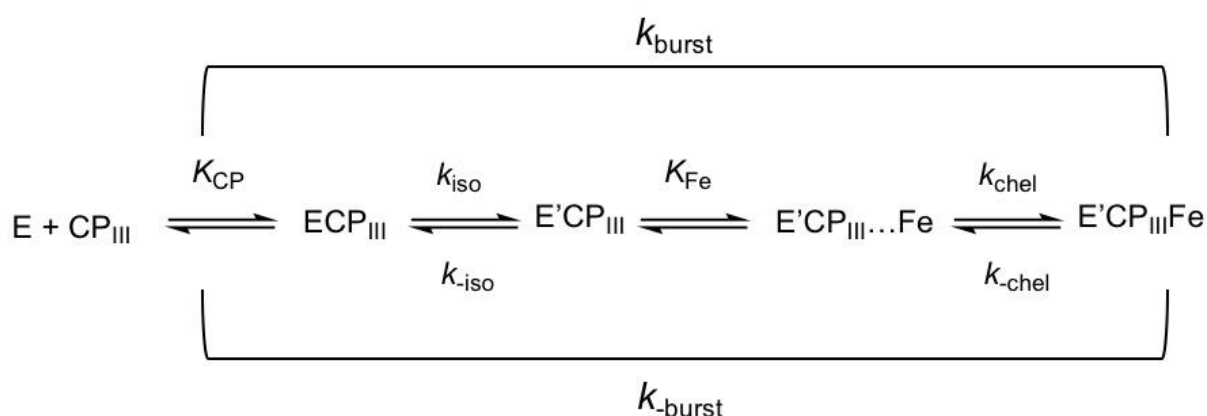
$$E + CP_{III} \xrightleftharpoons[]{K_{CP}} ECP_{III} \xrightleftharpoons[k_{-iso}]{k_{iso}} E'CP_{III} \xrightleftharpoons[]{K_{Fe}} E'CP_{III}\ldots Fe \xrightleftharpoons[k_{-chel}]{k_{chel}} E'CP_{III}Fe$$

with k_{burst} (forward, top) and k_{-burst} (reverse, bottom) spanning the whole scheme.

Scheme 3 – Enzymatic scheme of ferrochelatase reaction from start to rate determining step

4.6. Chapter summary

In this chapter, expression protocols and protein purification of *B. subtilis* and *S. aureus* HemH have been changed slightly compared to the published methods. *B. subtilis* HemH can be expressed using a standard IPTG induction method and purification involves normal IMAC and IEX chromatography. *S. aureus* HemH must be expressed in nutrient rich media with no IPTG protein induction (as stated in the literature) but can be purified in the absence of the detergent sodium cholate and MOPS following the same protocol previously published (Hobbs et al., 2017). The presence of sodium cholate has shown that the activity of *S. aureus* HemH is severely

impaired (data incomplete, appendix 7.6.2) compared to its activity in the absence of detergent. In the absence of detergent, the activity of *S. aureus* HemH is comparable to *B. subtilis* HemH. Circular dichroism has shown that these two proteins have similar structural elements and *B. subtilis* HemH is more thermostable than *S. aureus* HemH.

In kinetic characterisation using steady state kinetics the kinetic parameters for each of the ferrochelatases were similar, *S. aureus* HemH seems to have a slightly higher k_{cat} value indicating that it is more efficient at releasing metalloporphyrin product. Also, its slightly lower K_m value for iron (K_m^{Fe}) means it can work more capably at lower iron concentrations compared to *B. subtilis* HemH. Binding assays and steady state data reveal that *B. subtilis* and *S. aureus* HemH have the same K_m and K_d values for CP_{III} (summary of values shown in table 4.16)

Table 4.16 Calculated kinetic parameters for steady state kinetics and binding assays

Experiment	Parameters	*B. subtilis* HemH	*S. aureus* HemH
STEADY STATE KINETICS [1]	K_m^{CP} / µM	0.14 ± 0.02 0.15 ± 0.05	0.1 ± 0.03 0.21 ± 0.06
	K_m^{Fe} / µM	3.8 ± 0.4 1.8 ± 0.3	0.58 ± 0.5 1.1 ± 0.2
	k_{cat} / s^{-1}	0.32 ± 0.01 0.35 ± 0.01	0.44 ± 0.02 0.36 ± 0.02
	$K^{CP.Fe}$ / µM^2	0.02 ± 0 (held) 0.01 ± 0 (held)	0.023 ± 0.2 0.1 ± 0 (held)
CP$_{III}$ BINDING ASSAYS	K_d / µM	0.048 ± 0.02	0.046 ± 0.007

[1] Data re-represented for clarity.

Stopped flow fluorescence spectroscopy was able to show upon binding CP$_{III}$ the ferrochelatases both undergo an isomerisation. The rates for this isomerisation show that it occurs much quicker in *S. aureus* HemH however the K_{CP} values appear lower in *B. subtilis* HemH. The backward reaction for the isomerisation (k$_{-iso}$) was held at zero as this rate is very small. The rate of this can be calculated from the kinetic parameters gained in the binding assay and binding kinetics and is estimated as 0.25 s^{-1} and 0.42 s^{-1} in *B. subtilis and S. aureus* HemH, respectively. The rates acquired in these experiments are summarised in table 4.17.

A combination of rapid scanning kinetics, standard scanning kinetics and stopped flow fluorescence spectroscopy was used to show that a spectral shift occurred when free porphyrin became bound to either ferrochelatase. Tests were undertaken to confirm that this spectral shift occurred due to complex formation between CP_{III} and *B. subtilis* ferrochelatase. In the spectral shift the λ_{max} for the Soret band shifts from 393 nm to 405 nm, as a result transient kinetics were undertaken using the preassembled complex. The complex (in *B. subtilis* HemH) was excited at 405 nm and revealed that there is two step binding. These two steps have been attributed to iron binding and porphyrin metalation. The iron binding constant at 90 µM was relatively high and the k_{chel} was estimated at 16 s^{-1} (see table 4.17).

Table 4.17 Calculated kinetic parameters for stopped flow fluorescence spectroscopy

Stopped Flow	Parameters	*B. subtilis* HemH	*S. aureus* HemH
CP$_{III}$ BINDING	K_{CP} / μM	4.8 ± 0.3	7.6 ± 2
	k_{iso} / s^{-1}	25 ± 0.4	70 ± 7
	k_{-iso} / s^{-1}	0 ± 0 (held)	0 ± 0 (held)
IRON BINDING AND PORPHYRIN METALATION	K_{Fe} / μM	90 ± 20	ND
	k_{chel} / s^{-1}	16 ± 2	ND
	k_{-chel} / s^{-1}	0 ± 0 (held)	ND
ALL STEPS BEFORE RATE DETERMINING STEP	K_{Fe} / μM	-	1.1 ± 0.2
	k_{burst} / s^{-1}	-	30 ± 0.8
	k_{-burst} / s^{-1}	-	0 ± 0 (held)

The final experimental design used in stopped flow looked at the rates of steps in the ferrochelatase mechanism prior to the rate determining step. These were consistent with the rates gained in the CP$_{III}$ binding experiment and the iron binding and porphyrin metalation setup (*B. subtilis* HemH only). These results show that whilst most calculated kinetic parameters for the two enzymes have been similar *S. aureus* is generally more capable of producing coproheme from coproporphyrin III. It is likely that the slight difference in sequence may be attributed to the difference observed between *B. subtilis* and *S. aureus* HemH. The enzymatic scheme for the overall mechanism investigated is shown in scheme 4.

$$E + CP_{III} \xrightleftharpoons{K_{CP}} ECP_{III} \xrightleftharpoons[k_{-iso}]{k_{iso}} E'CP_{III} \xrightleftharpoons{K_{Fe}} E'CP_{III}...Fe \xrightleftharpoons[k_{-chel}]{k_{chel}} E'CP_{III}Fe \xrightarrow{k_{cat}} E + CP_{III}Fe$$
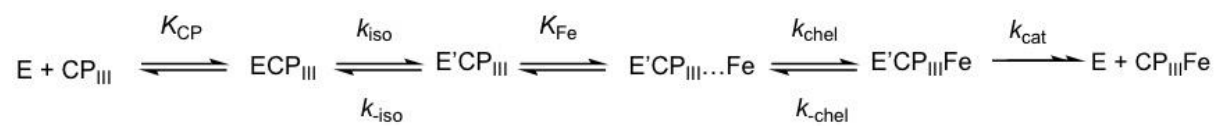
Scheme 4- Overall enzymatic mechanism of ferrochelatase

5. Defining the role of active site residues in the function of the *B. subtilis* HemH enzymatic mechanism

5.1. Chapter introduction

B. subtilis is a Gram positive bacterium that utilises the coproporphyrin-dependent heme biosynthetic pathway. The *B. subtilis* HemH has been extensively studied before the discovery of the coproporphyrin-dependent pathway and as a result, our view of the structure-function relationship is distorted by the assumption that protoporphyrin IX was the substrate. The work presented here addresses the role of a set of *B. subtilis* HemH active site residues in the reaction with CP_{III}.

Several structures of wildtype *B. subtilis* HemH and its mutants have been resolved using X-ray crystallography (Hansson et al., 2007, Hansson et al., 2011, Hansson et al., 2006, Karlberg et al., 2008, Lecerof et al., 2000, Lecerof et al., 2003, Shipovskov et al., 2005, Al-Karadaghi et al., 1997) and kinetic characterisation of the wildtype and mutant proteins has been performed (Hansson et al., 2007, Hansson et al., 2006, Hansson et al., 2011, Shipovskov et al., 2005). The main limitations of these kinetic experiments are that the porphyrin substrates used are not endogenous. In the kinetic assays performed, the protoporphyrin IX and related molecules such as deuteroporphyrin IX and mesoporphyrin IX have been used. As a result, the wildtype *B. subtilis* HemH has appeared relatively inactive compared to the *H. sapiens* HemH and mutation of the active site residues in *B. subtilis* HemH has reduced the activity of the ferrochelatase even more.

The active site for the *B. subtilis* HemH is larger than the active site for the *H. sapiens* HemH and so the smaller more planar porphyrin molecules such as protoporphyrin can enter the active site of the ferrochelatase. These porphyrin molecules may bind in an orientation that is not correct and different to what is expected as shown in the crystal structure of *B. subtilis* HemH and N-methyl mesoporphyrin (Lecerof et al., 2000). The N-methyl mesoporphyrin bound *B. subtilis* ferrochelatase structure (PDB ID: 1C1H) shows the porphyrin bound in a different orientation to the PP_{IX} bound *H. sapiens* ferrochelatase (PDB: ID 2HRE) (Lecerof et al., 2000, Medlock et al., 2007a) shown in figure 1.18. As these smaller molecules can enter the active site of the *B. subtilis* HemH it may indicate why metalation of PP_{IX} is still observed (Hansson et al., 2007, Hansson et al., 2006).

Additionally, other divalent metal ions have been used in ferrochelatase assays instead ferrous iron due to its propensity to oxidise to ferric iron and ferrochelatase cannot insert ferric iron into the porphyrin ring. Zn^{2+} is the most commonly used metal ion used in the assays as it does not oxidise however it has its own limitations. For an example zinc can insert itself into the porphyrin molecule without the help of ferrochelatase (unpublished data), this is much faster when using CP_{III} compared to PP_{IX}. The combination of using the incorrect porphyrin molecule and other divalent metal ions in the ferrochelatase assays may not correctly report the actual activity of the *B. subtilis* HemH.

The mutant proteins that have been previously investigated (K87A, H88A, H183A, E264Q and E264A) were selected for investigation (see figure 5.1 for location in active

site). These mutants were selected as they represent active site residues that are thought to be important in the enzymatic mechanism. There is an ongoing debate about which active site residues are involved in the key reaction steps; binding iron, metalating porphyrin and abstracting protons. Two main arguments have been proposed. The first argument is that the conserved His-Glu pair bind iron and deliver it to the porphyrin ring, and the non-conserved face is responsible for proton abstraction. In contrast, the second argument proposes that the non-conserved face delivers the iron to the porphyrin ring and the pyrrole protons are abstracted by the conserved histidine residue(Hansson et al., 2007, Hunter et al., 2016, Sellers et al., 2001, Dailey et al., 2007, Hoggins et al., 2007). Two of the mutants selected target the non-conserved face of the active site (K87A and H88A) and the other three mutants target the conserved face of the active site (H183A, E264Q and E264Q), a combination of kinetic experiments could give a deeper insight to the enzymatic mechanism of *B. subtilis* HemH.
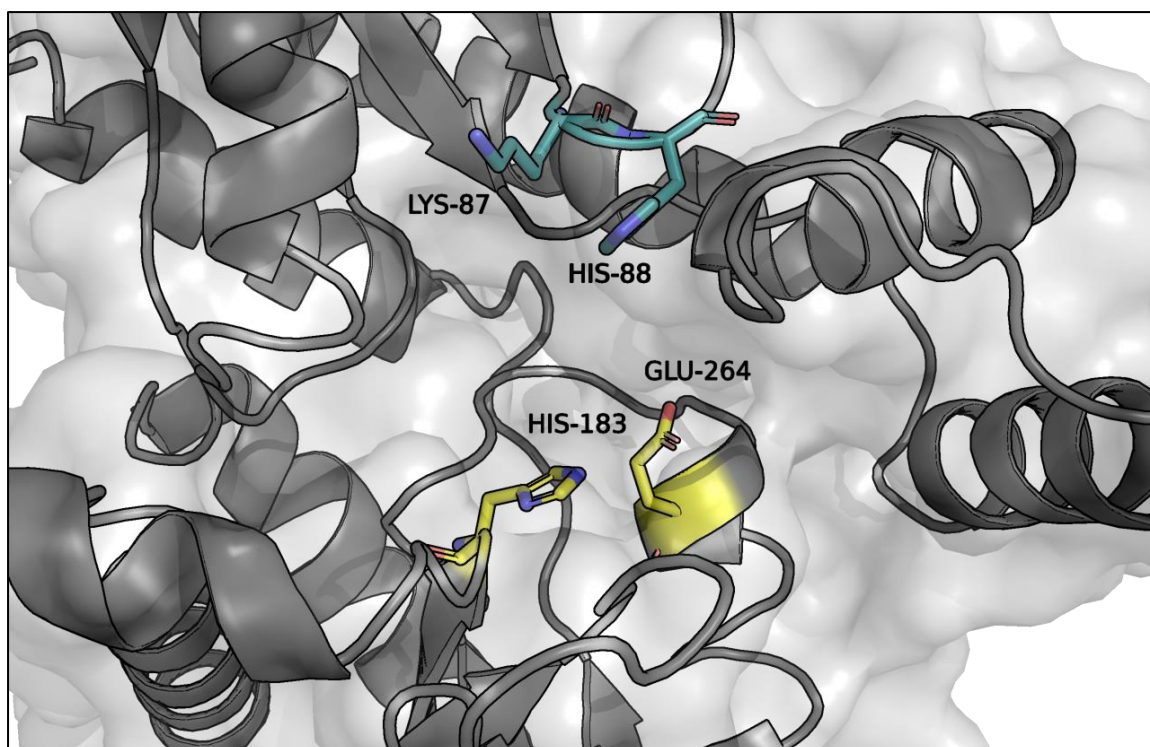
Figure 5.1 – Structure of the *B. subtilis* HemH active site

The secondary structure and surface of *B. subtilis* HemH (PDB:1AK1) are shown in dark grey and white, respectively. The non-conserved residues of the active site (K87 and 88) are highlighted in teal and labelled. The conserved residues of the active site (H183 and E264) are coloured yellow and labelled. The planar ring structure of the porphyrin would most likely fit in between these residues.

The five mutants selected were successfully cloned and expressed. The H183A mutant was found in inclusion bodies and was not investigated any further. The other four mutants (K87A, H88A, E264Q and E264Q) were successfully purified, their secondary structures were similar and thermostability was comparable to wildtype. A combination of kinetic approaches were used to investigate the activity of each of the mutants, the extent of the investigation was dependent on the activity of the mutants. The H88A mutant protein was completely active and so more kinetic experiments were completed.

5.2. Gene cloning *B. subtilis* ferrochelatase HemH

The five *B. subtilis* HemH mutant genes (K87A, H88A, H183A, E264A, and E264Q) were produced using the Q5 mutagenesis kit and the wildtype *B. subtilis hemH* plasmid was the DNA template. The primers were designed so that they were adjacent to each other and one primer contained the mutation (table 2.1). After mutagenesis the mutated gene was sequenced (GATC Biotech) confirming that only the desired change was present.

5.3. Protein expression and purification of active site mutants

Four of the five *B. subtilis* HemH mutants (K87A, H88A, E264A and E264Q) were expressed and purified successfully. The H183A HemH was not successfully purified and remained insoluble despite several attempts to solubilise it. Plasmids containing the mutated *hemH* genes were inserted in BL21-DE3 *E. coli* and grown on LB agar in the presence of ampicillin. The large-scale protein expression of each of these mutants followed a conventional IPTG induction protocol. The four mutants were purified using a 1 mL Talon GraviTrap column. Poor binding to Nickel-NTA HiTrap columns were observed. Imidazole was removed using a 20 mL Sephadex G50 column. The purified proteins were stored at -80 °C, SDS-PAGE analysis (figure 5.2) demonstrates the single step procedure provides pure (>95%) protein.
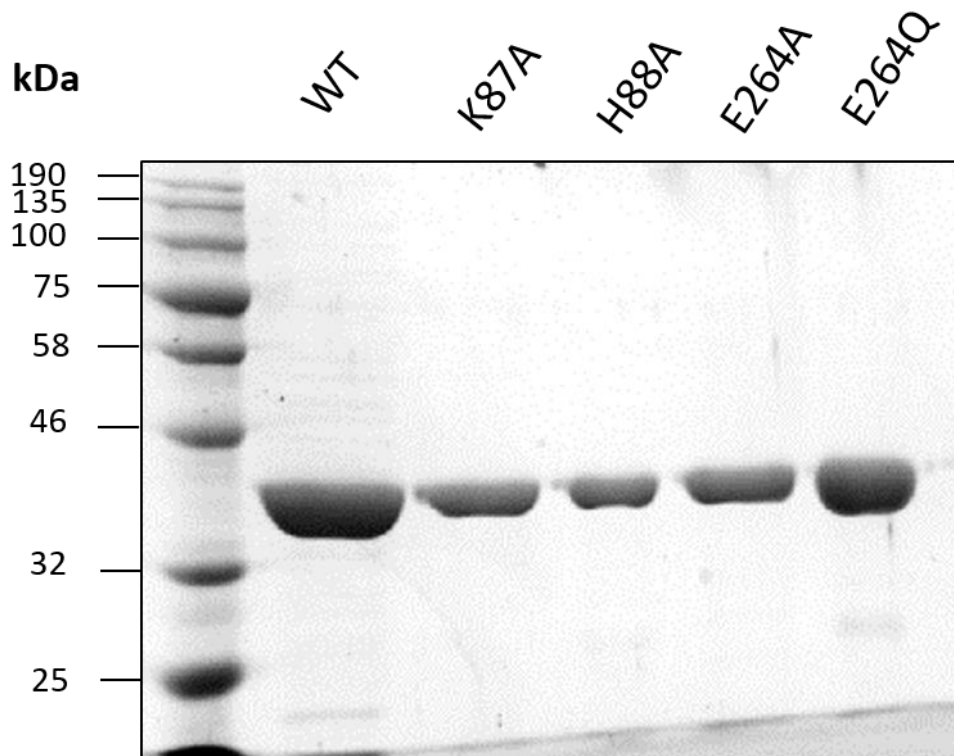
Figure 5.2 – Purification of _B. subtilis_ HemH mutations

SDS PAGE gel of the purified protein of K87A, H88A, E264A and E264Q compared to wildtype.

5.4. Investigating protein secondary structure and thermostability of ferrochelatase active site mutations

Circular dichroism spectroscopy shows that the _B. subtilis_ HemH mutants contained similar structural elements to wildtype _B. subtilis_ HemH (figure 5.3). The CD spectra of the HemH mutants was monitored between 200-260 nm.
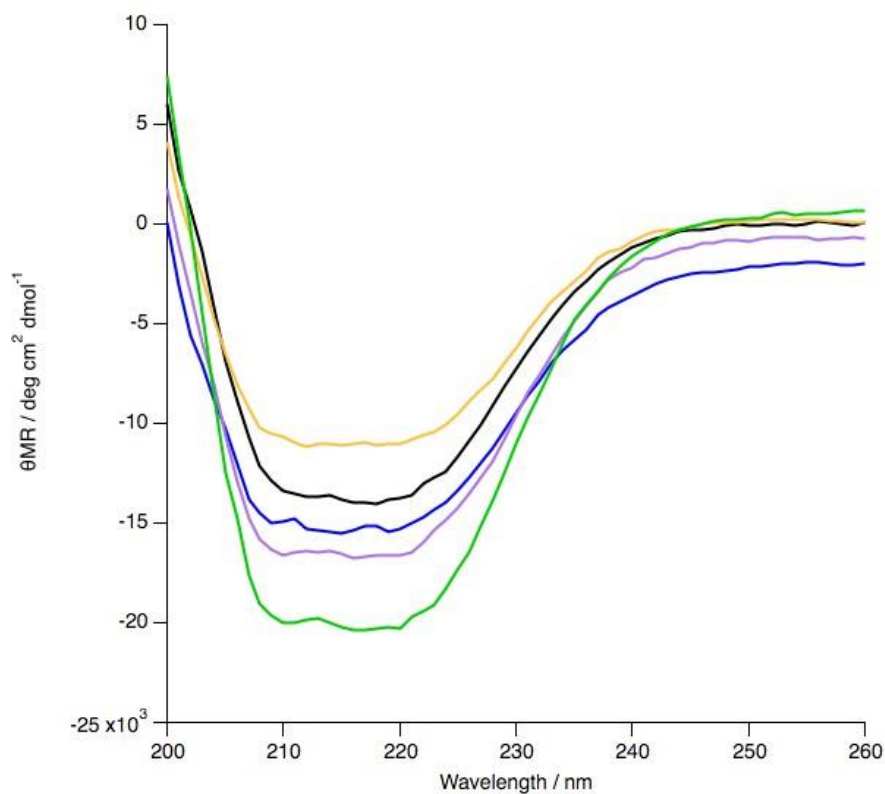
Figure 5.3 – CD spectra of *B. subtilis* mutants

The ellipticity of the ferrochelatase mutants was monitored between 200-260 nm. These were compared the wild-type (WT) protein shown in black. K87A (green), H88A (yellow), E264A (blue) and E264Q (purple) show folding similar to wildtype. All proteins were approximately 4 μM.

The thermostability of the each of the mutants was tested. The circular dichroism signal was monitored at 220 nm and the temperature was increased from 5-100 °C. The temperature increase lead to protein unfolding (figure 5.4A) and at 100 °C the temperature was slowly dropped to 5 °C to allow protein refolding (figure 5.4B). Sigmoidal curves were observed, and these were fit to the equation 1 and T_m values for unfolding and refolding in each mutant were estimated. The T_m values for K87A, H88A, E264A and E264Q were 53 °C, 51 °C, 53 °C and 51 °C for unfolding and 49 °C, 52 °C, 51 °C and 55 °C for refolding, respectively. The calculated T_m values for wildtype HemH was 53 °C for unfolding and 52 °C for refolding. This shows that the melting temperatures for the mutant proteins are relatively similar to the wildtype,

therefore mutation has not affected their thermostability. More importantly, all of the mutant proteins contain consistent secondary structure at their assaying temperature (25 °C).
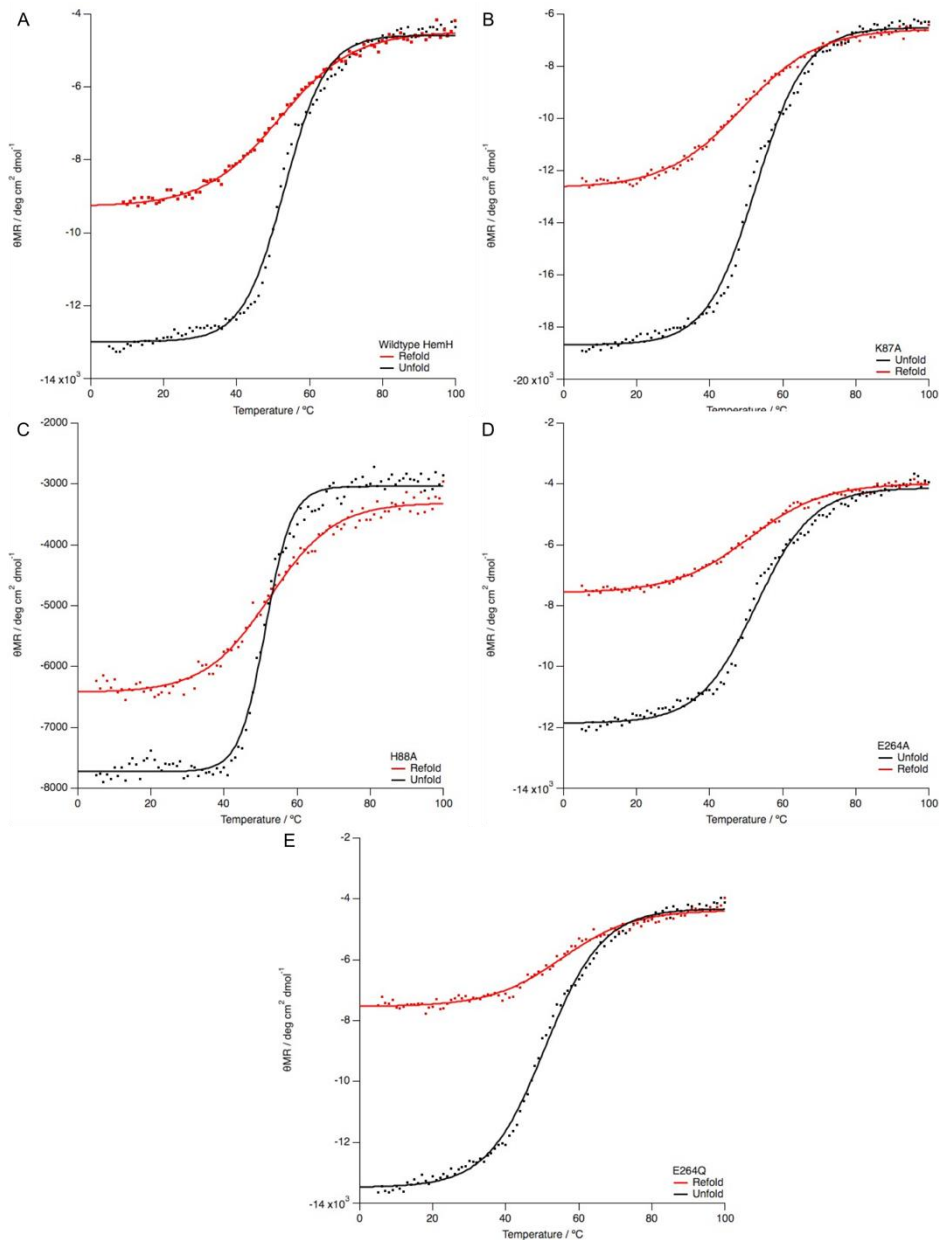
Figure 5.4 –Thermostability of *B. subtilis* HemH mutants compared to wildtype

Thermostability of the mutants were tested using circular dichroism, the ellipticity was monitored at 220 nm and the temperature was raised from 5 –100 °C, showing each of the mutants unfolding (black). The temperature was then dropped from 100 to 5 °C over the same timeframe allowing the proteins to refold (**red**). The thermal melting point (T_m) for unfolding and refolding was calculated using equation 1. The calculated T_m values for unfolding were 53 ± 0.2 °C (K87A), 51 ± 0.2 °C (H88A), 53 ± 0.3 °C (E264A) and 51 ± 0.2 °C (E264Q). The calculated T_m values for refolding were 49 ± 0.3 °C (K87A), 52 ± 0.4 °C (H88A), 51 ± 0.3 °C (E264A) and 55 ± 0.5 °C (E264Q). The unfolding and refolding for the wildtype (WT) protein are 53 ± 0.2 °C and 52 ± 0.3 °C, respectively. Each mutant is in one graph K87A (B), H88A (C), E264A (D) and E264Q (E). The WT traces are shown in A. Each of the errors are ± one standard deviation.

5.5. Activity assays on the *B. subtilis* HemH mutants

The activity of the *B. subtilis* HemH mutants were compared to the activity of the wild type protein in the presence of saturating substrate concentrations. The mutant proteins were assayed in the presence of 50 μM ferrous iron and 4 μM CP$_{III}$. The H88A mutant had activity comparable to wild type. E264Q was completely inactive whereas K87A and E264A retained a small fraction of activity. The activity assays are shown in figure 5.5. Due to the exceptionally low activity of E264Q, E264A and K87A steady-state kinetics were not attempted on these mutants.
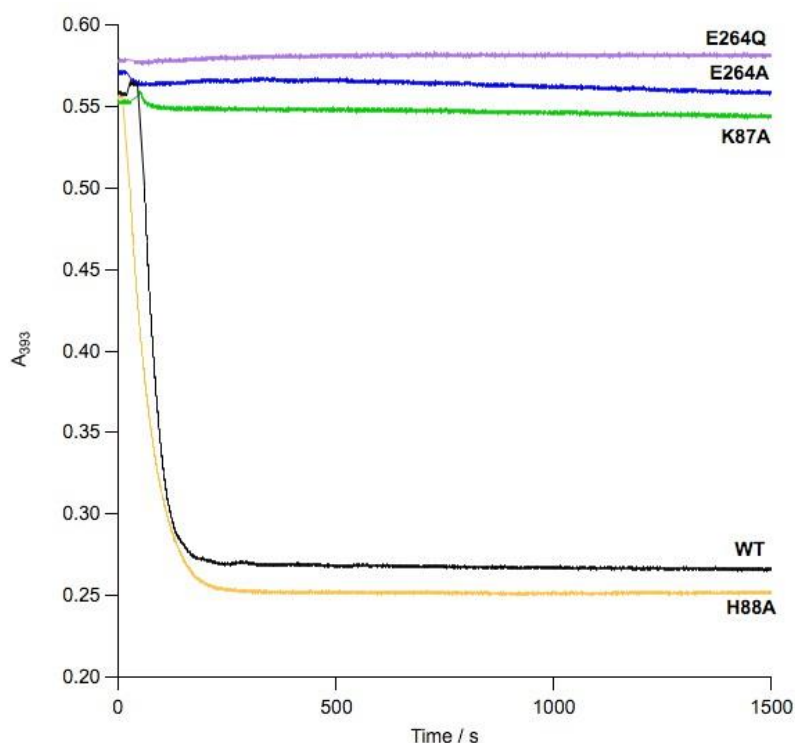
Figure 5.5- Activity assays of *B. subtilis* HemH mutants

Each of the mutants (K87A, H88A, E264A and E264Q) were assayed in the presence of 4 μM CP$_{III}$ and 50 μM Fe^{2+}, the reactions were monitored at 393 nm. The concentration of each of the mutants was approximately 0.2 μM. The mutant activity was compared to the wildtype (WT) protein. K87A is shown in green, H88A is shown in yellow, E264A is shown in blue, E264Q is shown in purple and WT is shown in black.

5.6. Characterising the H88A *B. subtilis* HemH mutant

In chapter 4 the wildtype proteins *B. subtilis* and *S. aureus* HemH were kinetically characterised used several different approaches and these approaches were used to characterise the *B. subtilis* mutants. Firstly, the overall activity of the mutant proteins were tested and those that were active enough (H88A HemH) were characterised using steady state kinetics. Steady state kinetics looked at the overall enzyme mechanism and deduced rate constant for the rate determining step (k_{cat}).

The substrate binding in ferrochelatase is ordered with CP_{III} binding first and Fe^{2+} binding second. As a result, CP_{III} binding in the mutants was the first step of the enzymatic mechanism isolated for investigation. CP_{III} static binding assays (monitoring intrinsic tryptophan fluorescence) and CP_{III} binding kinetics were performed to gain dissociation constants (K_d and K_{CP}) and rate constants (k_{iso} and k_{-iso}) for CP_{III} binding. In addition, scanning kinetics were performed to observe CP_{III} binding across a wavelength range. Scanning kinetics performed in the presence of the wildtype ferrochelatases and CP_{III} show that the complex formation between the substrate and enzyme causes a change in the spectral properties of the CP_{III}, modelled structure of the H88A mutant is shown in figure 5.6.
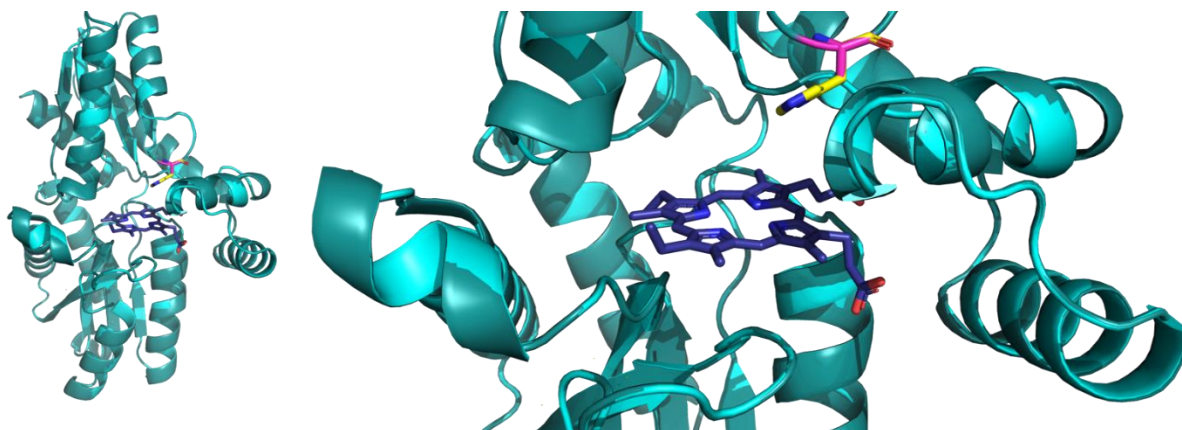
Figure 5.6 – Structure of H88A *B. subtilis* ferrochelatase

Overlay of wildtype *B. subtilis* ferrochelatase (PDB ID: 1AK1, cyan) and a model (generated by Swiss-Model (Waterhouse et al., 2018) of the H88A mutant (template used PDB ID:1AK1, deep teal), the H88 (wildtype) and A88 (mutant) are shown in sticks and coloured yellow and magenta, respectively. The overlay was aligned to PP$_{IX}$ bound *H. sapiens* ferrochelatase (2HRE) to show porphyrin placement in the active site (dark blue) (Al-Karadaghi et al., 1997, Medlock et al., 2007a).

Binding of the second substrate and resultant porphyrin metalation was assessed next. Scanning kinetics established whether the mutant HemH proteins were capable of binding iron or metalating porphyrin. Rate and dissociation constants for iron binding (K_{Fe}) and porphyrin metalation (k_{chel} and k_{-chel}) were determined for the mutant proteins that were capable of binding iron and metalating porphyrin (H88A HemH).

Finally, burst kinetics were completed on mutants that were able to turnover substrate. Burst kinetics measured rate constants for all enzymatic steps prior to the rate determining step (k_{cat}). These burst kinetics can be used to decide whether the results obtained in the CP$_{III}$ binding and the Fe^{2+} binding experiments were consistent and whether additional steps should be added to the mechanism.

In these kinetic experiments different spectroscopic conditions were used dependent on the experiment completed. Steady state characterisation of the mutant proteins monitored the porphyrin absorbance at 393 nm. In the CP_{III} static binding assays the enzymes were excited at 280 nm and emission was recorded from 330 -700 nm. Three emission peaks were observed, the peak with a λ_{max} of 371 nm is indicative of emission produced from excitation of tryptophan. This peak decreases in intensity as the CP_{III} concentration increases. The two additional peaks correspond to porphyrin fluorescence (600-700 nm) and increase in intensity as CP_{III} concentration increases. These peaks result from direct excitation of porphyrin as well as energy transfer from tryptophan to porphyrin.

In the binding kinetics and burst kinetics the porphyrin is most commonly excited at 393 nm and emission is recorded from 405 nm. In the K87A mutant binding kinetics the tryptophan residues are excited at 280 nm and emission is recorded from 330-600 nm, the use of band pass filters removes the signal corresponding to direct excitation of porphyrin (table 2.4). In the iron binding and porphyrin metalation kinetics the ferrochelatase-CP_{III} complex was excited at 405 nm for the wildtype proteins whereas it is excited at 396 nm for the H88A HemH mutant. These wavelengths are used as the spectral properties of free CP_{III} are different from the ferrochelatase-CP_{III} in all of the mutants.

The *B. subtilis* H88A HemH mutant is the most active mutant investigated in this chapter, as shown in the activity assays in section 5.5. The activity assays show that H88A has activity comparable to wildtype this means that a fuller kinetic

characterisation must be completed unlike the other mutants (K87A, E264A and E264Q) where activity has been significantly affected. In chapter 4, *B. subtilis* and *S. aureus* HemH were characterised using steady state kinetics and the H88A mutant can be characterised in the same way.

5.6.1. Steady state characterisation of H88A HemH

The previously described experimental design for the characterisation of the wildtype proteins provides a convenient starting point for the characterisation of the H88A mutant. As previously described, the consumption of the porphyrin substrate can be readily be monitored at 393 nm. To maintain the steady state conditions the substrate concentrations was at least 10-fold excess over enzyme. A simplified design was used where the concentration of one substrate was held at saturation while the other was varied. This approach provides good estimates for k_{cat} and K_m for both substrates, provided the concentration of the fixed substrate is sufficiently close to saturation. Initial rates were taken from the progress curves and changed from absorbance units into µM using the extinction coefficient for the reaction.

The converted initial rates were converted into $v_i/[E]_T$ values making them independent of enzyme concentration and they were plotted against the substrate concentration. Each individual data set was fit to the Michaelis-Menten equation (equation 2B). This enabled estimation of each of the kinetic parameters and optimised them for each data set (figure 5.7). When CP_{III} was varied (0-8 µM) the ferrous iron concentration was approximately 100 µM, the calculated kinetic parameters for this data were: k_{cat} 0.37 s^{-1} and K_m^{Fe} 28 µM (figure 5.7A). When Fe^{2+} concentration was varied (0-200 µM) the

CP$_{III}$ concentration was held at 2 µM, the calculated kinetics parameters for this data were: k_{cat} 0.46 s^{-1}, K_m^{CP} 0.2 µM (figure 5.7B).

The results of steady-state kinetics on the H88A mutant reveal that it has a slightly higher k_{cat} value (0.37 and 0.46 s^{-1}) to the wildtype (0.32 and 0.35 s^{-1}) and so the H88A mutant slightly faster at turning over substrate compared to wildtype *B. subtilis* HemH, however they appear broadly comparable. The K_m^{CP} value of H88A HemH (0.2 µM) is comparable to the wildtype protein (0.14 and 0.15 µM) indicating that the mutation does not affect the concentration of CP$_{III}$ corresponding to 50% activity. The K_m^{Fe} was estimated as 28 µM in the H88A mutant and the calculated K_m^{Fe} value for the wildtype is 1.8 and 3.8 µM, which is substantially lower than the mutant thus showing that the mutant's ability to handle the second substrate, ferrous iron, is affected.

In the activity assays the H88A mutant appears to turnover substrate similarly to the wild-type, steady state characterisation has shown that whilst this is the case there are other factors involving the substrate iron that have been affected due to mutation at the His88 residue. To understand the functional implication of the mutation at position 88, the enzymatic mechanism of the H88A mutant protein was investigated in greater detail. Other spectroscopic experiments such as stopped flow fluorescence spectroscopy, rapid scanning kinetics and scanning kinetics were performed to isolate and assess steps in the enzymatic mechanism.
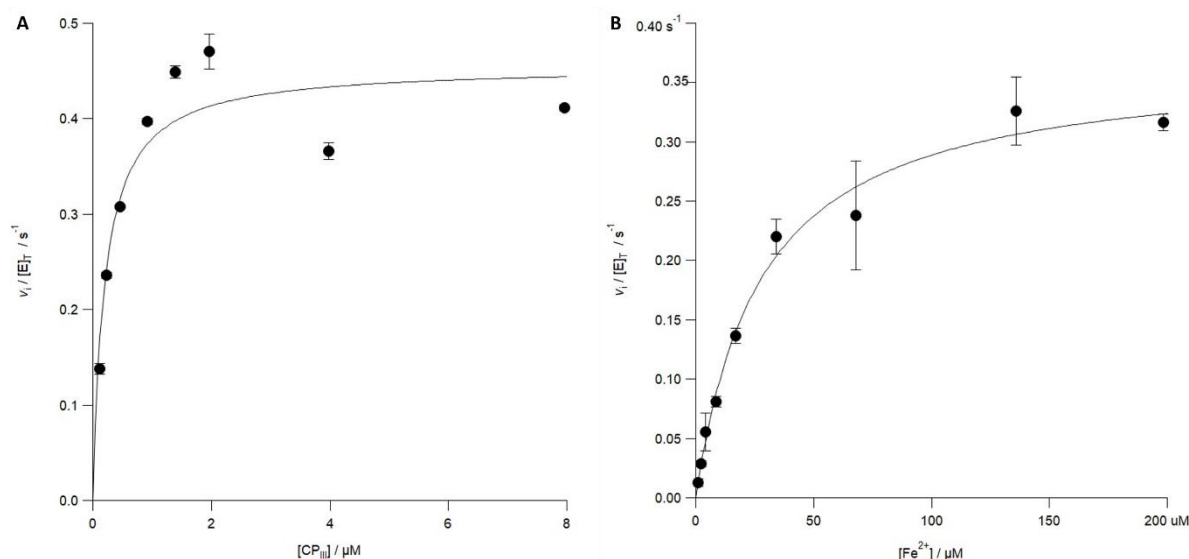
Figure 5.7- Steady state kinetics of H88A *B. subtilis* HemH

The traces show the rate of substrate consumption at 393 nm when one substrate is varied and the other is held. **A** shows when CP_{III} is varied (0-8 μM), ferrous iron (Fe^{2+}) is held at 100 μM and ferrochelatase concentration is 10 nM. **B** shows when Fe^{2+} is varied (0-200 μM); CP_{III} is held at 2 μM and the ferrochelatase concentration is 75 nM. These curves were produced using the Michaelis-Menten equation (equation 2B). The calculated kinetic parameters in **A** were k_{cat} 0.46 ± 0.03 s^{-1} and K_m^{CP} 0.20 ± 0.07 μM. The calculated parameters for **B** were k_{cat} 0.37 ± 0.02 s^{-1} and K_m^{Fe} 28 ± 4 μM. Calculated errors are ± one standard deviation.

5.6.2. CP_{III} binding to H88A HemH

In static binding assays, the H88A mutant protein was excited at 280 nm and emission was recorded from 310-700 nm in different in concentrations of CP_{III} (0-100 μM). As previously described, the emission spectra show three peaks similar to those observed in the wildtype (shown in figure 4.8) and the emission peak with λ$_{max}$ 371 nm was integrated. Quenching of tryptophan/tyrosine fluorescence by increased concentrations of CP_{III} show a weak binding relationship between the mutant ferrochelatase and CP_{III}. The weak binding equation (equation 3B) was fitted to the data and estimated a K_d value of 5.0 μM (figure 5.8). The wildtype *B. subtilis* HemH shows tight binding and estimates a K_d of 0.048, this shows that the H88A mutant binds CP_{III} approximately 100-fold weaker compared to wildtype.
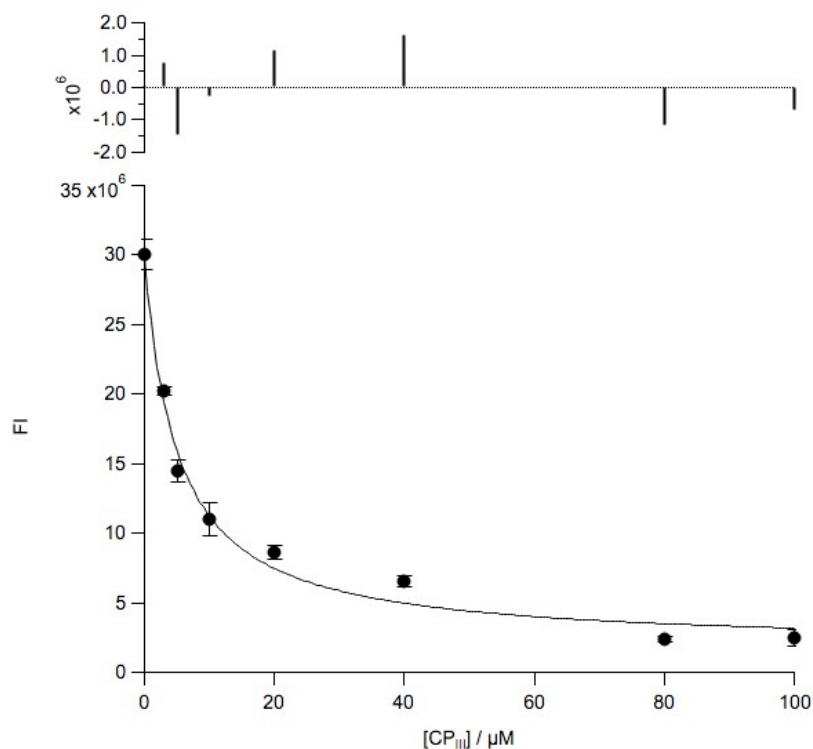
Figure 5.8- Static binding assays of H88A *B. subtilis* HemH

The emission peak representing tryptophan fluorescence of the H88A mutant was integrated between 330-510 nm and plotted against CP_{III} concentration giving rise to the binding curve observed. The curve was fitted using equation 3B, the weak binding equation and the calculated K_d was 5.0 ± 0.91 µM. Each data point is an average of three and the error bars are ± one standard deviation.

The results from the steady state characterisation and static binding assays indicate that the K_m^{CP} value is lower than the K_d value in the H88A mutant protein (0.2 vs 5 µM). In contrast, the K_m^{CP} value is higher than the K_d value in the wildtype protein (0.1 vs 0.048 µM) and the K_m values are similar in both proteins. This shows that dissociation constant (K_m^{CP}) for the dissociation of CP_{III} from the ternary complex (E'CPIII...Fe) remains the same whereas the dissociation of CP_{III} from the enzyme-substrate complex (E'CPIII) significantly increases when histidine is mutated at position 88 (Cornish-Bowden, 2012).

After static binding assays, binding kinetics were completed to determine the rate constants for each stage in the binding of CP_{III}. As high concentrations of CP_{III} were required to saturate the binding system, kinetics were performed where the intrinsic tryptophan fluorescence in ferrochelatase was excited at 280 nm (0.1 µM) and CP_{III} was varied (0-120 µM). The binding progress curves for wildtype *B. subtilis* HemH appeared single exponential and k_{obs} values were estimated by fitting a single exponential to the data (equation 4A). In contrast, the H88A mutant shows traces that are biphasic and can be described as double exponential. This double exponential behaviour observed disappears as CP_{III} concentration increases (figure 5.9A) making it difficult to decipher what has led to this behaviour. When the binding progress curves were fitted to the double exponential (equation 4C), the second observed rate constant had errors that were comparable to the instrumental signal-to-noise ratio. As a result, no further analysis of this second phase was conducted. The existence of this second phase could indicate an additional step in the porphyrin binding reaction (porphyrin binding is weak so the step could be observed) or it could indicate a small amount of optical drift or non-specific interaction at the high porphyrin concentration used.
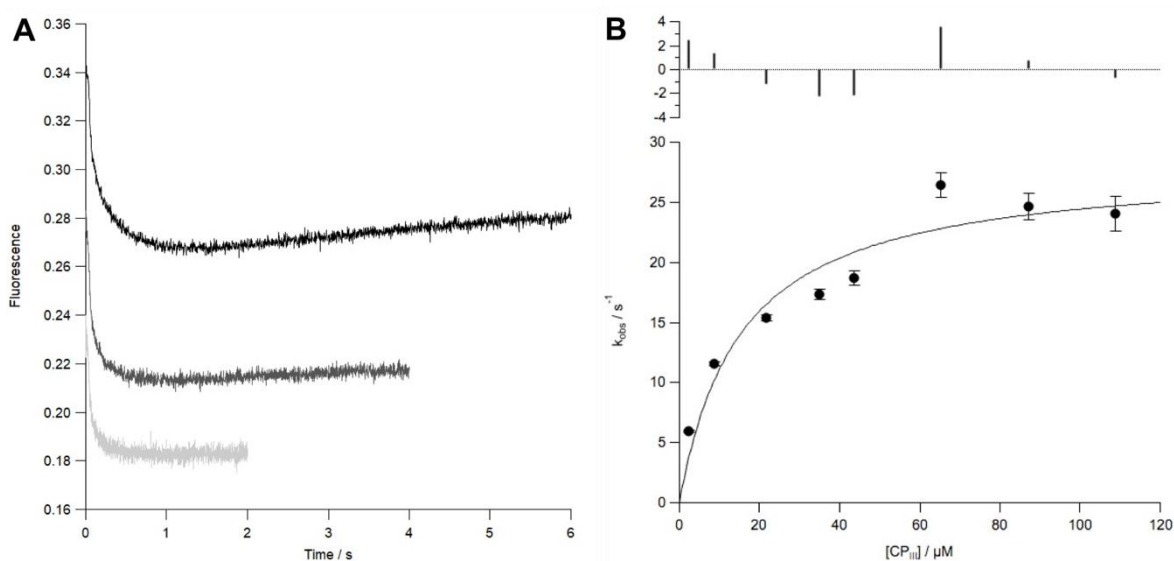
Figure 5.9- Stopped flow binding kinetics of H88A B. subtilis HemH

A shows raw traces of CP_{III} binding in the H88A mutant. As the concentration of CP_{III} increases (black to light grey) the second phase of the double exponential decreases. **B** shows the estimated k_{obs} values against CP_{III} concentration, the data is fitted to equation 5. The estimated kinetic parameters for the curve fitting are: 15 ± 5.3 µM, 28 ± 2.6 s^{-1} for K_{CP} and k_{iso}, respectively and k_{-iso} was constrained at zero. The error bars are $\pm$ one standard deviation

The double exponential equation (equation 4C) was fitted to the progress curves displaying biphasic behaviour. The single exponential equation (equation 4A) was applied to those displaying monophasic behaviour and k_{obs} values were estimated for the first exponential phase. The k_{obs} data had similar characteristics to the kinetic binding data observed in the wildtype proteins *B. subtilis* and *S. aureus* HemH. They displayed two-step binding (scheme 1) indicative of initial porphyrin binding followed by enzyme/porphyrin isomerisation, this data was fit to equation 5. The estimated K_{CP} and k_{iso} values are 15 µM and 28 s^{-1}, respectively and k_{-iso} value was held at zero. The K_{CP} value for the H88A mutant is almost three-fold higher than the wildtype protein suggesting that it is less able to bind CP_{III}, this is consistent with the static binding assays. The k_{iso} values for the wildtype protein (25 s^{-1}) and H88A mutants (28 s^{-1})

remain similar indicating that the isomerisation after substrate binding is not affected by mutation at His88 (figure 5.9B).

In these binding kinetics, the k_{-iso} was held at zero. Binding kinetics on wildtype *B. subtilis* HemH show that the k_{-iso} value is small (0.25 s^{-1}) and therefore no distinguishable from zero in the experiment. Holding the k_{-iso} value at zero may not be an accurate representation of the data as steady state kinetics and static binding assays suggest that CP$_{III}$ binding overall is likely to be reversible. Estimation of k_{-iso} from the binding assays and kinetics in the H88A mutant approximates the rate constant as 9.3 s^{-1}. This is large enough to be observed. However, holding the k_{-iso} value at 9.3 s^{-1} results in less optimal fitting, a five-fold higher K_{CP} value (79 µM) and similar k_{iso} value (29 s^{-1}). If left unconstrained the k_{-iso} is estimated as 4.6 s^{-1}, the K_{CP} value (33 µM) is higher and the k_{iso} value (27 s^{-1}) is similar. This suggests that the k_{iso} is consistent despite any changes in k_{-iso} value whereas the accuracy in estimating the K_{CP} changes dependent on the value of the k_{-iso} rate constant.

$$E + CP_{III} \xrightleftharpoons{K_{CP}} ECP_{III} \xrightleftharpoons[k_{-iso}]{k_{iso}} E'CP_{III}$$

Scheme 1- Two step substrate (CP$_{III}$) binding to enzyme (E)

In addition to static binding assays and binding kinetics, rapid scanning kinetics (millisecond time base) were completed on the H88A mutant. In the wildtype protein complex formation between ferrochelatase and CP$_{III}$ causes a spectral shift in the Soret band, the λ_{max} shifts from 393 nm to 405 nm. Complex formation between H88A

ferrochelatase and CP$_{III}$ shows that whilst a spectral shift occurs the λ_{max} moves from 393 nm to 399 nm (figure 5.10). This suggests that the porphyrin molecule is in a different environment when bound by the H88A mutant protein when compared to the wildtype protein. The H88A mutant or porphyrin molecule may adopt a different conformation when bound to each other compared to the wildtype protein. The spectra produced during rapid scanning kinetics shows that the shift occurs within 10 s (comparable to wildtype). Accurate rates for this shift cannot be deduced as the concentration of CP$_{III}$ (0.64 µM) and H88A ferrochelatase (1 µM) were not pseudo-first order with respect to one another, although the presence of one isosbestic point indicates the presence of two species.

Scanning kinetics (second time base) were performed to determine whether any further shifting was observed at later time points. Scans were taken for free CP$_{III}$ (2 µM) and bound CP$_{III}$ (2 µM of CP$_{III}$ and ferrochelatase). This showed a spectral shift in the Soret band λ_{max} from 393 nm to 396 nm. Monitoring this shift over a longer time frame indicated that the binding between the porphyrin and enzyme was stable (figure 5.11).
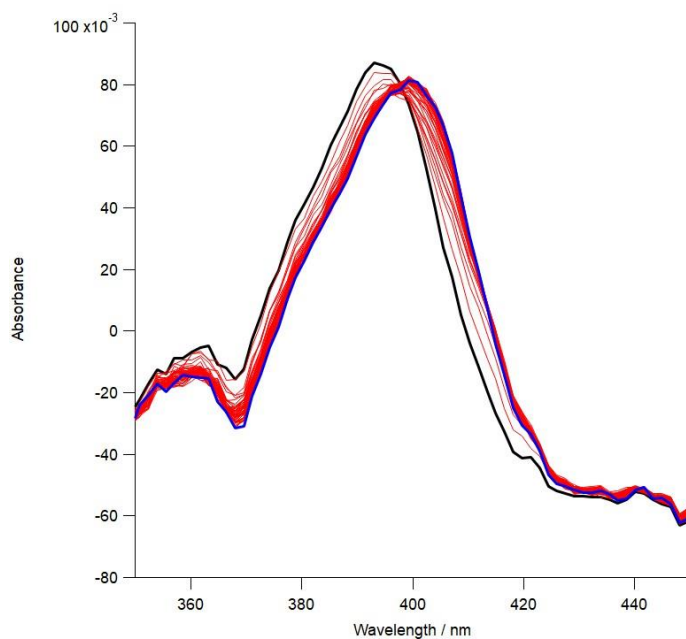
Figure 5.10- Rapid scanning kinetics of the H88A mutant

Rapid scanning kinetics was performed to monitor complex formation between H88A (1 µM) and CP_{III} (0.64 µM). The λ_{max} of the Soret band shifts from 393 nm to 399 nm. Each trace shown is an average of 10 raw data traces. Black indicates the first spectrum and blue indicates the final spectrum, the red spectra are intermediary spectra (averages of 10 consecutive scans).

5.6.3. Iron binding and porphyrin metalation in H88A HemH

The activity assays described in section 5.5 show that mutation of His88 to alanine does not significantly affect the function of ferrochelatase, the H88A mutant is capable of consuming substrate at rates comparable to the wildtype protein. The mutant is able to bind iron and metalate coproporphyrin and so the iron binding and porphyrin metalation studies completed on the wildtype protein can also be performed on *B. subtilis* H88A HemH.

Scanning kinetics (second time base) were used determine whether the H88A mutant was capable of binding iron and metalating porphyrin similar to the wildtype protein.

The enzyme porphyrin complex (2 μM) was scanned before 10-fold excess of ferrous iron was added (20 μM) and the absorbance peak at 396 nm drops rapidly, (figure 5.11), thus showing conclusively that the mutant is capable of porphyrin metalation.
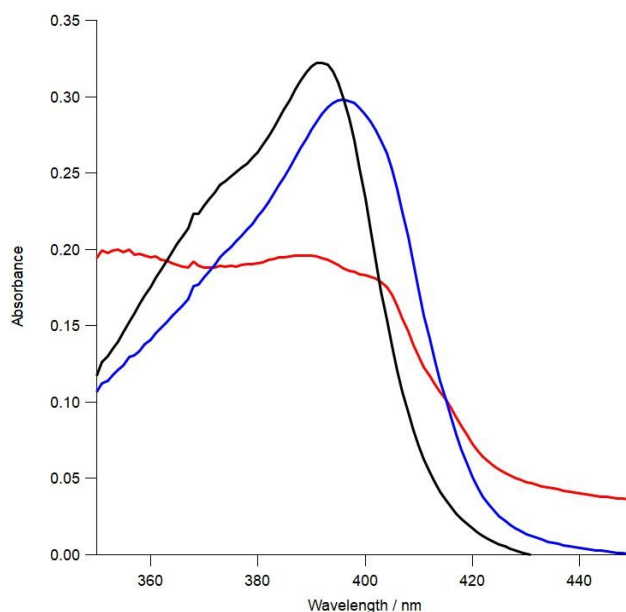
Figure 5.11- Spectral change upon formation of enzyme-substrate complex in H88A HemH and subsequent porphyrin metalation after the addition of iron

Scanning kinetics were performed to show the spectral properties of CP_{III} binding and porphyrin metalation across 350- 450 nm. The black spectrum indicates 2 μM CP_{III} only (λ_{max} 393 nm) and the blue spectrum show the spectral shift in the λ_{max} when 2 μM of H88A ferrochelatase is added (λ_{max} 396 nm). Upon completion of the shift at least 10-fold iron (20 μM) was added and the red trace indicates the spectrum after the addition of iron.

After confirming that the mutant is able to bind iron and metalate porphyrin the dissociation and rate constants for this part of the mechanism can be determined using stopped flow fluorescence spectroscopy. The scanning kinetics revealed that 396 nm was a suitable wavelength to use as the spectrum with λ_{max} 396 nm showed stable formation of the ferrochelatase-CP_{III} complex over minutes. The experimental design for the transient kinetics were similar to those used for the wildtype in section 4.5.5.1. The CP_{III} and ferrochelatase were incubated in equimolar concentrations (1 μM), this ensured that they formed a complex, removing any rate or dissociation constants that

were associated with CP_{III} binding and ensuring that the spectral shift was complete. The iron (varied 5-200 µM) was also incubated with ferrochelatase (1 µM), this prevented dissociation of the complex upon mixing. When ferrochelatase was not incubated with iron the progress curves showed biphasic behaviour, the first phase was attributed to the equilibrium between bound and unbound porphyrin. In the experiment using the H88A mutant protein, the complex was excited at 396 nm whereas the wildtype-CP_{III} complex was excited at 405 nm. When mixed the final concentration of CP_{III} and H88A HemH were 0.5 µM and 1 µM, respectively. The reaction mechanism for this experiment is shown in scheme 2.

$$E'CP_{III} \xrightleftharpoons{K_{Fe}} E'CP_{III}...Fe \mathrel{\mathop{\rightleftharpoons}^{k_{chel}}_{k_{-chel}}} E'CP_{III}Fe$$
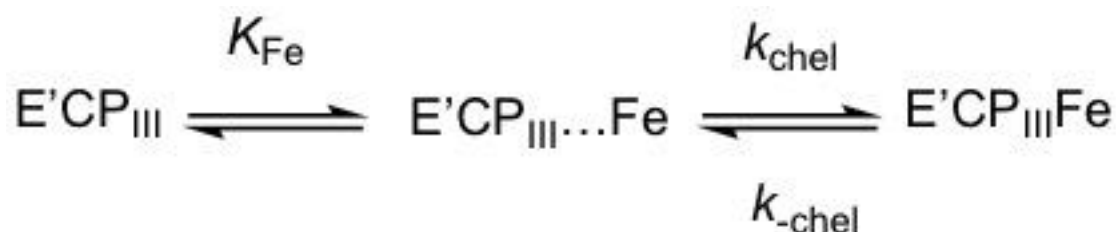
Scheme 2- Iron binding and porphyrin metalation

The raw traces were fitted to equation 4B and k_{obs} values were estimated. The k_{obs} values were plotted against ferrous iron concentration and showed data consistent with a two-step mechanism. The two steps in the mechanism are iron binding (K_{Fe}) and subsequent porphyrin metalation (k_{chel}). Fitting equation 6 to the data calculated K_{Fe} and k_{chel} as 3.1 µM and 32 s^{-1}, respectively whilst k_{-chel} was constrained at zero (figure 5.12). In comparison to the wildtype protein, the H88A mutants has a 30-fold lower K_{Fe} value (3.1 µM compared to 90 µM) indicating can bind iron more efficiently and its k_{chel} value is two-fold higher (32 s^{-1} vs 16 s^{-1}) suggesting that it can metalate porphyrin faster. Previously literature has suggested that iron binding and porphyrin metalation may occur too quickly for accurate estimation of rates using stopped flow

fluorescence spectroscopy (Hoggins et al., 2007) however the data presented shows this is not the case in the *B. subtilis* ferrochelatase enzyme.
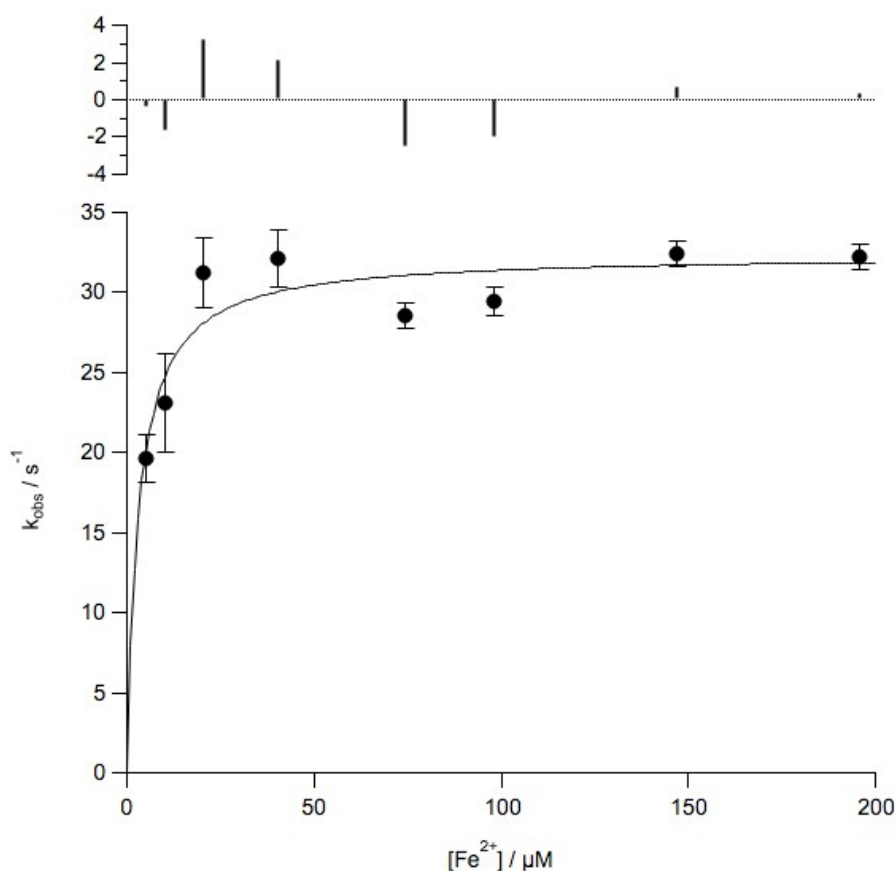
Figure 5.12- Stopped flow fluorescence spectroscopy of iron binding and porphyrin metalation in H88A *B. subtilis* HemH

The raw data was fitted to equation 4B (single exponential + linear phase) to estimate the k_{obs} values. The graph shows the estimated k_{obs} values against Fe^{2+} concentration fitted to equation 6 to give the kinetic parameters K_{Fe} and k_{chel} and k_{-chel}. The estimated K_{Fe} and k_{chel} are 3.1 ± 0.84 µM and 32 ± 1.1 s^{-1}, respectively and k_{-chel} was held at zero. The error bars are $\pm$ one standard deviation.

5.6.4. *Calculation of rates in the enzymatic mechanism of* B. subtilis *H88A HemH prior to the rate determining step*

The third and final stopped flow spectroscopy experiment investigates the kinetics of the H88A from the start of the enzymatic mechanism until the rate determining step (the step corresponding to k_{cat}). Kinetic characterisation of *H. sapiens* wildtype HemH

and *H. sapiens* E343D HemH has been performed previously. The results of these experiments suggest that the rate determining step is product release (Hoggins et al., 2007). If this is correct then the experiment measures the rate constants for CP_{III} binding, enzyme/porphyrin isomerisation, iron binding and porphyrin metalation collectively (see scheme 3 for enzymatic mechanism) as well as any other potential steps prior to product release.
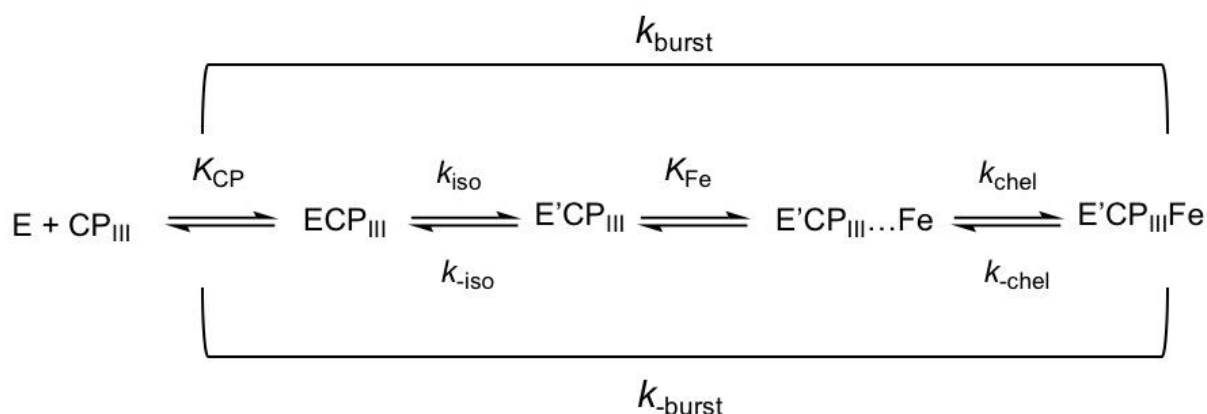
Scheme 3 – Enzymatic scheme of ferrochelatase reaction from start to rate determining step

The substrates are incubated together and exposed to the H88A mutant at the same time. The enzyme concentration is held at 0.2 µM, the CP_{III} concentration is held at 2 µM and the ferrous iron is varied from 0-200 µM. The porphyrin is excited at 393 nm and its consumption is measured against time. The raw traces represent bursts and they initially fit to the same equation 4B allowing the estimation of k_{obs} values.

Fitting of equation 4B (single exponential + linear phase) assumes that only one exponential phase was observed, and the raw data looks consistent with this curve

fitting. However, studies on CP_{III} binding (section 5.6.2) and iron binding and porphyrin metalation (section 5.6.3) have shown that an exponential phase is observed in each experiment and so two exponential phases should be observed in this experiment. Exponential phases can only be distinguished from one another easily when there is at least a 10-fold difference in their rate constants. In these experiments the two exponential phases are too close together and so the only way to determine the separate rate constants would be to average more progress curves (25-100) and reduce the signal-to-noise ratio significantly. To overcome this issue rate constants were taken from the CP_{III} binding data and the iron binding and porphyrin metalation data and used to fit a double exponential equation (equation 4C) to each of the progress curves (figure 5.13). This showed that the results gained from the previous two stopped flow experiments were consistent with the results of the third stopped flow experiment.
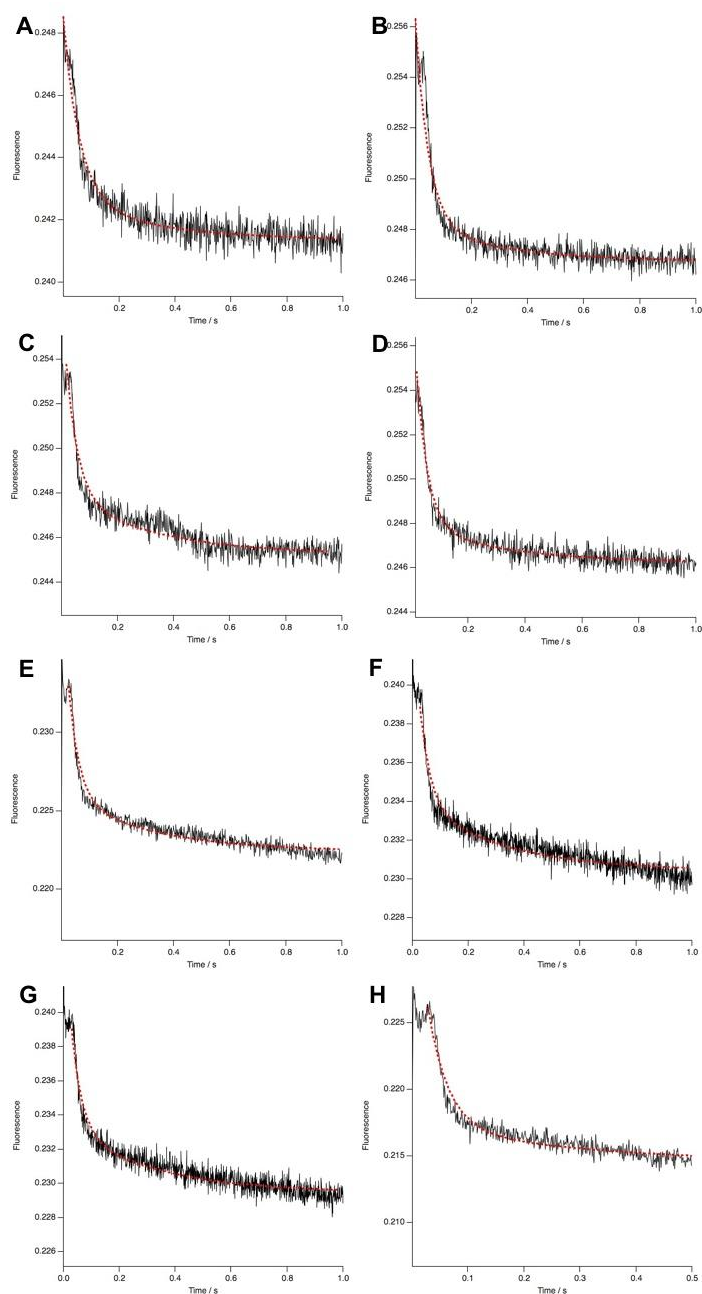
Figure 5.13- Stopped flow fluorescence spectroscopy of all enzymatic steps prior to the rate-determining step in the H88A mutant

In this experiment, the substrates were exposed to the ferrochelatase at the same time, the enzyme concentration was 0.2 μM, the CP_{III} concentration was held at 2 μM and the ferrous iron was varied (2 μM (**A**), 4 μM (**B**), 8 μM (**C**),12 μM (**D**), 25 μM (**E**), 49 μM (**F**), 98 μM (**G**) and 196 μM (**H**)). The porphyrin was excited at 393 nm and progress curves measured the change in fluorescence (black). The progress curves were fitted to a double exponential equation (equation 4C). The rate of the first exponential phase was held at 3.25 s^{-1}(the rate constant for the CP_{III} binding at 2 μM). The rate of the second exponential phase was held at rate constants for the porphyrin metalation at different iron concentrations (17.4 s^{-1} (**A**), 21.5 s^{-1} (**B**), 24.3 s^{-1} (**C**), 25.4 s^{-1} (**D**), 26.7 s^{-1} (**E**), 27.3 s^{-1} (**F**), 27.6 s^{-1} (**G**) and 27.8 s^{-1} (**H**). The curve fitting for the double exponential equation is shown in red.

226

5.6.5. Summary of H88A mutant

The *B. subtilis* H88A mutant was successfully expressed and purified and CD spectroscopy confirmed that protein folding and thermostability are similar to wildtype. Activity assays show that the H88A mutant had comparable activity to wildtype and so steady state kinetic characterisation was performed. Steady state kinetics show that the K_m^{Fe} value is higher in the H88A mutant compared to the wildtype ferrochelatase indicating that wildtype *B. subtilis* HemH can work more efficiently at lower iron concentration compared to H88A HemH. The K_m^{CP} and k_{cat} values remain similar between the wildtype protein and the H88A mutant protein showing that these are not greatly affected by the mutation (see table 5.1).

After steady-state characterisation of the H88A mutant, CP_{III} binding was investigated. Static binding assays and binding kinetics show that mutation of H88 to an alanine causes higher estimated K_d and K_{CP} values compared to the wildtype protein and this is different from the K_m^{CP} calculated in the steady-state kinetics. These values are reporting on different steps in the enzymatic mechanism, the K_d is the dissociation constant for the interaction between ferrochelatase and CP_{III}, whereas the K_m is the dissociation constant of the substrate from the ternary complex (when both substrates are bound). Whilst a difference is observed in the rate constants involving CP_{III}, the rate constant for the isomerisation of ferrochelatase is similar in the wildtype and mutant indicating the mutation has not altered the rate of isomerisation (table 5.1). Rapid scanning kinetics and scanning kinetics show that a spectral shift in the Soret band occurs when CP_{III} binds to H88A HemH this is similar to the wildtype, but the

shift is less extensive insinuating that the environment of the porphyrin is different when bound to the H88A mutant compared to wildtype.

Iron binding and porphyrin metalation were assessed after CP_{III} binding, scanning kinetics showed that the mutant protein was capable of binding iron and metalating porphyrin. Transient kinetics were performed to gain rate constants for each of these steps. These kinetics showed that the H88A mutant had a lower K_{Fe} value and a higher k_{chel} value compared to wildtype *B. subtilis* HemH thus indicating it is more capable of iron binding and porphyrin metalation compared to wildtype *B. subtilis* ferrochelatase. Finally, a third stopped flow fluorescence spectroscopy experiment assessed the combined rate constants for all of the steps prior to the rate determining steps. This showed that the three stopped flow fluorescence spectroscopy experiments were consistent (see scheme 4 for full mechanism).

$$E + CP_{III} \underset{}{\overset{K_{CP}}{\rightleftharpoons}} ECP_{III} \underset{k_{-iso}}{\overset{k_{iso}}{\rightleftharpoons}} E'CP_{III} \underset{}{\overset{K_{Fe}}{\rightleftharpoons}} E'CP_{III}...Fe \underset{k_{-chel}}{\overset{k_{chel}}{\rightleftharpoons}} E'CP_{III}Fe \overset{k_{cat}}{\longrightarrow} E + CP_{III}Fe$$
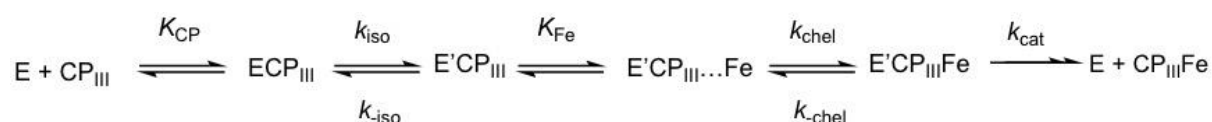
Scheme 4- Overall enzymatic mechanism of ferrochelatase

As the activity of the H88A mutant was comparable to the wildtype, it was characterised to the same degree of the wildtype protein. Transient kinetic characterisation of the H88A mutant shows that the mutation at the H88 residue is detrimental to CP_{III} binding but is better at iron binding and porphyrin metalation compared to the wildtype protein.

Table 5.1- Summary table of the H88A mutant activity compared to wildtype

EXPERIMENT	PARAMETERS	H88A HEMH	WILDTYPE HEMH [1]
STEADY STATE KINETICS	K_m^{CP} / µM	0.20 ± 0.07	0.14 ± 0.02
			0.15 ± 0.05
	K_m^{Fe} / µM	28 ± 4	3.8 ± 0.4
			1.8 ± 0.3
	k_{cat} / s^{-1}	0.37 ± 0.02	0.32 ± 0.01
		0.46 ± 0.03	0.35 ± 0.01
CP$_{III}$ BINDING ASSAYS	K_d / µM	5.0 ± 0.9	0.048 ± 0.02
CP$_{III}$ BINDING KINETICS	K_{CP} / µM	15 ± 5	4.8 ± 0.3
	k_{iso} / s^{-1}	28 ± 3	25 ± 0.4
	k_{-iso} / s^{-1}	9.3 (calculated)	0.25 (calculated)
IRON BINDING AND PORPHYRIN METALATION KINETICS	K_{Fe} / µM	3.1 ± 0.9	90 ± 20
	k_{chel} / s^{-1}	32 ± 1	16 ± 1
	k_{-chel} / s^{-1}	0 ± 0 (held)	0 ± 0 (held)

[1] Wildtype data re-represented for comparison

5.7. Characterising the K87A *B. subtilis* HemH mutant

The second *B. subtilis* HemH mutant is K87A HemH, the activity assays (section 5.5) showed that this mutant protein has significantly reduced activity compared to the wildtype suggesting that it was unable complete part of its enzymatic mechanism. The characterisation of the K87A mutant began with assessing its CP_{III} binding capability.
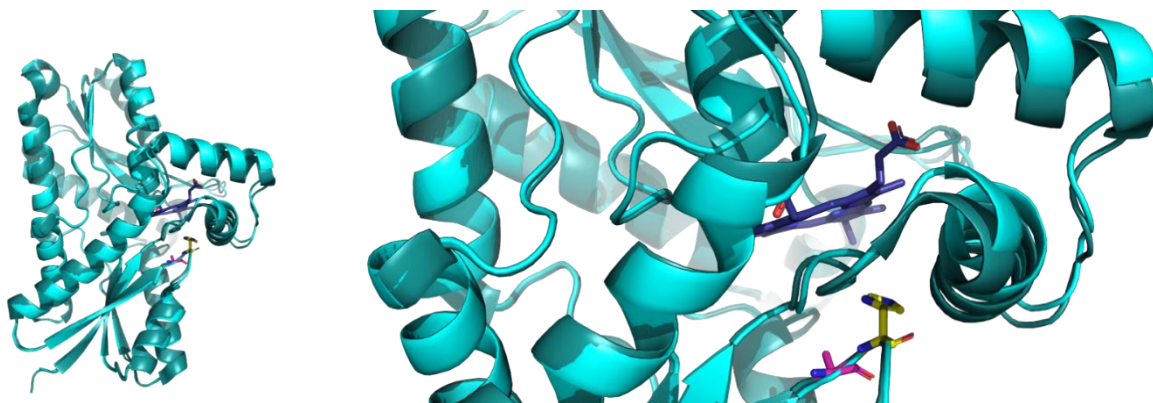
Figure 5.14 – Structural model of the K87A mutant *B. subtilis* ferrochelatase overlayed with wildtype ferrochelatase

Overlay of wildtype *B. subtilis* ferrochelatase (PDB ID: 1AK1, cyan) and a crystal structure of the K87A mutant (PDB ID: 2H1V, deep teal), the K87 (wildtype) and A87 (mutant) are shown in sticks and coloured yellow and magenta, respectively. The overlay was aligned to PP_{IX} bound *H. sapiens* ferrochelatase (2HRE) to show porphyrin placement in the active site (dark blue) (Al-Karadaghi et al., 1997, Medlock et al., 2007a).

5.7.1. CP_{III} binding to K87A HemH

Using fluorescence spectroscopy, static binding assays were performed on the K87A mutant to determine if it was able to bind its first substrate CP_{III}. Previous studies with the wildtype *B. subtilis* HemH protein (section 4.5.4) showed that CP_{III} could bind tightly to ferrochelatase.

Analysis of the integrated tryptophan emission peak and the CP_{III} concentration demonstrates that the relationship between the K87A enzyme and substrate is tight

binding (figure 5.15). The tight binding equation (equation 3A) was fit to the data and a K_d value of 0.016 µM was determined. In comparison, the K_d for the wildtype protein was 0.048 µM. This shows that the K87A mutant has 3-fold tighter binding compared to the wildtype. The concentration of K87A assayed was 50 nM, higher than the calculated K_d value, under these conditions the estimated K_d value depends on the accuracy of the protein concentration. Despite this potential limitation it is clear that the K_d value is very low and there is tight binding between the K87A ferrochelatase and its substrate CP_{III}.
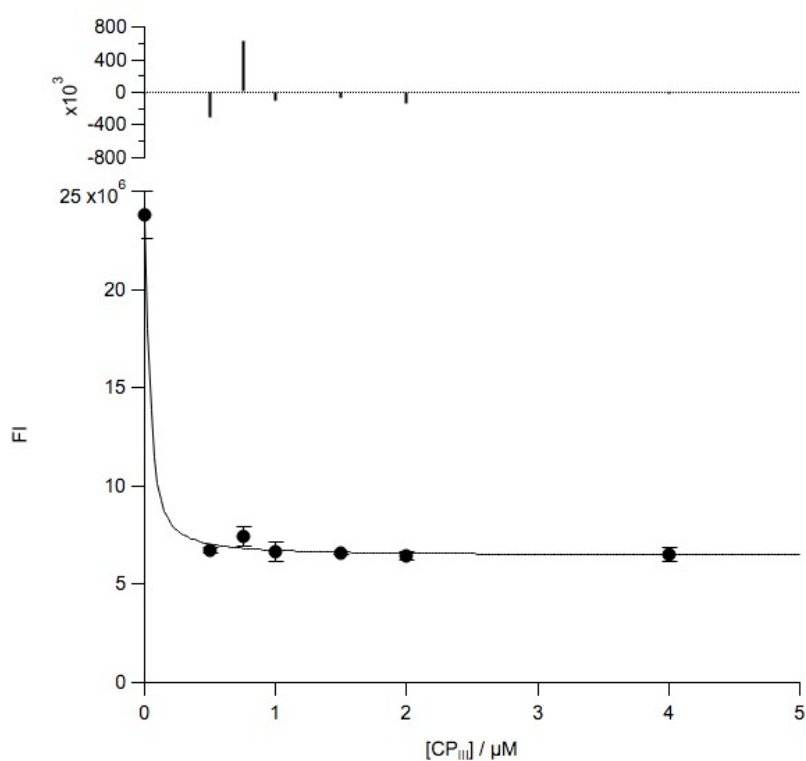
Figure 5.15– Static quenching of K87A *B. subtilis* ferrochelatase tryptophan/tyrosine fluorescence by CP_{III}

The graph shows the quenching of tryptophan/tyrosine fluorescence in the K87A mutant in increasing concentrations of CP_{III}. The enzyme concentration is held at approximately 50 nM and the CP_{III} concentration is varies (0-4 µM). Each point corresponds to the peak area of the tryptophan/tyrosine emission peak (330-510 nm) when it is excited at 280 nm. Each data point is an average of three measurements and the error bars are ± one standard deviation. The curve was fitted using equation 3A and the calculated K_d was 0.016 ± 0.01 µM.

The static binding assay of the K87A mutant revealed that there was tighter binding with CP_{III} compared to the wildtype protein. As there is tight binding between the enzyme and its substrate the rate constants for this interaction can be determined using stopped flow fluorescence spectroscopy. There are two signals in this binding experiment that can be used to estimate rate constants: tryptophan/tyrosine fluorescence (280 nm) and porphyrin fluorescence (393 nm). Generally, the favoured signal is for this experiment is tryptophan/tyrosine fluorescence as this means the concentration of CP_{III} can be varied and a greater range of CP_{III} can be obtained. When the porphyrin signal is used the enzyme, concentration is varied instead. Both signals were used to delineate the rate constants for the binding reaction in the K87A mutant however, the CP_{III} signal was more successful.

$$E + CP_{III} \underset{}{\overset{K_{CP}}{\rightleftharpoons}} ECP_{III} \underset{k_{-iso}}{\overset{k_{iso}}{\rightleftharpoons}} E'CP_{III}$$

Scheme 1- Two step substrate (CP_{III}) binding to enzyme (E)

To begin with, the tryptophan/tyrosine signal was measured and the K87A mutant concentration was held at 0.1 µM. The raw traces obtained at different CP_{III} concentrations (1-4 µM) were fitted to a single exponential equation (equation 4A) and the k_{obs} values were estimated (figure 5.16) The k_{obs} data is fitted to equation 5. The data shows behaviour consistent with two-step binding, the first step indicates initial CP_{III} binding (K_{CP}) and the second step corresponds to an enzyme/porphyrin isomerisation (k_{iso}) (see scheme 1).

The calculated K_{CP} for this experiment was 0.48 µM however, the lowest concentration of CP$_{III}$ is above K_{CP}. This means that the estimated K_{CP} is unreliable. The calculated k_{iso} value was 43 s^{-1}, which was between 1.5-2-fold faster than the wildtype protein whilst the k_{-iso} was held at zero (appendix 7.6.5). However, these experiments were preliminary, and analysis of the raw data showed the reaction was fast and timeframe for each of the reactions were too long. When shorter timeframes were used there was high signal to noise and so more repeats were needed. In these binding kinetics it was challenging to measure the kinetics of a tight binding system under pseudo first order conditions. The difficulty arose as low concentrations of reagents were required and as a result signal changes are exceptionally low. This problem was circumvented by using porphyrin signal as it is more intense. In the binding kinetics using porphyrin signal, the CP$_{III}$ concentration (10 nM) was held and the concentration of the K87A mutant (0-5 µM) was varied. This meant that the concentration of K87A HemH could go lower that the estimate K_{CP} in the first binding experiment. The data was processed in the same way as the first binding kinetic experiment.

In second binding kinetic experiment the K_{CP} values were a little higher that those previously calculated (0.48 µM compared to 1.3 µM) but still consistently lower than the wildtype protein (K_{CP} of 4.8 µM). The k_{iso} value is also much faster in the second setup at approximately 150 s^{-1} compared to 43 s^{-1}, this shows that the k_{iso} value is 6-fold faster than the wildtype *B. subtilis* ferrochelatase.

When equation 5 was fitted to the binding data, three rate constants were calculated, K_{CP}, k_{iso} and k_{-iso}. Generally, the k_{-iso} was held at zero this is because binding kinetics

on wildtype *B. subtilis* HemH show that the k_{iso} value is small (0.25 s^{-1}) and therefore close to zero. The k_{iso} value can be estimated using the parameters calculated from the binding assays and binding kinetics, the estimated k_{iso} value is 1.8 s^{-1} (calculated from the second binding experiment). The calculated parameters for K_{CP} and k_{iso} did not change when the k_{iso} values was held at zero, 1.8 s^{-1} or left unconstrained. If left unconstrained the k_{iso} value was calculated at 1.7 s^{-1} and had an error that was approximately 10-fold higher.
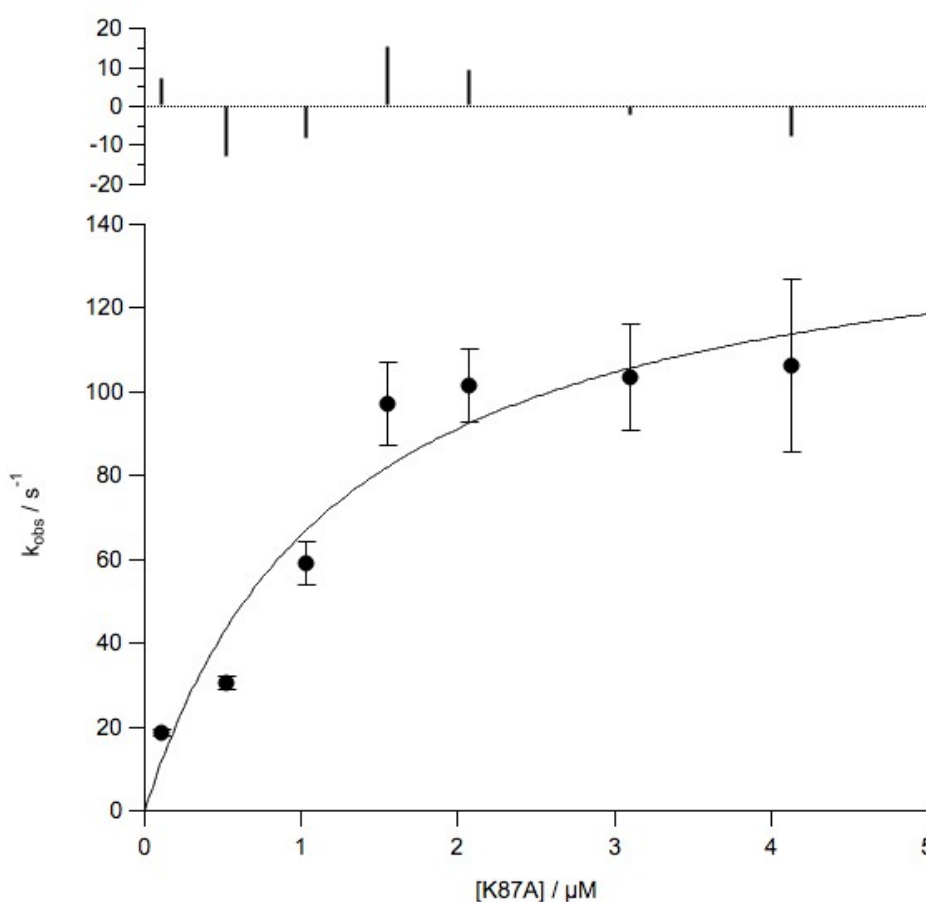
Figure 5.16 - CP$_{III}$ binding kinetics of K87A *B. subtilis* HemH

The data from the second binding kinetic experiment. The CP$_{III}$ concentration was held at 10 nM and the ferrochelatase concentration was varied (0.1-5 µM). Excitation occurred at 393 nm and the raw traces were averaged and fitted to equation 4A to estimate k_{obs} values. The k_{obs} values were plotted against enzyme concentration and equation 5 was fitted to the data. The kinetic parameters were estimate and are as follows: K_{CP} was 1.3 ± 0.5 µM and k_{iso} was 150 ± 20 s^{-1} and k_{iso} was held at zero. Error bars are ± one standard deviation.

The binding kinetics revealed rate constants for the forward and backward reaction of isomerisation (k_{iso} and k_{-iso}) are higher than the wildtype *B. subtilis* HemH whereas the dissociation constant (K_{CP}) is lower in the K87A mutant protein compared to wildtype. This shows that the mutant protein can binding CP_{III} more tightly and isomerise quicker as a result it can it is ready to receive iron more quickly when compared to the wildtype protein.

After confirming the K87A mutant is capable of binding substrate and deduction of the rate constants of the CP_{III} binding, the next step was to assess the spectral properties of the K87A-CP_{III} complex compared to the spectral properties of free CP_{III}. Spectral analysis of *B. subtilis* and *S. aureus* HemH revealed a spectral shift (393-405 nm) occurs when porphyrin complexes with the ferrochelatase. The progression of this shift indicates the presence of two spectrally distinct species (free porphyrin and bound porphyrin) (section 4.5.4.3).

Rapid scanning kinetics (millisecond time base) were used to observe any spectral shifts that occur when CP_{III} binds to the K87A mutant. Monitoring the complex formation between the K87A HemH mutant and CP_{III} indicates that a spectral shift occurs, and this is similar to the wildtype HemH proteins (393- 405 nm). However, the binding occurs so fast that approximately half of the spectral shift occurs in the dead time of the machine, the first spectrum recorded has λ_{max} 400 nm and the shift is complete in 0.5 seconds (figure 5.17). This spectral shift is much faster the wildtype *B. subtilis* HemH where the shift was completed by 5 seconds. Spectral analysis of the K87A mutant also reveals the presence of two spectrally distinct species. The static

binding assays and binding kinetics show that the K87A mutant binds tightly and quickly and rapid scanning kinetics support these findings.
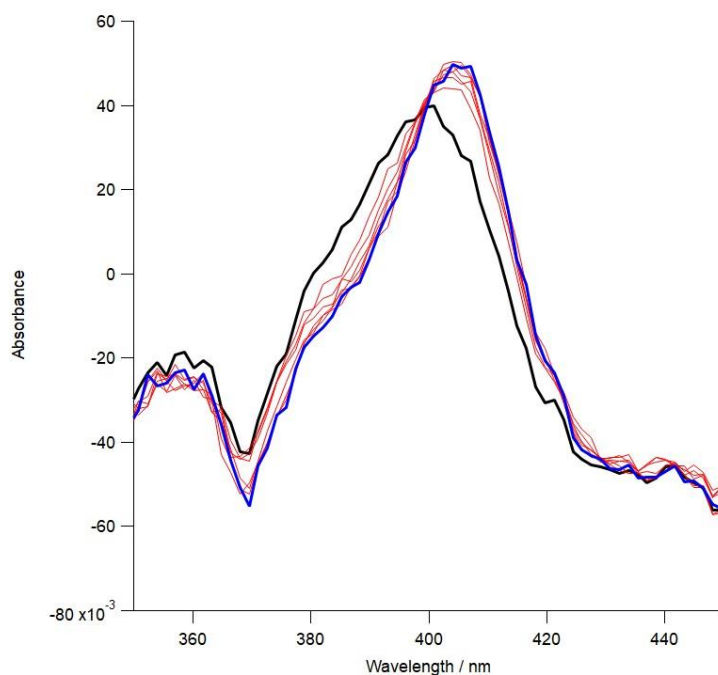
Figure 5.17 – Rapid scanning kinetics of K87A HemH

The spectra show the rapid scanning kinetics of 1 μM K87A ferrochelatase and 0.64 μM CP_{III} over 0.5 s, the black trace indicates the first spectral reading (λ_{max} 400 nm) and the blue trace shows the final reading (λ_{max} 405 nm). Each trace is an average of five consecutive scans.

5.7.2. Iron binding and porphyrin metalation in K87A HemH

The activity assay performed on the K87A mutant show that it is less active than the wildtype protein, this indicates that altering the side chain at position 87 reduces the activity of ferrochelatase. The static binding assays, binding kinetics and rapid scanning kinetics reveal that the K87A mutant is able to bind its coproporphyrin substrate more tightly and faster compared to the wildtype *B. subtilis* HemH. These

236

results show that the K87A mutation is capable of binding CP_{III} well and may affect the enzyme mechanism due to tighter binding. In order to investigate whether this was the reason for the inactivity of the K87A mutation, iron binding and porphyrin metalation were assessed.

The next stages that need to be investigated in the enzymatic mechanism of the K87A mutant were iron binding and porphyrin metalation. In order to determine iron binding and porphyrin metalation in the K87A mutant scanning kinetics (second time base) were utilised. Scans in the wavelength range 350-450 nm were taken for free CP_{III} (2 µM), the K87A-CP_{III} complex (2 µM) and when 10-fold excess (20 µM) of ferrous iron was added. The reaction was monitored across the wavelength range after the addition of the ferrous iron. Addition of 10-fold excess of ferrous iron shows a very slow decrease in the 405 nm peak (figure 5.18), suggesting that iron binding and porphyrin metalation is very slow.

Scanning kinetics (second time base) can show the full shift from 393-405 nm but gives no data on rate of shift as the conditions are not pseudo first order (figure 5.18). They are also able to show whether the mutant protein is capable of iron binding/metalating porphyrin. Addition of an excess of ferrous iron shows a very slow decrease in the 405 nm peak (figure 5.18) and a blue shift back towards 393 nm forming a less distinguished broad peak. These spectral shifts suggest that iron binding, porphyrin metalation and/or product release is severely affected but still occurring. As product is formed slowly transient kinetics were not performed on the later stages of the enzymatic mechanism.
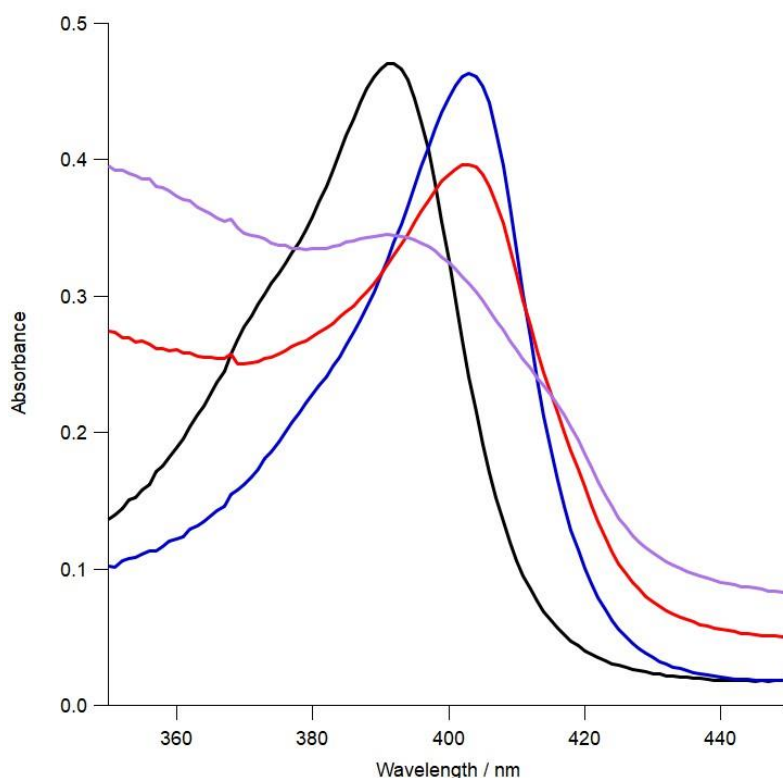
Figure 5.18 – Scanning kinetics of K87A HemH

The spectral changes occurring across 350-450 wavelength range in the K87A HemH mutant. CP_{III} (2 µM) only is shown by the black trace, the blue trace shows the formation of the complex between K87A HemH (2 µM) and CP_{III} (2 µM) and an immediate red shift from 393 nm to 405 nm in the λ_{max} of the Soret band. The red trace shows the spectra immediately after the addition of 100 µM of ferrous iron, the purple trace shows the progression of the reaction after 30 minutes.

5.7.3. Summary of K87A mutant

The K87A *B. subtilis* HemH mutant was successful purified and shown to have similar secondary structure and thermostability to the wildtype *B. subtilis* HemH. Activity assays show that the K87A mutation greatly reduces the ability for *B. subtilis* ferrochelatase to convert CP_{III} and ferrous iron into coproheme. Due to the inactivity of the K87A mutant, steady state kinetics were not completed. However, fluorescence spectroscopy, UV-visible spectroscopy and stopped flow fluorescence spectroscopy were used to identify the steps in the enzymatic mechanism that were affected by the mutation at Lys87 and those that are responsible for the lack of activity.

Static binding assays indicated that the K87A mutant had a lower K_d value for CP_{III} compared to the wildtype ferrochelatase, this was supported by the binding kinetics that showed that the K_{CP} values was also lower in the K87A mutant. The isomerisation that occurs after CP_{III} binding was much faster in the K87A mutant indicating that it is prepared to receive iron much quicker than the wildtype, this suggests that if CP_{III} binding is responsible for the lack of activity then it will be because of tight binding.

Scanning kinetics (second time base) and rapid scanning kinetics (millisecond time base) were performed using UV-visible spectroscopy, these showed that there is a spectral shift in the λ_{max} of Soret band from 393 nm to 405 nm when there is complex formation between K87A ferrochelatase and CP_{III}. This observed spectral shift was completed in 0.5 seconds compared to the 5 seconds required for the wildtype protein, supporting the results of the binding kinetics. The spectra produced in the rapid scanning kinetics show that there are two spectrally distinct species corresponding to free porphyrin and enzyme bound porphyrin. Scanning kinetics showed that in the presence of an excess of ferrous iron the ferrochelatase-CP_{III} complex is unable to turnover substrate very quickly, thus showing that iron binding, porphyrin metalation and/or product release is limited in the K87A mutant. As these stages of the enzymatic mechanism significantly impaired by mutation at Lys87, the other two stopped flow experiments used on the wildtype ferrochelatase were not completed. A summary of the kinetic results are shown in table 5.2.

Table 5.2 – Summary of the K87A *B. subtilis* HemH kinetics compared to wildtype

EXPERIMENT	PARAMETERS	K87A HEMH	WILDTYPE HEMH [1]
CP$_{\text{III}}$ BINDING ASSAYS	K_d / μM	0.016 ± 0.01	0.048 ± 0.024
CP$_{\text{III}}$ BINDING KINETICS	K_{CP} / μM	1.3 ± 0.52	4.8 ± 0.28
	k_{iso} / s^{-1}	150 ± 23	25 ± 0.44
	$k_{\text{-iso}}$ / s^{-1}	1.8 (calculated)	0.25 (calculated)

[1] Wildtype data re-represented for comparison

5.8. Characterising the E264Q and E264A *B. subtilis* HemH mutants

The E264 residue in *B. subtilis* HemH is completely conserved in all ferrochelatases and research has shown that it is important in the function of ferrochelatase (Hoggins et al., 2007, Hunter et al., 2016, Hansson et al., 2007, Sellers et al., 2001, Medlock et al., 2007a). Two different mutants were produced for the E264 residue, the first mutant E264Q is more conservative, conserving sidechain length and hydrogen bonding but removes the negative charge. The second mutant, E264A, completely removes the functionality of the glutamate. The activity assays reveal that both mutants are substantially less active than the wildtype protein. As a result, steady-state kinetic characterisation was not attempted. To discern which part of the enzymatic mechanism was affected by mutation at E264 a combination of fluorescence, UV-visible and stopped flow fluorescence spectroscopy was utilised.
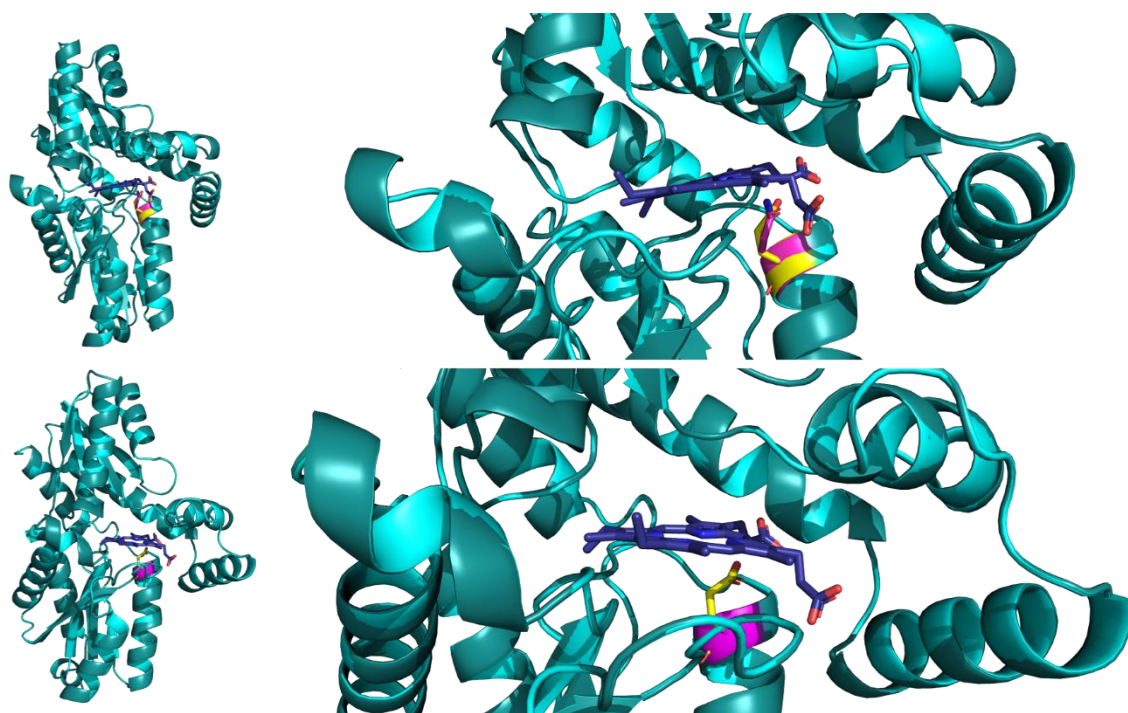
Figure 5.19 – Structural models of the E264Q (above) and the E264A (below) *B. subtilis* **ferrochelatase mutants**

Above: Overlay of wildtype *B. subtilis* ferrochelatase (PDB ID: 1AK1, cyan) and a model (generated by Swiss-Model (Waterhouse et al., 2018) of the E264Q mutant (template used PDB ID:1AK1, deep teal, top), the E264 (wildtype) and Q264 (mutant) are shown in sticks and coloured yellow and magenta, respectively. The overlay was aligned to PP_{IX} bound *H. sapiens* ferrochelatase (2HRE) to show porphyrin placement in the active site (dark blue) (Al-Karadaghi et al., 1997, Medlock et al., 2007a). **Below:** Overlay of wildtype *B. subtilis* ferrochelatase (PDB ID: 1AK1, cyan) and a model (generated by Swiss-Model (Waterhouse et al., 2018) of the E264A mutant (template used PDB ID:1AK1, deep teal,), the E264 (wildtype) and Q264 (mutant) are shown in sticks and coloured yellow and magenta, respectively. The overlay was aligned to PP_{IX} bound *H. sapiens* ferrochelatase (2HRE) to show porphyrin placement in the active site (dark blue) (Al-Karadaghi et al., 1997, Medlock et al., 2007a).

5.8.1. CP_{III} binding to E264Q/A HemH

The CP_{III} binding to the E264Q and E264A mutants was investigated. Static binding assays were performed using fluorescence spectroscopy, assessing the ability of CP_{III} to quench the intrinsic tryptophan/tyrosine fluorescence of the E264 mutants. In the wildtype protein CP_{III} binding quenched tryptophan/tyrosine fluorescence and the degree of quenching was dependent on the concentration of CP_{III}. The peak area of the tryptophan/tyrosine emission (330-510, λ_{max} 371 nm) was plotted against CP_{III}

concentration, these data showed tight binding and consequently the tight binding equation (equation 3A) was fit to the data (figure 5.20). The estimated K_d for the E264Q mutant was 0.072 µM and 0.036 µM for the E264A mutant. The K_d value for the wildtype protein is 0.048 µM, so in all cases tight binding was observed.
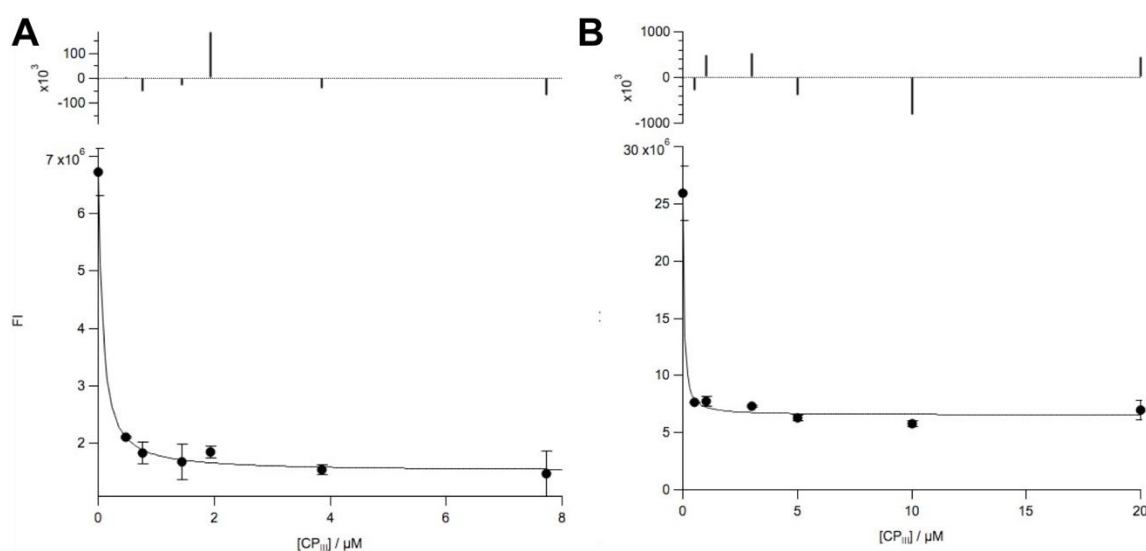
Figure 5.20- CP$_{III}$ binding assays of the E264Q and E264A mutants

Fluorescence spectroscopy was used to calculate binding constants (K_d) for the interaction between the E264Q/A mutant proteins and CP$_{III}$. The mutant ferrochelatase proteins (50 nM) were excited at 280 nm and emission was collected. The tryptophan/tyrosine emission peak was integrated (330-510 nm) and plotted against CP$_{III}$ concentration, the resulting graph was fitted to equation 3A. **A** shows the E264Q HemH binding curve where the K_d was estimated as 0.056 ± 0.08 µM. **B** shows the E264A HemH binding curve where the K_d was calculated as 0.036 ± 0.02 µM. The error bars are ± one standard deviation.

The static binding assays showed tight binding between CP$_{III}$ and the mutant ferrochelatases establishing the conditions needed to proceed with investigating CP$_{III}$ binding kinetics. The raw data for these binding kinetics were similar to those observed with the wildtype ferrochelatases (*B. subtilis* and *S. aureus*) (section 4.5.4.2) and as a result they were fit to a single exponential (equation 4A). From these fits k_{obs} values were estimated and plotted against CP$_{III}$ and subsequently fit to equation 5 allowing the definition of K_{CP} and k_{iso} (see scheme 1). The k_{-iso} rate constant was assumed to indistinguishable from zero (figure 5.21). The calculated k_{-iso} value from the binding

assay and kinetic parameters are 2.5 s^{-1} (E264Q) and 1.4 s^{-1} (E264A) which are not substantially different from each other. When the k_{-iso} values are held at these calculated values instead of zero, the estimated for K_{CP} and k_{iso} appears essentially unchanged.

$$E + CP_{III} \xrightleftharpoons{K_{CP}} ECP_{III} \underset{k_{-iso}}{\overset{k_{iso}}{\rightleftharpoons}} E'CP_{III}$$

Scheme 1- Two step substrate (CP$_{III}$) binding to enzyme (E)

The calculated K_{CP} parameter for the two mutants were similar, for the E264Q mutant it was 0.60 µM and 0.75 µM for E264A HemH. The K_{CP} values in these mutants are 6-8-fold lower than the estimated K_{CP} value in the wildtype protein indicating that they bind CP$_{III}$ more tightly. The k_{iso} values were 21 s^{-1} and 30 s^{-1} for E264Q HemH and E264A HemH, respectively, these are slightly different and indicate the E264A mutant ferrochelatase can isomerise relatively quickly after initial CP$_{III}$ binding. The k_{iso} value for wildtype protein is 25 s^{-1}, it is an intermediate value between the two mutants and so isomerisation in the mutants appears essentially unchanged from the wildtype HemH.
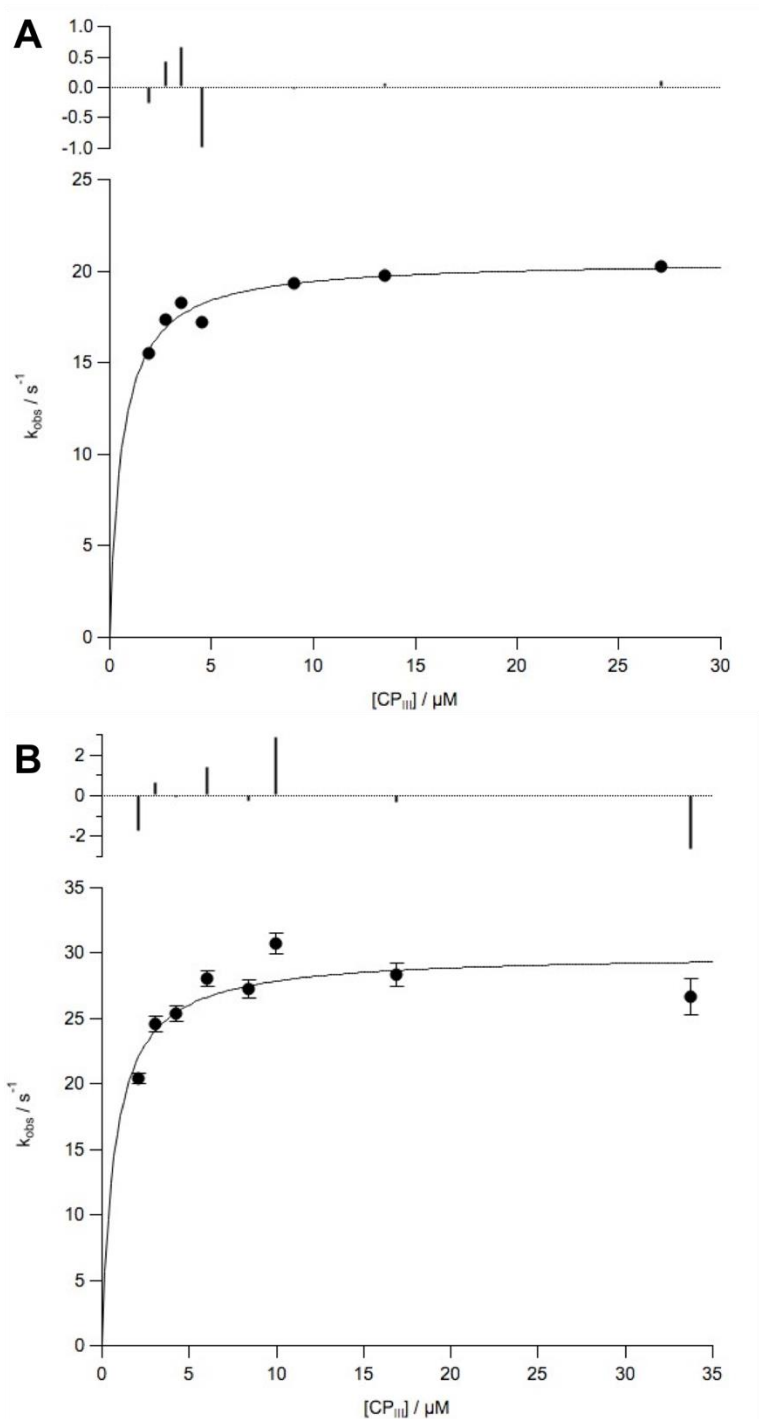
Figure 5.21- CP$_{III}$ binding kinetics of the E264Q and E264A mutants using stopped flow fluorescence spectroscopy

The mutant ferrochelatases E264Q (**A**) and E264A (**B**) were held at 0.2 µM and excited at 280 nm whilst the CP$_{III}$ concentration was varied 0-35 µM. The raw traces averaged and fitted to equation 4A and k_{obs} values were estimated. These were plotted against CP$_{III}$ to give the graphs **A** and **B**. The calculated kinetic parameters for E264Q (**A**) were K_{CP} 0.60 ± 0.10 µM, k_{iso} 21± 0.44 s^{-1} and k_{-iso} was constrained at zero. The calculated kinetic parameters for E264A (**B**) were K_{CP} 0.75 ± 0.26 µM, k_{iso} 30 ± 1.3 s^{-1} and k_{-iso} was constrained at zero. The error bars are ± one standard deviation (small and therefore not visible in **A**).

In addition to estimating the rate constants for the binding of CP_{III} to the E264 mutant proteins, a combination of scanning kinetics (second time base) and rapid scanning kinetics (millisecond time base) was used to investigate any spectral shift in the Soret band upon enzyme-substrate complex formation. This has been shown to occur in both wildtype ferrochelatases described in the previous chapter and the K87A and H88A mutant described above. Scanning kinetics instead of rapid scanning kinetics were used to assess spectral shift with the E264Q mutant. This was because the final stages of the spectral shift were slow (figure 5.22A). The λ_{max} of the Soret band moved from 393 nm to 401 nm and this occurred over approximately 20 minutes, much longer than the wildtype (5 seconds). As the spectral shift was complete at 401 nm this indicates that the porphyrin molecule is in a different environment when bound to the E264Q mutant when compared to the wildtype protein. Rapid scanning kinetics were utilised to observe the spectral shift in the E264A mutant, the shift in the λ_{max} of the Soret band was 393-402 nm and occurred within 10 seconds, a similar time frame to the wildtype protein (5 seconds) (figure 5.22B). The spectral changes observed in each of the E264 mutants show that they behave differently when compared to each other. The spectral shift corresponding to the E264Q mutant protein is very slow compared to the spectral shift that occurs when CP_{III} binds E264A this spectral change is similar to the wildtype protein.
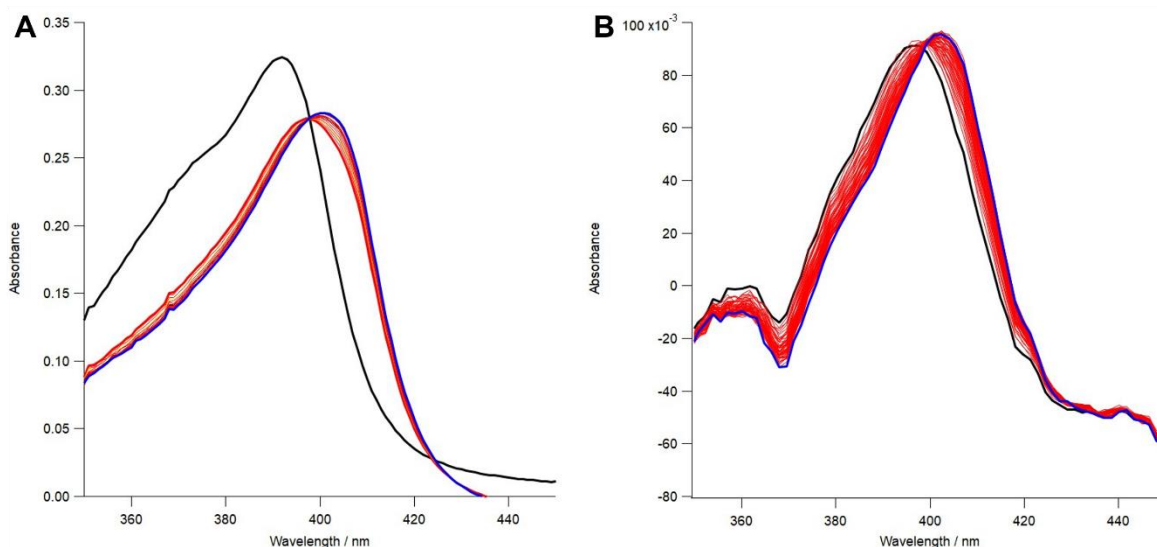
Figure 5.22- Rapid Scanning kinetics of E264Q and E264A *B. subtilis* HemH showing a spectral shift of CP$_{III}$ upon binding to HemH

Scanning kinetics (350-450 nm) of complex formation between CP$_{III}$ (2 µM) and *B. subtilis* E264Q HemH (2 µM) (**A**). The black traces shows CP$_{III}$ alone, the red traces show the shifting of the Soret band once 2 µM E264Q ferrochelatase has been added and the blue trace shows the final spectrum once the shift has finished, the peak shifts from 393-401 nm. **B** shows the spectral shift of the Soret band using rapid scanning kinetics, the black indicates the first averaged spectra, the blue indicates the final averaged spectra and the red indicates intermediate spectra, the λ$_{max}$ of the peak shifts from 393-402 nm. Each spectrum shown in the rapid scanning kinetics is an average of 10 consecutive traces.

5.8.2. Iron binding and porphyrin metalation in E264Q and E264A HemH

After the deducing the rate constants for CP$_{III}$ binding and confirming that the spectral properties of the enzyme-substrate complex with the E264 mutants, iron binding and porphyrin metalation were assessed. Scanning kinetics were used to isolate the iron binding and porphyrin metalation steps and investigate whether the mutation affected these. Before addition of the enzyme the CP$_{III}$ shows a characteristic Soret band with a λ$_{max}$ of 393 nm. The spectral shift from free CP$_{III}$ to bound CP$_{III}$ on adding the mutant ferrochelatase (E264Q) was slow (~20 mins) and the λ$_{max}$ of the complex was 401 nm. On addition of a 10-fold excess of ferrous the iron the absorbance at 401 nm increases slightly and remains stable at the higher absorbance. This indicates that the E264Q

mutant is incapable of iron binding or porphyrin metalation and the slight increase in absorbance is most likely due to increased scattering caused by the addition of iron (figure 5.23A). When investigating the spectral properties of the complex between E264A ferrochelatase and CP_{III}, it appears similar to wildtype (shift from 393- 405 nm). The addition of ferrous iron (100 µM) causes a slow decrease in the peak at 405 nm (over 105 mins) thus suggesting that the mutant is capable of iron binding or porphyrin metalation, but it is severely affected by the mutation (figure 5.23B). The E264A mutant protein retains a fraction of activity whereas the E264Q mutant is completely inactive. Alanine has a smaller amino acid sidechain compared to glutamine, this leave spaces for a water molecule to substitute the mutated glutamate sidechain. The presence of the water molecule could lead to the activity observed in the E264A HemH protein. As the iron binding or porphyrin metalation in both mutations were reduced, kinetic investigation of the rates of iron binding and porphyrin metalation was not performed.
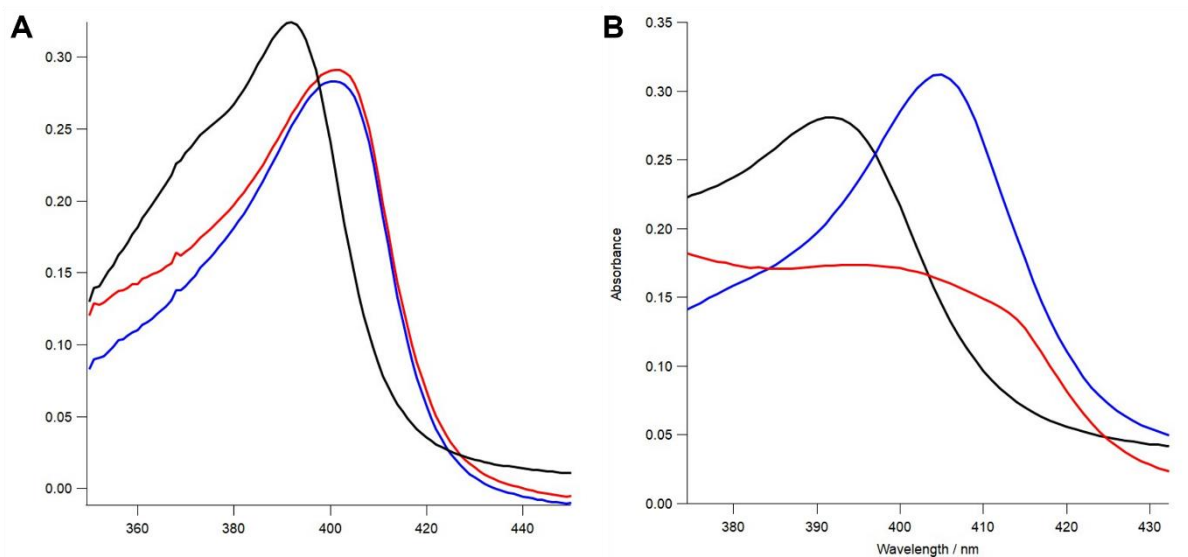
Figure 5.23- Scanning kinetics of E264Q and E264A *B. subtilis* HemH showing a spectral shift of CP$_{III}$ upon binding to HemH

Standard scanning kinetics (350- 450 nm) show a shift in λ_{max} of the Soret band upon complex formation between CP$_{III}$ and either E264Q HemH (**A**) or E264A HemH (**B**). The black traces show the spectra of 2 µM of CP$_{III}$. The blue traces show the spectra where 2 µM of ferrochelatase has been added, in **A** the shift in λ_{max} is 393-401 nm and in **B** the shift in λ_{max} is 393-405 nm. After the shift stabilised excess of ferrous iron was added (20 µM (**A**) and 100 µM (**B**)), the red traces indicate the spectra produced after iron has been added. **B** shows a decrease in absorbance at 405 nm indicating iron binding and porphyrin metalation is occurring however this is very slow (105 mins).

5.8.3. Summary of E264Q/A mutants

Activity assays of the two E264 mutants show that they can either turnover substrate very slowly or cannot do this at all. Compared to the wildtype they look almost completely inactive and as a result, steady state kinetic characterisation was not performed on these mutants. CP$_{III}$ binding assays show that they are both able to bind their substrate CP$_{III}$ tightly and the estimated K_d values are comparable to wildtype. Binding kinetics were performed to deduce the rate constants for CP$_{III}$ binding and these show that the K_{CP} values are much lower that the wildtype and the rate of enzyme/porphyrin isomerisation (k_{iso}) is similar compared to wildtype. The lower K_{CP} values show that both mutants are better at initial binding than the wildtype protein. In

addition, to the binding kinetics a combination of scanning kinetics and rapid scanning kinetics were used to identify any shift in the Soret band when CP_{III} is bound by the mutant proteins. The E264Q mutant shows very slow shifting that reaches 401 nm rather than the 405 nm observed in the wildtype *B. subtilis* HemH. However, the shifting in the E264A mutant shows rate of shift and degree of shift equivalent to wildtype protein (393-405 nm, ~10 seconds).

After determining the degree of spectral shift in the E264 mutant proteins' ability for them to bind iron and metalate porphyrin was tested. Scanning kinetics show that the E264Q mutant is completely incapable of binding iron and metalating porphyrin as there is no decrease in the absorbance at 401 nm. The E264A mutant is capable of turning over substrate however this is very slow, too slow for stopped flow fluorescence spectroscopy. Due to the lack of iron binding and porphyrin metalation capability, kinetics investigating the rate of iron binding and porphyrin metalation were not completed. It is clear that mutation at E264 is detrimental to the function of ferrochelatase; it appears to mostly affect the ability of the enzyme during the iron binding and porphyrin metalation phase. However, slow product release could be affecting the turnover of substrate. A summary of the E264A and E264Q is shown in table 5.3.

Table 5.3- Summary of E264Q and E264A *B. subtilis* HemH mutants

EXPERIMENT	PARAMETERS	E264Q HEMH	E264A HEMH	WILDTYPE HEMH [1]
CP$_{III}$ BINDING ASSAYS	K_d / μM	0.072 ± 0.082	0.036 ± 0.020	0.048 ± 0.024
CP$_{III}$ BINDING KINETICS	K_{CP} / μM	0.60 ± 0.10	0.75 ± 0.26	4.8 ± 0.28
	k_{iso} / s^{-1}	21 ± 0.44	30 ± 1.3	25 ± 0.44
	k_{-iso} / s^{-1}	2.5 (calculated)	1.4 (calculated)	0.25 (calculated)

[1] Wildtype data re-represented for comparison

5.9. Co-crystallisation of mutant HemH proteins with CP$_{III}$

Currently, there are no resolved crystal structures of any coproporphyrin ferrochelatase where CP$_{III}$ is bound in the active site. In combination with kinetic analysis crystallisation of the mutant proteins (K87A, H88A and E264A) in the presence of CP$_{III}$ was attempted. Crystallisation of these and the wildtype protein in the presence or absence of CP$_{III}$ could provide information about the orientation of the active site residues in the mutant proteins and when CP$_{III}$ is bound. Analysing the orientation of the active site residues could provide data on the enzymatic mechanism and the importance of each residue in the mechanism.

The three mutant proteins and wildtype were purified as usual and concentrated to approximately 10 mg mL^{-1}. Pre-crystallisation trials were performed on each of the mutant proteins to determine whether they were concentrated to a suitable concentration, all mutants were sufficiently concentrated for crystallisation screens. Seven standard crystal screens (JSCG+, Morpheus, pH Clear, MPD, Ammonium

sulphate, PACT and Proplex) were used for the proteins in the presence of equimolar CP_{III}. Protein crystals did not form in any of these conditions. A custom screen of the wildtype protein in the presence of CP_{III} was attempted. This custom screen contained a buffer composition similar to the conditions used to crystallise the wildtype protein (PDB ID: 1AK1). This resulted in the crystals that diffracted at 1.8 Å however, the protein structure did not contain bound CP_{III}. The lack of crystal formation could be due to homogenous structures within the protein samples as the proteins did not undergo SEC prior to crystallisation. Also, when analysing the crystal trays CP_{III} frequently aggregated in the wells which is not surprised given the high concentration required. The apoprotein structure of K87A has previously been resolved (PDB: 2H1V).

5.10. Chapter summary

5.10.1.   Overview of chapter results

Four mutants of the five produced were successfully expressed and purified. CD spectroscopy confirmed that they contained secondary structure and their thermostability was similar to wildtype. Activity assays showed that K87A, E264Q and E264Q HemH had very little activity whereas the H88A mutant had activity comparable to the wildtype ferrochelatase.

As the H88A mutant has activity comparable to wildtype, steady state characterisation was completed on the mutant, the results of these shown that the H88A mutant has a higher K_m value for iron and a similar $K_m{}^{CP}$ and k_{cat} values when compared to the wildtype protein. This indicates that the H88A mutant is less efficient at low iron

concentrations compared to the wildtype. Steady state kinetic characterisation was not performed on K87A, E264Q and E264A due to lack of activity.

To identify if the mutant ferrochelatases were still able to bind CP_{III}, fluorescent binding assays were performed. These binding assays show that all four mutants were still able to bind CP_{III}; the E264 mutants bound CP_{III} similarly to wildtype, the H88A mutant was worse at binding CP_{III} and the K87A was better at binding CP_{III} when compared to the wildtype protein. Binding kinetics reveal that the most inactive mutants (K87A, E264A and E264Q) have lower K_{CP} values than the wildtype whilst the H88A mutant has a higher K_{CP} value, this consistent with the binding assays. The isomerisation in H88A, E264Q and E264A ferrochelatases are broadly similar to the wildtype and the K87A ferrochelatase is significantly faster. The rapid scanning kinetics also show that the K87A mutant is much faster at binding and isomerising compared to the other proteins.

Investigation into the spectral shift that occurs when CP_{III} is bound shows that the λ_{max} of the Soret band shifts from 393-405 nm in that K87A and E264A HemH (comparable to wildtype). The H88A mutant causes a λ_{max} shift from 393-396 nm and E264Q λ_{max} shift from 393 nm to 401 nm. The shift in E264Q is much slower than wildtype and takes minutes instead of seconds. Scanning kinetics also showed the change in spectral properties of the enzyme-substrate complex when 10-fold ferrous iron was added. The E264Q mutant remained unchanged indicating no product formation had occurred. The K87A and E264A mutant show that production of metalated porphyrin

was slow and H88A HemH produced metalated product almost immediately, this is similar to the wildtype HemH.

Slow or no formation of metalated porphyrin in the E264A, K87A or E264Q mutants meant that transient kinetics were not performed to deduce rate constants for iron binding and porphyrin metalation. Transient kinetics were performed on the H88A mutant and these showed that the K_{Fe} value was lower than wildtype and k_{chel} was faster in than wildtype indicating that the H88A mutant was better at iron binding and porphyrin metalation. Burst kinetics were completed on the H88A mutant and the rate constants from the two previous stopped flow experiments were fitted onto data from the third stopped flow spectroscopy experiment. This showed that all three stopped flow experiments were consistent. In addition to kinetic characterisation, crystallisation screens were attempted to resolve the apoprotein structure and CP$_{III}$ bound structure of the wildtype and mutant proteins (K87A, H88A and E264A). However, protein crystals were not produced.

Together these mutants give an insight into how the active site of *B. subtilis* HemH functions, it is clear that the K87A, E264A and E264Q mutations are not tolerated by the enzyme whereas the H88A mutation is.

5.10.2.   Assessing the role of the residues in the non- conserved of the active site

The K87 residue is part of the non-conserved face of the ferrochelatase active site and therefore there are different amino acids at corresponding positions in different species. In *H. sapiens* HemH the corresponding residue is R164 and steady state kinetics characterisation has been performed on this residue when it has been mutated conservatively to a leucine. Steady state kinetics of R164L reveal that upon mutation the K_m for the porphyrin and the k_{cat} was unchanged and the K_m^{Fe} was 2-fold higher when compared to the R115L mutant (similar to wildtype) (Sellers et al., 2001). As discussed before the K87A mutant in this work retained very little activity and evidence indicated that the activity and CP$_{III}$ binding is affected by mutation, no parameters were gained involving iron as turnover was very slow.

Mutation from arginine to leucine shown in Sellers et al. is more conservative than lysine to alanine in this work and perhaps the long side chain in lysine, arginine and leucine is important for maintaining activity in both species of ferrochelatase. Additionally, at this site in both species the residue is a long chain positively charged amino acid so whilst they are not completely conserved, they are similar. From these experiments Sellers et al. hypothesise that R164 is part of the final metal binding site prior to metal insertion, the data displayed here support these hypotheses as iron binding and porphyrin metalation was severely affected in the K87A mutant. However, these results do not indicate whether metal insertion occurs from the conserved side or non-conserved side of the active site, K87 may have a role in proton abstraction instead and the same behaviour may still be observed (Sellers et al., 2001).

Activity assays have also been performed on the K87A mutant (*B. subtilis*) using the incorrect porphyrin molecule (protoporphyrin IX) and zinc as the metal ion. These showed that the mutant was very active with 92% activity compared to the wildtype. The activity of the K87A mutant in the literature is grossly different to the activity of the K87A mutant observed here. Stopped flow fluorescence spectroscopy has revealed that the K87A mutant is capable of binding CP_{III} tightly and isomerising quickly compared to the wildtype protein. The tighter binding observed could indicate why the K87A mutant has limited activity when using its endogenous substrates, the CP_{III} may be bound so tightly it is not released easily whereas protoporphyrin may bind weakly and therefore turnover appears comparable to wildtype. However, there is no kinetic data to indicate how well protoporphyrin IX binds to *B. subtilis* K87A HemH (Hansson et al., 2007).

The H88 residue is the other residue on the non-conserved face of the active site that has been implicated in the ferrochelatase mechanism. In *H. sapiens* HemH the corresponding residues is Y165, whilst these residues are not identical, they are both aromatic and therefore similar. In Sellers et al., Y165 is mutated to phenylalanine which conserves the aromatic ring and removes the polar hydroxyl group, this is a conservative mutation compared to the conversion of histidine to alanine where there is no conservation of polarity or aromatic ring (Sellers et al., 2001).

Steady state kinetic characterisation of the Y165F showed a slightly higher K_m^{Fe} and k_{cat} and a slightly lower K_m^{PPIX} compared to the wildtype protein. In this work, the K_m^{Fe}, value is higher and the K_m^{CP} and k_{cat} values are similar wildtype protein, this is broadly consistent with the work completed with the Y165F mutant. The increases in the K_m^{Fe} value observed in the H88A mutant is more drastic, this most likely due to the severity of the mutation. Sellers et al., suggests that the Y165 and R164 residues in the *H. sapiens* ferrochelatase make up the final metal binding site prior to porphyrin metalation as they have higher K_m^{Fe} values compared to wildtype and relatively similar K_m^{PPIX} and k_{cat} values and the data shown in this chapter supports this (Sellers et al., 2001).

Further investigation into the kinetics of the H88A mutant revealed that CP_{III} binding is actually affected by the mutation. The K_{CP} and K_d values in the mutant are higher compared to wildtype and the rate constant for isomerisation subsequent to initial binding remains similar. The spectral shift that occurs when CP_{III} is bound by H88A ferrochelatase is different to the wildtype ferrochelatase further support its ability to affect CP_{III} binding. The iron binding and porphyrin metalation kinetics of the H88A HemH show rate constants faster (k_{chel}) and binding constants lower (K_{Fe}) than the wildtype protein indicating that they are better at iron binding and porphyrin metalation. Further assessment of the H88A mutant using transient kinetics and scanning kinetics reveal that CP_{III} binding is the main step affected by mutation.

Kinetic characterisation of the *B. subtilis* H88A mutant has been attempted before however as stated above for the K87A mutant the wrong porphyrin molecule was used.

Using protoporphyrin IX instead of CP$_{III}$ showed that the H88A mutant was only 5% active compared to wildtype extremely different from the activity of the H88A mutant when CP$_{III}$ is used. The CP$_{III}$ binding in the H88A is weak so the binding to protoporphyrin could be even weaker and therefore prevent turnover of substrate, however, there is no current published binding data for *B. subtilis* HemH and protoporphyrin IX so this cannot be determined.

5.10.3. Assessing the role of the residues in the conserved of the active site

The E264 residue in *B. subtilis* HemH is completely conserved in all ferrochelatases and is part of the conserved face of the active site. This residue is E343 in *H. sapiens* HemH, E289 in *M. musculus* and E314 in *S. cerevisiae.* Several kinetic experiments have been performed on this residue in all species mentioned above and mutagenesis appears to greatly reduce activity in most cases.

Mutation of E314 (*S. cerevisiae*) to alanine showed that the V_{max} and K_m^{PPIX} were significantly lower and the K_m^{Zn} was comparable to the wildtype protein. This is consistent with the findings in this work, steady state kinetic characterisation was not performed due to lack of activity in both E264Q and E264A. The K_{CP} values in the binding kinetics were lower than wildtype but the K_d values in the static binding assay were similar. Any kinetic parameter involving iron or zinc was not gained as the mutant protein was not active enough (Gora et al., 1996). In the research undertaken by Gora et al., they hypothesise that the conserved glutamate residue is involved in proton abstraction and the conserved histidine it is paired with, is responsible for iron binding.

Activity assays performed on *B. subtilis* HemH mutants E264V and E264Q show that <1% and 21% activity is retained, respectively. However, these mutant proteins were assayed using protoporphyrin IX and may not reflect the true activity of the enzyme. In the work presented here both E264Q and E264A are very inactive so the results are slightly different dependent on the porphyrin molecule used (Hansson et al., 2007).

Steady state kinetic characterisation has also been completed on the E343 mutants in *H. sapiens* HemH. The E343 residues has been mutated to aspartate (E343D), lysine (E343K), histidine (E343H) and glutamine (E343Q). The first mutant, E343D, was the only mutant that wasn't inactive suggesting that the negative charge of glutamate is important in its role, this is supported by the work here where both mutants (E264Q and E264A) are both relatively inactive. Kinetics of the E343D mutant shows the K_m values for iron and protoporphyrin IX are relatively similar to the wildtype HemH with the K_m^{PPIX} value being slightly higher in the mutant protein (Sellers et al., 2001).

Transient kinetics has also been performed on this mutant using the third stopped flow experiment described in this work. It looks at the rate constants for all enzymatic steps prior to the rate-determining step. These show that the K_{Fe} and K_{DIX} do not appear to change significantly upon mutation of E343D whereas the k_{burst} values were approximately 3-fold different (Hoggins et al., 2007). The transient kinetics performed on E264Q and E264A show that the iron binding and porphyrin metalation is affected by the mutation. The mutants are able to bind CP_{III} easily but cannot turnover quickly

(E264A) or at all (E264Q) (Hoggins et al., 2007) and so k_{burst} values for these mutants were not gained. Hoggins et al. suggested that mutation of the E343 residue in *H. sapiens* HemH affects several steps in the enzymatic mechanism.

6. Discussion

CpFCs are a recent discovery and ferrochelatases belonging to this group of ferrochelatases were previously annotated PpFCs (Dailey et al., 2015). Theses ferrochelatases were reallocated to the CpFC group after the discovery of the coproporphyrin-dependent pathway in 2015 (Dailey et al., 2015). As the endogenous substrate for CpFCs were assumed to be PP_{IX}, when CpFCs such as *B. subtilis* ferrochelatase was assayed with PP_{IX} or related porphyrin analogues they appeared largely inactive when compared to the activity of *H. sapiens* ferrochelatase (Sellers et al., 2001, Hansson and Hederstedt, 1994a, Hansson et al., 2010, Hansson et al., 2007, Hansson et al., 2006). The discovery of this new pathway meant that all previous kinetic analysis on CpFCs, particularly *B. subtilis* HemH, did not represent the actual capabilities of the ferrochelatase. Since 2015 new literature has been released where the correct substrate CP_{III} has been used in kinetic assays. This shows that the CpFCs are much more active than first observed however, the literature is still very limited (Lobo et al., 2015, Hobbs et al., 2017, Dailey et al., 2015).

In addition to kinetic analysis, several structures of *B. subtilis* HemH have been resolved using X-ray crystallography. The apoprotein structure of *B. subtilis* HemH was resolved in 1997 (Al-Karadaghi et al., 1997). When the apo-structure of *B. subtilis* HemH was compared to *H. sapiens* HemH there was structural conservation between the two ferrochelatase types with a few minor differences. The *H. sapiens* HemH has N-terminal and C-terminal extensions, the N-terminal binds to the membrane, the C-terminal extension contains an iron-sulphur cluster. Both extensions form H-bonds at the dimer interface and contribute to dimer formation (Lecerof et al., 2000, Al-Karadaghi et al., 1997, Wu et al., 2001). A second structure of *B. subtilis* HemH

containing a distorted porphyrin N-MeMP (inhibitor for PpFCs) was structurally resolved in 2000 (Lecerof et al., 2000). At the time, analysis of this structure showed a potential binding location and orientation within the active site. However, this binding location and orientation was different to what was observed in the PP$_{IX}$ bound structure of *H. sapiens* (Medlock et al., 2009). This suggested that N-MeMP binding in *B. subtilis* HemH may not represent the actual binding location and orientation for the porphyrin molecule. Despite this, the crystal structures are still useful for further investigation into CpFCs. To date, *B. subtilis* HemH is the most structurally investigated CpFC with 16 deposited structures (Lecerof et al., 2000, Lecerof et al., 2003, Hansson et al., 2010, Karlberg et al., 2008, Hansson et al., 2007, Shipovskov et al., 2005). There is only one other CpFC structure deposited, this is the apoprotein structure of *Bacillus anthracis* HemH (PDB ID: 2C8J, paper not published).

Table 6.1 Crystal structures of *B. subtilis* ferrochelatase

PDB ID	DESCRIPTION	AUTHORS
3M4Z	Co2+ bound in the active site	Hansson et al., 2010
3GOQ	Y13M mutant	Karlberg et al., 2010
2Q2O	H183C mutant with deuteroporphyrin IX 2,4-disulfonic acid dihydrochloride bound	Karlberg et al., 2008
2Q2N	In a complex with deuteroporphyrin IX 2,4-disulfonic acid dihydrochloride bound	Karlberg et al., 2008
2Q3J	H183A mutant with N-Methyl mesoporphyrin	Karlberg et al., 2008
2H1V	K87A mutant	Hansson et al., 2007
2H1W	H183A mutant	Hansson et al., 2007
2HK6	Fe2+ bound in the active site	Hansson et al., 2007
2AC2	Y13F mutant with Zn2+ bound in the active site	Shipovskov et al.,2005
2AC4	H183C mutant	Shipovskov et al.,2005
1N0I	Cd2+ bound in the active site	Lecerof et al., 2003
1LD3	Zn2+ bound at the active site	Lecerof et al., 2003
1C9E	Cu2+ N-methyl mesoporphyrin bound	Lecerof et al., 2003
1C1H	N-methyl mesoporphyrin bound	Lecerof et al., 2003
1DOZ	Apoprotein structure	Lecerof et al., 2000
1AK1	Apoprotein structure	Al-Karadaghi et al., 1997

The discovery of the coproporphyrin-dependent pathway also meant that HemQ (ChDC), the final enzyme in the pathway, was annotated as a decarboxylase instead of a chlorite dismutase. Prior to the discovery of the new pathway there was very little published information about HemQ. However, much more information is now available, most likely because of its high potential as a therapeutic target (Hofbauer et al., 2016a, Hofbauer et al., 2015, Hofbauer et al., 2016b, Hofbauer et al., 2016c, Celis et al., 2015, Streit et al., 2016, Dailey and Gerdes, 2015, Dailey et al., 2015, Dailey et al., 2010). One recent publication includes the first crystal structure of HemQ from *L. monocytogenes* (PDB ID: 5LOQ), bound to its substrate coproheme (Hofbauer et al., 2016c). HemQ is of interest in conjunction with HemH as in *P. acnes* they are fused together, this could indicate that the proteins may interact and shuttle substrates from one active site directly to the other.

6.1. Expression and purification of HemH and HemQ from different species to determine interaction between two consecutive enzymes in the coproporphyrin-dependent heme biosynthetic pathway

In the first results chapter we explored three different hypotheses, the first was whether the HemH and HemQ from the species *P. acnes* form a complex. To test this hypothesis, truncations of the *P. acnes* HemH-Q fusion protein were produced. The SEC trace showed formation of a complex between HemHL and HemQS. This complex was 1:1. The formation of the complex showed a strong interaction between the two proteins.

The second hypothesis questioned the substrate transfer mechanism between the two proteins. To answer this question the full-length fusion protein was required. Attempts were made to purify the full-length protein however; the protein degraded when concentrated. Further optimisation of the expression and purification of HemHQ could be completed.

To start the expression of the protein could be changed. The expression levels for HemH-Q were reasonable but use of a different expression system (e.g. insect cells) or expression conditions (temperature, media, cell line, addition of additives, presence of chaperones) may have stabilised the protein during expression and prevent the cleavage observed. The cell lysis procedure could be optimised, the power level of the sonicator could be reduced thereby reducing the chance of protein cleavage. The cell lysis method could be altered to lysozyme, a gentle method of lysis.

During the purification of the addition of different stabilising chemicals or proteins could reduce protein degradation. The purification buffers could be altered so that they promote stability of the protein. This could involve an addition of detergent or glycerol, change of pH, increased salt concentration or using a different buffer base (e.g. MOPS or HEPES). However, changing the buffer composition could alter the kinetic behaviour of the enzyme and as a result any potential substrate transfer assays. Additionally, pull down studies could be completed to identify a binding partner that is required for stabilisation. Tryptic digest and mass spectrometry of the degradation product has identified the area where cleavage occurs in the full-length fusion protein, this could be mutated to prevent degradation however, this could result in misfolding protein and the exact site of cleavage is unknown. There is limited literature on the

purification of the full-length *P. acnes* HemH-Q protein. One publication mentions a purification but notes that cleavage products were observed when analysed by SDS-PAGE (Dailey et al., 2010).

The final part of the chapter investigates complex formation between *S. aureus* HemH and HemQ. These two enzymes are not covalently linked unlike the *P. acnes* HemH-Q fusion protein. Protein-protein interactions were also tested across species of Gram-positive bacteria (*S. aureus*, *P. acnes* and *B. subtilis*) using SEC. SEC of *S. aureus* HemH and HemQ showed no interaction occurring between the two proteins and no interaction was observed when cross species combinations of HemH and HemQ species were used.

SEC relies on strong protein-protein interactions between the two proteins. If the interactions are weak or transient, then SEC would show that the proteins do not interact. As only one method was used to determine protein-protein interactions between the HemH and HemQ other methods could probe protein-protein interactions. We have shown that any protein-protein interactions occurring between *S. aureus* HemH and HemQ and cross species HemH and HemQ are not strong enough to be observed using SEC.

Coimmunoprecipitation or pulldown assays can also determine whether proteins interact with each other, these require an antibody specific to one protein or an affinity tag on one protein. As all HemH and HemQ proteins contained his-tags, a nickel resin could be used for pulldown assays, but the his-tag would need to be cleaved or engineered out of one of the protein constructs. Other techniques that probe protein-

protein interactions include surface plasmon resonance, analytical ultracentrifugation, atomic force microscopy, microscale thermophoresis and co-crystallisation. Surface plasmon resonance is frequently used in industry to determine association and dissociation constants of the protein-protein interaction. These techniques may be able to differentiate between weak interactions and no interaction. But as the hypothesis was that HemH and HemQ form a tight long-lived complex with obligatory substrate transfer, SEC is more than adequate to demonstrate that this doesn't take place.

6.2. Investigating the kinetic properties of *B. subtilis* and *S. aureus* HemH

The second results chapter demonstrates the kinetic behaviour of two CpFCs, *B. subtilis* and *S. aureus* HemH when assayed with their endogenous substrate. Both ferrochelatases have not been fully characterised kinetically with the correct substrate CP_{III}. As stated before very little available literature has described the kinetics of either ferrochelatase. In this chapter we have demonstrated the CpFCs are more active than previously described.

Steps within the mechanism were isolated and examined separately using stopped flow fluorescence spectroscopy and scanning kinetics. Rates of CP_{III} binding were calculated using stopped flow fluorescence spectroscopy. This technique revealed that CP_{III} binding was a two-step mechanism, initial binding followed by an isomerisation. The initial binding constants and rates of isomerisation are different in both proteins. *B. subtilis* HemH exhibits a tighter initial binding and a slower isomerisation rate compared to the *S. aureus* HemH.

The metal binding constant and iron chelation rate constant for the ferrochelatase reaction was isolated and investigated using stopped flow fluorescence spectroscopy. CP_{III} binds tightly to ferrochelatase and CP_{III} in an enzyme-substrate complex has different spectral properties when compared to unbound CP_{III}. This meant that the enzyme-substrate complex could be assembled before exposure to iron and enzymatic steps subsequent to CP_{III} binding could be assessed. This experiment was completed using *B. subtilis* HemH and not in *S. aureus* HemH. The results of these experiment showed two observable kinetic steps that have been attributed to iron binding and metal chelation. The rates of iron chelation were previously assumed to be very fast (Hoggins et al., 2007) and so could not be accurately determined using stopped flow fluorescence spectroscopy. The experiments shown in this chapter show that iron chelation is not as fast as predicted and can be estimated using stopped flow fluorescence. In fact, the estimate k_{chel} values are actually slower than the estimated k_{iso} constants for the ferrochelatase reactions.

Finally, the third stopped flow fluorescence experimental design considered all steps prior to the rate determining step in the mechanism of ferrochelatase. The substrates were exposed to the ferrochelatase simultaneously. The rate determining step is thought to be product release and the work here shows that this is likely to be the case. We have shown that the CP_{III} binding, enzyme/porphyrin isomerisation, iron binding and metal chelation stages are not rate determining. This experimental design ensured that the previous two experiments (CP_{III} binding and iron binding and porphyrin metalation) were consistent with each other. As the iron binding and porphyrin metalation experiment was not completed using *S. aureus* HemH equation 4B (single

exponential + linear phase) was fitted to the raw data of the third experiment. A double exponential equation (equation 4C) was not fitted to this data as accurate estimates of the second rate constant could not be obtained without data from the second experiment. Completing the iron binding and porphyrin metalation experiment on *S. aureus* would provide the information needed to check for consistency. The main caveat for this experiment is producing enough pure protein and protein yields were low and large scale up during protein expression would be required. The k_{burst} constant for *S. aureus* HemH was estimated at 30 s^{-1} this is the combined rate constant of k_{iso} *and* k_{chel} indicating that k_{chel} could be much slower.

Using stopped flow fluorescence spectroscopy, we have shown that there are four observable steps in the ferrochelatase mechanism. The three experiments isolate particular steps and are consistent with each other. We can confirm that product release is most likely to be rate determining and metal chelation is slow enough to be observed by stopped flow fluorescence spectroscopy. This information would not have been gained using simple steady-state kinetics and can be used to compare the potency of inhibitors in rational drug design. Co-crystallisation of the different CpFCs with their endogenous porphyrin substrate CP$_{III}$ could reveal interactions between CP$_{III}$ and ferrochelatase that could also aid drug design.

6.3. Defining the role of active site residues in the function of the *B. subtilis* HemH enzymatic mechanism

The final results chapter assesses the activity of mutants of the *B. subtilis* ferrochelatase. These proteins contain mutations in important active site residues. Two of the mutants contain changes to residues in the non-conserved face of the

active site whereas the other three mutants have mutations in the conserved face of the active site. In *B. subtilis* HemH the important residues in the conserved active site face are completely conserved in all ferrochelatases, H183 and E264 (*B. subtilis* numbering). The two mutants from the non-conserved active site face were K87A and H88A (in *B. subtilis* HemH). These residues are an arginine and tyrosine in the *H. sapiens* HemH but remain the same in *S. aureus* HemH. There has been a large debate as to which residues are involved in iron binding and porphyrin metalation. All the residues mutated (K87, H88, H183 and E264) have been implicated in iron binding and porphyrin metalation.

The mutant proteins were kinetically characterised using the same experiments used to characterise the wildtype ferrochelatase proteins. Fluorescence spectroscopy showed that despite the lack of activity observed in three of the mutants, all four mutants were capable of binding CP_{III}.

Using stopped flow fluorescence spectroscopy, we have shown that the rates and binding constants for CP_{III} binding in the mutants vary when compared to wildtype. We have shown that even though all of the mutants are all capable of binding their porphyrin substrate, they interact with CP_{III} differently and as a result this can alter the environment of the bound porphyrin and the spectral properties of the CP_{III}.

When the iron binding and porphyrin metalation ability was tested in each of the mutant proteins, we have shown that the H88A mutant was the only one able to bind iron and metalate on a time scale observable by stopped flow spectroscopy. The K87A and

E264A mutants were only able to bind iron and metalate CP$_{III}$ very slowly whereas the E264Q mutant was completely inactive after CP$_{III}$ binding.

Finally, the H88A mutant protein was assessed using the third and final stopped flow fluorescence experiment. This estimated the rate constants for the step in the ferrochelatase mechanism prior to the rate determining step. We have shown that in the H88A mutant it is likely that product release remains the rate determining step as CP$_{III}$ binding, enzyme/porphyrin isomerisation, iron binding and porphyrin metalation are all faster than the estimated k_{cat} value gained in the steady-state kinetics. The rate constants gained from the previous two stopped flow fluorescence experiments using the H88A mutant protein were fitted to the raw data gained from the third experiment using a double exponential curve (equation 4C). This showed that all three experiments are consistent with each other.

Investigation into the *B. subtilis* ferrochelatase active site mutant proteins originating from the conserved and non-conserved face of the ferrochelatase active site cannot provide evidence that specifically supports one of the hypotheses for iron binding and porphyrin metalation. What has been shown is that all mutants bind their first substrate. K87A, E264A and E264Q bind their substrate tightly and H88A binds CP$_{III}$ weakly. Three of the mutants are capable of iron binding and porphyrin metalation. The H88A mutant can bind iron and metalate porphyrin more effectively compared to wildtype whereas iron binding and porphyrin metalation in the mutant proteins K87A and E264A has been severely affected by mutation. The E264Q protein is incapable of binding iron and metalating porphyrin and this is the major difference observed between the E264A and E264Q mutants. In the K87A and E264A mutants iron binding and

porphyrin metalation may have become rate determining however this is difficult to determine with the data provided.

Using several different techniques, we have shown how steady-state kinetics are not substantial enough for kinetic characterisation of an enzyme. Steady-state kinetics do not provide a complete picture of the enzyme mechanism and the steps that are affected by mutation. If activity assays and steady-state kinetic were performed to characterise the H88A mutant, then it would seem as though the enzyme mechanism was not affected by mutation at His88. Stopped flow fluorescence and rapid scanning kinetics has shown that the mutation of H88 to an alanine has changed the ferrochelatase mechanism substantially and several steps have been affected.

Investigating specific the role of specific active site residues could indicate important reaction surfaces that could aid drug design in the absence of crystal structures. Co-crystallisation of the mutants with CP_{III} and apoprotein structures could provide more visual information on the interactions occurring in the active site and changes that occur when porphyrin is bound. Attempts were made to produce these structures but this beared no fruit, there are currently structures of apo-K87A (PDB ID: 2H1V) and apo-H183A (PDB ID: 2H1W) deposited in the PDB (Hansson et al., 2007).

6.4. Future work

We have demonstrated that there are interactions between *P. acnes* HemH and HemQ truncations and these interactions should be investigated further. The HemH-Q complex and the interaction interface between the two proteins could be investigated structurally using techniques such as X-ray crystallography, SAXS (small-angle X-ray

scattering), SEC-MALS (size exclusion multiple angle light scattering) and AUC (analytical ultracentrifugation). MST (microscale thermophoresis), AFM (atomic force microscopy) and SPR (surface plasmon resonance) could also deduce binding constants for this interaction. Substrate transfer assays could be developed to assess the movement of the substrate from one protein to the next and in the *P. acnes* and *S. aureus* species. Further attempts could be made to purify the full-length *P. acnes* HemH-Q protein so that it could be used in the substrate transfer assays instead. However, the protein may need fluorescent tagging if coproheme is not spectroscopically distinct.

With regard to the determining protein-protein interactions between *S. aureus* HemH and HemQ and the cross-species combinations, we have shown that they do not interact when tested using SEC. Other techniques probing protein-protein interactions are required. These techniques could be used to check consistency with the SEC results and perhaps determine whether weaker interactions occur between HemH and HemQ. Probing protein-protein interactions between HemH and HemQ in the presence of CP_{III} would be worth investigating as HemH is known to undergo an isomerisation when binding CP_{III}, this could reveal an interaction surface for HemQ.

In the second results chapter we have kinetically characterised two CpFCs (*B. subtilis* and *S. aureus*) using several different techniques and experimental designs. Iron binding and porphyrin metalation kinetics were not completed in *S. aureus* HemH. These kinetics are required to compare both ferrochelatases completely. After complete characterisation using the endogenous substrates the metal and porphyrin

substrates can be altered. The metal ions such as Zn^{2+}, Co^{2+}, Ni^{2+} or Cu^{2+} could be tested to determine differences in the behaviour of the enzyme. A combination of different porphyrin molecules could also be assayed. This collection of porphyrins could include analogues related to protoporphyrin IX and coproporphyrin III and the techniques described in this thesis could help the production of inhibitors specific to CpFCs. pH-dependent kinetics and isotopic kinetics could be used in combination with the different metals to gain more mechanistic information about metal entry (into the active site), metal binding and porphyrin metalation.

In the third results chapter, we have shown that both sides of the *B. subtilis* ferrochelatase active site are important in the function of the enzyme. We targeted residues from each of the active site faces and investigated their role in the enzymatic mechanism. All of the residues were mutated to alanine (K87A, H88A, H183A and E264A) and E264 was also mutated to a glutamine. As K87A, E264A and E264Q were very inactive these residues could be mutated to other amino acids that are more conservative, for an example E264 could be mutated to aspartate and K87 could be mutated to an arginine instead. These mutations could result in substantially higher ferrochelatase activity allowing more information to be gained from them. H88A was the most active mutant and more experiments could be used to determine the role of H88 in the enzymatic mechanism. Other residues in the active site could also be mutated to define their importance in ferrochelatase.

To investigate the roles of the H88A mutant further, pH-dependent kinetics or isotopic kinetics could be performed alongside the wildtype ferrochelatase. Each of the active

site residues have different pK_a values this means that changing the active site pH can change the protonation state of each of the residues independently. The protonation state of some residues will not change (pH independent) but others will be pH-dependent. Proton abstraction of the porphyrin pyrrole groups and iron entry and binding is essential in the ferrochelatase mechanism. If particular residues are protonated/deprotonated this could give an insight to residues important in these parts of the mechanism. Fine tuning the pH could lead to different protonation/deprotonation patterns and therefore different enzymatic activity. This could identify residues specifically involved in iron entry and binding and proton abstraction. Equally isotopic kinetics could identify residues that readily exchange their protons, this could also help identify pathways for metal entry and proton abstraction. Whilst the iron binding and porphyrin metalation transient kinetics has shown that there is a difference between the wildtype protein and the H88A mutant with regard to iron binding and porphyrin metalation, we cannot say conclusively that this is because iron utilises the non-conserved face of the active site to enter the active site and H88 makes up part of the final iron binding site prior to insertion. pH-dependent kinetics may be able to determine whether the H88A mutant is important in iron binding prior to insertion or proton abstraction.

In this thesis, we have shown a deep kinetic investigation into two CpFCs (*B. subtilis* and *S. aureus*) and several active site mutants of the *B. subtilis* ferrochelatase. This type of kinetic investigation has not been completed on any ferrochelatase before and provides substantial mechanistic information on the ferrochelatase reaction. In addition to this kinetic investigation, co-crystallisation of *B. subtilis* ferrochelatase (wildtype and mutants) with CP_{III} has been attempted to supplement this kinetic data.

Finally, protein-protein interactions between HemH and HemQ have been investigated in Gram positive bacteria (*P. acnes*, *B. subtilis* and *S. aureus*) to explore a potential substrate transfer mechanism. Gaining more data about the CpFCs and their interaction partners will aid the development of novel antibiotics targeting the coproporphyrin-dependent heme biosynthesis pathway found with Gram positive bacteria (Actinobacteria and Firmicutes).

7. Appendix

7.1. Structural alignments to determine domain boundaries of *P. acnes* HemHQ

7.1.1. P. acnes *HemH PRALINE output*

Red indicates alpha helical structure, blue indicates beta sheet structure

```
                    . . . . . . . . . . 10. . . . . . . . . 20. . . . . . . . . 30. . . . . . . . . 40. . . . . . . . . 50
(PRED) P__acnes     ---------- ---------- ---------- --------M TANFYAAF--
(PRED) H_Sapien     MRSLGANMAA ALRAAGVLLR DPLASSSWRV CQPWRWKSCA AAAAVTTETA
(PRED) S_cerevisiae ---------- -------MLS RTIRTQCSFL RRS----QLT ITRSFSVT--
(PRED) B_subtilis   ---------- ---------- ---------- ---------- ----------
(PRED) S_aureus     ---------- ---------- ---------- ---------- ----------
(PRED) E_coli       ---------- ---------- ---------- ---------- ----------

                    . . . . . . . . . . 60. . . . . . . . . 70. . . . . . . . . 80. . . . . . . . . 90. . . . . . . . . 100
(PRED) P__acnes     ---------- -TDPLAPYSA VLVVSFGGPR --SPEEVMPF LRRV------
(PRED) H_Sapien     QHAQCAKPQV QPQKRKPKTC ILMLNMGGPE --TLCDVHDF LLRLFLDRDL
(PRED) S_cerevisiae -------FNM QNAQKRSPTG IVLMNMGGPS --KVEETYDF LYQLFADNDL
(PRED) B_subtilis   ---------- ---MSRKKMG LLVMAYGTPY --KEEDIERY YTHIR-----
(PRED) S_aureus     ---------- ---M-TKKMG LLVMAYGTPY --KESDIEPY YTDIR-----
(PRED) E_coli       ---------- ---MRQTKTG ILLANLGTPD APTPEAVKRY LKQFLSDRRV

                    . . . . . . . . . . 110. . . . . . . . 120. . . . . . . . 130. . . . . . . . 140. . . . . . . . 150
(PRED) P__acnes     ---------- -SHGRIPEER LADVARHYDR FG--GVSPIN DATDVFVNAI
(PRED) H_Sapien     MTL-F--IQN KLAPFIAKRR TPKIQEQYRR IG--GGSPIK IWTSKQGEGM
(PRED) S_cerevisiae IPI-SAKYQK TIAKYIAKFR TPKIEKQYRE IG--GGSPIR KWSRYQATEV
(PRED) B_subtilis   ---------- -RGRKPEPEM LQDLKDRAHL IG--GISPLA QITEQQAHNL
(PRED) S_aureus     ---------- -HCKRPSEEK LQDLKDRYEF IG--GLSPLA GTTDDQADAL
(PRED) E_coli       VDTSRLLWWP LLRGVILPLR SPRVAKLYAS VWMEGGSPLM VYSRQQQQAL

                    . . . . . . . . . . 160. . . . . . . . 170. . . . . . . . 180. . . . . . . . 190. . . . . . . . 200
(PRED) P__acnes     CNELRRHG-- -VRVPVLLGN RNGTPFLEEA LTDMHAHCVR RVLAVVTSAY
(PRED) H_Sapien     VKLLDELSPN TAPHKYYIGF SYVHPLTEEA IEEMERDGLE RAIAFTQYFQ
(PRED) S_cerevisiae CKILDKTCPE TAPHKPYVAF RYAKPLTAET YKQMLKDGVK KAVAFSQYPH
(PRED) B_subtilis   EQHLNEIQDE -ITFKAYIGL KHIEPFIEDA VAEMHKDGIT EAVSIVLAPH
(PRED) S_aureus     VSALNKAYAD -VEFKLYLGL KHISPFIEDA VEQMHNDGIT EAITVVLAPH
(PRED) E_coli       AQRLPEM--- ----PVALGM SYGSPSLESA VDELLAEHVD HIVVLPLYPQ

                    . . . . . . . . . . 210. . . . . . . . 220. . . . . . . . 230. . . . . . . . 240. . . . . . . . 250
(PRED) P__acnes     ASYSCCRQYR EEIATALAHA G-ITDMQVDK VPPFNEAPGF IRANAEALMQ
(PRED) H_Sapien     YSCSTTCGSSL NAIYRYYNQV CRKPTMKWST IDRWPTHHLL IQCFADHILK
(PRED) S_cerevisiae FSYSTTGSSI NELWRQIKAL DSERSIWWSV IDRWPTNECL IKAFSENITK
(PRED) B_subtilis   FSTFSVQSYN KRAKEEAEKL G---GLTITS VESWYDEPKF VTEWVDRVKE
(PRED) S_aureus     YSSFSVGSYD KRADEEAAKY ----GIQLTH VKHYYEQPKF IEYWTNKVHE
(PRED) E_coli       FSCSTVGAVM DELARILARK R--SIPGISF IRDYADNHDY INALANSVRA

                    . . . . . . . . . . 260. . . . . . . . 270. . . . . . . . 280. . . . . . . . 290. . . . . . . . 300
(PRED) P__acnes     AFMHIPPTPL EATRVVFVTH SIPDSMQDAS GAGQPGTDYI SQHKAVCERV
(PRED) H_Sapien     ELDHFPLEKR SEYVILFSAH SLPMSVVNR- ------GDPY P QEVSATVQKV
(PRED) S_cerevisiae KLQKFPQPVR DKVVLLFSAH SLPMDVVNT- ------GDAYP AEVAATVINI
(PRED) B_subtilis   TYASMPEDER ENAMLIVSAH SLPEKIKEF- ------GDPYP DQLEESAKLI
(PRED) S_aureus     TLAQIPEEEH KDTVLVVSAH SLPKGLIEKN ------NDPYP QELEHTALLI
(PRED) E_coli       SFAE----HG EPDLLLLSYH GIPQRYADE- ------GDDYP QRCRTTTREL

                    . . . . . . . . . . 310. . . . . . . . 320. . . . . . . . 330. . . . . . . . 340. . . . . . . . 350
(PRED) P__acnes     AGQVRQVFGN M-PQWDLAYC SRSGRPSDPW LEPDIIDHLR SLPEQ-GVQS
(PRED) H_Sapien     M----EHLEY C-NPYRLVWQ SKVG--PMPW LGPQTDESIK GLCER-GRKN
(PRED) S_cerevisiae M----QKLKF K-NPYRLVWQ SQVG--FKPW LGAQTAEIAE FLGF--KVDG
(PRED) B_subtilis   A----EGACV --SEYAVGWQ SEGNT-PDPW LGPDVQDLTR DLFEQKGYQA
(PRED) S_aureus     K----EQSNI --EHIAIGWQ SEGNT-GTPW LGPDVQDLTR DLYEKHQYKN
(PRED) E_coli       A----SALGM APEKVMMTFQ SRFG--REPW LMPYTDETLK MLGEK-GVGH

                    . . . . . . . . . . 360. . . . . . . . 370. . . . . . . . 380. . . . . . . . 390. . . . . . . . 400
(PRED) P__acnes     VVVAPIGFVA DHMEVVNDLD YEAAE-AAKE SGL-AFTRAA TAGTEHAFIA
(PRED) H_Sapien     ILLVPIAFTS DHIETLYELD IEYSQVLAKE CCVENIRRAE SLNGNPLFSK
(PRED) S_cerevisiae LMFIPIAFTS DHIETLHEID LGV---IGES EYKDKFKRCE SLNGNQTFIE
(PRED) B_subtilis   FVYWPVGFVA DHLEVLYDND YECKV-VTDD ICA-SYYRPE MPNAKPEFID
(PRED) S_aureus     FIYTPVGFVC EHLEVLYDND YECKV-VCDD IGA-NYYRPK MPNTEPLFIG
(PRED) E_coli       IQVMPGFAA DCLETLEEIA EQNRE-VFLG AGGKKYEYIP ALNATPEHIE

                    . . . . . . . . . . 410. . . . . . . . 420. . . . . . . . 430. . . . . . . . 440. . . . . . . . 450
(PRED) P__acnes     DLAGLILSQA AAARGEGCNL TSWPAPC-VA GCCRRYPDAQ DIPAVSGGDV
(PRED) H_Sapien     ALADLVHSHI QSNELCSKQL TLSCPLC-VN PVCRETK--S FFTSQQL---
(PRED) S_cerevisiae CMADLVKSHL QSNQLYSNQL PLDFALGKSN DPVKDLS--L VFGNHEST--
(PRED) B_subtilis   ALATVVLKKL GR-------- ---------- ---------- ----------
(PRED) S_aureus     AIVDEIKSIF ---------- ---------- ---------- ----------
(PRED) E_coli       MMANLVAAYR ---------- ---------- ---------- ----------
```

7.1.2.P. acnes *HemQ PRALINE output*

Red indicates alpha helical structure, blue indicates beta sheet structure. *P. acnes*

HemQ was start at residue 326.

```
                ..........10 ..........20 ..........30 ..........40 ..........50
(PRED) S_aureus_HemQ   ----------  ----------  ----------  ----------  ----------
(PRED) _B__subtilis_He ----------  ----------  ----------  ----------  ----------
(PRED) L__monocytogene ----------  ----------  ----------  ----------  ----------
(PRED) P__acnes_HemQ   SQAAAARGEG  GNLTSWPAPC  VAGCCRRYPD  AQDIPAVSGG  DVESVAAGAD

                ..........60 ..........70 ..........80 ..........90 ..........100
(PRED) S_aureus_HemQ   ----------  ----------  ----------  ----------  ----------
(PRED) _B__subtilis_He ----------  ----------  ----------  ----------  ----------
(PRED) L__monocytogene ----------  ----------  ----------  ----------  ----------
(PRED) P__acnes_HemQ   VVDAEPGGVD  FVPSGSASAV  DRPGPEAVEL  ETPPSPYNPL  TKETPMSDHS

                ..........110..........120..........130..........140..........150
(PRED) S_aureus_HemQ   ----------  ----------  ----------  MSQAAETLDG  WYSLHLFYAV
(PRED) _B__subtilis_He ----------  ----------  ----MSEQQM  TNEAAKTLDG  WYALHDFRTM
(PRED) L__monocytogene ----------  ----------  ----------  MNEAVKTLDG  WFCLHDFRSI
(PRED) P__acnes_HemQ   SADSVIEGPR  DDEVPAGSYT  APTDPRDTPV  IPEEVNASSK  WAMYSVFRVA

                ..........160..........170..........180..........190..........200
(PRED) S_aureus_HemQ   DWASLRLVPK  DERDALVTEF  QSFLENTATV  RSSKSGDQAI  YNITGQK--A
(PRED) _B__subtilis_He DWASWKLLSS  DERQSIIHEF  TGLLEKWGVA  QKEGKGSQTL  YSIVGQK--A
(PRED) L__monocytogene DWAAWRELNP  GNQELMLNEL  SHFLSDMEIT  KNIGEGEHTI  YSILGQK--A
(PRED) P__acnes_HemQ   TALPAE---D  DERRRLVEGS  DEWAGQ----  --SGVDTRGW  YDLSGLRANA

                ..........210..........220..........230..........240..........250
(PRED) S_aureus_HemQ   DLLLWFLRPE  MKSLNHIENE  FNKLRIADFL  IPTYSYVSVI  ELSNYLAG--
(PRED) _B__subtilis_He DFMLMILRPT  MEELNQIELE  FNKSRLAEFT  IPAYSYVSVV  ELSNYLAS--
(PRED) L__monocytogene DLVFFTLRDS  LEALNEVENR  FNKLAIADYL  LPTYSYISVV  ELSNYLASHM
(PRED) P__acnes_HemQ   DLLVWWVSDD  PAVLQDAYHR  FRASGLGRHL  EPVWSNVGVH  RPA-------

                ..........260..........270..........280..........290..........300
(PRED) S_aureus_HemQ   KSDEDPYENP  HIKARLYPEL  PHSDYICFYP  MNKRRNETYN  WYMLTMEERQ
(PRED) _B__subtilis_He -GDGDPYENP  HVRARLYPEL  PESKYVCFYP  MDKRRSGNDN  WYMLSMEERR
(PRED) L__monocytogene AGGDDPYQNK  GVRARLYPAL  PPKKHICFYP  MSKKRDGADN  WYMLPMEERQ
(PRED) P__acnes_HemQ   -----EFNKS  HLPSCF-AGI  APRRWAAFYP  FIRSK----E  WYLLPAADRS

                ..........310..........320..........330..........340..........350
(PRED) S_aureus_HemQ   KLMYDHGMIG  RKYAGKIKQF  ITGSVGFDDF  EWGVTLFSDD  VLQFKKIVYE
(PRED) _B__subtilis_He NLMRSHGLIG  RSYAGKVKQI  ITGSVGFDDY  EWGVTLFSDD  VLQFKKLVYE
(PRED) L__monocytogene QLIRDHGLIG  RSYAGKVQQI  IGGSIGFDDY  EWGVTLFSDD  ALEFKRIVTE
(PRED) P__acnes_HemQ   RMLREHGIVG  AASS-DVKAS  TLAAFALGDY  EWILALEGDD  LARIVDVMKD

                ..........360..........370..........380
(PRED) S_aureus_HemQ   MRFDETTARY  GEFGSFFVGH  IIN-TNEFDQ  FFAIS
(PRED) _B__subtilis_He MRFDEVSARY  GEFGSFFVGN  HLS-LDTLPQ  FLYV-
(PRED) L__monocytogene MRFDEASARY  AEFGSFFIGN  LLL-SEQLSK  LFTI-
(PRED) P__acnes_HemQ   LRYVEARRYV  DVDTPFFTGE  RVSPVVWADR  QMRA-
```

7.2. Plasmid and sequence information for constructs

7.2.1. P. acnes *HemHQ constructs*

7.2.1.1. *P. acnes HemHQ truncations*

P. acnes HemHL (2-459)

Amino acid sequence

MGGSHHHHHHGMASTANPYAAPTDPLAPYSAVLVVSFGGPRSPEEVMPFLRRVS
HGRIPEERLADVARHYDRFGGVSPINDATDVFVNAIGNELRRHGVRVPVLLGNRNG
TPFLEEALTDMHAHGVRRVLAVVTSAYASYSGCRQYREEIATALAHAGITDMQVDK
VPPFNEAPGFIRANAEALMQAFMRIPPTPLEATRVVFVTHSIPDSMQDASGAGQPG
TDYISQHKAVCERVAGQVRQVFGNMPQWDLAYCSRSGRPSDPWLEPDIIDHLRSL
PEQGVQSVVVAPIGFVADHMEVVNDLDYEAAEAAKESGLAFTRAATAGTHSAFIAD
LAGLILSQAAAARGEGGNLTSWPAPCVAGCCRRYPDAQDIPAVSGGDVESVAAGA
DVVDAEPGGVDFVPSGSASAVDRPGPEAVELETPPSPYNPLTKETPMSDHSSADS
VIEGPRDDEVPAGSYTAPTDPRDTPVI

Analysis	Entire protein
Length	470 aa
Molecular Weight	49846.08
Molar extinction coefficient	33150
Isoelectric point	4.99
1 microgram =	20.062 pMol

DNA sequence

ATGGGGGGTTCTCATCATCATCATCATCATGGTATGGCTAGCACCGCTAATCCC
TACGCTGCTCCCACGGACCCGTTGGCCCCTTATAGCGCCGTGCTTGTCGTTTC
TTTTGGCGGTCCGCGTTCCCCTGAAGAGGTCATGCCTTTTCTGAGAAGGGTCT
CCCACGGTCGCATTCCTGAAGAACGCTTGGCTGATGTCGCCCGACACTATGAC
CGTTTCGGCGGTGTCAGCCCGATTAACGATGCGACGGACGTTTTCGTCAACGC
GATTGGGAATGAACTGCGCCGTCACGGAGTACGAGTTCCAGTGCTGTTAGGGA
ACCGCAACGGCACCCCCTTCCTTGAGGAAGCGCTGACTGACATGCACGCGCAC
GGGGTGCGTCGGGTGTTAGCGGTTGTCACCTCTGCCTACGCCAGTTACTCCGG
GTGCCGTCAGTATCGCGAGGAGATCGCGACTGCCCTGGCTCACGCCGGTATC
ACCGATATGCAGGTCGACAAGGTACCTCCCTTTAACGAGGCGCCGGGATTCAT
TCGCGCTAACGCGGAAGCTCTGATGCAGGCGTTTATGCGGATCCCGCCTACTC

CTCTTGAGGCTACCCGCGTCGTTTTCGTCACTCACTCCATCCCTGACTCTATGC
AGGACGCATCTGGCGCTGGGCAGCCGGGGACGGATTACATTTCTCAGCACAA
GGCGGTTTGTGAGAGGGTCGCTGGTCAGGTGCGCCAGGTCTTCGGGAATATG
CCGCAGTGGGACTTGGCCTATTGCTCGAGGTCGGGGCGACCCAGCGACCCGT
GGCTTGAACCGGACATTATCGATCACCTCCGCAGTCTTCCCGAACAGGGCGTG
CAATCTGTTGTCGTCGCTCCAATTGGCTTCGTTGCTGACCACATGGAGGTCGTT
AATGACCTTGATTACGAGGCCGCCGAGGCAGCTAAGGAGTCCGGGCTCGCCTT
CACGCGGGCGGCGACCGCTGGTACCCATTCCGCCTTTATCGCTGATCTCGCCG
GGCTCATCTTGTCCCAGGCCGCGGCGGCTCGTGGTGAGGGTGGCAATCTAAC
GTCGTGGCCGGCTCCTTGCGTCGCCGGTTGTTGCCGACGCTACCCGGACGCT
CAGGACATTCCAGCCGTCTCCGGTGGTGATGTCGAGTCCGTAGCTGCCGGTGC
CGATGTAGTCGATGCTGAACCAGGAGGTGTGGATTTTGTGCCAAGCGGCTCAG
CGAGTGCAGTCGATCGCCCGGGGCCAGAGGCGGTCGAACTGGAGACTCCTCC
TTCCCCCTACAACCCGTTGACTAAGGAGACCCCCATGTCTGATCATTCGAGTGC
TGATTCGGTGATTGAGGGACCACGCGACGACGAAGTTCCCGCCGGCTCCTACA
CCGCACCGACCGATCCCCGCGATACCCCGGTCATTAAGCTTGGCTGTTTTGGC
GGATGAGAGAAGATTTTCAGCCTGATACAGATTAAATCAGAACGCAGAAGCGGT
CTGATAAAACAGAATTTGCCTGGCGGCAGTAGCGCGGTGGTCCCACCTGACCC
CATGCCGAACTCAGAAGTG

Plasmid Map

pTrcHisA-P.acnes-HemHL(1-459)
5822 bp

lacO
trc
T7 translational enhancer
RBS
lacI
mini cistron
6X His
P. acnes HemHL
pBR322
Ampicillin resistance
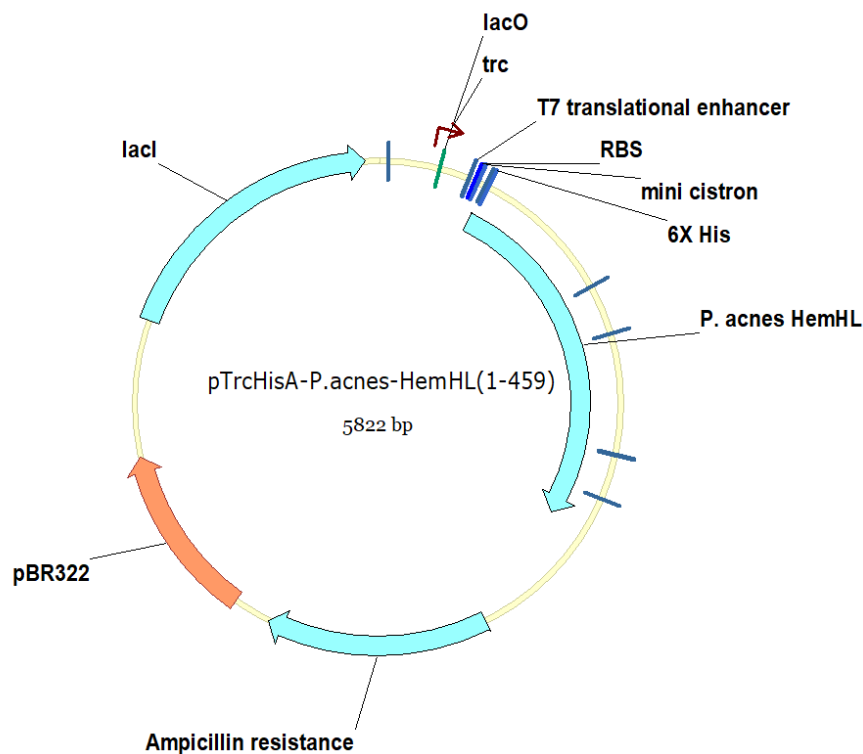
P. acnes HemQS (478-683)

Amino acid sequence

MGGSHHHHHHGMASEEVNASSKWAMYSVFRVATALPAEDDERRRLVEGSDEWA
GQSGVDTRGWYDLSGLRANADLLVWWVSDDPAVLQDAYHRFRASGLGRHLEPV
WSNVGVHRPAEFNKSHLPSCFAGIAPRRWAAFYPFIRSKEWYLLPAADRSRMLRE
HGIVGAASSDVKASTLAAFALGDYEWILALEGDDLARIVDVMKDLRYVEARRYVDV
DTPFFTGERVSPVVWADRQMRA

Analysis	Entire protein
Length	239 aa
Molecular Weight	27006.32
Molar extinction coefficient	67260
Isoelectric point	6.12
1 microgram =	37.028 pMol

DNA

ATGGGGGGGTTCTCATCATCATCATCATCATGGTATGGCTAGCGAGGAGGTCAA
CGCCTCCAGCAAGTGGGCGATGTACTCGGTATTCCGCGTCGCGACCGCGCTTC
CTGCCGAGGATGACGAGCGTCGCCGCCTTGTTGAGGGCTCCGACGAGTGGGC
GGGACAGTCCGGTGTCGACACCCGAGGATGGTACGACCTGTCGGGCCTGCGC
GCTAACGCCGACCTGCTGGTGTGGTGGGTTAGCGACGATCCGGCGGTGCTGC
AGGATGCCTACCATCGTTTCCGCGCATCTGGGCTGGGGCGCCACCTGGAACC
GGTGTGGTCGAACGTAGGAGTTCATCGTCCTGCGGAGTTCAACAAGTCTCACC
TGCCCTCATGCTTTGCCGGCATCGCCCCGAGGCGTTGGGCTGCGTTCTACCCC
TTCATTCGCTCCAAGGAGTGGTACCTCCTTCCGGCGGCTGATCGTTCCCGCAT
GCTGCGCGAACACGGCATCGTCGGCGCGGCCAGCTCCGACGTCAAAGCGTCG
ACGTTGGCGGCATTCGCGCTCGGGGACTACGAGTGGATTCTCGCGTTGGAGG
GTGACGACCTCGCCCGTATTGTCGATGTCATGAAGGACCTTCGTTACGTTGAAG
CCCGTCGTTATGTCGACGTGGATACCCCCTTCTTCACCGGCGAGCGCGTTTCT
CCGGTGGTGTGGGCCGACCGTCAGATGAGAGCCTGA

Plasmid Map

pTrcHisA-P. acnes HemQS (461-683)

4988 bp

Labels: trc, lacO, T7 translational enhancer, RBS, mini cistron, P. acnes HemQS, lacI, Ampicillin resistance, pBR322

P. acnes HemHS (2-330)

Amino acid sequence

MGGSHHHHHHGMASTANPYAAPTDPLAPYSAVLVVSFGGPRSPEEVMPFLRRVS
HGRIPEERLADVARHYDRFGGVSPINDATDVFVNAIGNELRRHGVRVPVLLGNRNG
TPFLEEALTDMHAHGVRRVLAVVTSAYASYSGCRQYREEIATALAHAGITDMQVDK
VPPFNEAPGFIRANAEALMQAFMRIPPTPLEATRVVFVTHSIPDSMQDASGAGQPG
TDYISQHKAVCERVAGQVRQVFGNMPQWDLAYCSRSGRPSDPWLEPDIIDHLRSL
PEQGVQSVVVAPIGFVADHMEVVNDLDYEAAEAAKESGLAFTRAATAGTHSAFIAD
LAGLILSQAAKLGCFGG

Analysis	Entire protein
Length	343 aa
Molecular Weight	37019.19
Molar extinction coefficient	23260
Isoelectric point	5.83
1 microgram =	27.013 pMol

DNA sequence

ATGGGGGGGTTCTCATCATCATCATCATCATGGTATGGCTAGCACCGCTAATCCC
TACGCTGCTCCCACGGACCCGTTGGCCCCTTATAGCGCCGTGCTTGTCGTTTC
TTTTGGCGGTCCGCGTTCCCCTGAAGAGGTCATGCCTTTTCTGAGAAGGGTCT
CCCACGGTCGCATTCCTGAAGAACGCTTGGCTGATGTCGCCCGACACTATGAC
CGTTTCGGCGGTGTCAGCCCGATTAACGATGCGACGGACGTTTTCGTCAACGC
GATTGGGAATGAACTGCGCCGTCACGGAGTACGAGTTCCAGTGCTGTTAGGGA
ACCGCAACGGCACCCCCTTCCTTGAGGAAGCGCTGACTGACATGCACGCGCAC
GGGGTGCGTCGGGTGTTAGCGGTTGTCACCTCTGCCTACGCCAGTTACTCCGG
GTGCCGTCAGTATCGCGAGGAGATCGCGACTGCCCTGGCTCACGCCGGTATC
ACCGATATGCAGGTCGACAAGGTACCTCCCTTTAACGAGGCGCCGGGATTCAT
TCGCGCTAACGCGGAAGCTCTGATGCAGGCGTTTATGCGGATCCCGCCTACTC
CTCTTGAGGCTACCCGCGTCGTTTTCGTCACTCACTCCATCCCTGACTCTATGC
AGGACGCATCTGGCGCTGGGCAGCCGGGGACGGATTACATTTCTCAGCACAA
GGCGGTTTGTGAGAGGGTCGCTGGTCAGGTGCGCCAGGTCTTCGGGAATATG
CCGCAGTGGGACTTGGCCTATTGCTCGAGGTCGGGGCGACCCAGCGACCCGT
GGCTTGAACCGGACATTATCGATCACCTCCGCAGTCTTCCCGAACAGGGCGTG
CAATCTGTTGTCGTCGCTCCAATTGGCTTCGTTGCTGACCACATGGAGGTCGTT
AATGACCTTGATTACGAGGCCGCCGAGGCAGCTAAGGAGTCCGGGCTCGCCTT
CACGCGGGCGGCGACCGCTGGTACCCATTCCGCCTTTATCGCTGATCTCGCCG
GGCTCATCTTGTCCCAGGCCGCGAAGCTTGGCTGTTTTGGCGGATGA

Plasmid Map

pTrcHisA-P.acnes-HemHS(2-330)
5297 bp

trc
lacO
T7 translational enhancer
RBS
mini cistron
lacI
P. acnes HemHS
pBR322
Ampicillin resistance

P. acnes HemQL

Amino acid sequence

MGGSHHHHHHGMASAARGEGGNLTSWPAPCVAGCCRRYPDAQDIPAVSGGDVE
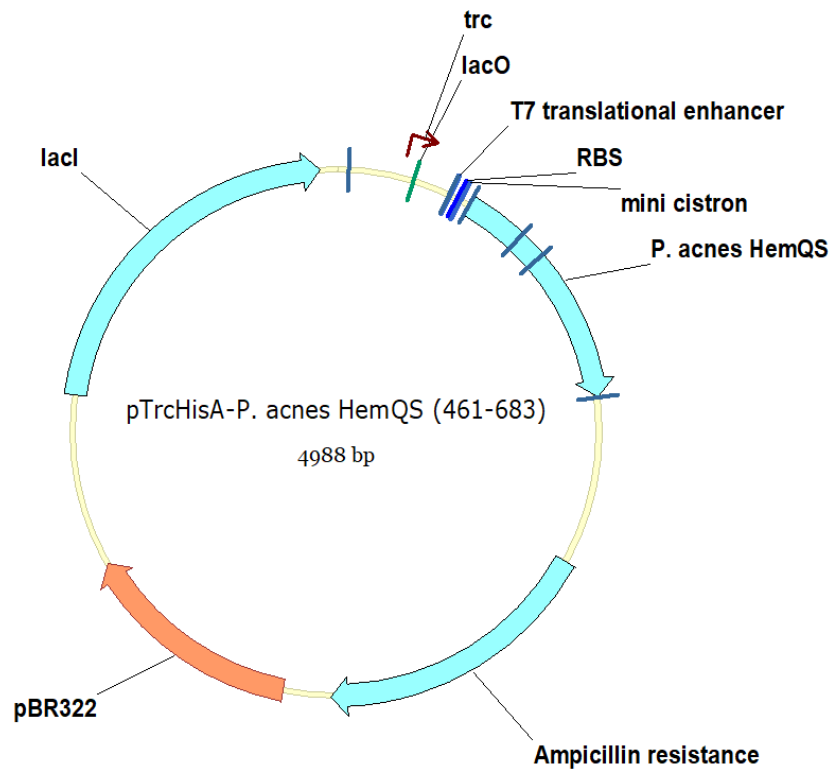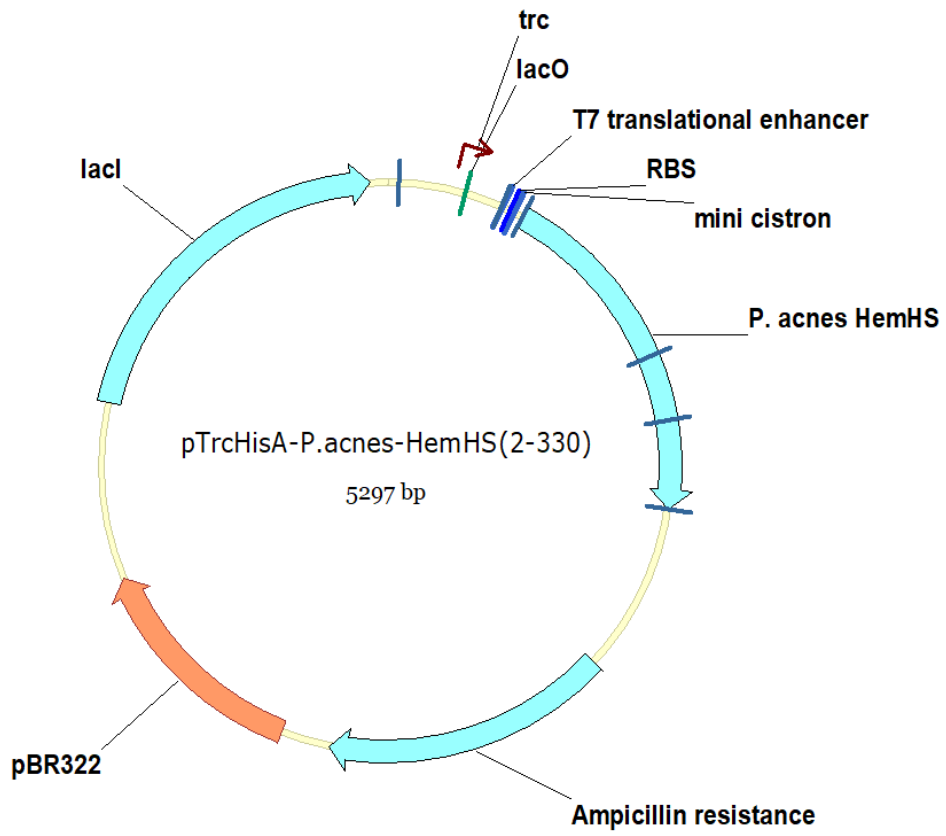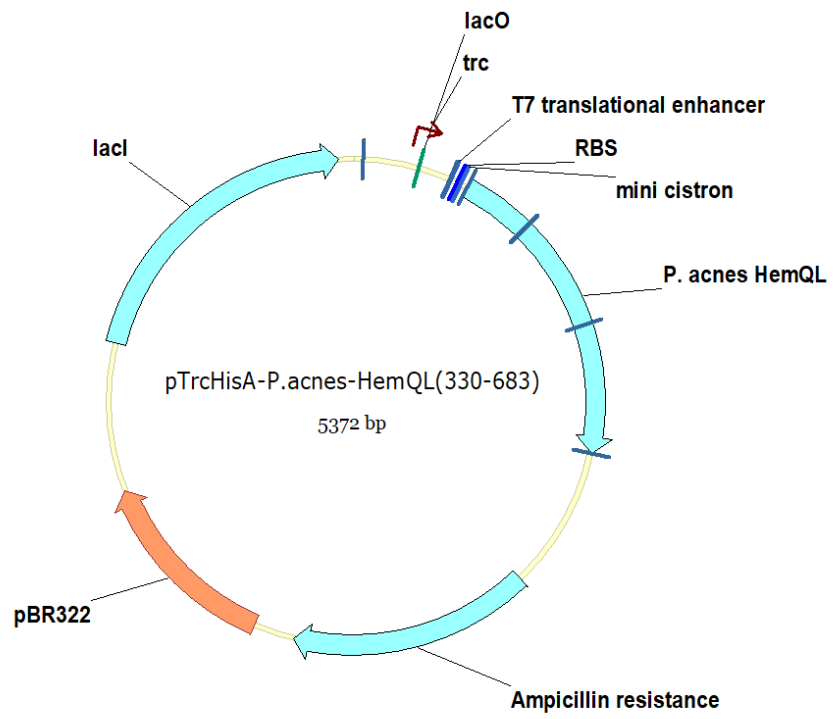SVAAGADVVDAEPGGVDFVPSGSASAVDRPGPEAVELETPPSPYNPLTKETPMSD
HSSADSVIEGPRDDEVPAGSYTAPTDPRDTPVIPEEVNASSKWAMYSVFRVATALP
AEDDERRRLVEGSDEWAGQSGVDTRGWYDLSGLRANADLLVWWVSDDPAVLQD
AYHRFRASGLGRHLEPVWSNVGVHRPAEFNKSHLPSCFAGIAPRRWAAFYPFIRS
KEWYLLPAADRSRMLREHGIVGAASSDVKASTLAAFALGDYEWILALEGDDLARIV
DVMKDLRYVEARRYVDVDTPFFTGERVSPVVWADRQMA

Analysis	Entire protein
Length	366 aa
Molecular Weight	39774.14
Molar extinction coefficient	77150
Isoelectric point	4.91
1 microgram =	25.142 pMol

DNA sequence

ATGGGGGGGTTCTCATCATCATCATCATCATGGTATGGCTAGCGCGGCTCGTGG
TGAGGGTGGCAATCTAACGTCGTGGCCGGCTCCTTGCGTCGCCGGTTGTTGCC
GACGCTACCCGGACGCTCAGGACATTCCAGCCGTCTCCGGTGGTGATGTCGA
GTCCGTAGCTGCCGGTGCCGATGTAGTCGATGCTGAACCAGGAGGTGTGGATT
TTGTGCCAAGCGGCTCAGCGAGTGCAGTCGATCGCCCGGGGCCAGAGGCGGT
CGAACTGGAGACTCCTCCTTCCCCCTACAACCCGTTGACTAAGGAGACCCCCA
TGTCTGATCATTCGAGTGCTGATTCGGTGATTGAGGGACCACGCGACGACGAA
GTTCCCGCCGGCTCCTACACCGCACCGACCGATCCCCGCGATACCCCGGTCAT
TCCCGAGGAGGTCAACGCCTCCAGCAAGTGGGCGATGTACTCGGTATTCCGCG
TCGCGACCGCGCTTCCTGCCGAGGATGACGAGCGTCGCCGCCTTGTTGAGGG
CTCCGACGAGTGGGCGGGACAGTCCGGTGTCGACACCCGAGGATGGTACGAC
CTGTCGGGCCTGCGCGCTAACGCCGACCTGCTGGTGTGGTGGGTTAGCGACG
ATCCGGCGGTGCTGCAGGATGCCTACCATCGTTTCCGCGCATCTGGGCTGGG
GCGCCACCTGGAACCGGTGTGGTCGAACGTAGGAGTTCATCGTCCTGCGGAG
TTCAACAAGTCTCACCTGCCCTCATGCTTTGCCGGCATCGCCCCGAGGCGTTG
GGCTGCGTTCTACCCCTTCATTCGCTCCAAGGAGTGGTACCTCCTTCCGGCGG
CTGATCGTTCCCGCATGCTGCGCGAACACGGCATCGTCGGCGCGGCCAGCTC
CGACGTCAAAGCGTCGACGTTGGCGGCATTCGCGCTCGGGGACTACGAGTGG
ATTCTCGCGTTGGAGGGTGACGACCTCGCCCGTATTGTCGATGTCATGAAGGA
CCTTCGTTACGTTGAAGCCCGTCGTTATGTCGACGTGGATACCCCCTTCTTCAC
CGGCGAGCGCGTTTCTCCGGTGGTGTGGGCCGACCGTCAGATGAGAGCCTGA

Plasmid Map

7.2.1.2.   P. acnes HemHQ full length

Amino acid sequence

MGGSHHHHHHGMASTANPYAAPTDPLAPYSAVLVVSFGGPRSPEEVMPFLRRVS
HGRIPEERLADVARHYDRFGGVSPINDATDVFVNAIGNELRRHGVRVPVLLGNRNG
TPFLEEALTDMHAHGVRRVLAVVTSAYASYSGCRQYREEIATALAHAGITDMQVDK
VPPFNEAPGFIRANAEALMQAFMRIPPTPLEATRVVFVTHSIPDSMQDASGAGQPG
TDYISQHKAVCERVAGQVRQVFGNMPQWDLAYCSRSGRPSDPWLEPDIIDHLRSL
PEQGVQSVVVAPIGFVADHMEVVNDLDYEAAEAAKESGLAFTRAATAGTHSAFIAD
LAGLILSQAAAARGEGGNLTSWPAPCVAGCCRRYPDAQDIPAVSGGDVESVAAGA
DVVDAEPGGVDFVPSGSASAVDRPGPEAVELETPPSPYNPLTKETPMSDHSSADS
VIEGPRDDEVPAGSYTAPTDPRDTPVIPEEVNASSKWAMYSVFRVATALPAEDDER
RRLVEGSDEWAGQSGVDTRGWYDLSGLRANADLLVWWVSDDPAVLQDAYHRFR
ASGLGRHLEPVWSNVGVHRPAEFNKSHLPSCFAGIAPRRWAAFYPFIRSKEWYLL
PAADRSRMLREHGIVGAASSDVKASTLAAFALGDYEWILALEGDDLARIVDVMKDL
RYVEARRYVDVDTPFFTGERVSPVVWADRQMRA

Analysis	Entire protein
Length	695 aa
Molecular Weight	75298.72
Molar extinction coefficient	100410
Isoelectric point	5.14
1 microgram =	13.280 pMol

DNA sequence

ATGGGGGGTTCTCATCATCATCATCATCATGGTATGGCTAGCACCGCTAATCCC
TACGCTGCTCCCACGGACCCGTTGGCCCCTTATAGCGCCGTGCTTGTCGTTTC
TTTTGGCGGTCCGCGTTCCCCTGAAGAGGTCATGCCTTTTCTGAGAAGGGTCT
CCCACGGTCGCATTCCTGAAGAACGCTTGGCTGATGTCGCCCGACACTATGAC
CGTTTCGGCGGTGTCAGCCCGATTAACGATGCGACGGACGTTTTCGTCAACGC
GATTGGGAATGAACTGCGCCGTCACGGAGTACGAGTTCCAGTGCTGTTAGGGA
ACCGCAACGGCACCCCCTTCCTTGAGGAAGCGCTGACTGACATGCACGCGCAC
GGGGTGCGTCGGGTGTTAGCGGTTGTCACCTCTGCCTACGCCAGTTACTCCGG
GTGCCGTCAGTATCGCGAGGAGATCGCGACTGCCCTGGCTCACGCCGGTATC
ACCGATATGCAGGTCGACAAGGTACCTCCCTTTAACGAGGCGCCGGGATTCAT
TCGCGCTAACGCGGAAGCTCTGATGCAGGCGTTTATGCGGATCCCGCCTACTC
CTCTTGAGGCTACCCGCGTCGTTTTCGTCACTCACTCCATCCCTGACTCTATGC
AGGACGCATCTGGCGCTGGGCAGCCGGGGACGGATTACATTTCTCAGCACAA
GGCGGTTTGTGAGAGGGTCGCTGGTCAGGTGCGCCAGGTCTTCGGGAATATG
CCGCAGTGGGACTTGGCCTATTGCTCGAGGTCGGGGGCGACCCAGCGACCCGT
GGCTTGAACCGGACATTATCGATCACCTCCGCAGTCTTCCCGAACAGGGCGTG
CAATCTGTTGTCGTCGCTCCAATTGGCTTCGTTGCTGACCACATGGAGGTCGTT
AATGACCTTGATTACGAGGCCGCCGAGGCAGCTAAGGAGTCCGGGCTCGCCTT
CACGCGGGCGGCGACCGCTGGTACCCATTCCGCCTTTATCGCTGATCTCGCCG

GGCTCATCTTGTCCCAGGCCGCGGCGGCTCGTGGTGAGGGTGGCAATCTAAC
GTCGTGGCCGGCTCCTTGCGTCGCCGGTTGTTGCCGACGCTACCCGGACGCT
CAGGACATTCCAGCCGTCTCCGGTGGTGATGTCGAGTCCGTAGCTGCCGGTGC
CGATGTAGTCGATGCTGAACCAGGAGGTGTGGATTTTGTGCCAAGCGGCTCAG
CGAGTGCAGTCGATCGCCCGGGGCCAGAGGCGGTCGAACTGGAGACTCCTCC
TTCCCCCTACAACCCGTTGACTAAGGAGACCCCATGTCTGATCATTCGAGTGC
TGATTCGGTGATTGAGGGACCACGCGACGACGAAGTTCCCGCCGGCTCCTACA
CCGCACCGACCGATCCCCGCGATACCCCGGTCATTCCCGAGGAGGTCAACGC
CTCCAGCAAGTGGGCGATGTACTCGGTATTCCGCGTCGCGACCGCGCTTCCTG
CCGAGGATGACGAGCGTCGCCGCCTTGTTGAGGGCTCCGACGAGTGGGCGGG
ACAGTCCGGTGTCGACACCCGAGGATGGTACGACCTGTCGGGCCTGCGCGCT
AACGCCGACCTGCTGGTGTGGTGGGTTAGCGACGATCCGGCGGTGCTGCAGG
ATGCCTACCATCGTTTCCGCGCATCTGGGCTGGGGCGCCACCTGGAACCGGT
GTGGTCGAACGTAGGAGTTCATCGTCCTGCGGAGTTCAACAAGTCTCACCTGC
CCTCATGCTTTGCCGGCATCGCCCCGAGGCGTTGGGCTGCGTTCTACCCCTTC
ATTCGCTCCAAGGAGTGGTACCTCCTTCCGGCGGCTGATCGTTCCCGCATGCT
GCGCGAACACGGCATCGTCGGCGCGGCCAGCTCCGACGTCAAAGCGTCGACG
TTGGCGGCATTCGCGCTCGGGGACTACGAGTGGATTCTCGCGTTGGAGGGTG
ACGACCTCGCCCGTATTGTCGATGTCATGAAGGACCTTCGTTACGTTGAAGCCC
GTCGTTATGTCGACGTGGATACCCCCTTCTTCACCGGCGAGCGCGTTTCTCCG
GTGGTGTGGGCCGACCGTCAGATGAGAGCCTGA

Plasmid Map

pTrcHisA-P.acnes- HemHQ_FL
6359 bp

lacO
trc
T7 translational enhancer
RBS
mini cistron
lacI
P. acnes HemHQ FL
pBR322
Ampicillin resistance

### 7.2.2. B. subtilis HemH construct

Amino acid sequence

MGGSHHHHHHGMASMSRKKMGLLVMAYGTPYKEEDIERYYTHIRRGRKPEPEML
QDLKDRYEAIGGISPLAQITEQQAHNLEQHLNEIQDEITFKAYIGLKHIEPFIEDAVAE
MHKDGITEAVSIVLAPHFSTFSVQSYNKRAKEEAEKLGGLTITSVESWYDEPKFVTY
WVDRVKETYASMPEDERENAMLIVSAHSLPEKIKEFGDPYPDQLHESAKLIAEGAG
VSEYAVGWQSEGNTPDPWLGPDVQDLTRDLFEQKGYQAFVYVPVGFVADHLEVL
YDNDYECKVVTDDIGASYYRPEMPNAKPEFIDALATVVLKKLGR

Analysis	Entire protein
Length	324 aa
Molecular Weight	36846.21
Molar extinction coefficient	45920
Isoelectric point	5.06
1 microgram =	27.140 pMol

DNA sequence

ATGGGGGGTTCTCATCATCATCATCATCATGGTATGGCTAGCGTGAGTAGAAAG
AAAATGGGGCTTCTCATGATGGCGTACGGCACGCCTTATAAGGAAGAAGATATT
GAACGTTATTATACACATATCAGAAGAGGCAGAAAGCCTGAACCTGAAATGCTT
CAAGATTTGAAAGACAGATACGAAGCGATTGGCGGCATTTCACCGCTTGCCCAA
ATCACAGAACAGCAGGCGCATAATCTGGAACAGCACTTGAATGAAATTCAGGAT
GAGATTACGTTTAAAGCGTATATCGGACTGAAGCATATCGAGCCGTTTATTGAA
GACGCCGTAGCAGAGATGCATAAGGATGGCATTACAGAAGCAGTCAGCATCGT
GCTGGCGCCGCATTTCTCCACGTTCAGCGTTCAGTCCTACAACAAACGCGCCA
AAGAAGAGGCTGAAAAACTCGGCGGCTTAACGATTACGTCAGTTGAAAGCTGG
TACGATGAACCGAAGTTCGTGACATATTGGGTTGACCGAGTGAAGGAAACATAT
GCGTCAATGCCTGAGGATGAAAGAGAAACGCAATGCTCATCGTATCCGCACA
CAGCCTGCCGGAAAAAATCAAAGAATTTGGAGACCCGTACCCGGACCAGCTTC
ATGAATCGGCGAAATTAATTGCTGAAGGCGCAGGCGTTTCCGAATATGCTGTCG
GCTGGCAAAGTGAAGGGAACACGCCTGATCCTTGGCTCGGACCCGATGTTCAG
GATTTAACACGTGATTTATTCGAACAAAAGGCTATCAAGCATTTGTATATGTTC
CTGTTGGGTTTGTCGCGGATCACTTAGAAGTGCTTTATGATAATGATTATGAATG
CAAAGTGGTTACTGACGATATCGGCGCAAGCTATTACCGGCCGGAAATGCCAA
ATGCCAAGCCTGAATTTATTGATGCTTTGGCAACAGTCGTATTAAAAAAATTAGG
ACGTTAA

Plasmid Map
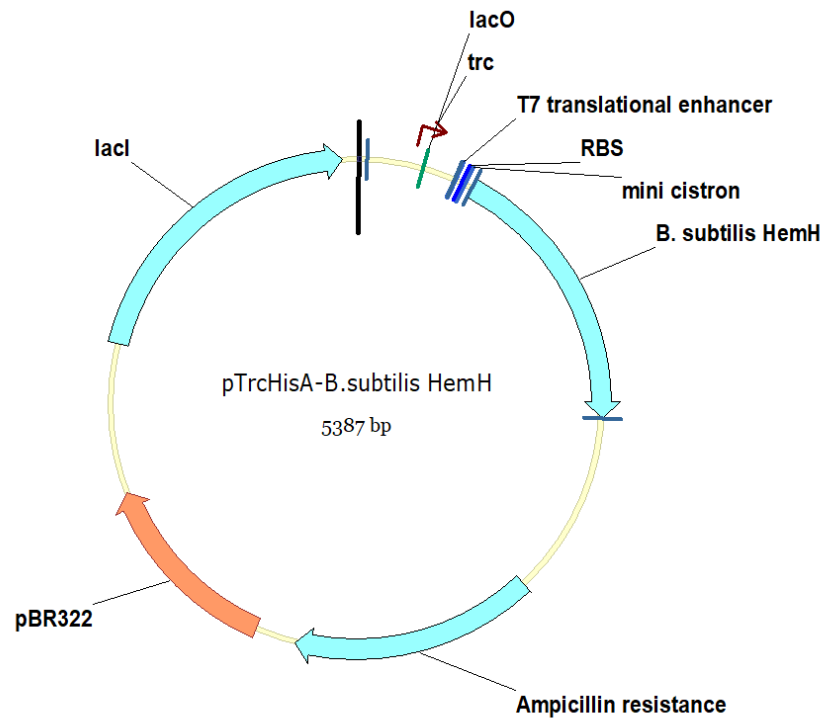
7.2.3. S. aureus *HemH and HemQ constructs*

S. aureus HemH

Amino acid sequence

MGGSHHHHHHGMASTKKMGLLVMAYGTPYKESDIEPYYTDIRHGKRPSEEELQDL
KDRYEFIGGLSPLAGTTDDQADALVSALNKAYADVEFKLYLGLKHISPFIEDAVEQM
HNDGITEAITVVLAPHYSSFSVGSYDKRADEEAAKYGIQLTHVKHYYEQPKFIEYWT
NKVNETLAQIPEEEHKDTVLVVSAHSLPKGLIEKNNDPYPQELEHTALLIKEQSNIEHI
AIGWQSEGNTGTPWLGPDVQDLTRDLYEKHQYKNFIYTPVGFVCEHLEVLYDNDY
ECKVVCDDIGANYYRPKMPNTHPLFIGAIVDEIKSIF

Analysis	Entire protein
Length	320 aa
Molecular Weight	36423.40
Molar extinction coefficient	44310
Isoelectric point	5.15
1 microgram =	27.455 pMol

DNA sequence

ATGGGGGGTTCTCATCATCATCATCATCATGGTATGGCTAGCACTAAAAAAATG
GGATTATTAGTTATGGCTTATGGCACACCTTATAAAGAAAGTGACATAGAGCCAT
ATTATACAGATATTAGACATGGTAAACGTCCATCTGAAGAAGAACTTCAAGATTT
GAAAGATAGATATGAATTTATAGGTGGTTTATCACCATTAGCAGGTACAACAGAT
GACCAGGCTGATGCGCTAGTTTCAGCATTAAATAAAGCATATGCAGATGTTGAA
TTTAAACTATACTTAGGATTAAAACACATTTCACCATTTATCGAAGATGCGGTTG
AACAAATGCACAATGATGGCATTACTGAAGCAATCACGGTAGTACTAGCACCAC
ATTATTCTTCATTTTCAGTAGGATCATATGACAAACGTGCTGATGAAGAAGCTGC
AAAATATGGTATTCAACTTACACATGTGAAACATTATTATGAACAACCTAAATTTA
TTGAATATTGGACGAATAAAGTCAACGAAACATTAGCTCAAATACCGGAAGAGG
AACATAAAGACACGGTATTAGTTGTTTCGGCACATAGTTTGCCAAAAGGTTTAAT
CGAAAAGAATAATGATCCATATCCACAAGAACTAGAACATACTGCGCTTTTAATT
AAAGAACAATCTAATATTGAACATATCGCGATTGGTTGGCAATCTGAAGGTAATA
CAGGTACACCTTGGTTAGGGCCAGATGTACAAGATTTAACACGTGATTTATATG
AAAAACATCAGTATAAAAACTTTATATATACGCCAGTAGGTTTTGTATGTGAGCA
TTTAGAGGTGCTTTATGACAATGATTATGAATGTAAAGTAGTTTGCGATGATATT
GGTGCGAATTATTATCGTCCAAAAATGCCGAATACACATCCATTATTTATCGGTG
CAATTGTTGATGAAATCAAGTCTATATTTTAA

S. aureus HemQ

Amino acid sequence

MGGSHHHHHHGMASSQAAETLDGWYSLHLFYAVDWASLRLVPKDERDALVTEFQ
SFLENTATVRSSKSGDQAIYNITGQKADLLLWFLRPEMKSLNHIENEFNKLRIADFLI
PTYSYVSVIELSNYLAGKSDEDPYENPHIKARLYPELPHSDYICFYPMNKRRNETYN
WYMLTMEERQKLMYDHGMIGRKYAGKIKQFITGSVGFDDFEWGVTLFSDDVLQFK
KIVYEMRFDETTARYGEFGSFFVGHIINTNEFDQFFAIS

Analysis	Entire protein
Length	263 aa
Molecular Weight	30757.89
Molar extinction coefficient	49050
Isoelectric point	5.62
1 microgram =	32.512 pMol

DNA sequence

ATGGGGGGTTCTCATCATCATCATCATCATGGTATGGCTAGCAGTCAAGCAGCC
GAAACATTAGATGGTTGGTATAGTCTACATTTATTTTATGCAGTTGATTGGGCAT
CATTACGTCTAGTTCCAAAGGACGAACGCGATGCACTTGTCACTGAATTTCAAT
CATTTTTAGAAAATACAGCAACTGTAAGATCATCAAAATCTGGTGATCAAGCTAT
TTATAATATAACTGGTCAAAAGCAGATTTGTTATTATGGTTCTTACGTCCTGAAA
TGAAGTCTTTAAATCATATTGAAAATGAATTTAACAAATTGCGCATTGCTGACTTC
CTAATCCCTACATATTCATATGTATCAGTCATTGAATTGAGCAATTATTTAGCTG
GTAAATCTGATGAAGATCCTTATGAGAACCCTCATATCAAAGCAAGATTATACCC
AGAATTACCACATTCTGATTATATTTGTTTCTATCCAATGAACAAACGTCGTAATG
AAACTTATAACTGGTACATGTTAACTATGGAAGAACGCCAAAAATTAATGTATGA
CCATGGTATGATTGGTAGAAAATATGCTGGCAAAATCAAACAATTTATTACTGGT
TCTGTAGGGTTTGATGATTTCGAATGGGGCGTAACATTGTTCTCAGATGACGTA
TTACAATTCAAAAAAATTGTATACGAAATGCGCTTTGATGAAACAACAGCACGAT
ACGGTGAATTCGGTAGTTTCTTTGTAGGACATATTATTAACACAAACGAATTCGA
TCAATTCTTTGCGATTTCTTAA

7.3. Derivation of kinetics equations

7.3.1. Derivation of equation 2A
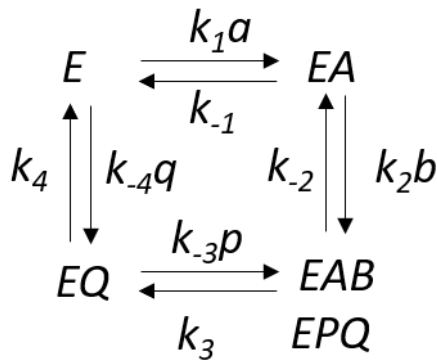
Notation	Expressions
V^+	$\dfrac{k_3 k_4 e_0}{k_3+k_4}$
V^-	$\dfrac{k_{-1} k_{-2} e_0}{k_{-1}+k_{-2}}$
K_{mA}	$\dfrac{k_3 k_4}{k_1(k_3+k_4)}$
K_{mB}	$\dfrac{(k_{-2}+k_3)k_4}{k_2(k_3+k_4)}$
K_{mP}	$\dfrac{(k_{-2}+k_3)k_{-1}}{k_{-3}(k_{-1}+k_{-2})}$
K_{mQ}	$\dfrac{k_{-1}k_{-2}}{k_{-4}(k_{-1}+k_{-2})}$
K_{iA}	$\dfrac{k_{-1}}{k_1}$
K_{iB}	$\dfrac{(k_{-1}+k_{-2})}{k_2}$
K_{iP}	$\dfrac{(k_3+k_4)}{k_{-3}}$
K_{iQ}	$\dfrac{k_4}{k_{-4}}$

First equation with all parameters

$$v = \frac{\dfrac{V^+ ab}{K_{iA}K_{mB}} - \dfrac{V^- pq}{K_{iQ}K_{mP}}}{1 + \dfrac{a}{K_{iA}} + \dfrac{K_{mA}b}{K_{iA}K_{mB}} + \dfrac{K_{mQ}p}{K_{mP}K_{iQ}} + \dfrac{q}{K_{iQ}} + \dfrac{ab}{K_{iA}K_{mB}} + \dfrac{K_{mQ}ap}{K_{iA}K_{mP}K_{iQ}} + \dfrac{K_{mA}bq}{K_{iA}K_{mB}K_{iQ}} + \dfrac{pq}{K_{iQ}K_{mP}} + \dfrac{abq}{K_{iA}K_{mB}K_{iP}} + \dfrac{bpq}{K_{iB}K_{mP}K_{iQ}}}$$

As no products are in the reaction mixture all terms containing *p* or *q* are removed, this gives:

$$v = \frac{\dfrac{V^+ ab}{K_{iA}K_{mB}}}{1 + \dfrac{a}{K_{iA}} + \dfrac{K_{mA}b}{K_{iA}K_{mB}} + \dfrac{ab}{K_{iA}K_{mB}}}$$

This can be tidied by multiply all terms by $K_{iA}K_{mB}$

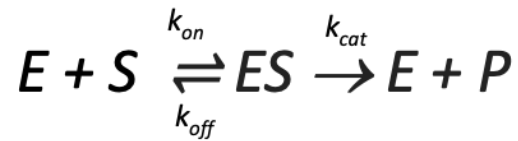$$v = \frac{V^+ ab}{K_{iA}K_{mB} + K_{mB}a + K_{mA}b + ab}$$

This can be rearranged to the equation used by dividing all by ab

$$v = \frac{V^+}{1 + \dfrac{K_{mA}}{a} + \dfrac{K_{mB}}{b} + \dfrac{K_{iA}K_{mB}}{ab}}$$

In the equation 2A used the terms have altered to appropriate notations.

$$v_i = \frac{V}{1 + \dfrac{K_m^{Fe}}{[Fe]} + \dfrac{K_m^{CP}}{[CP]} + \dfrac{K^{CP.Fe}}{[Fe][CP]}}$$

7.3.2. Derivation of equation 3A

$$E + S \underset{k_{off}}{\overset{k_{on}}{\rightleftharpoons}} ES \xrightarrow{k_{cat}} E + P$$

Kinetic equation is derived from the scheme above but does not resort to the free ligand approximation, rates of change of different species are given by the four differentials below:

$$\frac{d[S]}{dt} = -k_{on}[E][S] + k_{off}[ES]$$

$$\frac{d[E]}{dt} = -k_{on}[E][S] + (k_{off} + k_{cat})[ES]$$

$$\frac{d[P]}{dt} = k_{cat}[ES]$$

$$\frac{d[ES]}{dt} = k_{on}[E][S] - (k_{off} + k_{cat})[ES]$$

Assume [ES] reaches steady-state

$$\frac{d[ES]}{dt} = 0 \Rightarrow k_{on}[E][S] = (k_{off} + k_{cat})[ES]$$

Free Enzyme concentration, [E], is equal to total enzyme concentration, [E_T], minus [ES]. [S] equals [E_T].

$$k_{on}([E_T] - [ES])([S_T] - [ES]) = (k_{off} + k_{cat})[ES]$$

Rearrangement gives:

$$k_{on}([E_T] - [ES])([S_T] - [ES]) = (\frac{k_{off} + k_{cat})}{k_{on}}[ES] = K_M[ES]$$

$$[ES^2] - ([E_T] + [S_T] + K_M)[ES] + [E_T][S_T] = 0$$

This is a quadratic equation; the roots are calculated using:

$$(-b \pm \sqrt{b^2 - 4ac})/2a$$

Substitute in

$$a = 1$$

$$b = -([E_T] + [S_T] + K_M)$$

$$c = [E_T][S_T]$$

To give:

$$[ES] = \frac{([E_T] + [S_T] + K_M) - \sqrt{([E_T] + [S_T] + K_M)^2 - 4[E_T][S_T]}}{2}$$

Then substitute into:

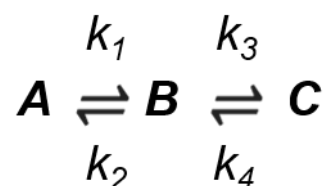$$v = k_{cat}[ES] = \frac{V_{max}}{[E_T]}[ES]$$

To give:

$$v = V_{max} \frac{([E_T] + [S_T] + K_M) - \sqrt{([E_T] + [S_T] + K_M)^2 - 4[E_T][S_T]}}{2[E_T]}$$

In the equation 3A used the terms have altered to appropriate notations. F accounts for the baseline fluorescence.

$$FI = F + \Delta F \frac{([S]+[E]+K_d) - \sqrt{([S]+[E]+K_d)^2 - 4[S][E]}}{2[E]}$$

7.3.3. Derivation of equation 5,6,7

$$
\begin{array}{ccc}
k_1 & & k_3 \\
A \rightleftharpoons B & \rightleftharpoons & C \\
k_2 & & k_4
\end{array}
$$

Differential equations from the scheme above

$$\frac{dA}{dt} = -k_1 A + k_2 B$$

$$\frac{dB}{dt} = k_1 A - (k_2 + k_3)B + k_4 C$$

$$\frac{dC}{dt} = k_3 B - k_4 C$$

In matrix form:

$$
\begin{bmatrix}
-k_1 & k_2 & 0 \\
k_1 & -k_2 - k_3 & k_4 \\
0 & k_3 & -k_4
\end{bmatrix}
\begin{bmatrix} A \\ B \\ C \end{bmatrix}
=
\begin{bmatrix}
dA/dt \\
dB/dt \\
dC/dt
\end{bmatrix}
$$

Using Eigenvalues:

$$
\begin{vmatrix}
-(k_1 + \lambda) & k_2 & 0 \\
k_1 & -(k_2 + k_3 + \lambda) & k_4 \\
0 & k_3 & -(k_4 + \lambda)
\end{vmatrix} = 0
$$

Divide through by $-\lambda$ to give this quadratic equation

$$\lambda^2 + \lambda(k_1 + k_2 + k_3 + k_4) + (k_1k_3 + k_2k_4 + k_1k_4) = 0$$

It's difficult to solve the quadratic but note that

$$\lambda_1 + \lambda_2 = k_1 + k_2 + k_3 + k_4$$

$$\lambda_1\lambda_2 = k_1k_3 + k_1k_4 + k_2k_4$$

Interest in conditions where only one exponential is visible, this assumes that one step is faster than the another. If the first step is the fast step then $k_1 + k_2 \gg k_3 + k_4$

As a result

$$\lambda_1 + \lambda_2 \approx \lambda_1 \approx k_1 + k_2$$

This gives

$$\lambda_2 = \frac{k_1k_3 + k_1k_4 + k_2k_4}{k_1 + k_2}$$

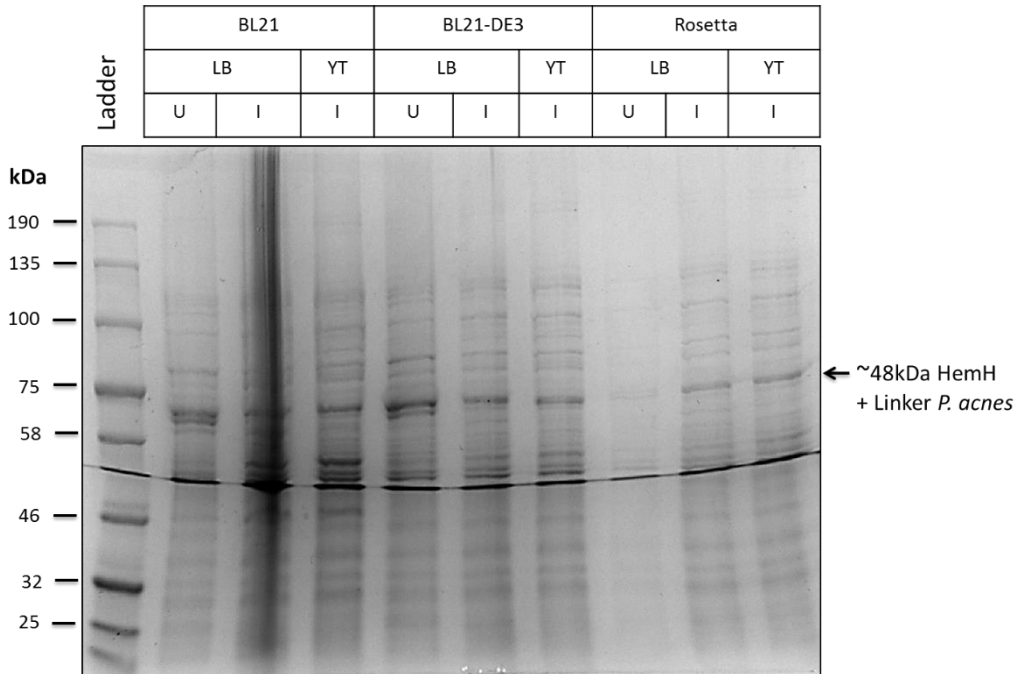$$\lambda_2 = \frac{k_3 + k_4}{1 + \frac{k_2}{k_1}} + \frac{k_2k_4}{k_1 + k_2}$$

$$\lambda_2 = \frac{k_3}{1 + \frac{k_2}{k_1}} + k_4 \left(\frac{k_1}{k_1 + \frac{k_2}{k_1}} + \frac{k_2}{k_1 + k_2} \right)$$

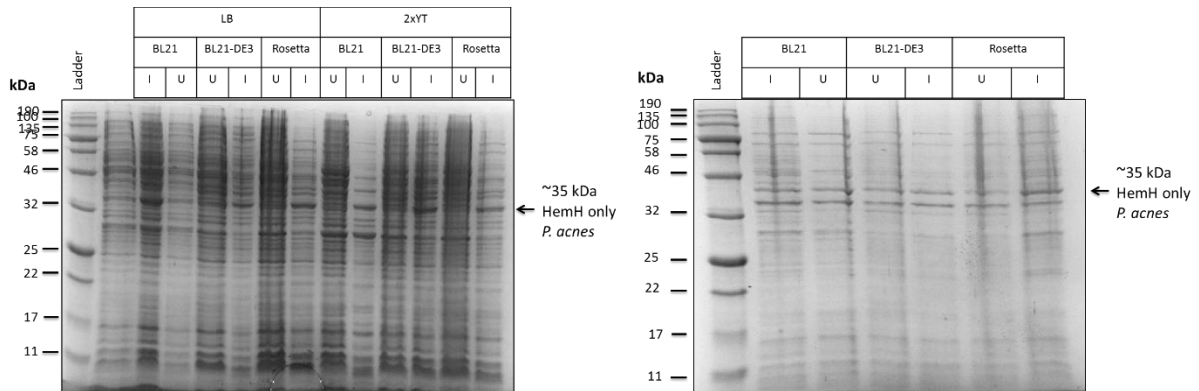$$\lambda_2 = \frac{k_3}{1 + \frac{k_2}{k_1}} + k_4$$

In the equation 5,6,7 used the terms have altered to appropriate notations.

7.4. Protein expression trials

7.4.1. *P. acnes HemHL protein expression gels*

	BL21			BL21-DE3			Rosetta		
Ladder	LB		YT	LB		YT	LB		YT
	U	I	I	U	I	I	U	I	I

kDa

190 —

135 —

100 —

75 —

58 —

46 —

32 —

25 —

← ~48kDa HemH
   + Linker *P. acnes*

7.4.2. *P. acnes HemHS protein expression gels*

Left gel:

		LB			2xYT		
kDa	Ladder	BL21	BL21-DE3	Rosetta	BL21	BL21-DE3	Rosetta
		I	U	U I	U I	U I	U I	U I

190
135
100
75
58
46
32
25
22
17
11

← ~35 kDa
   HemH only
   P. acnes

Right gel:

		BL21		BL21-DE3		Rosetta	
kDa	Ladder	I	U	U	I	U	I

190
135
100
75
58
46
32
25
22
17
11

← ~35 kDa
   HemH only
   P. acnes

Right is in LB and 2xYT media and left is in auto induction media

7.4.3. P. acnes HemQL protein expression gels

	BL21			BL21-DE3	Rosetta			BL21-DE3	
	LB		YT	LB		LB	YT	LB	YT
	U	I	I	U	U	I	I	I	I

~38kDa HemQ + Linker *P. acnes*
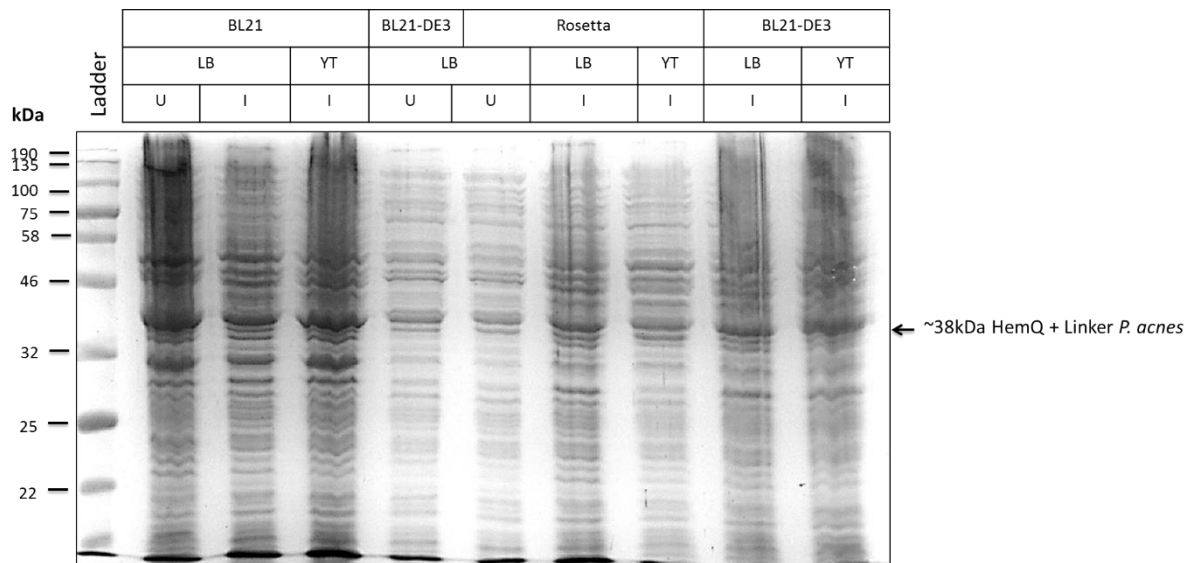
7.5. Purification gels

7.5.1. P. acnes HemQL purification gel

~38kDa
HemQ + Linker
P. acnes
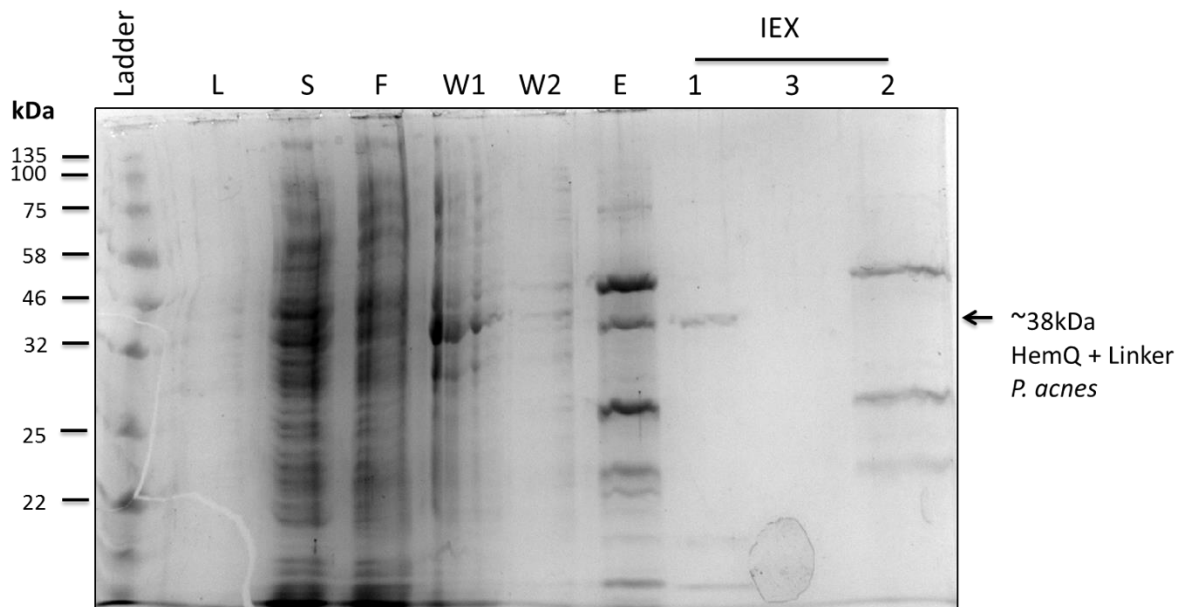
7.5.2. P. acnes *HemHQ heat trials*
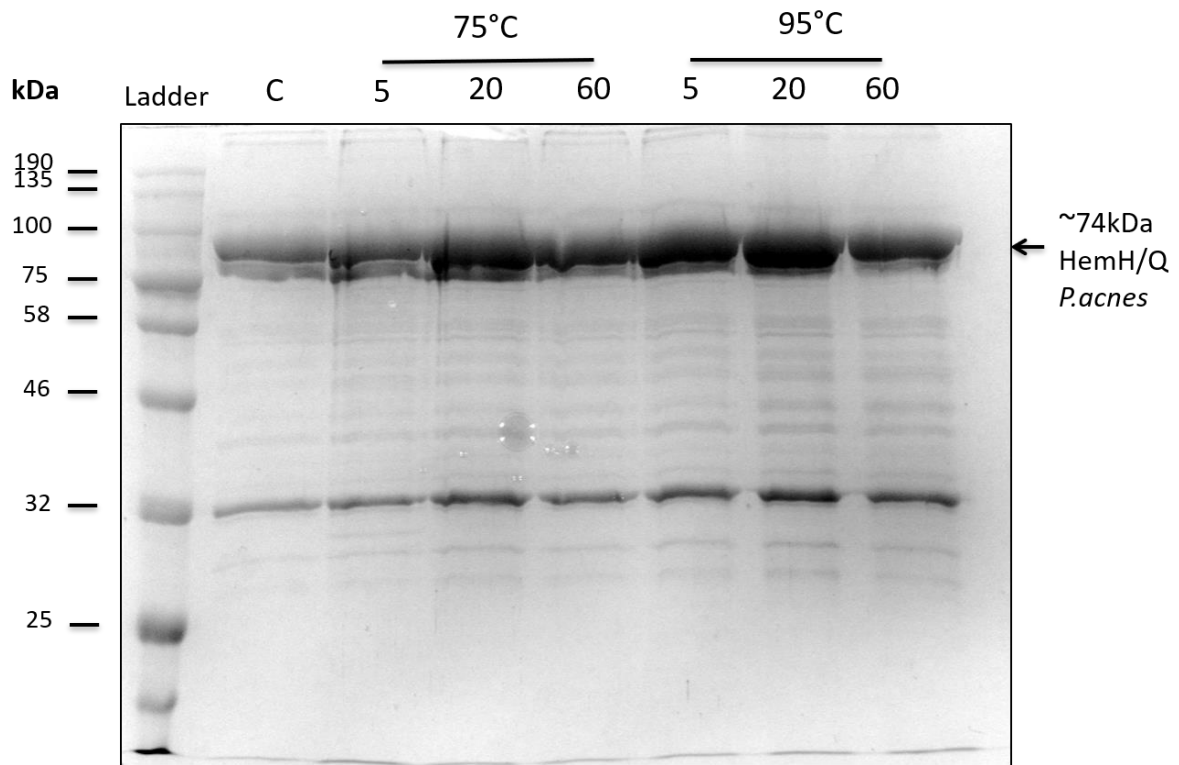
7.5.3. S. aureus *HemQ purification gel*
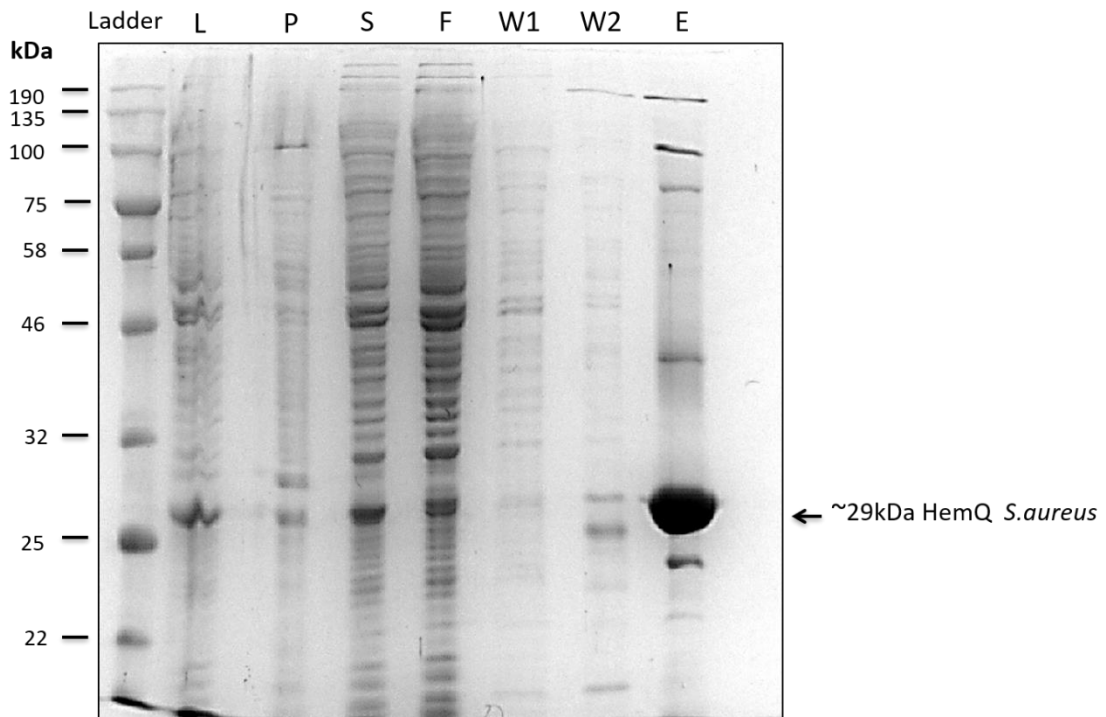
7.6. Additional kinetic data

7.6.1.Zn uncatalysed
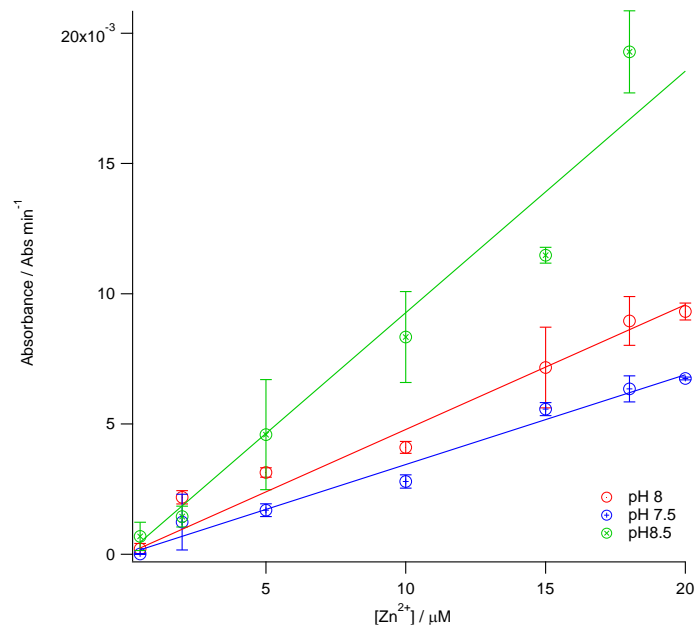
7.6.2. *Detergent-dependent activity of CP_{III} binding in* S. aureus HemH
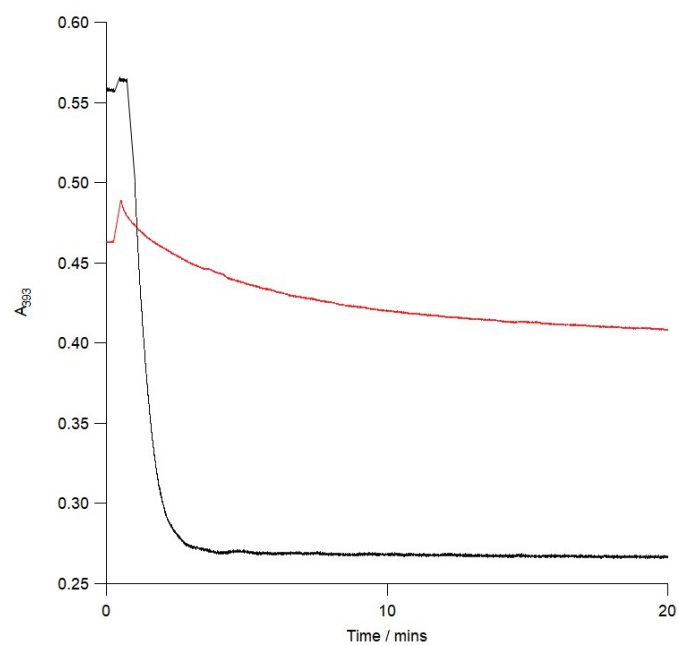
Red line indicates assay in the presence of detergent, Black line indicates assay without detergent (enzyme concentration 0.2 µM, CP_{III} 4 µM and Fe^{2+} 50 µM)
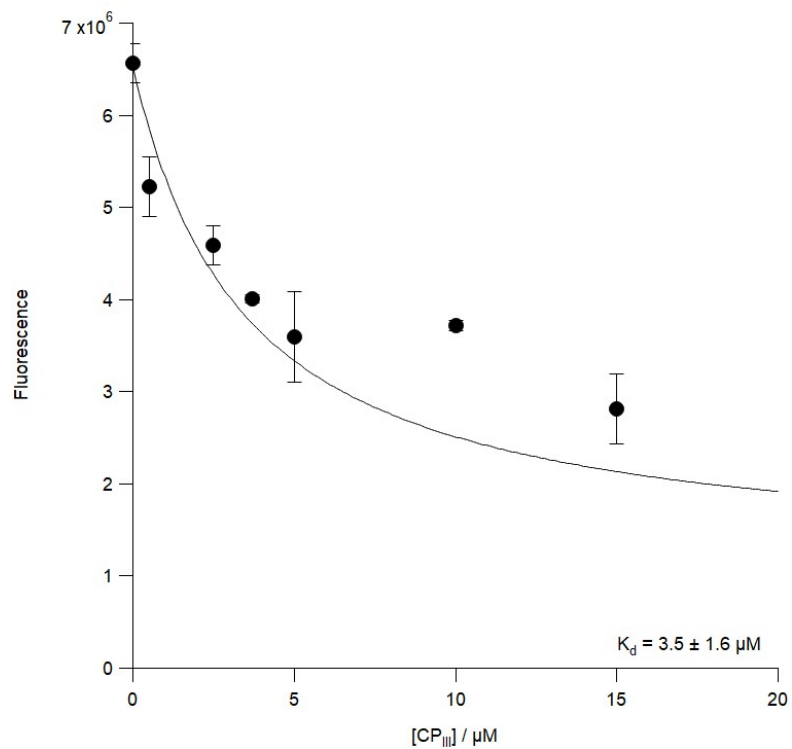
Static CP_{III} binding assay with *S. aureus* HemH (50 nM) monitoring tryptophan quenching in the presence of increasing concentrations of CP_{III}. The *S. aureus* HemH was purified in the presence of 1% cholate.

7.6.3. Global fit for S. aureus *HemH and* B. subtilis *HemH steady kinetics*

B. subtilis ferrochelatase global fit
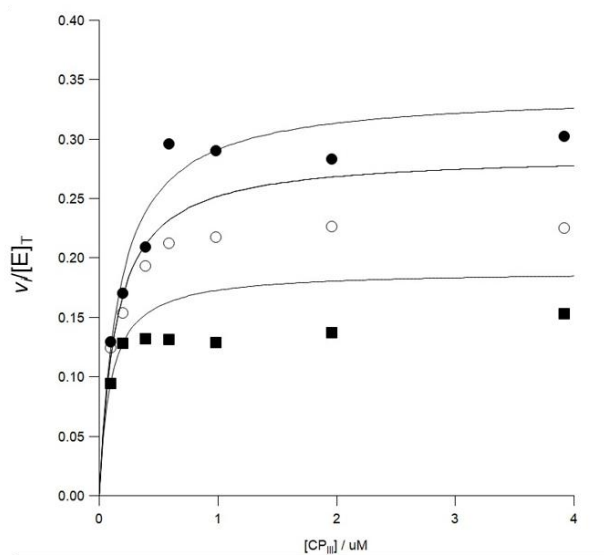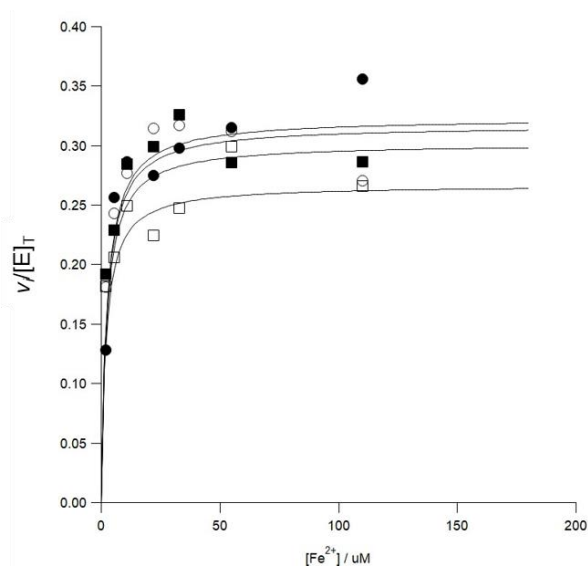
Parameter	Value
k_{cat}	0.35 ± 0.01 s^{-1}
K_m^{Fe}	2.6 ± 0.4 µM
K_m^{CP}	0.17 ± 0.03 µM
$K^{Fe.CP}$	0.01 ± 0 µM^2

S. aureus ferrochelatase global fit
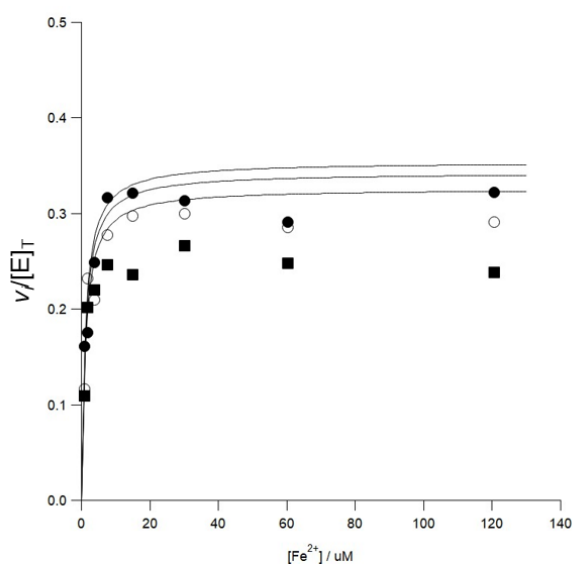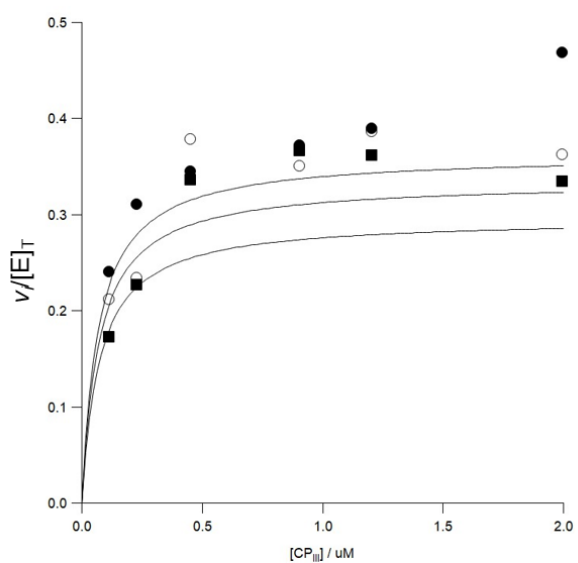
Parameter	Value
k_{cat}	0.37 ± 0.02 s^{-1}
K_m^{Fe}	1.1 ± 0.5 µM
K_m^{CP}	0.068 ± 0.04 µM
$K^{Fe.CP}$	0.1 ± 0.3 µM^2

8.   References

AIZAWA, S.-I. 2014. Chapter 21 - Rhodobacter sphaeroides — A Resourceful Little Bug. *In:* AIZAWA, S.-I. (ed.) *The Flagellar World.* Academic Press.

AIZENCANG, G. I., BISHOP, D. F., FORREST, D., ASTRIN, K. H. & DESNICK, R. J. 2000. Uroporphyrinogen III Synthase: An Alternative Promoter Controls Erythroid-Specific Expression in the Murine Gene. *Journal of Biological Chemistry,* 275**,** 2295-2304.

AL-KARADAGHI, S., FRANCO, R., HANSSON, M., SHELNUTT, J. A., ISAYA, G. & FERREIRA, G. C. 2006. Chelatases: distort to select? *Trends Biochem Sci,* 31**,** 135-42.

AL-KARADAGHI, S., HANSSON, M., NIKONOV, S., JÅNSSON, B. & HEDERSTEDT, L. 1997. Crystal structure of ferrochelatase: the terminal enzyme in heme biosynthesis. *Structure,* 5**,** 1501-1510.

ANDRADE, M. A., CHACON, P., MERELO, J. J. & MORAN, F. 1993. Evaluation of secondary structure of proteins from UV circular dichroism spectra using an unsupervised learning neural network. *Protein Eng,* 6**,** 383-90.

ARAKAWA, T. & TIMASHEFF, S. N. 1982. Preferential interactions of proteins with salts in concentrated solutions. *Biochemistry,* 21**,** 6545-52.

ASURU, A. P. & BUSENLEHNER, L. S. 2011. Analysis of human ferrochelatase iron binding via amide hydrogen/deuterium exchange mass spectrometry. *International Journal of Mass Spectrometry,* 302**,** 76-84.

BALI, S., LAWRENCE, A., LOBO, S., SARAIVA, L., GOLDING, B., PALMER, D., HOWARD, M., FERGUSON, S. & WARREN, M. 2011. Molecular hijacking of siroheme for the synthesis of heme and d1 heme. *Proc Natl Acad Sci U S A,* 108**,** 18260-65.

BALI, S., PALMER, D. J., SCHROEDER, S., FERGUSON, S. J. & WARREN, M. J. 2014. Recent advances in the biosynthesis of modified tetrapyrroles: the discovery of an alternative pathway for the formation of heme and heme d 1. *Cell Mol Life Sci,* 71**,** 2837-63.

BEALE, S. I., GOUGH, S. P. & GRANICK, S. 1975. Biosynthesis of delta-aminolevulinic acid from the intact carbon skeleton of glutamic acid in greening barley. *Proceedings of the National Academy of Sciences of the United States of America,* 72**,** 2719-2723.

BEVAN, D. R., BODLAENDER, P. & SHEMIN, D. 1980. Mechanism of porphobilinogen synthase. Requirement of Zn2+ for enzyme activity. *Journal of Biological Chemistry,* 255**,** 2030-2035.

BLACKWOOD, M. E., JR., RUSH, T. S., III, MEDLOCK, A., DAILEY, H. A. & SPIRO, T. G. 1997. Resonance raman spectra of ferrochelatase reveal porphyrin distortion upon metal binding. *Journal of the American Chemical Society,* 119**,** 12170-12174.

BLACKWOOD, M. E., JR., RUSH, T. S., III, ROMESBERG, F., SCHULTZ, P. G. & SPIRO, T. G. 1998. Alternative modes of substrate distortion in enzyme and antibody catalyzed ferrochelation reactions. *Biochemistry,* 37**,** 779-782.

BOLLIVAR, D. W., CLAUSON, C., LIGHTHALL, R., FORBES, S., KOKONA, B., FAIRMAN, R., KUNDRAT, L. & JAFFE, E. K. 2004. Rhodobacter capsulatus porphobilinogen synthase, a high activity metal ion independent hexamer. *BMC Biochem,* 5.

BOLLIVAR, D. W., ELLIOTT, T. & BEALE, S. I. 1995. Anaerobic protoporphyrin biosynthesis does not require incorporation of methyl groups from methionine. *Journal of Bacteriology,* 177**,** 5778–5783.

BOYNTON, T. O., DAUGHERTY, L. E., DAILEY, T. A. & DAILEY, H. A. 2009. Identification of Escherichia coli HemG as a novel, menadione-dependent flavodoxin with protoporphyrinogen oxidase activity. *Biochemistry,* 48**,** 6705-11.

BOYNTON, T. O., GERDES, S., CRAVEN, S. H., NEIDLE, E. L., PHILLIPS, J. D. & DAILEY, H. A. 2011. Discovery of a gene involved in a third bacterial protoporphyrinogen oxidase activity through comparative genomic analysis and functional complementation. *Appl Environ Microbiol,* 77**,** 4795-801.

BRECKAU, D., MAHLITZ, E., SAUERWALD, A., LAYER, G. & JAHN, D. 2003. Oxygen-dependent coproporphyrinogen III oxidase (HemF) from Escherichia coli is stimulated by manganese. *J Biol Chem,* 278**,** 46625-31.

BRINDLEY, A. A., RAUX, E., LEECH, H. K., SCHUBERT, H. L. & WARREN, M. J. 2003. A story of chelatase evolution: identification and characterization of a small 13-15-kDa "ancestral" cobaltochelatase (CbiXS) in the archaea. *J Biol Chem,* 278**,** 22388-95.

BURDEN, A. E., WU, C., DAILEY, T. A., BUSCH, J. L., DHAWAN, I. K., ROSE, J. P., WANG, B. & DAILEY, H. A. 1999. Human ferrochelatase: crystallization, characterization of the [2Fe-2S] cluster and determination that the enzyme is a homodimer. *Biochim Biophys Acta,* 1435**,** 191-197.

CELIS, A., STREIT, B., MORASKI, G., KANT, R., LASH, T., LUKAT-RODGERS, G., RODGERS, K. & DUBOIS, J. 2015. Unusual Peroxide-Dependent, Heme-Transforming Reaction Catalyzed by HemQ. *Biochemistry,* 54**,** 4022-32.

CHOI, H. P., HONG, J. W., RHEE, K. H. & SUNG, H. C. 2004. Cloning, expression, and characterization of 5-aminolevulinic acid synthase from Rhodopseudomonas palustris KUGB306. *FEMS Microbiol Lett,* 236**,** 175-81.

CORNISH-BOWDEN, A. 2012. *Fundamentals of Enzyme Kinetics*, Wiley VCH.

CROCKETT, N., ALEFOUNDER, P. R., BATTERSBY, A. R. & ABELL, C. 1991. Uroporphyrinogen III synthase-studies on its mechanism of action, molecular biology and biochemistry. *Tetrahedron,* 47**,** 6003-6014.

DAILEY, H., DAILEY, T., GERDES, S., JAHN, D., JAHN, M., O'BRIAN, M. & WARREN, M. 2017. Prokaryotic Heme Biosynthesis: Multiple Pathways to a Common Essential Product. *Microbiol Mol Biol Rev,* 81.

DAILEY, H. & GERDES, S. 2015. HemQ: An iron-coproporphyrin oxidative decarboxylase for protoheme synthesis in Firmicutes and Actinobacteria. *Arch Biochem Biophys,* 574**,** 27-35.

DAILEY, H., GERDES, S., DAILEY, T., BURCH, J. & PHILLIPS, J. 2015. Noncanonical coproporphyrin-dependent bacterial heme biosynthesis pathway that does not use protoporphyrin. *Proc Natl Acad Sci U S A*.

DAILEY, H. A. & DAILEY, T. A. 1996. Protoporphyrinogen Oxidase of Myxococcus xanthus: Expression, Purification, and Characterization of the Cloned Enzyme. *Journal of Biological Chemistry,* 271**,** 8714-8718.

DAILEY, H. A. & DAILEY, T. A. 2003. Ferrochelatase. *In:* KADISH, K. M., SMITH, K. M. & GUILDARD, R. (eds.) *The Porphyrin Handbook, vol. 12.* London: Academic Press.

DAILEY, H. A., DAILEY, T. A., WU, C. K., MEDLOCK, A. E., WANG, K. F., ROSE, J. P. & WANG, B. C. 2000. Ferrochelatase at the millennium: structures, mechanisms and [2Fe-2S] clusters. *Cell Mol Life Sci,* 57**,** 1909-26.

DAILEY, H. A. & FLEMING, J. E. 1986. The role of arginyl residues in porphyrin binding to ferrochelatase. *J Biol.Chem.,* 261**,** 7902-7905.

DAILEY, H. A., JONES, C. S. & KARR, S. W. 1989. Interaction of free porphyrins and metalloporphyrins with mouse ferrochelatase. A model for the active site of ferrochelatase. *Biochim. Biophys. Acta,* 999**,** 7-11.

DAILEY, H. A., WU, C. K., HORANYI, P., MEDLOCK, A. E., NAJAHI-MISSAOUI, W., BURDEN, A. E., DAILEY, T. A. & ROSE, J. 2007. Altered orientation of active site residues in variants of human ferrochelatase. Evidence for a hydrogen bond network involved in catalysis. *Biochemistry,* 46**,** 7973-9.

DAILEY, T., BOYNTON, T., ALBETEL, A., GERDES, S., JOHNSON, M. & DAILEY, H. 2010. Discovery and Characterization of HemQ: an essential heme biosynthetic pathway component. *J Biol Chem,* 285**,** 25978-86.

DAILEY, T. A. & DAILEY, H. A. 2002. Identification of [2Fe-2S] Clusters in Microbial Ferrochelatases. *Journal of Bacteriology,* 184**,** 2460-2464.

DAILEY, T. A., MEISSNER, P. & DAILEY, H. A. 1994. Expression of a cloned protoporphyrinogen oxidase. *Journal of Biological Chemistry,* 269**,** 813-815.

DAVIDSON, R., CHESTERS, C. & REID, J. 2009. Metal ion selectivity and substrate inhibition in the metal ion chelation catalyzed by human ferrochelatase. *J Biol Chem,* 284**,** 33795-9.

DE GEUS, D., THOMASSEN, E.A.J, HAGEDOOM, P.L., PANNU, N.S., VAN DUIJN, E. & ABRAHAMS, J.P. 2019. Crystal Structure of Chlorite Dismutase, a Detoxifying Enzyme Producing Molecular Oxygen. *Journal of Molecular Biology, 387, 192-206.*

FAGAN, R., PALFEY, B., LEW, M. & HUNG-WEN, L. 2010. Flavin-dependent enzymes. *Comprehensive natural products II,* 7**,** 37-113.

FALK, J. E. 1964. *Porphyrins and metalloporphyrins,* London, Elsevier.

FERREIRA, G. C., FRANCO, R., MANGRAVITA, A. & GEORGE, G. N. 2002. Unraveling the substrate-metal binding site of ferrochelatase: an X-ray absorption spectroscopic study. *Biochemistry,* 41**,** 4809-18.

FODJE, M. N. & AL-KARADAGHI, S. 2002. Occurrence, conformational features and amino acid propensities for the pi-helix. *Protein Eng,* 15**,** 353-8.

FRANCO, R., AL-KARADAGHI, S. & FERREIRA, G. 2011. Resonance Raman Spectroscopic Examination of Ferrochelatase-induced Porphyrin Distortion. *J Porphyr Phthalocyanines,* 15**,** 357-363.

FRANCO, R., MA, J. G., LU, Y., FERREIRA, G. C. & SHELNUTT, J. A. 2000. Porphyrin interactions with wild-type and mutant mouse ferrochelatase. *Biochemistry,* 39**,** 2517-2529.

GILLAM, M. E., HUNTER, G. A. & FERREIRA, G. C. 2018. Ferrochelatase pi-helix: Implications from examining the role of the conserved pi-helix glutamates in porphyrin metalation and product release. *Arch Biochem Biophys,* 644**,** 37-46.

GORA, M., GRZYBOWSKA, E., RYTKA, J. & LABBE-BOIS, R. 1996. Probing the active-site residues in Saccharomyces cerevisiae ferrochelatase by directed mutagenesis. In vivo and in vitro analyses. *Journal of Biological Chemistry,* 271**,** 11810-11816.

HANSSON, M. & AL KARADAGHI, S. 1995. Purification, crystallization, and preliminary X-ray analysis of Bacillus subtilis ferrochelatase. *Proteins,* 23**,** 607-609.

HANSSON, M. & HEDERSTEDT, L. 1992. Cloning and characterization of the Bacillus subtilis hemEHY gene cluster, which encodes protoheme IX biosynthetic enzymes. *Journal of Bacteriology,* 174**,** 8081-8093.

HANSSON, M. & HEDERSTEDT, L. 1994a. Bacillus subtilis HemY is a peripheral membrane protein essential for protoheme IX synthesis which can oxidize coproporphyrinogen III and protoporphyrinogen IX. *Journal of Bacteriology,* 176**,** 5962-5970.

HANSSON, M. & HEDERSTEDT, L. 1994b. Purification and characterisation of a water-soluble ferrochelatase from Bacillus subtilis. *European Journal of Biochemistry,* 220**,** 201-208.

HANSSON, M., KARLBERG, T., SODERBERG, C., RAJAN, S., WARREN, M., AL-KARADAGHI, S., RIGBY, S. & HANSSON, M. 2010. Bacterial ferrochelatase turns human: Tyr13 determines the apparent metal specificity of Bacillus subtilis ferrochelatase. *J Biol Inorg Chem*.

HANSSON, M., RUTBERG, L., SCHRÖDER, I. & HEDERSTEDT, L. 1991. The Bacillus subtilis hemAXCDBL gene cluster, which encodes enzymes of the biosynthetic pathway from glutamate to uroporphyrinogen III. *Journal of bacteriology,* 173**,** 2590-2599.

HANSSON, M. D., KARLBERG, T., RAHARDJA, M. A., AL-KARADAGHI, S. & HANSSON, M. 2007. Amino Acid Residues His183 and Glu264 in Bacillus subtilis Ferrochelatase Direct and Facilitate the Insertion of Metal Ion into Protoporphyrin IX. *Biochemistry,* 46**,** 87-94.

HANSSON, M. D., KARLBERG, T., SÖDERBERG, C. A. G., RAJAN, S., WARREN, M. J., AL-KARADAGHI, S., RIGBY, S. E. J. & HANSSON, M. 2011. Bacterial ferrochelatase turns human: Tyr13 determines the apparent metal specificity of Bacillus subtilis ferrochelatase. *JBIC Journal of Biological Inorganic Chemistry,* 16**,** 235-242.

HANSSON, M. D., LINDSTAM, M. & HANSSON, M. 2006. Crosstalk between metal ions in Bacillus subtilis ferrochelatase. *J Biol Inorg Chem,* 11**,** 325-33.

HART, G. J., MILLER, A. D., LEEPER, F. J. & BATTERSBY, A. R. 1987. Biosynthesis of the natural porphyrins: proof that hydroxymethylbilane synthase (porphobilinogen deaminase) uses a novel binding

group in its catalytic action. *Journal of the Chemical Society, Chemical Communications*, 1762-1765.

HEINEMANN, I. U., JAHN, M. & JAHN, D. 2008. The biochemistry of heme biosynthesis. *Arch Biochem Biophys,* 474, 238-51.

HOBBS, C., DAILEY, H. A. & SHEPHERD, M. 2016. The HemQ coprohaem decarboxylase generates reactive oxygen species: implications for the evolution of classical haem biosynthesis. *Biochem J,* 473, 3997-4009.

HOBBS, C., REID, J. & SHEPHERD, M. 2017. The coproporphyrin ferrochelatase of Staphylococcus aureus: mechanistic insights into a regulatory iron-binding site. *Biochem J,* 474, 3513-3522.

HOFBAUER, S., DALLA SEGA, M., SCHEIBLBRANDNER, S., JANDOVA, Z., SCHAFFNER, I., MLYNEK, G., DJINOVIĆ-CARUGO, K., BATTISTUZZI, G., FURTMÜLLER, P., OOSTENBRINK, C. & OBINGER, C. 2016a. Chemistry and Molecular Dynamics Simulations of Heme b-HemQ and Coproheme-HemQ. *Biochemistry,* 55, 5398-5412.

HOFBAUER, S., HAGMULLER, A., SCHAFFNER, I., MLYNEK, G., KRUTZLER, M., STADLMAYR, G., PIRKER, K. F., OBINGER, C., DAIMS, H., DJINOVIC-CARUGO, K. & FURTMULLER, P. G. 2015. Structure and heme-binding properties of HemQ (chlorite dismutase-like protein) from Listeria monocytogenes. *Arch Biochem Biophys,* 574, 36-48.

HOFBAUER, S., HOWES, B. D., FLEGO, N., PIRKER, K. F., SCHAFFNER, I., MLYNEK, G., DJINOVIC-CARUGO, K., FURTMULLER, P. G., SMULEVICH, G. & OBINGER, C. 2016b. From chlorite dismutase towards HemQ - the role of the proximal H-bonding network in haeme binding. *Biosci Rep,* 36.

HOFBAUER, S., MLYNEK, G., MILAZZO, L., PUHRINGER, D., MARESCH, D., SCHAFFNER, I., FURTMULLER, P. G., SMULEVICH, G., DJINOVIC-CARUGO, K. & OBINGER, C. 2016c. Hydrogen peroxide-mediated conversion of coproheme to heme b by HemQ-lessons from the first crystal structure and kinetic studies. *FEBS J,* 283, 4386-4401.

HOGGINS, M., DAILEY, H. A., HUNTER, C. N. & REID, J. D. 2007. Direct Measurement of Metal Ion Chelation in the Active Site of Human Ferrochelatase. *Biochemistry,* 46, 8121-8127.

HONEYBOURNE, C. L., JACKSON, J. T. & JONES, O. T. 1979. The interaction of mitochondrial ferrochelatase with a range of porphyrin substrates. *FEBS Letters,* 98, 207-210.

HUANG, D.-D., Y WANG, W., GOUGH, S. & G KANNANGARA, C. 1984. δ-Aminolevulinic acid-synthesizing enzymes need an RNA moiety for activity. *Science,* 225, 1482-4.

HUNTER, G., AL-KARADAGHI, S. & FERREIRA, G. 2011. Ferrochelatase: The Convergence of the Porphyrin Biosynthesis and Iron Transport Pathways. *J Porphyr Phthalocyanines,* 15, 350-356.

HUNTER, G. & FERREIRA, G. 2010. Identification and characterization of an inhibitory metal ion-binding site in ferrochelatase. *J Biol Chem,* 285 41836–41842.

HUNTER, G., SAMPSON, M. & FERREIRA, G. 2008. Metal ion substrate inhibition of ferrochelatase. *J Biol Chem,* 283, 23685-91.

HUNTER, G. A., VANKAYALA, S. L., GILLAM, M. E., KEARNS, F. L., LEE WOODCOCK, H. & FERREIRA, G. C. 2016. The conserved active site histidine-glutamate pair of ferrochelatase coordinately catalyzes porphyrin metalation. *Journal of Porphyrins and Phthalocyanines,* 20, 556-569.

ISHIDA, T., YU, L., AKUTSU, H., OZAWA, K., KAWANISHI, S., SETO, A., INUBUSHI, T. & SANO, S. 1998. A primitive pathway of porphyrin biosynthesis and enzymology in Desulfovibrio vulgaris. *Proc.Natl.Acad.Sci.U.S.A,* 95, 4853-4858.

JACKSON, A. H., SANCOVICH, H. A., FERRAMOLA, A. M., EVANS, N., GAMES, D. E., MATLIN, S. A., ELDER, G. H., SMITH, S. G., NEUBERGER, A. & KENNER GEORGE, W. 1976. Macrocyclic intermediates in the biosynthesis of porphyrins. *Philosophical Transactions of the Royal Society of London. B, Biological Sciences,* 273, 191-206.

JACOBS, N. J. & JACOBS, J. M. 1976. Nitrate, fumarate, and oxygen as electron acceptors for a late step in microbial heme synthesis. *Biochimica et Biophysica Acta,* 449, 1-9.

JAFFE, E. K. & LAWRENCE, S. H. 2012. Allostery and the dynamic oligomerization of porphobilinogen synthase. *Arch Biochem Biophys,* 519, 144-53.

JORDAN, P. M. & WARREN, M. J. 1987. Evidence for a dipyrromethane cofactor at the catalytic site of E. coli porphobilinogen deaminase. *FEBS Letters,* 225**,** 87-92.

KALIPATNAPU, S. & CHATTOPADHYAY, A. 2005. Membrane protein solubilization: recent advances and challenges in solubilization of serotonin1A receptors. *IUBMB Life,* 57**,** 505-12.

KANNANGARA, C. G. & GOUGH, S. P. 1978. Biosynthesis of Δ-aminolevulinate in greening barley leaves: Glutamate 1-semialdehyde aminotransferase. *Carlsberg Research Communications,* 43**,** 185.

KARLBERG, T., HANSSON, M., YENGO, R., JOHANSSON, R., THORVALDSEN, H., FERREIRA, G., HANSSON, M. & AL-KARADAGHI, S. 2008. Porphyrin binding and distortion and substrate specificity in the ferrochelatase reaction: the role of active site residues. *J Mol Biol,* 378**,** 1074-83.

KARLBERG, T., LECEROF, D., GORA, M., SILVEGREN, G., LABBE-BOIS, R., HANSSON, M. & AL KARADAGHI, S. 2002. Metal Binding to Saccharomyces cerevisiae Ferrochelatase. *Biochemistry,* 41**,** 13499-13506.

KRIEGER, F., MÖGLICH, A. & KIEFHABER, T. 2005. Effect of Proline and Glycine Residues on Dynamics and Barriers of Loop Formation in Polypeptide Chains. *Journal of the American Chemical Society,* 127**,** 3346-3352.

KUHNER, M., HAUFSCHILDT, K., NEUMANN, A., STORBECK, S., STREIF, J. & LAYER, G. 2014. The alternative route to heme in the methanogenic archaeon Methanosarcina barkeri. *Archaea,* 2014.

KURIEN, B. T. & SCOFIELD, R. H. 2012. Common artifacts and mistakes made in electrophoresis. *Methods Mol Biol,* 869**,** 633-40.

LAYER, G., REICHELT, J., JAHN, D. & HEINZ, D. 2010. Structure and function of enzymes in heme biosynthesis. *Protein Sci,* 19**,** 1137-61.

LAYER, G., VERFURTH, K., MAHLITZ, E. & JAHN, D. 2002. Oxygen-independent coproporphyrinogen-III oxidase HemN from Escherichia coli. *J Biol Chem,* 277**,** 34136-42.

LECEROF, D., FODJE, M., HANSSON, A., HANSSON, M. & AL KARADAGHI, S. 2000. Structural and mechanistic basis of porphyrin metallation by ferrochelatase. *Journal of Molecular Biology,* 297**,** 221-232.

LECEROF, D., FODJE, M. N., ALVAREZ LEON, R., OLSSON, U., HANSSON, A., SIGFRIDSSON, E., RYDE, U., HANSSON, M. & AL-KARADAGHI, S. 2003. Metal binding to Bacillus subtilis ferrochelatase and interaction between metal sites. *J Biol Inorg Chem,* 8**,** 452-8.

LOBO, S., SCOTT, A., VIDEIRA, M., WINPENNY, D., GARDNER, M., PALMER, M., SCHROEDER, S., LAWRENCE, A., PARKINSON, T., WARREN, M. & SARAIVA, L. 2015. Staphylococcus aureus haem biosynthesis: characterisation of the enzymes involved in final steps of the pathway. *Mol Microbiol,* 97**,** 472-87.

MARTINS, B. M., GRIMM, B., MOCK, H. P., HUBER, R. & MESSERSCHMIDT, A. 2001. Crystal structure and substrate binding modeling of the uroporphyrinogen-III decarboxylase from Nicotiana tabacum. Implications for the catalytic mechanism. *J Biol Chem,* 276**,** 44108-44116.

MATHEWS, M. A., SCHUBERT, H. L., WHITBY, F. G., ALEXANDER, K. J., SCHADICK, K., BERGONIA, H. A., PHILLIPS, J. D. & HILL, C. P. 2001. Crystal structure of human uroporphyrinogen III synthase. *The EMBO journal,* 20**,** 5832-5839.

MEDLOCK, A., CARTER, M., DAILEY, T., DAILEY, H. & LANZILOTTA, W. 2009. Product Release Rather than Chelation Determines Metal Specificity for Ferrochelatase. *J Mol Biol,* 393**,** 308-19.

MEDLOCK, A., NAJAHI-MISSAOUI, W., ROSS, T., DAILEY, T., BURCH, J., O'BRIEN, J., LANZILOTTA, W. & DAILEY, H. 2012. Identification and Characterization of Solvent Filled Channels in Human Ferrochelatase. *Biochemistry,* 51**,** 5422–5433.

MEDLOCK, A., SWARTZ, L., DAILEY, T. A., DAILEY, H. A. & LANZILOTTA, W. N. 2007a. Substrate interactions with human ferrochelatase. *Proc Natl Acad Sci U S A,* 104**,** 1789-93.

MEDLOCK, A. E., DAILEY, T. A., ROSS, T. A., DAILEY, H. A. & LANZILOTTA, W. N. 2007b. A pi-helix switch selective for porphyrin deprotonation and product release in human ferrochelatase. *J Mol Biol,* 373**,** 1006-16.

MUNRO, A. W., GIRVAN, H. M., MCLEAN, K. J., CHEESMAN, M. R. & LEYS, D. 2009. Heme and Hemoproteins. *In:* WARREN, M. J. & SMITH, A. G. (eds.) *Tetrapyrroles: Birth, Life and Death.* New York, NY: Springer New York.

NEEDLEMAN, S. B. & WUNSCH, C. D. 1970. A general method applicable to the search for similarities in the amino acid sequence of two proteins. *J Mol Biol,* 48**,** 443-53.

OLSSON, U., BILLBERG, A., SJOVALL, S., AL-KARADAGHI, S. & HANSSON, M. 2002. In vivo and in vitro studies of Bacillus subtilis ferrochelatase mutants suggest substrate channeling in the heme biosynthesis pathway. *J Bacteriol,* 184**,** 4018-24.

PANEK, H. & O'BRIAN, M. R. 2002. A whole genome view of prokaryotic haem biosynthesis. *Microbiology,* 148**,** 2273-2282.

PERNG, J. H. & BOCIAN, D. F. 1992. Resonance Raman spectra of chlorin and chlorophyll radical anions. *The Journal of Physical Chemistry,* 96**,** 10234-10240.

PHILLIPS, J. D., WHITBY, F. G., KUSHNER, J. P. & HILL, C. P. 1997. Characterization and crystallization of human uroporphyrinogen decarboxylase. *Protein science : a publication of the Protein Society,* 6**,** 1343-1346.

PIROVANO, W. & HERINGA, J. 2010. Protein secondary structure prediction. *Methods Mol Biol,* 609**,** 327-48.

RAUX, E., LEECH, H., BECK, R., SCHUBERT, H., SANTANDER, P., A ROESSNER, C., IAN SCOTT, A., H MARTENS, J., JAHN, D., THERMES, C., RAMBACH, A. & WARREN, M. 2003. Identification and functional analysis of enzymes required for precorrin-2 dehydrogenation and metal ion insertion in the biosynthesis of sirohaem and cobalamin in Bacillus megaterium. *Biochem J,* 370**,** 505-16.

RAUX, E., MCVEIGH, T., PETERS, S. E., LEUSTEK, T. & WARREN, M. J. 1999. The role of Saccharomyces cerevisiae Met1p and Met8p in sirohaem and cobalamin biosynthesis. *Biochem J,* 338**,** 701-708.

SCHUBERT, H. L., RAUX, E., BRINDLEY, A. A., LEECH, H. K., WILSON, K. S., HILL, C. P. & WARREN, M. J. 2002. The structure of Saccharomyces cerevisiae Met8p, a bifunctional dehydrogenase and ferrochelatase. *EMBO J,* 21**,** 2068-2075.

SEEHRA, J. S., JORDAN, P. M. & AKHTAR, M. 1983. Anaerobic and aerobic coproporphyrinogen III oxidases of Rhodopseudomonas spheroides. Mechanism and stereochemistry of vinyl group formation. *The Biochemical journal,* 209**,** 709-718.

SELLERS, V. M., WU, C.-K., DAILEY, T. A. & DAILEY, H. A. 2001. Human ferrochelatase: characterization of substrate-iron binding and proton-abstracting residues. *Biochemistry,* 40**,** 9821-9827.

SHELDON, J. R. & HEINRICHS, D. E. 2015. Recent developments in understanding the iron acquisition strategies of gram positive pathogens. *FEMS Microbiol Rev,* 39**,** 592-630.

SHEMIN, D. & KUMIN, S. 1952. The Mechanism of Porphyrin Formation: the Formation of a Succinyl Intermediate from Succinate. *Journal of Biological Chemistry,* 198**,** 827-837.

SHEMIN, D. & RITTENBERG, D. 1945. The utilization of glycine for the synthesis of a porphyrin. *Journal of Biological Chemistry,* 159**,** 567-568.

SHI, Z. & FERREIRA, G. C. 2004. Probing the active site loop motif of murine ferrochelatase by random mutagenesis. *J Biol Chem,* 279**,** 19977-86.

SHIPOVSKOV, S., KARLBERG, T., FODJE, M., HANSSON, M. D., FERREIRA, G. C., HANSSON, M., REIMANN, C. T. & AL-KARADAGHI, S. 2005. Metallation of the Transition-state Inhibitor N-methyl Mesoporphyrin by Ferrochelatase: Implications for the Catalytic Reaction Mechanism. *J Mol Biol,* 352**,** 1081-90.

SIGFRIDSSON, E. & RYDE, U. 2003. The importance of porphyrin distortions for the ferrochelatase reaction. *Journal of Biological Inorganic Chemistry,* 8**,** 273-282.

SONG, G., LI, Y., CHENG, C., ZHAO, Y., GAO, A., ZHANG, R., JOACHIMIAK, A., SHAW, N. & LIU, Z.-J. 2008. Structural insight into acute intermittent porphyria. *The FASEB Journal,* 23**,** 396-404.

STOOKEY, L. L. 1970. Ferrozine-A New Spectrophotometric Reagent for Iron. *Analytical chemistry,* 42**,** 779-781.

STORBECK, S., ROLFES, S., RAUX-DEERY, E., WARREN, M. J., JAHN, D. & LAYER, G. 2010. A novel pathway for the biosynthesis of heme in Archaea: genome-based bioinformatic predictions and experimental evidence. *Archaea*.

STREIT, B., CELIS, A., SHISLER, K., RODGERS, K., LUKAT-RODGERS, G. & DUBOIS, J. 2016. Reactions of Ferrous Coproheme Decarboxylase (HemQ) with O2 and H2O2 Yield Ferric Heme b. *Biochemistry*, 189-201.

TAIT, G. H. 1972. Coproporphyrinogenase activities in extracts of Rhodopseudomonas sphaeroides and Chromatium strain D. *Biochem.J.,* 128**,** 1159-1169.

TANAKA, R. & TANAKA, A. 2007. Tetrapyrrole biosynthesis in higher plants. *Annu Rev Plant Biol,* 58**,** 321-46.

TROUP, B., JAHN, M., HUNGERER, C. & JAHN, D. 1994. Isolation of the hemF operon containing the gene for the Escherichia coli aerobic coproporphyrinogen III oxidase by in vivo complementation of a yeast HEM13 mutant. *Journal of bacteriology,* 176**,** 673-680.

TSUMOTO, K., EJIMA, D., KUMAGAI, I. & ARAKAWA, T. 2003. Practical considerations in refolding proteins from inclusion bodies. *Protein Expression And Purification,* 28**,** 1-8.

VELDKAMP, C. T., PETERSON, F. C., HAYES, P. L., MATTMILLER, J. E., HAUGNER, J. C., 3RD, DE LA CRUZ, N. & VOLKMAN, B. F. 2007. On-column refolding of recombinant chemokines for NMR studies and biological assays. *Protein Expr Purif,* 52**,** 202-9.

VENKATESHRAO, S., YIN, J., JARZECKI, A. A., SCHULTZ, P. G. & SPIRO, T. G. 2004. Porphyrin distortion during affinity maturation of a ferrochelatase antibody, monitored by Resonance Raman spectroscopy. *J Am Chem Soc,* 126**,** 16361-7.

WARREN, M. J., BOLT, E. L., ROESSNER, C. A., SCOTT, A. I., SPENCER, J. B. & WOODCOCK, S. C. 1994. Gene dissection demonstrates that the Escherichia coli cysG gene encodes a multifunctional protein. *The Biochemical journal,* 302 (Pt 3)**,** 837-844.

WARREN, M. J. & JORDAN, P. M. 1988. Investigation into the nature of substrate binding to the dipyrromethane cofactor of Escherichia coli porphobilinogen deaminase. *Biochemistry,* 27**,** 9020-9030.

WARREN, M. J., RAUX, E., SCHUBERT, H. L. & ESCALANTE-SEMERENA, J. C. 2002. The biosynthesis of adenosylcobalamin (vitamin B12). *Natural Product Reports,* 19**,** 390-412.

WATERHOUSE, A., BERTONI, M., BIENERT, S., STUDER, G., TAURIELLO, G., GUMIENNY, R., HEER, F.T., DE BEER, T.A.P., REMPFER, C., BORDOLI, L., LEPORE, R. & SCHWEDE, T. 2018. SWISS-MODEL: Homology Modelling of Protein Structures and Complexes. *Nucleic Acids Res*. 46, W296-W303

WHITBY, F. G., PHILLIPS, J. D., KUSHNER, J. P. & HILL, C. P. 1998. Crystal structure of human uroporphyrinogen decarboxylase. *EMBO J,* 17**,** 2463-2471.

WILKINS, M. R., GASTEIGER, E., BAIROCH, A., SANCHEZ, J. C., WILLIAMS, K. L., APPEL, R. D. & HOCHSTRASSER, D. F. 1999. Protein identification and analysis tools in the ExPASy server. *Methods Mol Biol,* 112**,** 531-52.

WU, C. K., DAILEY, H. A., ROSE, J. P., BURDEN, A., SELLERS, V. M. & WANG, B. C. 2001. The 2.0 A structure of human ferrochelatase, the terminal enzyme of heme biosynthesis. *Nat Struct Biol,* 8**,** 156-160.